Origin of mafic and potassic to ultrapotassic rocks, Manicouagan area, central Grenville Province: Geochemical and geochronological constraints on the evolution of the Mesoproterozoic SE Laurentian margin and the Grenvillian LHO

by

Barun Maity

A Thesis submitted to the School of Graduate Studies
in partial fulfillment of the requirements for the degree of
Doctor of Philosophy

Department of Earth Sciences
Memorial University of Newfoundland
St. John's, Newfoundland and Labrador

October, 2019

Abstract

The southeastern margin of Laurentia preserves evidence for a long episode of juvenile crustal growth and recycling extending from the late Paleoproterozoic and throughout the Mesoproterozoic (~1.9–1.2 Ga). This was terminated by the onset of the Grenvillian continental collision (~1.1–0.98 Ga), forming a large, hot, long-duration orogen (LHO), comparable in scale to the modern day Himalayan-Tibet LHO. The Grenvillian LHO has been subdivided into the ca. 1090-1020 Ma Ottawan phase for which evidence is preserved in allochthonous rocks in the orogenic hinterland, and the ca. 1005-980 Ma Rigolet phase for which evidence is mainly preserved in the parautochthonous foreland (Rivers et al. 2012).

Mesoproterozoic to early Neoproterozoic metamorphosed mafic and unmetamorphosed potassic to ultrapotassic rocks from the Canyon domain, part of the polycyclic allochthonous, medium-pressure (aM*P*) belt of the Grenville Orogen in the Manicouagan area, central Grenville Province, were investigated using integrated petrographic, geochronological, isotopic, and geochemical methods. The principal results of the thesis, presented as three Chapters (2 - 4), are summarized below.

In Chapter 2, U-Pb TIMS geochronology of zircon, and whole-rock geochemical and Sm-Nd isotopic analyses of two granulite-facies mafic tholeiitic suites, provide constraints on: (i) the emplacement of crust-contaminated, depleted to enriched MORB-type, high Fe-Ti-P mafic sills at $1439\ ^{+76}_{-68}$ Ma within a ca. 1.5 Ga supracrustal sequence that was under limited extension at that time, probably in a back-arc setting; and (ii) emplacement of a crust-contaminated, enriched MORB to arc-type mafic intrusive suite, previously dated at 1410 ± 16 Ma, in a transitional back-arc to arc

setting. Integrated with published information, these results support the existing model of a long-lived continental margin arc on the southeastern margin of Laurentia, with intermittent back-arc opening and closure during Geons 15-14.

In Chapter 3, U-Pb TIMS geochronology of zircon from two suites of granulite-facies mafic rocks has yielded ages of 1007.7 ± 2.0 Ma for the syn-metamorphic emplacement of dykes, and 997.0 ± 3.8 Ma for the emplacement of sills. Whole-rock geochemical and Sr-Nd isotopic compositions of the mafic rocks, coupled with petrogenetic modelling, indicate that they are tholeiitic intraplate basalts derived from ~4-10% decompression melting of upwelled asthenosphere, followed by ~4-20% contamination by crust or subcontinental lithospheric mantle (SCLM). Combined with published data, these results provide evidence for late-orogenic (post-Ottawan) lithospheric extension, which led to melting of Proterozoic SCLM, decompression melting of upwelling asthenosphere, and granulite-facies metamorphism in the crust.

In Chapter 4, whole-rock geochemical and isotopic (Sr, Nd, Pb, and O) data for a suite of ca. 980 Ma, late- to post-tectonic, potassic to ultrapotassic dykes suggest two geochemically distinct groups, which formed by melting of spinel and garnet peridotite that were metasomatized by MARID-type vein assemblages containing amphibole, phlogopite, and accessory Fe-Ti-P phases. Their enriched EM I-type mantle sources were metasomatized by ancient subduction of carbonate, phosphate, and pelagic sediments. The late-tectonic group was derived from Proterozoic SCLM, whereas the post-tectonic group was derived from depleted late-Archean SCLM that had undergone early Paleoproterozoic metasomatism. Moreover, both the sources experienced an early Neoproterozoic metasomatism that is mainly attributed to late-Grenvillian continental subduction and asthenospheric upwelling. These data suggest that the terminal Rigolet

phase convergence of the Grenvillian orogeny was intracontinental, characterized by foreland subduction, where progressively older components of SCLM underwent partial melting. Hence, with continued subduction, SCLM, initially of Proterozoic age and eventually of late-Archean age, became transported beneath the orogenic core, with the Archean Superior lithosphere being situated beneath the Grenvillian hinterland by ca. 980 Ma.

The late-Grenvillian mafic rocks (Chapter 3) and potassic to ultrapotassic rocks (Chapter 4), together with published structural, geochronological and metamorphic data from the nearby Parautochthonous Belt, suggest that post-Ottawan lithospheric extension was followed by Rigolet intracontinental subduction beginning at ca. 1005 Ma, which in turn led to termination of the long-duration Grenvillian LHO by ca. 980 Ma.

Acknowledgements

I would like to extend my sincere thanks to the many people, who supported me and contributed to my work that is presented here.

First and foremost, I would like to thank my supervisor, Toby Rivers, for his tremendous and unconditional academic support, generosity, infectious enthusiasm, and constant faith in me. I have benefitted tremendously from countless stimulating discussions with him, and from his thorough and thoughtful revisions of all the chapters. He stood by me during the most challenging times and inspired me throughout to complete this arduous task. Special thanks also go to his wife Pat for her kindness and warmth. They have hosted me graciously on many occasions at their place, and I have very fond memories of my time there.

My sincere and wholehearted appreciation goes to Graham Layne, my formal supervisor and a great mentor, for supporting me gracefully throughout a very toilsome period, and providing thoughtful comments on several chapters.

My sincere gratitude also goes to my former supervisor Jyotisankar Ray, and thanks to all my teachers and friends, who remained great sources of inspiration for me.

I am deeply indebted to Len Zedel, former Associate Dean of Science, for his remarkable support.

Aphrodite Indares contributed significantly towards this thesis, and Greg Dunning performed U-Pb mass spectrometry, and both are thankfully acknowledged. Special thanks go to Sherri Strong, Pam King, Mike Shaffer, David Grant, Dylan Goudie, Amanda Langille, and Anne Westhues for their support in labs, and to Michelle, Diane, and all other staff in the department. Kier Hiscock was extremely

tenderhearted and facilitated in every possible way to make my life easier here at MUN. Zahra was a great colleague and I am very thankful for her patience, kindness, and friendship.

I am deeply humbled by the positive and appreciative remarks by the thesis examiners Brendan J. Murphy, John Greenough, and Hamish Sandeman. Their inputs have improved the quality of this thesis and are thankfully acknowledged.

My heartfelt gratitude goes to the people of Newfoundland and Labrador, who generously welcomed and supported me here. I am deeply indebted to my managers, supervisors, staffing office, and all my colleagues and staff members at Eastern Health, who cordially extended their friendships and supported graciously during this period.

Finally, I would like to thank my parents, and especially to my mother who remained supportive and unbelievably patient despite taking extraordinary hardships during this period. This thesis is dedicated to them.

Table of Contents

List of Acronyms

A.I	Alteration index
a/pH*P*	Allochthonous/Parautochthonous high-pressure
AB	Allochthonous Belt
ABT/ABD	Allochthonous Boundary Thrust/Detachment
AFC	Assimilation fractional crystallization
ALC	Archean lower crust
AMCG	Anorthosite-mangerite-charnockite-granite
BAB	Back-arc basalt
BSE	Back-scattered electron/ Bulk Silicate Earth
CA-TIMS	Chemical abrasion- thermal ionization mass spectrometry
CCPI	Carbonate-chlorite-pyrite index
CHUR	Chondrite Uniform Reservoir
CL	Cathodoluminescence
CN	Chondrite normalized
CRUML	Château- Richer, St. Urbain, Lac Chaudiere, Lac à Jack, Mattawa, and Labrieville
DM	Depleted mantle
EDS	Energy Dispersive X-Ray Spectroscopy
EM	Enriched mantle
FEG-SEM	Field emission gun- scanning electron microscope
GF	Grenville Front
GPAO	Great Proterozoic accretionary orogens
HFSE	High field-strength element
IAT	Island arc tholeiite
K-S	Kensington Schoottamatta
KLG	Knob Lake Group
L/M/HREE	Light/Middle/Heavy Rare earth element
LA-ICP-MS	Laser ablation- inductively coupled- plasma mass spectrometry
LBS	Layered Bimodal Suite

LBV	Labrieville
LCC	Lower continental crust (post-Archean)
LHO	Large hot (long-duration) orogens
LILE	Large ion lithophile element
MERNQ	Ministère de l'Énergie et des Ressources naturelles du Québec
MIU	Mafic to Intermediate Unit
MIZ	Manicouagan Imbricate Zone
MLA	Mineral liberation analysis
MORB	Mid-ocean ridge basalt
M*P*/L*P*	Medium-pressure/Low-pressure
MSWD	Mean square weighted deviation
OIB	Ocean island basalt
OOL	Ottawan orogenic lid
P.I	Peraluminous index
PB	Parautochthonous Belt
PGD	Pegmatitic granite dyke
PLV	Plus Value Complex (Complexe de la Plus Value)
PM	Primitive mantle
PUD	Potassic to ultrapotassic dykes
QFU	Quartzofeldspathic Unit
SCLM	Subcontinental lithospheric mantle
SSZM	Suprasubduction zone mantle
TSZ	Thachic shear zone
UCC	Upper continental crust
VAG	Volcanic arc granite
VC	Vein Complex
WG	Wakeham Group
WIP	Within plate basalt
WPG	Within plate granite

List of Tables

List of Figures

1. Introduction

1.1 Overview and scope of study

Convergent plate boundaries, such as active margins and continental collision belts, are major sites of the formation, preservation, and recycling of Earth's crust (Percival et al., 2001; Cawood et al., 2009; Scholl and Huene, 2007; Condie, 2013). The Grenville Province (fig. 1.1), the focus of this study, was part of a Himalaya-Tibet-scale large hot long-duration orogen (LHO; Beaumont et al., 2006) that developed on crust formed in the long-lived (~1.7-1.2 Ga), Paleo- to Mesoproterozoic active margin of southeastern Laurentia, termed the Great Proterozoic Accretionary Orogen (GPAO; Condie, 2013). Continental growth along the active margin of the GPAO started during the late Paleoproterozoic, with several spatially and temporally distinct periods of accretionary orogenesis (e.g., Penokean, Makkovikian, and Labradorian orogenies; ca. 1.90-1.62 Ga; Hoffman, 1988), followed by the development of early-Pinwarian (>1.5 Ga) supracrustal sequences (e.g., Wakeham Group in the eastern Grenville Province and Plus Value Complex in the central Grenville Province) that were deposited on the southeastern Laurentian margin in a setting variably interpreted as a passive margin (Gower, 1996; Gower and Krogh, 2002), or an active margin intra-arc or back-arc setting (Rivers and Corrigan, 2000; Wodicka et al., 2003; Corriveau et al., 2007; Rivers et al., 2012; Augland et al., 2015). Prolonged, extensive, and widespread early- to mid-Mesoproterozoic (ca. 1.5-1.3 Ga) juvenile crust formation, island arc accretion (e.g., Montauban arc; Sappin et al., 2009; Escoumins supracrustal belt; Groulier et al., 2018a) and reworking is inferred to have involved distinct phases of continental arc and back-arc activity along the entire length of the Laurentian margin, and was followed in the

southwest Grenville Province by the ca. 1.28-1.23 Ga Elzevirian and 1.19-1.12 Ga Shawinigan arc-accretionary phases (van Breemen and Davidson, 1988; Gower et al., 1990; Gower and Tucker, 1994; Tucker and Gower, 1994; Nadeau and van Breemen, 1994; Gower, 1996; Rivers, 1997; Rivers and Corrigan, 2000; Gower and Krogh, 2002; Slagstad et al., 2004, 2009; Bonnet et al., 2005; van Breemen and Corriveau, 2005; Whitmeyer and Karlstrom, 2007; Hynes and Rivers, 2010; Rivers et al., 2012; McNutt and Dickin, 2012; and references therein).

The terminal continental collision (the Grenvillian Orogeny *sensu stricto* from 1.09-0.98 Ga; Rivers, 2008), leading to formation of the large hot long-duration Grenville Orogen, has been empirically subdivided into the Ottawan (1090-1020 Ma) and the Rigolet (1005-980 Ma) phases (Rivers, 2008). The Ottawan phase is characterized by continental collision leading to lithospheric thickening, followed by slab break-off, delamination, or convective thinning of the lithospheric mantle, which may have resulted in asthenospheric upwelling and formation of an orogenic plateau (e.g., Groulier et al., 2018b). The plateau is inferred to have collapsed ~1060-1030 Ma in the central Grenville Province (Indares and Dunning, 2004; Groulier et al., 2018a), due to melt-weakening and associated channel flow of the hot and ductile middle crust, resulting in rapid extrusion of deep crustal levels (Indares et al., 1998), which were juxtaposed with mid- and upper-crustal levels along first reverse- and then normal-sense shear zones (Rivers, 2008, 2012). In this part of the orogen, the latest phase of collapse was recorded ca. 1017-1007 Ma along normal-sense shear zones that run between (previously extruded) high-pressure (H*P*) units and medium- to low-pressure (M-L*P*) units and at the base of the orogenic suprastructure (Indares et al., 1998; Indares and Dunning, 2004). The ensuing Rigolet orogenic phase is inferred to have been a time

of renewed crustal shortening and thickening in the northern margin of the province as the Grenville Orogen propagated towards the foreland within the Parautochthonous Belt. The period between the Ottawan and Rigolet orogenic phases, lacking a record of tectonothermal activity in the hinterland, was referred to as a "hiatus" (Rivers, 2008). Therefore, the relations between the Ottawan and Rigolet phases, and the processes leading to the transition between them, are unclear.

This thesis is primarily concerned with using mantle-derived intrusions as probes of their magma sources, magmatic processes, and tectonic settings – and, more specifically, it involves determination, interpretation, and evaluation of the crystallization ages, metamorphism, and geochemical and isotopic characterization of four suites of metamafic rocks and one suite of potassic to ultrapotassic rocks. These data are used to provide an improved understanding of three distinct periods in the evolution of the Laurentian margin: (i) the Geon 14 evolution of the active margin of Laurentia; (ii) the post-Ottawan tectonic and metamorphic evolution of the orogenic hinterland; and (iii) the characteristics of the Rigolet phase in the hinterland and its relation to the evolution of the foreland in the Parautochthonous Belt. Mafic and potassic to ultrapotassic rocks were chosen for this study because of their geochemical and isotopic sensitivity to their tectonic settings of formation and the nature of their mantle sources. Moreover, the metamorphic mineral assemblages developed in metamafic rocks are diagnostic of metamorphic facies and the *P-T* conditions of their formation. Therefore, this study has the potential to provide insights into the changing mantle sources in an evolving orogen, the tectonic settings of formation of the investigated suites, and the metamorphic evolution of metamafic rocks during the Grenvillian orogeny.

1.2 Regional geology

The first-order division of the orogenic architecture of the Grenville Province, into the Parautochthonous Belt in the north and the structurally overlying Allochthonous Belt in the south (fig. 1.1; Rivers et al., 1989), is exposed in the Manicouagan area, where high-grade gneiss complexes in both of these first-order belts can be observed. In the central Grenville Province, the Parautochthonous Belt is represented by the Gagnon terrane, which consists of a Paleoproterozoic continental margin sequence that overlies the Archean basement. Both were metamorphosed and deformed during the Rigolet phase (~1005- 980 Ma) of the Grenvillian Orogeny, with the grade of metamorphism ranging from greenschist-facies near the Grenville Front, to high-pressure granulite- and eclogite-facies conditions in the south (Rivers, 2008, and references therein).

The Gagnon terrane is tectonically overlain by the Allochthonous Belt (AB), which in the central Grenville Province comprises the Manicouagan Imbricate Zone (MIZ; Indares et al., 1998). The MIZ is mainly composed of Labradorian (~1.65 Ga) anorthosite-mangerite-charnockite-granite (AMCG) rocks and Pinwarian (~1.45 Ga) granitoids. The MIZ is part of the Allochthonous high-pressure (aH*P*) belt that was metamorphosed at ~750- 920 °C and 1700-1900 MPa from ca. 1060-1040 Ma (Indares, 1997, 2003; Indares et al., 1998; Cox and Indares, 1999a, b; Cox et al., 1998; Yang and Indares, 2005), during the Ottawan phase of the Grenvillian Orogeny (Rivers, 2008; Rivers et al., 2012).

To the south and southeast of the MIZ, the late Paleoproterozoic to mid-Mesoproterozoic supracrustal and plutonic rocks comprising the Island domain,

Canyon domain, Gabriel Complex, and Banded Complex (Hynes et al., 2000; Indares and Dunning, 2004; Dunning and Indares, 2010) were subjected to Ottawan granulite-facies metamorphism at 800-900 °C and 600-1100 MPa conditions from ca. 1080-1040 Ma (Indares and Dunning, 2004; Dunning and Indares, 2010; Lasalle et al., 2013; Lasalle et al., 2014; Lasalle and Indares, 2014; Patrick and Indares, 2017), and belong to the Allochthonous medium-pressure (aM*P*) belt of Rivers (2008). In addition, the Hart Jaune terrane to the southeast of the MIZ consists of 1.47 Ga mafic granulites (Hynes et al., 2000) that lack evidence for high-grade Ottawan metamorphism (Indares and Dunning, 2004), and therefore the terrane represents part of the Ottawan Orogenic Lid (OOL) of Rivers (2008).

1.2.1 Geology of the study area: Canyon domain

The Canyon domain, first defined by Hynes et al. (2000), is situated in the southern Manicouagan Reservoir area (fig. 1.2) and structurally overlies Labradorian units to the north that were metamorphosed to Ottawan M-H*P* conditions (Indares et al., 2000; Dunning and Indares, 2010). Following regional mapping by the Ministère de l'Énergie et des Ressources naturelles du Québec (MERNQ; see Moukhsil et al., 2012), detailed field investigations led to recognition of distinct lithologic units in the Canyon domain (Indares and Moukhsil, 2013), which are described briefly below, in geochronological order.

The oldest unit from the southern part of the Canyon domain is the widespread, supracrustal Plus Value Complex (PLV), a granulite-facies, predominantly metaclastic unit that is inferred to have been deposited in an early Pinwarian (~1.5 Ga) active-margin, intra-arc or back-arc setting (Moukhsil et al., 2012; Lasalle et al., 2013; Augland et al., 2015), and that was subsequently intruded by several orthogneissic

plutons of felsic to intermediate composition between ca. 1497-1015 Ma (Gobeil et al., 2002, 2005; Moukhsil et al., 2012, 2013; Augland et al., 2015). In the central part of the domain, a more restricted suite of mafic to intermediate rocks that structurally underlies the PLV, consists of 1416 ± 10 Ma (Dunning and Indares, 2010) plutons inferred to have formed in an island arc (Dunning and Indares, 2010) or a mature continental arc setting (Valverde Cardenas et al., 2012). The northern part of the Canyon domain consists of the supracrustal Quartzofeldspathic Unit (QFU) of undetermined origin and depositional age, but inferred to be ~1.4 Ga based on the presence of transposed felsic pegmatites within it and also in the >1.4 Ga units to the south, but which are absent in <1.3 Ga units to the north (Indares and Mouksil, 2013). The units to the north include the undated Vein Complex (VC), which exhibits an intricate anastomosing "vein-like" pattern of felsic and mafic layers inferred to have resulted from ca. 1.2 Ga felsic intrusion into the ca. 1.4 Ga mafic units (Indares and Moukhsil, 2013). The ca. 1.24 Ga (Lasalle et al., 2013) supracrustal Layered Bimodal Suite (LBS), composed of felsic and mafic layers and interpreted to have formed in an extensional setting (Valverde Cardenas et al., 2012; Indares and Moukhsil, 2013; Hindemith et al., 2017; Moukhsil and Solgadi, 2017), underwent Ottawan M*P* granulite-facies metamorphism ca. 1080-1050 Ma (Lasalle and Indares, 2014). The VC and LBS also include several massive and variably deformed mafic layers, rafts, and attenuated dykes, some of which occur in the LBS and cross-cut the QFU and VC (Indares and Mouksil, 2013). Finally, the older units in the Canyon domain are intruded by a suite of undeformed, leucocratic, late-Grenvillian pegmatitic granite dykes that have yielded crystallization ages of ca. 1005-995 Ma (Dunning and Indares, 2010; Turlin et al., 2017, 2019), and a suite of variably deformed and recrystallized, potassic

to ultrapotassic dykes (PUD), one of which has yielded a U-Pb zircon (TIMS) crystallization age of ca. 980 Ma (Dunning and Indares, 2010; Valverde et al., 2012).

1.3 Objectives of this study

In spite of many recent studies in the Manicouagan area of the central Grenville Province, several aspects of the tectonic evolution of this part of the Province remain poorly constrained. This thesis builds on the lithological, geochronological, geochemical, and tectonometamorphic information in the Manicouagan area and its vicinity that was available at the time the project was designed and started, to investigate the ages, sources, and tectonic settings of the suites of mafic tholeiitic and potassic to ultrapotassic rocks that span ~450 M.y interval from the Mesoproterozoic to the earliest Neoproterozoic, and to integrate the new information into the current understanding of the Grenville Orogen. More specifically, the main objectives of the thesis were as follows:

1. **Protolith characterization of a suite of meta-mafic rocks to test the hypothesis that an inferred ca. 1.4 Ga Laurentian margin arc and outboard island arc system was eventually accreted to the continental margin.**

Based on a preliminary geochronological study (U-Pb of zircon, monazite, and titanite in TIMS; Dunning and Indares, 2010), ca. 1.4 Ga mafic rocks in the Canyon domain were inferred to represent remnants of an accreted island arc terrane (Dunning and Indares, 2010), which was compared to the Montauban Group of similar age farther southwest (Sappin et al., 2009), and ca. 1.2 Ga mafic rocks were interpreted to be remnants of an intracontinental rift that subsequently developed within the accreted are terrane (Dunning and Indares, 2010). The ca. 1.4 Ga mafic rocks exposed at the type

outcrop was thought to be part of a layered supracrustal sequence (Dunning and Indares, 2010), although subsequent fieldwork in 2011 at the extension of the same outcrop revealed a more diverse range of lithologies, including magmatically interlayered mafic rocks with light to intermediate grey, and dark grey colour indices. Based on field relations and geochemical evidence, it was subsequently suggested that the ca. 1.4 Ga light grey rocks in the Canyon domain were formed in a mature continental arc setting, and that these were intruded, in an extensional setting, by the ca. 1.2 Ga mafic rocks (Valverde Cardenas, 2009; Valverde Cardenas et al., 2012). Given the differeing interpretations, a more detailed investigation was required to more fully characterize the relationship between, and origins of, the 1.4 and 1.2 Ga units. To this end, the first part of this thesis is an investigation of the geochemical (whole-rock major and trace elements and Nd isotopes) signature of the light to intermediate and dark grey samples from the ca. 1.4 Ga mafic suite, in order to better constrain the Geon 14 tectonic evolution of the Canyon domain.

2. Characterization of the age and tectonic setting of a suite of mafic layers within the ca. 1.5 Ga volcano-sedimentary Plus Value Complex.

Mafic layers in the high-grade supracrustal Plus Value Complex (PLV; Moukhsil et al., 2012) yielded an inherited monazite age of 1467 ± 5 Ma (Dunning and Indares, 2010), suggesting the presence of an older crustal component in the Complex. Based on a detrital zircon study, the PLV was later constrained to have been deposited shortly before ca. 1.5 Ga (Lasalle et al., 2013). Hence, on the basis of these data, the mafic layers within PLV could be either *in situ* supracrustal layers within the paragneiss sequence, or intrusive sills emplaced during later (i.e., 1.4-1.2 Ga) events. Samples of the mafic layers collected from within the PLV were investigated for their

geochronology (U-Pb TIMS in zircon) and geochemical signature (whole-rock major and trace element and Nd isotope) in order to constrain their age of formation and possible tectonic setting.

3. **Characterization of the age and tectonic setting of mafic rocks within the undated Vein Complex (VC) and the ca. 1.2 Ga Layered Bimodal Suite (LBS).**

The mafic rocks within the Vein Complex (VC) and the Layered Bimodal Suite (LBS) were originally inferred to have been emplaced during a ca. 1.2 Ga extensional event (Dunning and Indares, 2010; Valverde Cardenas et al., 2012; Indares and Moukhsil, 2013). However, subsequent re-evaluation of their field relations by the present author, and recognition of their less intense structural overprint compared to the country rocks (this study), suggest they could plausibly be late-orogenic intrusions. U-Pb TIMS dating of zircon revealed their post-Ottawan age (this study), making them attractive candidates to better characterize the poorly understood, post-Ottawan evolution of the Canyon domain by means of investigating their petrographic, geochemical, and isotopic features, and tectonic settings of emplacement.

4. **Geochemical and isotopic investigation of the ca. 980 Ma potassic to ultrapotassic dykes (PUDs) to identify the depletion and enrichment events of their mantle sources, the nature of mantle metasomatism, and to characterize the tectonic setting of Rigolet phase of the Grenville Orogeny.**

The geological significance of Rigolet phase in the hinterland of the Grenville Province is rather poorly documented. However, it is known to include a variety of small-volume intrusions, and in the Canyon domain it includes sporadic occurrences of ca. 995 Ma granite pegmatite dykes and a suite of ca. 980 Ma PUDs (Dunning and

Indares, 2010; Valverde Cardenas et al., 2012). On the basis of a geochemical and isotopic study of the PUD suite, it was suggested that late-orogenic extension led to upwelling of hot asthenosphere that caused melting in ancient, metasomatized Archean subcontinental lithospheric mantle that was introduced beneath the Grenville hinterland as a result of northwest-directed thrusting of the latter over its Archean foreland (Valverde Cardenas et al., 2012). On the other hand, based on age, metamorphism, and structural features, the Rigolet phase in the Gagnon terrane (foreland) has been interpreted to have resulted either from propagation of the orogen over its foreland (van Gool et al., 2008; Hynes and Rivers, 2010; Rivers et al., 2012; Rivers, 2015), or from underthrusting of the foreland beneath the hinterland (Jordan et al., 2006), in both cases leading to extrusion of the parautochthonous rocks from progressively deeper crustal levels along the hanging wall of the Grenville Front (van Gool et al., 2008). Although kinematically equivalent in terms of relative crust and mantle motions, these interpretations differ in their implications for mantle melting and involvement in the evolution of the orogenic hinterland during the Rigolet phase. Therefore, additional isotopic investigations of the potassic to ultrapotassic rocks were undertaken in order to further characterize their mantle sources and to clarify the Rigolet plate tectonic setting.

5. Tectonic synthesis: integration of new data with the published literature to produce revised tectonic models for the evolution of the Mesoproterozoic Laurentian margin, and for the transition from the post-Ottawan to the Rigolet phases of the Grenvillian Orogeny.

The first part of this study was designed to provide further constraints on the Geon 14 tectonic setting of the Laurentian margin as preserved in the Canyon domain,

especially with respect to the continental margin arc and the timing of emplacement of mafic layers as sills within the PLV supracrustal sequence, and was successful in this regard. For the second part of the study, integrating the results for the late-orogenic mafic rocks (now known to be post-Ottawan) with those for the Rigolet potassic to ultrapotassic dykes was expected to provide a better understanding of the tectonic processes involved, which in turn would shed light on the late-Grenvillian evolution of the orogenic hinterland. With respect to this latter goal, research discoveries made during the course of this study have provided opportunity and an incentive to substantially broaden its purview, especially with respect to the significance of the hiatus period separating the Ottawan and Rigolet phases, and its connection with the Rigolet convergence in the Parautochthonous Belt.

1.4 Methods of study

A combination of analytical tools was used in this research to constrain the age of emplacement, the style of metamorphism and alteration history, the nature of mantle sources and mantle metasomatism, and the tectonic settings of emplacement of the mafic tholeiitic and potassic to ultrapotassic rocks. The analyses were performed on samples previously collected by Dr. Aphrodite Indares in 2004 and 2011 during regional mapping campaigns led by the Ministère de l'Énergie et des Ressources naturelles du Québec (MERNQ) in the Manicouagan area (see Moukhsil et al. 2012).

Hand samples, outcrop photographs and field notes provided the first sources of information, followed by a detailed petrographic study of selected polished thin sections using an optical microscope. Next, a subset of thin sections was chosen for electron imaging and mineralogical mapping using a Quanta 650 field emission gun

scanning electron microscope (FEG-SEM) at the Micro Analysis Facility (MAF-IIC) in the Bruneau Centre for Research and Innovation at Memorial University of Newfoundland and Labrador (MUN). The Energy Dispersive X-Ray Spectroscopy (EDS) system in the SEM was used to semi-quantitatively identify and calculate modal abundances of mineral phases. Analyses were carried out under a 25 keV acceleration potential and a 10 nA beam current condition to obtain back-scattered electron (BSE) images and EDS analyses. False colour mineralogical maps, showing the distribution of, and relationships among the phases, were produced by post-processing the BSE and EDS data using Mineral Liberation Analysis software.

For geochronological analyses, the fresh interiors of selected samples were crushed in a steel-plated jaw crusher and disk mill so that the majority of material processed was less than 500 μm and larger than 63 μm, followed by powdering in an agate ball mill, with all equipment carefully cleaned before use. A portion of the powdered samples was selected for zircon separation using standard techniques (Wilfley Table, manual separation of the magnetic fraction, heavy liquid separation, and a Frantz magnetic separator), followed by handpicking of different morphological groups (e.g., prisms and 'soccer balls'). Representative grains from each morphological group were mounted for cathodoluminescence (CL) imaging, which was carried out using a CL detector attached to a FEI Quanta 400 SEM, operating with a 15 keV acceleration potential and a 10 nA beam current. U-Pb geochronology was performed on selected single- and multi-grain fractions using chemical abrasion thermal ionization mass spectrometry (CA-TIMS) at MUN, using the standard laboratory methodology (Sparkes and Dunning, 2014).

For whole-rock analyses, selected splits of samples previously crushed using the jaw crusher and disc mill were then pulverized for whole-rock major and trace element analyses, performed at the Activation Laboratories Ltd., Ancaster, Ontario, using the fusion–inductively coupled plasma–mass spectrometry (FUS-ICP-MS) technique. Selected whole-rock samples were prepared for tracer radiogenic isotope (Sr, Nd, and Pb) analyses by a multi-collector Finnigan Mat 262 thermal ionization mass spectrometry (TIMS) at MUN. Stable isotope (O) ratios were measured on selected whole-rock samples using a dual-inlet, triple-collecting Thermo Scientific Delta Plus XL isotope ratio mass spectrometer (IRMS) at Western University, London, Ontario.

1.5 Structure of thesis

Following this introduction (Chapter 1), which provides an overview of the research project, geological background, objectives, and methods used, the principal results of this work are presented in three core Chapters (2 - 4), each representing a stand-alone manuscript either published, submitted, or in preparation for submission in peer-reviewed journals.

Chapter 2 is entitled "*The Geon 14 arc-related mafic rocks from the central Grenville Province*", co-authored by Barun Maity and Aphrodite Indares. The manuscript has been published in the Canadian Journal of Earth Sciences, 55, 545-570, 2018. In this chapter, field and petrographic observations, major and trace element chemistry, Sm-Nd isotopes, and CA-TIMS U-Pb geochronology of two contrasting suites of ca. 1.4 Ga mafic rocks are presented, which collectively provide improved understanding of the Geon 14 tectonic setting of the central Grenville Province.

Integrated with published information, the new data support a model of a long-lived continental-margin arc and intermittent back-arc development on southeast Laurentia in the mid-Mesoproterozoic (ca. 1.5-1.4 Ga), during which repeated short periods of extension and crustal thinning in the back-arc or intra-arc regions were followed by compression and crustal thickening.

Chapter 3 is entitled "*Late-orogenic mafic magmatism in the hinterland, central Grenville Province: lithospheric extension in the evolution of a large hot orogen*", co-authored by Barun Maity and Aphrodite Indares, and is in preparation for resubmission to Precambrian Research. In this chapter, the petrography, major and trace element geochemistry, Sr-Nd isotopes, and CA-TIMS U-Pb ages of two suites of late-orogenic, metamafic rocks from the VC and LBS are presented. This study provides the first recorded evidence for the post-Ottawan amphibolite- to granulite-facies metamorphism in the hinterland – and relates it to late-orogenic lithospheric extension, thinning and melting in the SCLM, and decompression melting of upwelled asthenosphere. Recent published studies on late-orogenic, within-plate-type, alkalic mafic to felsic plutons elsewhere have suggested an origin by melting of suprasubduction zone mantle and orogenic lower crust, in a continental margin arc to back-arc followed by slab break-off or retreat. Our study suggests that these post-Ottawan tholeiitic and alkalic rocks in the Canyon domain were derived from asthenospheric and subcontinental lithospheric mantle sources, respectively, as a result of lithospheric extension in a late-orogenic setting.

Chapter 4 is entitled "*Late-orogenic potassic to ultrapotassic dykes from the central Grenvillian hinterland: trace element and Sr-Nd-Pb-O isotopic perspectives*", co-authored by Barun Maity, Graham Layne, and Fred Longstaffe, and a manuscript is

under preparation for submission to a peer-reviewed journal. This paper presents new radiogenic and stable isotope data for a suite of late-orogenic potassic to ultrapotassic dykes that, in combination with previously published geochemical data on the same suite, are used to present new insights on the involvement of different SCLM sources, and their distinct incompatible element depletion and metasomatic enrichment processes and ages ranging from late-Archean to Proterozoic. Combined with recently published metamorphic, structural, geochronological, and geophysical data from the study area, it is proposed that the late-orogenic evolution of the Grenville Province was characterized by intracontinental subduction of the Superior foreland lithosphere beneath the Grenvillian hinterland.

Chapter 5 summarizes the findings of the three main chapters and places them in a larger context. Specifically, the findings of Chapter 2 are presented in the context of understanding of the mid-Mesoproterozoic evolution of the Laurentian margin. On the other hand, the conclusions of the Chapters 3 and 4 are placed in the context of the late-orogenic evolution of a large hot orogen that was characterized by lithospheric extension followed by final termination of the orogen during continental subduction.

1.6 Co-authorship statement

The manuscript in Chapter 2 entitled "*The Geon 14 arc-related mafic rocks from the central Grenville Province*" is published in the Canadian Journal of Earth Sciences (vol. 55, p. 545-570, 2018), and is co-authored by Barun Maity and Aphrodite Indares. As first author, Barun Maity formulated the specific research questions, undertook literature review, data collection (for Sm-Nd isotopes), data analyses, interpretation, and conclusions. Dr. Aphrodite Indares was responsible for formulation of the general

research topic, and provided helpful comments and feedback on sections related to field relations, petrography, metamorphic petrology, and the significance of geochronology data. The manuscript was written and submitted by Barun Maity.

The manuscript in Chapter 3 entitled "*Late-orogenic mafic magmatism in the hinterland, central Grenville Province: lithospheric extension in the evolution of a large hot orogen*" is co-authored by Barun Maity and Aphrodite Indares, and is in preparation for resubmission to Precambrian Research. As first author, Barun Maity formulated the specific research questions, undertook literature review, data collection (Sm-Nd isotopes), data analysis, interpretation, and formulation of the conclusions. Dr. Aphrodite Indares again proposed the general topic, and provided helpful comments and feedback on sections related to field relations, petrography, metamorphic petrology, and the significance of geochronological data. The manuscript was written and will be re-submitted by Barun Maity.

The manuscript in Chapter 4 entitled "*Late-orogenic potassic to ultrapotassic dykes from the central Grenvillian hinterland: trace element and Sr-Nd-Pb-O isotopic perspective*" is co-authored by Barun Maity, Graham Layne, and Fred Longstaffe, and is in preparation for submission to a peer-reviewed journal. As first author, Barun Maity formulated the specific research questions, undertook literature review, data analyses, interpretation, and formulation of the conclusions. The Sr, Nd, and Pb analyses for this study were performed by Sherri Strong, CREAIT labs, MUN, and the oxygen analyses were carried out by Dr. Fred Longstaffe in his laboratory at the Western University, London, Ontario. Dr. Longstaffe also provided comments on interpretation of the O data, and Dr. Graham Layne provided comments on interpreting the Pb data and on

overall interpretations. The manuscript was written and will be submitted by Barun Maity.

1.7 References

Augland, L.E., Moukhsil, A., Solgadi, F., Indares, A. 2015. Pinwarian to Grenvillian magmatic evolution in the central Grenville Province: new constraints from ID–TIMS U–Pb ages and coupled Lu–Hf S–MC–ICP–MS data. Canadian Journal of Earth Sciences, 52: 701–721. doi:10.1139/cjes-2014-0232.

Beaumont, C., Nguyen, M.H., Jamieson, R. A., Ellis, S. 2006. Crustal flow modes in large hot orogens. Geological Society London Special Publication, 268: 91–145. doi:10.1144/GSL.SP.2006.268.01.05

Bonnet, A.-L., Corriveau, L., La Flèche, M.R. 2005. Chemical imprint of highly metamorphosed volcanic-hosted hydrothermal alterations in the La Romaine Supracrustal Belt, eastern Grenville Province, Quebec. Canadian Journal of Earth Sciences, 42: 1783–1814. doi:10.1139/e05-098.

Cawood, P. a., Kroner, a., Collins, W.J., Kusky, T.M., Mooney, W.D., Windley, B.F. 2009. Accretionary orogens through Earth history. Geological Society, London, Special Publications, 318: 1–36. doi:10.1144/SP318.1.

Condie, K.C. 2013. Preservation and recycling of crust during accretionary and collisional phases of Proterozoic orogens: a bumpy road from Nuna to Rodinia. Geosciences, 3: 240–261. doi:10.3390/geosciences3020240.

Corriveau, L., Perrault, S., Davidson, A., 2007. Prospective metallogenic settings of the Grenville Province. *In* Mineral deposits of Canada: a synthesis of major deposit-types, district metallogeny, the evolution of geological provinces, and exploration methods. *Edited by* W.D. Goodfellow. Geological Survey of Canada, Mineral Deposits Division, pp. 819–847 (special publication 5)

Cox, R., Indares, A. 1999a. High-pressure and high-temperature metamorphism of the mafic and ultramafic Lac Espadon suite, Manicouagan Imbricate Zone, eastern Grenville Province, Quebec. Canadian Mineralogist, 37: 335–357.

Cox, R., Indares, A. 1999b. Transformation of Fe-Ti gabbro to coronite, eclogite and amphibolite in the Baie du Nord segment, Manicouagan Imbricate Zone, eastern Grenville Province. Journal of Metamorphic Geology, 17(5): 537–555. doi:10.1046/j.1525-1314.1999.00216.x

Cox, R.A., Dunning, G.R., Indares, A.D. 1998. Petrology and U–Pb geochronology of mafic, high-pressure, metamorphic coronites from the Tshenukutish domain, eastern Grenville Province. Precambrian Research, 90: 59–83. doi:10.1016/S0301-9268(98)00033-3.

Dunning, G., Indares, A. 2010. New insights on the 1.7–1.0 Ga crustal evolution of the central Grenville Province from the Manicouagan – Baie Comeau transect. Precambrian Research, 180: 204–226. doi:10.1016/j.precamres.2010.04.005.

Gobeil, A., Hébert, C., Clarck, C., Beaumier, M., Perreault, S. 2002. Géologie de la région du lac De La Blache (22K03/22K04). Ministère des Ressources Naturelles, Québec, Qué., RG2002-01: pp. 50.

Gobeil, A., Hébert, C., Clark, T., David, J., Davis, D. 2005. Nouvelles données géochronologiques dans l'est du Grenville: précisions sur l'évolution magmatique. Ministère des Ressources naturelles du Québec, Résumé des conférences et de l'exposition géoscientifique. Congrès de Québec Exploration 2005. 21 au 24 novembre 2005, Quebec, Que. DV 2005-03 pp. 118.

Gower, C.F. 1996. The evolution of the Grenville Province in eastern Labrador, Canada. Geological Society, London, Special Publications, 112: 197–218. doi:10.1144/GSL.SP.1996.112.01.11.

Gower, C.F., Krogh, T.E. 2002. A U-Pb geochronological review of the Proterozoic history of the eastern Grenville Province. Canadian Journal of Earth Sciences, 39: 795. doi:10.1139/e01-090.

Gower, C.F., Tucker, R.D. 1994. Distribution of pre-1400 Ma crust in the Grenville province: Implications for rifting in Laurentia-Baltica during geon 14. Geology, 22: 827.830. doi: 10.1130/0091-7613(1994)022<0827:DOPMCI>2.3.CO;2

Gower, C.F., Ryan, A.B., Rivers, T. 1990. Mid-Proterozoic Laurentia-Baltica: an overview of its geological evolution and a summary of the contributions made by this volume. *In* Mid-Proterozoic Laurentia-Baltica. *Edited by* C.F Gower, T. Rivers, and A.B. Ryan. Geological Association of Canada Special Paper, Special Paper 38: 1–20.

Groulier, P.-A., Indares, A., Dunning, G., Moukhsil, A., Jenner, G. 2018a. Syn-orogenic magmatism over 100 m.y. in high crustal levels of the central Grenville Province: characteristics, age and tectonic significance. Lithos, 312–313: 128–152. doi:10.1016/J.LITHOS.2018.04.025.

Groulier, P.-A., Indares, A., Dunning, G., Moukhsil, A., Wälle, M. 2018b. Peri-Laurentian, Pinwarian-age oceanic arc crust preserved in the Grenville Province: insights from the Escoumins supracrustal belt. Precambrian Research, 311: 37–64. doi:10.1016/J.PRECAMRES.2018.04.001.

Hindemith, M., Indares, A., Piercey, S. 2017. Hydrothermally altered volcanic rocks metamorphosed at granulite-facies conditions: an example from the Grenville Province. Canadian Journal of Earth Sciences, 54: 622–638. doi:10.1139/cjes-2016-0146.

Hoffman, P.F. 1988. United plates of America, the birth of a craton: early Proterozoic assembly and growth of Laurentia. Annual Review of Earth and Planetary Sciences, 16: 543–603. doi:10.1146/annurev.ea.16.050188.002551.

Hynes, A., Rivers, T. 2010. Protracted continental collision – evidence from the Grenville Orogen. Canadian Journal of Earth Sciences, 47: 591–620. doi:10.1139/E10-003.

Hynes, A., Indares, A., Rivers, T., Gobeil, A. 2000. Lithoprobe line 55: integration of out-of-plane seismic results with surface structure, metamorphism, and geochronology, and the tectonic evolution of the eastern Grenville Province. Canadian Journal of Earth Sciences, 37: 341–358. doi:10.1139/e99-076.

Indares, A. 1997. Garnet-kyanite clinopvroxenites and garnet-kyanite restites from the manicouagan imbricate zone: a case of high-P - High-T metamorphism in the Grenville Province. Canadian Mineralogist, 35: 1161–1171.

Indares, A., Dunning, G. 2004. Crustal architecture above the high-pressure belt of the Grenville Province in the Manicouagan area: new structural, petrologic and U-Pb age constraints. Precambrian Research, 130: 199–228. doi:10.1016/j.precamres.2003.11.005.

Indares, A., Moukhsil, A. 2013. Geon 12 crustal extension in the central Grenville Province, implications for the orogenic architecture, and potential influence on the emplacement of anorthosites. Canadian Journal of Earth Sciences, 50: 955–966. doi:10.1139/cjes-2012-0161.

Indares, A., Dunning, G., Cox, R., Gale, D., Connelly, J. 1998. High-pressure, high-temperature rocks from the base of thick continental crust: Geology and age constraints from the Manicouagan Imbricate Zone, eastern Grenville Province. Tectonics, 17: 426–440. doi:10.1029/98TC00373.

Indares, A.D. 2003. Metamorphic textures and P-T evolution of high-P granulites from the Lelukuau terrane, NE Grenville Province. Journal of Metamorphic Geology, 21: 35–48. doi:10.1046/j.1525-1314.2003.00414.x.

Lasalle, S., Dunning, G., Indares, A., McFarlane, C., 2014. In situ LA–ICP–MS dating of monazite from aluminous gneisses: insights on the tectono-metamorphic history of a granulite-facies domain in the central Grenville Province. Canadian Journal of Earth Sciences, 51: 558–572. doi:10.1139/cjes-2013-0170

Lasalle, S., Fisher, C.M., Indares, A., Dunning, G., 2013. Contrasting types of Grenvillian granulite facies aluminous gneisses: insights on protoliths and metamorphic events from zircon morphologies and ages. Precambrian Research, 228: 117–130. doi:10.1016/j.precamres.2013.01.014

Lasalle, S., Indares, A., 2014. Anatectic record and contrasting P–T paths of aluminous gneisses from the central Grenville Province. Journal of Metamorphic Geology, 32: 627–646. doi:10.1111/jmg.12083

Maity, B., Indares, A. 2018. The Geon 14 arc-related mafic rocks from the central Grenville Province. Canadian Journal of Earth Sciences, 55: 545–570. doi:10.1139/cjes-2017-0197.

McNutt, R.H., and Dickin, A.P. 2012. A comparison of Nd model ages and U-Pb zircon ages of Grenville granitoids: Constraints on the evolution of the Laurentian margin from 1.5 to 1.0Ga. Terra Nova, 24: 7–15. doi:10.1111/j.1365-3121.2011.01031.x.

Moukhsil, A., Solgadi, F., Lacoste, P., Gagnon, M., David, J. 2012. Géologie de la région du lac du Milieu (SNRC 22O03, 22O04, 22O06, 22J13 et 22J14). RG 2012-01, pp. 31.

Moukhsil, A., Solgadi, F., Thomas, C., Séverine, B., Indares, A., Davis, D.W. 2013. Géologie du nord-ouest de la région du barrage Daniel-Johnson (Manic 5), Côte-Nord. Ministère des Ressources naturelles, Québec. RG 2013-01.

Moukhsil, A., Solgadi, F. 2017. Géologie, potentiel minéral et cadre géodynamique des roches de la région du réservoir Daniel-Johnson (Manicouagan), partie centrale de la Province de Grenville. *In* Géologie, potentiel minéral et cadre géodynamique des roches de la région du réservoir Daniel-Johnson (Manicouagan), partie centrale de la Province de Grenville. Moukhsil, A. *coordonnateur*. Ministère de l'Énergie et des Ressources naturelles, Québec, MM 2017-1: 7-92. Available from: http://gq.mines.gouv.qc.ca/documents/EXAMINE/MM201701/MM201701.pdf.

Nadeau, L., van Breemen, O. 1994. Do the 1.45–1.39 Ga Montauban group and the La Bostonnais complex constitute a Grenvillian accreted terrane? In Program with Abstracts. Geological Association of Canada, 19: pp. A81.

Patrick, M.E., Indares, A. 2017. Petrography and phase equilibria modeling of mid-P aluminous gneisses derived from hydrothermally altered protoliths, Grenville Province, Canada. Canadian Journal of Earth Sciences, 54: 1103–1118. doi:10.1139/cjes-2016-0162.

Percival, J.A., Stern, R.A., Skulski, T. 2001. Crustal growth through successive arc magmatism: reconnaissance U–Pb SHRIMP data from the northeastern Superior

Province, Canada. Precambrian Research, 109: 203–238. doi:10.1016/S0301-9268(01)00148-6.
Rivers, T. 1997. Lithotectonic elements of the Grenville Province: review and tectonic implications. Precambrian Research, 86: 117–154. doi:10.1016/S0301-9268(97)00038-7.
Rivers, T. 2008. Assembly and preservation of lower, mid, and upper orogenic crust in the Grenville Province—implications for the evolution of large hot long-duration orogens. Precambrian Research, 167: 237–259. doi:10.1016/j.precamres.2008.08.005.
Rivers, T. 2015. Tectonic Setting and Evolution of the Grenville Orogen: An Assessment of Progress Over the Last 40 Years. Geoscience Canada, 42: 77–124. doi:10.12789/geocanj.2014.41.057.
Rivers, T., Corrigan, D. 2000. Convergent margin on southeastern Laurentia during the Mesoproterozoic: tectonic implications. Canadian Journal of Earth Sciences, 37: 359–383. doi:10.1139/e99-067.
Rivers, T., Culshaw, N., Hynes, A., Indares, A., Jamieson, R., Martignole, J. 2012. The Grenville Orogen–a post-Lithoprobe perspective. *In* Tectonic styles in Canada: the Lithoprobe perspective. *Edited by* J.A. Percival, F.A. Cook, and R.M. Clowes. Geological Association of Canada, Special Paper, 49: 97–236.
Rivers, T., Martignole, J., Gower, C.F., Davidson, A. 1989. New tectonic divisions of the Grenville Province, Southeast Canadian Shield. Tectonics, 8: 63–84. doi:10.1029/TC008i001p00063.
Sappin, A.-A., Constantin, M., Clark, T., van Breemen, O. 2009. Geochemistry, geochronology, and geodynamic setting of Ni–Cu ± PGE mineral prospects hosted by mafic and ultramafic intrusions in the Portneuf–Mauricie Domain, Grenville Province, Quebec. Canadian Journal of Earth Sciences, 46: 331–353. doi:10.1139/E09-022.
Scholl, D.W., von Huene, R. 2007. Crustal recycling at modern subduction zones applied to the past—Issues of growth and preservation of continental basement crust, mantle geochemistry, and supercontinent reconstruction. *In* 4-D framework of continental crust. *Edited by* Robert D. Hatcher, Jr., Marvin P. Carlson, John H. McBride, and José R. Martínez Catalán. Geological Society of America Memoir, 200: 9–32. doi:10.1130/2007.1200(02).
Slagstad, T., Culshaw, N.G., Daly, J.S., Jamieson, R. a. 2009. Western Grenville Province holds key to midcontinental Granite-Rhyolite Province enigma. Terra Nova, 21: 181–187. doi:10.1111/j.1365-3121.2009.00871.x.
Slagstad, T., Culshaw, N.G., Jamieson, R.A., Ketchum, J.W.F., Tollo, R.P., Corriveau, L., McLelland, J., Bartholomew, M.J. 2004. Early Mesoproterozoic tectonic history of the southwestern Grenville Province, Ontario: constraints from geochemistry and geochronology of high-grade gneisses. *In* Proterozoic tectonic evolution of the Grenville orogen in North America: Boulder, Colorado. Edited by R.P. Tollo, L. McLelland, and M.J. Bartholomew. Geological Society of America Memoir, 197: 209–241. doi:10.1130/0-8137-1197-5.209.
Sparkes, G.W., Dunning, G.R. 2014. Late Neoproterozoic epithermal alteration and mineralization in the western Avalon zone: a summary of mineralogical investigations and new U/Pb geochronological results. Current Research, Newfoundland and Labrador Department of Natural Resources, Geological Survey, Report 14-1: 99–128. Available

from:https://www.nr.gov.nl.ca/nr/mines/geoscience/publications/currentresearch/2014/Sparkes-2014.pdf.
Tucker, R.D., Gower, C.F. 1994. A U-Pb geochronological framework for the Pinware terrane, Grenville Province, southeast Labrador. The Journal of Geology, 102: 67–78. doi:10.1086/629648.
Turlin, F., André-Mayer, A.-S., Moukhsil, A., Vanderhaeghe, O., Gervais, F., Solgadi, F., Groulier, P.-A., and Poujol, M. 2017. Unusual LREE-rich, peraluminous, monazite- or allanite-bearing pegmatitic granite in the central Grenville Province, Québec. Ore Geology Reviews, 89: 627–667. doi:10.1016/j.oregeorev.2017.04.019.
Turlin, F., Vanderhaeghe, O., Gervais, F., André-Mayer, A.-S., Moukhsil, A., Zeh, A., Solgadi, F., I.P.T.N. 2019. Petrogenesis of LREE-rich pegmatitic granite dykes in the central Grenville Province by partial melting of Paleoproterozoic-Archean metasedimentary rocks: evidence from zircon U-Pb-Hf-O isotope and trace element analyses. Precambrian Research,. Elsevier. doi:10.1016/j.precamres.2019.02.009.
Valverde Cardenas, C. 2009. Geochemical constraints on the origin of mafic and ultrapotassic dykes from the southern Manicouagan area, Grenville Province. M.Sc. Thesis. Memorial University of Newfoundland, St. John's, Canada.
Valverde Cardenas, C., Indares, A., Jenner, G. 2012. Mafic and ultrapotassic rocks from the Canyon domain (central Grenville Province): geochemistry and tectonic implications. Canadian Journal of Earth Sciences, 49: 412–433. doi:10.1139/e11-065.
van Breemen, O., Corriveau, L. 2005. U-Pb age constraints on arenaceous and volcanic rocks of the Wakeham Group, eastern Grenville Province. Canadian Journal of Earth Sciences, 42: 1677–1697. doi:10.1139/e05-079.
van Breemen, O., Davidson, A. 1988. Northeast extension of Proterozoic terranes of mid-continental North America. Geological Society of America Bulletin, 100(5): 630–638. doi:10.1130/0016-7606(1988)100<0630:NEOPTO>2.3.CO;2.
van Gool, J.A.M., Rivers, T., Calon, T. 2008. Grenville Front zone, Gagnon terrane, southwestern Labrador: configuration of a midcrustal foreland fold-thrust belt. Tectonics, 27: 1–35. doi:10.1029/2006TC002095.
Whitmeyer, S., Karlstrom, K.E. 2007. Tectonic model for the Proterozoic growth of North America. Geosphere, 3: 220–259. doi:10.1130/GES00055.1.
Wodicka, N., David, J., Parent, M., Gobeil, A., Verpaelst, P. 2003. Géochronologie U–Pb et Pb–Pb de la région de Sept-Îles– Natashquan, Province de Grenville, Moyenne-Côte-Nord. In Synthèse géologique et métallogénique de la partie est de la Province de Grenville. Edited by D. Brisebois and T. Clark. Ministère des Ressources naturelles, de la Faune et des Parcs, Québec, DV 2002-03, pp. 59–118.
Yang, P., Indares, A.D. 2005. Mineral zoning, phase relations, and P-T evolution of high-pressure granulites from the Lelukuau terrane, northeastern Grenville Province, Quebec. The Canadian Mineralogist, 43: 443–462. doi:10.2113/gscanmin.43.1.443.

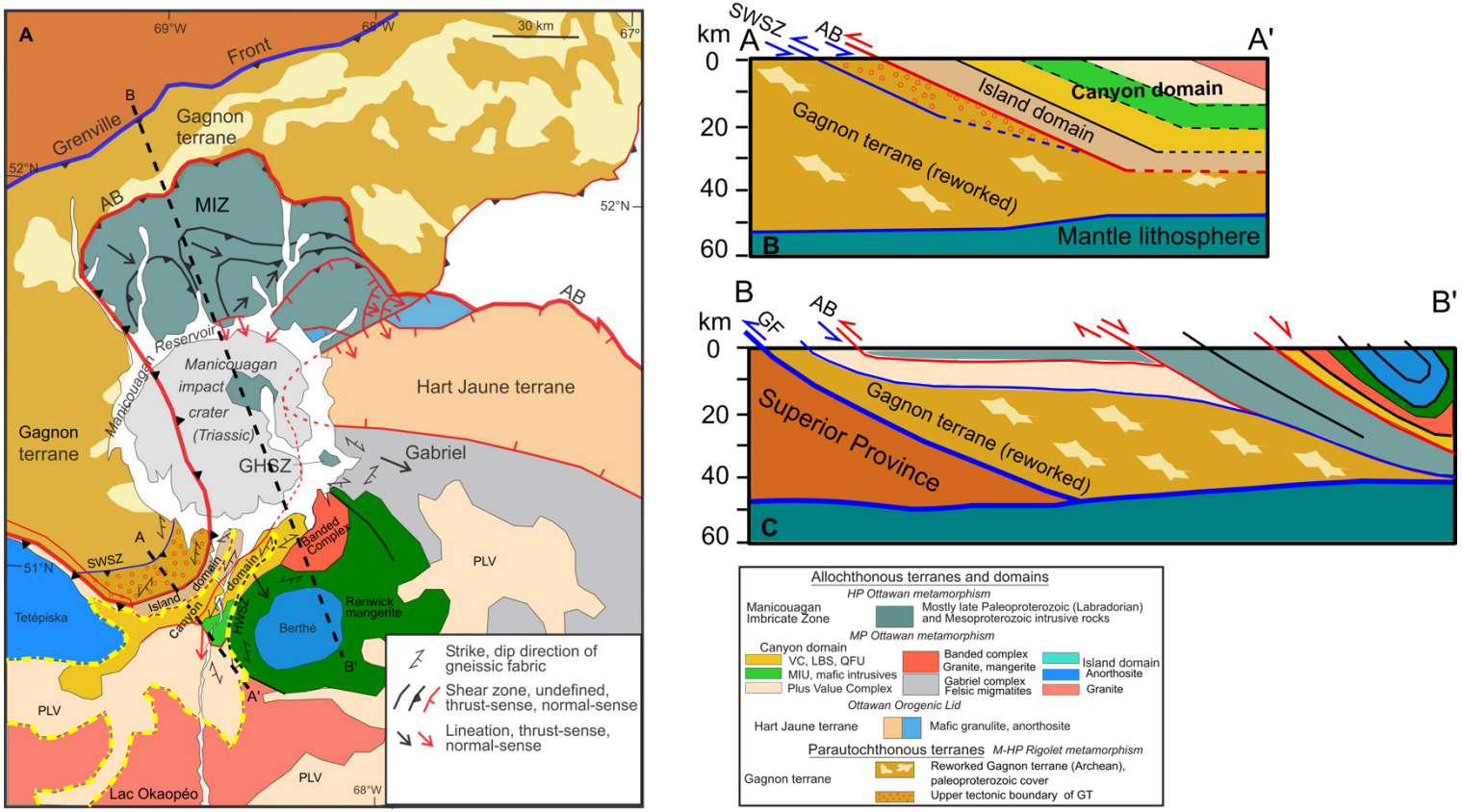

Figure 1.1. (A) Simplified geological map of the Manicouagan area showing the general tectonic boundaries (modified from Indares and Dunning, 2004; Rivers et al., 2012; Maity and Indares, 2018); (B-C) cross-sections along A-A' and B-B' (modified from Hynes et al., 2000). AB, Allochthon Boundary; MIZ, Manicouagan Imbricate Zone; MIU, Mafic to Intermediate Unit; QFU, quartzofeldspathic unit; LBS, layered bimodal suite; VC, Vein Complex; GT, Gagnon terrane; SWSZ, southwest shear zone; HWSZ, Highway Shear Zone; including zones of hydrothermal alteration; PLV, Complexe de la Plus Value; GHSZ, Gabriel high-strain shear zone.

2 The Geon 14 Arc-Related Mafic Rocks from the Central Grenville Province

2.1 Abstract

The late Paleoproterozoic to Mesoproterozoic (~1.7-1.2 Ga) evolution of the active southeastern margin of Laurentia terminated with the Grenvillian continental collision and the development of a large, hot, long-duration orogen at ~1.09-0.98 Ga. As a result, much of the hinterland of the Grenville Province consists of Paleo- and Mesoproterozoic rocks, mostly preserved as an imbricate stack of high-grade gneisses, that represent a potential repository of active-margin processes. This study presents geochronologic, geochemical, and isotopic analyses of two granulite-facies suites of ca. 1.45-1.40 Ga mafic tholeiites from the Canyon domain (Manicouagan area, central Grenville Province). One suite consists of 1439 $^{+76}_{-68}$ Ma high-Fe-Ti mafic sills with εNd values of -0.4 (T_{DM} 2.57-2.72 Ga), indicating derivation from variably depleted to enriched MORB-type mantle sources, probably in an extensional back-arc setting, before intrusion in a ca. 1.5 Ga supracrustal metasedimentary sequence. The other, previously dated, 1410 ± 16 Ma Mafic to Intermediate Unit exhibits εNd values of 0.0 to +0.9 (T_{DM} 2.02-2.25 Ga), and variably enriched MORB to arc geochemical signatures, for which formation in a transitional back-arc to arc setting is suggested.

Integrated with published information, the new data support a model of a long-lived continental-margin arc and intermittent back-arc development on southeast Laurentia during the mid-Mesoproterozoic (ca. 1.5-1.4 Ga), in which repeated short periods of extension and crustal thinning in the back-arc or intra-arc regions were followed by compression and crustal thickening.

2.2 Introduction

Convergent plate boundary zones are major sites of formation, consumption, and recycling of Earth's continental crust (Clift and Vannucchi, 2004; Cawood et al., 2009), so the study of magmatic processes in such zones can provide crucial understanding on the evolution of continental crust through time. This study is concerned with crust of Mesoproterozoic age preserved within the Grenville Province, part of the late Mesoproterozoic to early Neoproterozoic Grenville Orogen that is exposed on the southeast margin of the Canadian Shield and beyond. The Grenville Province (fig. *2.1a*) has been modelled as a part of a large hot long-duration orogen (LHO; Jamieson et al., 2002; Beaumont et al., 2006; Rivers, 2008; Rivers et al., 2012) that incorporated and reworked the long-lived Paleo- to Mesoproterozoic active margin of southeastern Laurentia (Rivers and Corrigan, 2000). Continental outgrowth along the active margin started during late Paleoproterozoic accretionary orogenesis (e.g., Penokean, Makkovikian, and Labradorian orogenies; ca. 1.90-1.62 Ga; Hoffman, 1988). In the eastern Grenville Province, it was followed by the development of early-Pinwarian (> 1.5 Ga) supracrustal sequences (e.g., Wakeham Group) deposited on the southeastern Laurentian margin in a setting variably interpreted as a passive margin (Gower, 1996; Gower and Krogh, 2002) or an active margin intra-arc or back-arc setting (Rivers and Corrigan, 2000; Wodicka et al., 2003; Corriveau et al., 2007; Rivers et al., 2012). Prolonged, extensive and widespread Mesoproterozoic (1.5-1.23 Ga) juvenile crust formation (and reworking), is inferred to have involved distinct phases of arc and back-arc activity along the entire stretch of the Laurentian continental margin, with 1.28-1.23 Ga accretionary activity limited to the southwestern Grenville Province. This was followed by the final continental collision during the Grenvillian

Orogeny (1.09-0.98 Ga; *sensu stricto* of Rivers, 2008) (van Breemen and Davidson, 1988; Gower et al., 1990; Gower and Tucker, 1994; Tucker and Gower, 1994; Nadeau and van Breemen, 1994; Gower, 1996; Rivers, 1997; Rivers and Corrigan, 2000; Gower and Krogh, 2002; Slagstad et al., 2004, 2009; Bonnet et al., 2005; van Breemen and Corriveau, 2005; Whitmeyer and Karlstrom, 2007; Hynes and Rivers, 2010; Rivers et al., 2012; and references therein). As a result, it is reasonable to assume that the Grenville Province contains a record of crustal addition, loss, and recycling in rocks that were formed and accreted to the south-eastern margin of Laurentia from 1.9-1.1 Ga. An outline of the orogen-wide development of active-margin arcs and back-arcs, outboard island arcs, oceanic back-arc basins, and accretion of arc terranes was reported previously (Rivers and Corrigan, 2000), but at the time details were sparse, especially from the central Grenville Province.

A major issue confronting any study of the high-grade gneissic rocks in the hinterland of the Grenville Province is that many primary characteristics of the protoliths may be obscured by high-grade metamorphism and deformation related to subsequent arc formation, accretionary orogenesis, and finally by the Grenvillian continental collision. High-grade metamorphism also has the potential to modify the isotopic and geochemical compositions of these rocks, which are presently mostly preserved in upper amphibolite to granulite-facies gneiss complexes. Given the low strain and good preservation of primary features in the study area, described in more detail below, we assume that their geochemical and isotopic signatures are preserved, and hence their study has the potential to provide insights on the processes operating on the ancient active continental margin of southeastern Laurentia. This assumption is evaluated in the course of the analysis.

Geon 14 mafic magmatism in the central Grenville Province constitutes an important part of the pre-Grenvillian evolution of the southeastern Laurentian margin, as revealed by recent studies by several workers. In particular, there is now good evidence for the deposition of a large widespread Mesoproterozoic supracrustal sequence (the Complexe de la Plus Value or PLV; Moukhsil et al., 2012, 2013a) before ca. 1.5 Ga (Lasalle et al., 2013), and the development of a continental margin volcanic arc on the southeastern Laurentian margin during Geon 14 (Dunning and Indares, 2010; Valverde Cardenas et al., 2012; Augland et al., 2015), all of which are of special interest in this study. In this paper, we have examined two contrasting suites of ca. 1.4 Ga mafic rocks, one occurring as sills in the recently recognized ca. 1.5 Ga supracrustal sequence of the PLV, and the other from the ca. 1.4 Ga Mafic to Intermediate Unit, both occurring in the Canyon domain of the central Grenville Province. Here we report the field and petrographic observations, major and trace element chemistry, Sm-Nd isotopes, and CA-TIMS U-Pb geochronology for these mafic rocks in order to characterize their age and tectonic setting.

2.3 Geological Context

2.3.1 The central Grenville Province: Manicouagan area

The first-order orogenic architecture of the Grenville Province is divided into the Parautochthonous Belt in the north and the structurally overlying Allochthonous Belt in the south (fig. 2.1a; Rivers et al., 1989), and the Manicouagan area exposes high-grade gneiss complexes in which these first-order divisions can be observed. The Parautochthonous Belt is represented by the Gagnon terrane, a Paleoproterozoic continental margin sequence that overlies an Archean basement, and both were

metamorphosed and deformed during the Rigolet phase (~1005- 980 Ma) of the Grenvillian Orogeny, with the grade of metamorphism ranging from greenschist-facies (near the Grenville Front) to high-pressure granulite- and eclogite-facies conditions to the south (Rivers, 2008, and references therein).

The Gagnon terrane is tectonically overlain by the allochthonous terranes of the Manicouagan Imbricate Zone (MIZ; Indares et al., 1998), which mainly consists of Labradorian (~1.65 Ga) anorthosite-mangerite-charnockite-granite (AMCG) rocks and Pinwarian (~1.45 Ga) granitoids. The MIZ, part of the Allochthonous high-pressure belt, was metamorphosed at 750- 920 °C and 1700-1900 MPa conditions from ca. 1060-1040 Ma (Indares, 1997, 2003; Indares et al., 1998; Cox and Indares, 1999a, b; Cox et al., 1998; Yang and Indares, 2005) during the Ottawan phase of the Grenvillian Orogeny (Rivers, 2008; Rivers et al., 2012). To the southeast of the MIZ, the late Paleoproterozoic to mid-Mesoproterozoic supracrustal and plutonic rocks comprising the Island domain, Canyon domain, Gabriel Complex, and Banded Complex (Hynes et al., 2000; Indares and Dunning, 2004; Dunning and Indares, 2010) were subjected to Ottawan mid-pressure granulite-facies metamorphism at 800-900 °C and 600-1100 MPa conditions from ca. 1080-1040 Ma (Dunning and Indares, 2010; Lasalle et al., 2013; Lasalle et al., 2014; Lasalle and Indares, 2014; Patrick and Indares, 2017), and belong to the mid-pressure belt of Rivers (2008). In addition, the Hart Jaune terrane to the southeast of MIZ consists of 1.47 Ga mafic granulites (Hynes et al., 2000) that lack evidence for high-grade Ottawan metamorphism (Indares and Dunning, 2004) and therefore, the terrane represents part of the Ottawan Orogenic Lid (OOL) of Rivers (2008).

On the basis of numerous Nd model ages, the Manicouagan area in the central Grenville Province has also been identified by Dickin and co-workers to be a junction of several crustal domains or terranes (fig. 2.1b; Dickin and Higgins, 1992; Dickin, 2000; Martin and Dickin, 2005; Thomson et al., 2011). The most recent work by these authors shows four crustal terranes with distinct ages of formation: Archean (~2.7 Ga, restricted to the Parautochthonous Belt), Makkovikia (2.0-1.7 Ga), Labradoria (1.75 Ga), and Quebecia (1.55 Ga). Labradoria and Quebecia were interpreted as juvenile arc terranes accreted to the Laurentian margin at around 1.65 and 1.45 Ga, respectively. In this study, we re-examine this interpretation in the light of the currently available detrital zircon data from the central and eastern Grenville Province.

The rocks for this study come from the mid-pressure Canyon domain (Hynes et al., 2000; Dunning and Indares, 2010), which is described in more detail below.

2.3.2 Geology of the study area: Canyon domain

The Canyon domain, first defined by Hynes et al. (2000), is situated in the southern Manicouagan Reservoir area (fig. 2.2) and structurally overlies mid-pressure and high- pressure Labradorian units to the north (Indares et al., 2000; Dunning and Indares, 2010). 'Canyon domain' is a working term, used here to characterize a thrust package of supracrustal units and associated plutonic rocks (Dunning and Indares, 2010; Indares and Moukhsil, 2013) with distinct boundaries in the east (Berthé anorthosite) and in the west (Tétépiska anorthosite), but a poorly defined boundary in the south with the intrusive Bardoux and Castoréum Plutonic Suites. Following a regional mapping campaign led by the Ministère de l'Énergie et des Ressources naturelles du Québec (MERNQ; see Moukhsil et al., 2012), detailed field investigations

have led to characterization of the domain into distinct lithologic units (see Indares and Moukhsil, 2013), which are described briefly below in their geochronological order.

2.3.2.1 The Complexe de la Plus Value (PLV)

The oldest unit is a supracrustal sequence formally named the Complexe de la Plus Value (PLV) by Moukhsil et al. (2012) in the Lac du Milieu area located east of fig. 2.2. In the study area the PLV occurs in the southern part of the Canyon domain near the Manic 5 reservoir, and consists of a layered sequence of granulite-facies gneissic rocks with inferred protoliths of greywacke, pelite, quartzite, calc-silicate, and mafic compositions. The upper age limit for the deposition of the PLV was initially determined to be 1482 ± 21 Ma (U-Pb igneous zircon crystallization age of granite from the Bardoux Plutonic Suite intruding the PLV in the Lac du Milieu area, Moukhsil et al., 2012), but has recently been more precisely constrained by Augland et al. (2015) to be 1497 ± 5 Ma based on TIMS U-Pb zircon dating of an augen granite with arc signature from the Bardoux Plutonic Suite in the Lac Okaopéo area south of our study area. The upper limit of deposition of the PLV has been constrained by detrital zircons studies (Lasalle et al., 2013) of two aluminous paragneisses from the Canyon domain, in which igneous cores of the youngest detrital zircon are ~1500 Ma, and the metamorphic grains and rims yield ages ranging between ~1450 and 1000 Ma, suggesting that the PLV was deposited at ~1.5 Ga, and underwent Pinwarian and Grenvillian metamorphisms. In addition, the core of a metamorphic monazite from an aluminous paragneiss in the PLV has yielded an age of 1445 ± 27 Ma (Lasalle et al., 2014).

The PLV is intruded by several plutonic suites in which it occurs as enclaves, e.g., granite and charnockite of the Bardoux Plutonic Suite (1497 Ma; Augland et al., 2015), felsic orthogneisses (including both older and younger tonalites of the Hulot Complex; ~1370-1440 Ma; Gobeil et al., 2002, 2005; Augland et al., 2015), granite, monzonite, and tonalite of the Castoréum Plutonic Suite (1393 ± 8 Ma, Moukhsil et al., 2013b; Augland et al., 2015), and undeformed mangerite of the Okaopéo Plutonic Suite (1014.6 ± 2.1 Ma; Augland et al., 2015). Furthermore, the PLV has been intruded by numerous younger dykes including those of gabbronorite composition (1383.4 ± 1.1 Ma; Augland et al., 2015) in the Hulot Complex and many discordant felsic pegmatites and ultrapotassic dykes of late Grenvillian age (~980-990 Ma; Dunning and Indares, 2010) in the Canyon domain.

The PLV in the Canyon domain has a high-grade metamorphic signature as revealed by the dominant metamorphic assemblage of Grt+Sill+Kfs±Bt+Liq (abbreviations after Whitney and Evans, 2010) in aluminous rocks that were metamorphosed under the peak metamorphic conditions of 600-1100 MPa and 800-900 °C (Lasalle and Indares, 2014; Patrick and Indares, 2017) during the Ottawan phase of the Grenvillian Orogeny as indicated by monazite ages of ~1081-1038 Ma and metamorphic zircon ages of ~1076-1044 Ma (Dunning and Indares, 2010; Lasalle et al., 2013, 2014).

2.3.2.2 The Mafic to Intermediate Unit (MIU)

The Mafic to Intermediate Unit (MIU) was first described from the type location (#395), near its boundary with the PLV, as an exposure of dark and light grey layers with the latter dated at 1410 ± 16 Ma (fig. 4a in Dunning and Indares, 2010). At that

location, the layers are massive, medium-grained, and lack coarse plutonic texture, and the layering was interpreted as an original feature indicative of a supracrustal volcaniclastic origin, with the rocks being meta-tuffs. The dark grey layers were also observed to contain leucocratic melts with Grt ± Opx, and to occur as lenses or rafts within the light grey components. On the basis of lithology and age, Dunning and Indares (2010) tentatively correlated this unit with the Montauban Group to the southwest, which consists of remnants of an island arc accreted to the Laurentian margin (Nadeau and van Breemen, 1994; Sappin et al., 2009). Later geochemical and isotopic data from a sample collected from the light grey layer of the unit was interpreted to indicate an origin in a mature continental arc setting (Valverde Cardenas et al., 2012). Subsequently, another exposure of the same belt to the north was discovered to consist of relict plutonic textures and original compositional layering (fig. 2a in Indares and Moukhsil, 2013), which were interpreted as part of the MIU formed as a shallow-depth layered intrusion. Based on pronounced compositional layering between different mafic parts and from the overall association of the unit, Indares and Moukhsil (2013) named it as the Layered Mafic Suite (LMS). This name was not intended to imply that the whole unit consisted of layered intrusions in the classical sense, and both the names have been alternatively used in recent literatures (e.g., Lasalle et al., 2013, 2014; Patrick and Indares, 2017). This unit at the type location has been pervasively cross-cut by late Grenvillian granite pegmatities dated at 995 ± 3.5 Ma (Dunning and Indares, 2010).

2.3.2.3 The Quartzofeldspathic unit

The MIU is in local contact with a supracrustal sequence named the Quartzofeldspathic unit (QFU; Indares and Moukhsil, 2013). Although of uncertain

origin, the QFU contains (i) mafic rafts that exhibit a geochemical signature similar to modern mature continental arcs (Valverde Cardenas et al., 2012), (ii) patches of a bimodal hydrothermally altered volcanic sequence (Hindemith and Indares, 2017; Patrick and Indares, 2017) named the Layered Bimodal Suite (LBS) that formed at 1238 ± 13 Ma (Indares and Moukhsil, 2013; Lasalle et al., 2013), and (iii) an apparently younger magmatic complex named the Vein Complex (VC), which was thought to have formed due to felsic intrusion within the MIU (Indares and Moukhsil, 2013). The age of the QFU and the mafic rafts within it were inferred by these authors to be ~1.4 Ga based on the presence of transposed felsic pegmatites in the unit that also occur in the PLV and MIU, but are absent from the LBS. Together these five units, the PLV, MIU, QFU, LBS, and VC constitute the major units exposed in the central and northern part of the Canyon domain (fig. 2.2).

2.3.2.4 Previous interpretations on tectonic evolution

Based on the inferred depositional age of the PLV at > 1500 Ma, and the intrusion of Bardoux suite at ca. 1497 Ma in an arc setting, the PLV was compared with the Wakeham Group farther east by Augland et al. (2015), who proposed that the former was deposited in a back-arc or intra-arc setting, consistent with previous interpretations (Larbi et al., 2003; Corriveau and Bonnet, 2005; Bonnet et al., 2005; Corriveau et al., 2007). A recent seismic study has revealed that the Wakeham Group continues to the southeast under Paleozoic cover on Anticosti Island (fig. 2.1; Pinet, 2016), considerably enlarging the known extent of this unit.

On the basis of geochemical and Hf isotope data, the tectonic settings of the central Grenville Province have been inferred to have evolved from a ca. 1500 Ma continental margin arc to a ca. $1434\ ^{+7}_{-11}$ Ma distal-arc or microcontinent-arc setting,

followed by crustal shortening due to terrane accretion and subsequent arc formation at ca. 1413 Ma (Augland et al., 2015). Additionally, the voluminous metaluminous Renwick mangerite with a within-plate signature was emplaced at 1402 ± 72 Ma and is in thrust contact with the PLV (Moukhsil et al., 2012, 2013a). An age of 1403 $^{+32}_{-25}$ Ma, was obtained by Indares and Dunning (2004) from a granodiorite body in the northeastern part of the Canyon domain near the Banded Complex, and is apparently also part of the Renwick mangerite.

2.3.3 Field Relations of the mafic rocks

The mafic samples in the PLV come from concordant layers up to a few tens of centimeters thick that show sharp contacts with the layering in the paragneiss (fig. 2.3a). There is no evidence of intrusive or tectonic contact between the mafic layers and the PLV paragneiss, and therefore, the layers could be interpreted to be *in situ*. Alternatively, they could have intruded the paragneiss sequence as concordant sills. The mafic gneisses commonly contain thin leucocratic films or veins parallel to or crosscutting the layering (fig. 2.3b), and in places leucocratic pods enclose clusters of coarse-grained ferromagnesian minerals. These features are consistent with derivation by partial melting, either of the mafic layers, or of the host paragneiss, or both, and in the latter case raising the possibility of felsic melt injection within the mafic sills. Our samples for this study were collected from well preserved homogeneous regions within the mafic layers that lacked leucocratic veins (fig. 2.3c), and hence are most likely to represent the original compositions.

As described above, the MIU at the type outcrop #395 was initially interpreted to be supracrustal in origin (Dunning and Indares, 2010), but following recognition at

a different location (#210) farther north that the unit also included components of shallow mafic intrusions that gave it a 'layered' appearance, it was renamed the Layered Mafic Suite (LMS; Indares and Moukhsil, 2013). Follow-up fieldwork in 2011 at the extension of the type outcrop for the unit (#395) led to the identification of a wider range of lithologic types, varying from dark through intermediate to light grey in colour (D, I, and L, respectively; fig. 2.3d), which are documented in more detail in this study. The dark grey components are locally observed to be intruded by the light grey components, and feature sharp to diffuse, cuspate and lobate contacts (fig. 2.3e). Elsewhere the dark and intermediate grey components are enclosed within the light grey components and exhibit evidence for partial disintegration, brecciation, and rounded to sub-rounded margins (fig. 2.3d, f). Moreover, the dark and intermediate grey components are commonly associated with thin leucocratic films or pods, in the absence of which the contacts range from sharp to diffuse. These contact relationships, together with the variable colour (and hence composition) of the mafic components ranging from dark grey through intermediate to light grey (fig. 2.3d), along with the contained leucocratic films and pods, are indicative of multiple injections of different magma batches, magma mingling, and possible mixing in a sub-volcanic or shallow plutonic settings, such as has been documented in many intrusive complexes elsewhere (e.g., Vernon et al., 1988; Sutcliffe, 1989; Sutcliffe et al., 1989; Castro et al., 1990; Lindline et al., 2004; Barbarin, 2005). However, in addition to the original igneous complexity, dark grey components contain occasional garnet- and pyroxene-bearing leucocratic veins (Dunning and Indares, 2010) that are inferred to be the result of localized dehydration melting along the margins of dark and light grey (hornblende-rich) rocks (fig. 2.3d and e). Such melts are mostly small-volume and in-situ. As such, these mafic

rocks are not similar to the migmatites reported from the amphibolitized margins of Fe-Ti gabbros from the Baie du Nord segment of the MIZ (fig. 3c in Cox et al., 1998), and from the mafic migmatites in the Kapuskasing Structural Zone (fig. 2 in Hartel and Pattison, 1996). The samples collected for this study are massive and come from parts of the exposures free from leucocratic veins and visible hydrothermal alteration (fig. 2.3e).

Ideally, an appropriate informal name for this ca. 1.41 Ga unit should take into consideration its compositional range, intrusive mode of occurrence, and shallow plutonic origin. The name Layered Mafic Suite is no longer appropriate due to the lack of layering in the type outcrop and its unintended link with classical layered mafic intrusions. The original name, Mafic to Intermediate Unit, although coined to describe rocks that were inferred to be of volcaniclastic origin, is permissive of either a volcaniclastic or plutonic origin and sufficiently general to accommodate the observed major features of the unit described herein, and so is retained in this study pending more detailed evaluation of the unit as a whole. Thus henceforth in this paper we extend the original meaning of the term 'Mafic to Intermediate Unit' (MIU), for which an age of ca. 1.41 Ga has been determined for a mafic light grey component (Dunning and Indares, 2010), to include rocks of a somewhat wider range of compositions that are deduced to be part of a shallow plutonic, mixed intrusive unit. At the extension of outcrop #395 from which the samples in this study come, there are no known rocks of supracrustal origin.

2.4 Sampling and Analytical techniques

The rocks in our study area in the central Grenville Province have undergone relatively low-strain mid-pressure granulite-facies metamorphism. In order to minimize the effects of metamorphism, we have taken special care to collect samples from the most lithologically coherent and unmelted parts of representative units in large exposures. For analytical purposes, we have only sampled rocks that were free of leucosomes and cross-cutting veins, and all samples were cut to remove weathered portions before proceeding to standard thin section preparation and crushing to produce powders for analysis.

Detailed petrographic study was carried out on 7 selected polished thin sections using an optical microscope and 5 samples were chosen for SEM mineralogical mapping using a Quanta 650 FEG-SEM. The Energy Dispersive Scanning (EDS) system in the SEM was used to semi-quantitatively identify and calculate modal abundances of mineral phases. Analyses were carried out under 25 keV acceleration potential and 10 nA beam current condition to obtain BSE images and EDS analyses. False colour mineralogical maps (fig. 2.4) showing the relationships and the distribution of the phases were produced by post-processing the BSE and EDS data using Mineral Liberation Analysis software on the SEM.

Fresh interiors of selected samples were used for standard crushing in a steel-plated jaw crusher and powdering in an agate ball mill. A portion of the powdered samples was selected for separation of zircon and CL imaging and U-Pb geochronology. CL imaging (fig. 2.5) of selected zircon grains was carried out using a CL detector attached to the FEI Quanta 400 SEM using a 15 keV acceleration potential

and a 10 nA beam current. The procedure followed for U-Pb chemical abrasion thermal ionization mass spectrometry (CA-TIMS) analyses is given in appendix A.

Selected whole rock samples were crushed using standard jaw crusher and disk mill techniques, followed by further pulverization for analysis of major and trace element geochemistry and radiogenic tracer isotopes. Sm and Nd were separated from pulverized whole-rock powders of four samples following an in-house protocol at MUN, and Sm-Nd isotope ratio analyses were determined using a multi-collector Finnigan Mat 262 TIMS mass spectrometer at MUN. Details of trace isotope analytical methods are described in appendix A. For major and trace elements, pulverized whole-rock powders of six samples were analyzed at the Actlabs, Ancaster, Ontario (www.actlabs.com). The detection limits for the analyses are typically in the range of 0.01-0.001 % for major elements and 1-30 ppm for trace elements.

2.5 Results

2.5.1 Petrography

The mafic gneissic layers in the PLV are coarse-grained, heterogeneous, and display two different textural types. Type-I (#11-383c and M5-383E1; fig. 2.4a) is composed of Grt + Pl + Cpx + Opx + Qtz + Bt + Ilm ± Hbl. Garnet porphyroblasts are extensively corroded and partially replaced by Pl + Cpx + Bt ± Hbl ± Opx. The matrix is composed of subgranoblastic Pl + Cpx + Opx + Qtz + Bt + Ilm ± Hbl, with trace amounts of rutile, apatite, titanite, magnetite, sulphides, zircon, K-feldspar, allanite, monazite, and barite. K-feldspar is commonly associated with plagioclase, hornblende, and biotite. The samples with this textural type contain large, partly resorbed quartz grains (fig. 2.4b) of various shapes (sub-rounded to stretched ribbons) and sizes (up to

3.6 mm long ribbons) mantled by plagioclase, clino-, and orthopyroxene. Quartz grains in some of the PLV samples with Type-I texture are large and highly corroded indicating chemical disequilibrium with the matrix composition. Such large partially resorbed quartz grains in mafic rocks are generally interpreted to be xenocrystic (e.g., Kuno, 1950; Sato, 1975; Koyaguchi, 1986), and may provide a substrate in a hybrid melt to nucleate pyroxenes (e.g., Hibbard, 1981; Vernon, 1990; Lindline et al., 2004). Their occurrences in mafic magmas may be indicative of mingling with felsic melts that were either produced during emplacement and stagnation of mafic magma in a crustal magma chamber, or they may have been derived by wall-rock assimilation during the ascent of mafic magma through continental crust. The preservation of quartz xenocrysts in the mafic sills indicates that homogenization of the contaminant with the mafic melt was incomplete (Hibbard, 1981; Vernon, 1990; Lindline et al., 2004). Type-II (#11-383e1; fig. 2.4c) is composed of large garnet porphyroblasts embedded in a matrix of Pl + Cpx + Opx + Hbl + Bt + Ilm. Garnet is variably corroded and replaced by Hbl + Cpx + Pl + Opx with the relict shape still preserved in some cases. This type does not have large quartz grains as observed in type-I, and contains allanite as an accessory phase. The mineral assemblage for the peak metamorphic stage in both the textural types in the PLV comprises Grt + Pl + Cpx + Opx, which was retrogressed under hydrous conditions forming hornblende and biotite replacing garnet.

The main lithological components of the MIU analyzed in this study come from the dark, intermediate, and light grey components, which are Grt-Cpx-rich (fig. 2.4d), Hbl-Grt-Cpx-rich (fig. 2.4e), and Pl-Hbl-rich (fig. 2.4f), respectively. The dark grey component is characterized by granoblastic idiomorphic garnet (1–5.5 mm) and clinopyroxene, along with orthopyroxene, ilmenite, hornblende, and minor plagioclase.

Large apatite crystals, present both as inclusions (in garnet and clinopyroxene) as well as in the matrix, form a characteristic accessory phase in these samples. The intermediate grey component is composed of porphyroblastic garnet (0.8–3.7 mm) and clinopyroxene embedded in a matrix of Hbl + Pl + Opx + Ilm. Biotite constitutes an important minor phase. The light grey component contains large sub-idiomorphic garnet porphyroblasts embedded in an overall coarse, crudely foliated matrix composed of subgranoblastic Hbl + Pl + Bt + Ap + Ilm + Ttn. The large garnet poikiloblasts in a pyroxene-bearing matrix indicate their formation was favoured by vapour-absent dehydration reactions under upper amphibolite to granulite-facies conditions (e.g., Hartel and Pattison, 1996; Pattison, 2003; Pattison et al., 2003). Clinopyroxene is extremely rare in the matrix in the investigated sample and occurs as very small grains at two locations. Thin rims of Pl ± Hbl ± Bt wrap around large (6-15 mm) corroded poikiloblastic garnet, which contains inclusions of Plg + Cpx + Ilm + Ttn + Ap. Titanites in the matrix are less abundant and smaller in size than those within garnet. All the samples in the MIU contain accessory allanite, magnetite, and zircon. The petrographic evidence in the mafic rocks from the MIU is suggestive of different basaltic bulk compositions, and supports the field interpretation of mingling between heterogeneously sourced magmatic components.

All the mafic rocks in our study have the mineral assemblage Grt + Pl + Hbl ± Cpx ± Opx that is indicative of mid-pressure granulite-facies metamorphism (e.g., Pattison, 2003), which is consistent with the estimated *P-T* range for the peak metamorphism determined from the host paragneiss samples in the PLV mentioned earlier. The peak AFM mineral assemblage for dark grey samples comprises Grt + Cpx + Opx, whereas textures and abundance of hornblende in intermediate and light grey

samples indicate hornblende could have been part of peak assemblage in these samples. Both the PLV and the MIU were retrogressed under variably hydrous conditions leading to the development of rims of hornblende and biotite around garnet porphyroblasts and pyroxenes, and in the matrix. Moreover, modal estimation of minerals in SEM-MLA provides evidence for variable amounts of chlorite-sericite-magnetite-carbonate-sulphides that are suggestive of hydrothermal alteration. The abundances of carbonates, magnetite, and sulphides (total ~1.5 %) is highest in the dark grey rocks in the MIU, whereas sericite and chlorite (total ~5%) are most commonly developed after plagioclase and garnet in the light grey rocks.

2.5.2 U-Pb isotope analyses

One sample (#11-383C) from the mafic layers in the PLV was chosen for zircon U-Pb analysis. Zircons in this sample display three different morphologies– prisms, round to sub-round grains, and flat grains. The prisms show complex internal CL structures (fig. 2.5) e.g., relict prisms, xenocrystic and composite cores, sector zoning, local internal dissolution indicated by dark convolute structures, bright areas of recrystallization, and thin but well developed metamorphic rims. A few prisms are much larger than average (not shown in the figure) and are thought to be xenocrystic. The round to sub-round zircon have internal convolute structures in dark zones with low CL response that indicate dissolution, and bright areas with high CL response indicating local recrystallization, relict prisms, radial fractures, and sector zoning. These round to sub-round zircon grains are interpreted to be corroded and recrystallized prisms. The flat grains also show complex internal structures with well-developed metamorphic rims. We carried out five analyses of the euhedral clear prisms, comprising three single-grain analyses and two multigrain analyses composed of 3-4

grains each. The data are presented in table 2.1 and plotted on a Concordia diagram (fig. 2.5). The data points defined a discordia line that intersects the Concordia at an upper intercept of $1439\ ^{+76}_{-68}$ Ma, interpreted as the crystallization age, and a lower intercept of $1029\ ^{+33}_{-47}$ Ma, interpreted as the age of growth of metamorphic rims.

2.5.3 Sm-Nd isotopes

Four samples were selected for Nd isotope analyses (table 2.2; fig. 2.6), two from the mafic layers in the PLV (#RS383E, 11-383c) and two from the representative dark grey rocks in the MIU (#11-395dx, 11-395d1). The samples from the PLV possess initial Nd isotopic ratios ($^{143}Nd/^{144}Nd)_{ini}$ of 0.510807 and 0.510805, yield $\varepsilon Nd_{1.4\ Ga}$ values of -0.4, and T_{DM} model ages of 2.57 and 2.72 Ga, respectively. The samples from the dark grey rocks possess initial Nd isotope ratios of 0.510637 and 0.510595, and yield $\varepsilon Nd_{1.4\ Ga}$ values of -3.7 and -4.6, respectively. These two samples have yielded anomalously old model ages, which are not considered to be meaningful.

The high Sm/Nd ratios (> 30), shallow slopes, and anomalously old Archean model ages (> 3.7 Ga) in the dark grey rocks suggest that their Sm-Nd isotope systematics have been modified, possibly by hydrothermal processes unrelated to regional high-grade orogenic metamorphism. For instance, Rosing (1990) showed that even a small change in the Sm/Nd ratio due to fluid-rock interaction may result in significant deviation of the calculated initial $^{143}Nd/^{144}Nd$ ratio and model age, and that such deviation may be modified exponentially by the time interval between crystallization and secondary disturbance leading to anomalously old model ages. The effect of secondary alteration on Sm-Nd isotopes similar to the dark grey rocks has also been demonstrated on Na- and K-metasomatized igneous clasts from the

Paleoproterozoic Bonnetia volcanic arc terrane in Yukon (Nielsen et al., 2013; their figs. 11 and 12).

2.5.4 Geochemistry

Both the PLV and the MIU have been subjected to Grenvillian mid-pressure granulite-facies metamorphism, and both the suites record evidence for partial melting and low-grade hydrothermal alteration. Therefore, it is necessary to assess the effects of partial melting and hydrothermal alteration on the major and trace element composition of the mafic rocks.

2.5.4.1 Effects of metamorphism and hydrothermal alteration

Effects on major elements

The mafic rocks in our study exhibit alteration indices [A.I = 100 X (MgO + K_2O)/ (MgO + K_2O + Na_2O + CaO)] (Ishikawa et al., 1976) between 33-48 (median value 37) and peraluminous indices (P.I = Al_2O_3/ (CaO + Na_2O + $K_2O)_{mol.}$) between 0.56-0.89 (median value 0.62) (table 2.3), which are similar to fresh MORB and arc-related mafic volcanic rocks (A.I = 36 ± 8 and 34 ± 10, respectively, and P.I = 0.8 ± 0.2; Laflèche et al., 1992). However, the mafic rocks from the PLV and the dark and intermediate grey rocks from the MIU exhibit Al_2O_3/Na_2O > 10 suggesting Na-loss (Spitz and Darling, 1978), and high chlorite-carbonate-pyrite index or CCPI > 90 suggesting carbonate-sericite-chlorite-sulphide alteration [CCPI = 100 × (MgO + FeO_t)/ (MgO + FeO_t + K_2O + Na_2O)] (Large et al., 2001). However, caution should be taken with the CCPI index as it is strongly correlated with magmatic fractionation and primary compositional variations in mafic rocks (Large et al., 2001). The alteration index K/Na in the mafic rocks varies between 0.2-0.9, suggesting they are mostly unaltered (K/Na = 2.0-0.5) with four samples being moderately Na-altered (K/Na = 0.5-

0.1) (Nielsen et al., 2013). Overall, the major element data suggest that the mafic rocks in our study are mostly unaltered except for mobility in alkalis.

Effects on trace elements

One mafic sample from the PLV (RS383E1) exhibits depletions in LREE relative to MREE [$(La/Sm)_{CN} \leq 1$; subscript 'CN' stands for chondrite-normalized], strong negative Eu anomalies (Eu/Eu* = 0.38; Eu* refers to the value obtained by linear interpolation between adjacent elements), high Ti/Eu (~11000), strong depletions in Zr and Hf, enrichments in Nb and Ta compared to La, and strong fractionation in Zr/Hf ratio (26). Two dark grey samples from the MIU also exhibit evidence for LREE depletions, strong negative Eu anomalies (Eu/Eu* = 0.30-0.32), high Ti/Eu (> 11,000), and disturbance in Nd isotopic systematics due to fluid-rock interaction. These three samples are moderately altered with low K/Na and high CCPI values, as is the sample RS209-1 from QFU. The potential mobility in HFSE, REE, and Eu^{2+} in these samples depends on the pH, chemistry, pressure-temperature, and redox condition of hydrothermal fluids (Jiang et al., 2005). Recently, argillic and carbonate alteration of various degrees by high-temperature CO_2-rich fluids have been shown to have affected the ca. 1.24 Ga andesitic volcanic rocks from the LBS in the study area (Hindemith et al., 2017). Despite the widely accepted notion that the REE and HFSE are 'conservative' elements (Pearce, 1983; Tatsumi et al., 1986; Pearce and Peat, 1995), several recent studies have shown that these elements can be mobile in magmatic, metamorphic, and submarine-hydrothermal environments (e.g., Ludden et al., 1982; Sorensen and Grossman, 1989; Rubin et al., 1993; Jenner, 1996; Woodhead et al., 2001; Kamber et al., 2002).

The presence of negative Eu anomalies (Eu/Eu* < 1) in the remaining samples indicates that they have not been subjected to partial melting and melt loss, as mafic restitic compositions would show positive Eu anomalies, or decrease in original negative anomalies inherited from their protoliths (Rudnick, 1992). The K/Rb ratios (150-775) in the mafic rocks mostly fall within the range of the igneous fractionation trend (fig. 2.7a; Shaw, 1968; Rudnick et al., 1985), which along with their Eu/Eu* < 1 (fig. 2.7b) suggest that most of these samples have not been modified by partial melting or alteration. The increasing K/Rb ratios at K_2O < 1 wt% in the altered mafic samples from the PLV and the dark grey rocks from the MIU indicate Rb loss (Rudnick, 1992). However, LILE and LFSE are well known to be fluid-mobile under low-grade conditions, and hence will not be used in our study.

Thorium, although stable below amphibolite-facies conditions, can be mobile during high-grade metamorphism in a water-dominated system (Jenner, 1996). In Th/U vs. La/Th diagram, the moderately altered samples plot within the field of igneous rocks because of loss in La, as suggested by their low LREE contents. Some of the least altered mafic samples exhibit La/Th ratios (25-52; fig. 2.7c) higher than common igneous rocks (La/Th ≤ 21; Rudnick et al., 1985; Sun and McDonough, 1989) suggesting Th mobility relative to La. However, their La/Th ratios do not correlate with any of the alteration indices; and moreover, the mafic samples in our study plot well within the permissible range of other least altered mafic granulites (e.g., Blein et al., 2003; Bonnet et al., 2005; Montreuil and Constantin, 2010), for which Th has been successfully used as a tool in petrotectonic discrimination (e.g., Montreuil and Constantin, 2010). High La/Th (> 20) is common in many modern back-arc basin basalts e.g., the East Scotia and the Lau Basin Spreading Centres (Taylor and Martinez,

2003; and references therein). Therefore, variability in Th in the least altered mafic rocks in our study is considered to be a source characteristic and a result of the processes involved in the magma genesis (Valverde Cardenas et al., 2012).

Dehydration melting in mafic migmatites has been shown to produce leucosomes that are not significantly different in composition than their original protoliths (Sawyer, 1991), and many recent studies have shown that such process have only minor effect on immobile element remobilization in mafic gneisses (e.g., Smith et al., 2001; Blein et al., 2003). Although the large leucosomes were not sampled for this study, field observations suggest that the small-volume in-situ melts are locally restricted in a way suggestive of the overall preservation of bulk rock compositions (e.g., Vielzeuf et al., 1990). Another more proximal example comes from the poikiloblastic, garnet-bearing mafic migmatites in the marginal gabbro, Baie du Nord segment of the MIZ, which were shown have broadly retained their protolith compositions identical to the main unaltered Fe-Ti gabbro (Cox et al., 1998). Several recent studies of high-grade gneisses in the Grenville Province have demonstrated that high-grade metamorphism and hydrothermal alteration can be effectively isochemical for immobile-incompatible major and trace elements e.g., HFSE and REE (Blein et al., 2003; Bonnet et al., 2005; Dickin and McNutt, 2007; Sappin et al., 2009; Yardley, 2012; Corriveau and Spry, 2014).

In summary, since the mafic samples analyzed in this study were selected from the most homogeneous and least altered parts of outcrops in which no visible signs of partial melting or hydrothermal alteration were recognized, they are inferred to represent original protolith chemistry. This is also supported by lack of evidence for partial melting in hand specimens and in the thin-sections. Combined mineralogical,

isotopic, and geochemical evidence suggests that the mafic samples are mostly unaltered to moderately altered in few cases, and that their immobile major and trace element contents are largely unaffected by metamorphic or hydrothermal processes.

2.5.4.2 Major and trace element geochemistry

The major and trace element geochemistry of the mafic rocks from the PLV and the MIU is listed in table 2.3. All the oxide values are reported as weight percentages and the trace element concentrations are reported in ppm.

All the mafic samples from the PLV have fairly restricted major element compositions with low SiO_2 (44-46 wt%), high TiO_2 (2.64-3.44 wt%) and $FeO_{(total)}$ (17-19 wt%) characterizing them as 'ferro-basalt' or 'Fe-Ti basalt' (fig. 2.8a) according to the classification of Byerly et al. (1976). They also display average Al_2O_3 (12.7-14 wt%), low MgO (~6 wt%), Mg# (0.37-0.40), Ni (40-70 ppm), Cr (50-70 ppm), and high Sc (~55 ppm) and V (435-742 ppm). Based on the immobile major and trace elements they are classified as tholeiitic (fig. 2.8b) sub-alkaline (fig. 2.8c) basalt. Note that the moderately altered sample RS383E1 has shifted to higher TiO_2 and lower Zr/TiO_2 side compared to the other samples.

The dark, intermediate, and light grey rocks from the MIU have distinct major elements concentrations. The dark grey rocks have very low SiO_2 (~40 wt%) along with high TiO_2 (~3.5-4.1 wt%) and $FeO_{(total)}$ (19.8-22.9 wt%) characterizing them as high Fe-Ti basalt (fig. 2.8a) of Byerly et al. (1976). These samples also have average Al_2O_3 (12.3-14.1 wt%), low MgO (~6 wt%), Mg# (0.32-0.35), and high Sc (~60-66 ppm) and V (470-620 ppm). The intermediate grey sample is also a high Fe-Ti basalt and it exhibits low SiO_2 (42.6 wt%), high TiO_2 (3.0 wt%), $FeO_{(total)}$ (19.7 wt%), average Al_2O_3

(12.5 wt%), and relatively higher MgO (7 wt%), Mg# (0.39), Sc (60 ppm), and V (803 ppm). The light grey rocks have relatively higher SiO_2 (46-47 wt%) and Al_2O_3 (18.0-20.3 wt%), along with lower TiO_2 (~1.8 wt%), $FeO_{(total)}$ (~12 wt%), MgO (3.56-4.64 wt%), Mg# (0.35-0.42), Sc (19-34 ppm), and V (134-302 ppm). The Ni and Cr contents are below the detection limit of ICP-MS for the dark and light grey rocks. All the three components are classified as tholeiitic (fig. 2.8b) sub-alkaline (fig. 2.8c) basalt to basaltic andesite.

In the chondrite-normalized REE diagrams, the samples from the PLV show low to moderate REE fractionation (fig. 2.9a) as indicated by $(La/Yb)_{CN}$ = 2.0-2.6, and strong negative Eu anomalies [Eu/Eu* = 0.67-0.86; Eu* refers to the value obtained by linear interpolation between adjacent elements]. Their overall REE patterns are very similar to E-MORB (although exhibiting much higher abundances than E-MORB) except for the –ve Eu* anomalies. The moderately altered sample #RS383E1, however, is slightly depleted in LREE [$(La/Sm)_{CN}$ = 0.8] and relatively enriched in MREE [$(Gd/Yb)_{CN}$ = 2.0] with strong negative Eu anomaly (Eu/Eu* = 0.38). In the MIU, the dark grey rocks are moderately fractionated in REE [$(La/Yb)_{CN}$ = 1.9-3.5] with flat LREE [$(La/Sm)_{CN}$ = 0.8-1.3], slightly enriched MREE [$(Gd/Yb)_{CN}$ = 1.6-1.9] (fig. 2.9b), and strong negative Eu anomalies (Eu/Eu* = 0.30-0.58). Note that the two moderately altered samples (11-395dx and d1) are similar to #RS383E1 in the PLV. The intermediate grey sample is moderately fractionated in REE [$(La/Yb)_{CN}$ = 3.6] with enrichment in both LREE [$(La/Sm)_{CN}$ = 1.7] and MREE [$(Gd/Yb)_{CN}$ = 1.6], and a weaker negative Eu anomaly (Eu/Eu* = 0.89) compared to the dark grey rocks (fig. 2.9c). The light grey rocks are the most fractionated in REE [$(La/Yb)_{CN}$ = 5-7] with enrichment in both LREE [$(La/Sm)_{CN}$ = 1.7-2.3] and MREE [$(Gd/Yb)_{CN}$ = 1.6-2.1],

weak negative Eu anomalies (Eu/Eu* = 0.83-0.85), and similar REE patterns to the intermediate grey sample (fig. 2.9c).

In the primitive mantle-normalized multi-element diagram, the least altered mafic samples from the PLV and the dark grey rocks from the MIU display distinct but small depletions in Th, Nb, Zr, and Ti (fig. 2.9d and e), and variable depletion in P (not shown). The moderately altered dark grey rocks in the MIU show patterns similar to the PLV sample #RS383E1, such as depletion in Zr, Hf, Ti, P, and variable enrichment in Nb (fig. 2.9d and e). Despite negative anomalies, the samples in PLV and the dark grey rocks have high Fe, Ti, and P contents. The intermediate and light grey samples in the MIU exhibit depletion in all HFSE and are variably depleted or enriched in Th (fig. 2.9f). Their multi-element patterns match well with two mafic samples from the ~1.4 Ga QFU (Valverde Cardenas et al., 2012) and the average composition of the Andean arcs (Kelemen et al., 2004).

2.6 Discussion

2.6.1 Significance of the U-Pb isotope data

The age data obtained in this study along with other recent studies from the Canyon domain are presented in fig. 2.10. In this study, sample #11-383c from the PLV has yielded an imprecise upper intercept age of $1439\ ^{+76}_{-68}$ Ma (fig. 2.5). Considering the lower limit of uncertainty, there is a small overlap of about 11 Ma between the upper age bracket for PLV deposition of ~1.5 Ga and the age of emplacement of the dated mafic layer. However, our preferred interpretation, which is consistent with the interpreted field relationships, is that the mafic layers in the PLV are younger than the paragneiss sequence, and intruded the PLV at $1439\ ^{+76}_{-68}$ Ma as concordant sills. Despite

large uncertainties, this age is comparable with the age of emplacement of the 'older tonalites' in the Lac Okaopéo area farther south at $1434\ ^{+7}_{-11}$ Ma (Augland et al., 2015), and with the age of the core of a metamorphic monazite at 1445 ± 27 Ma (Lasalle et al., 2014).

The crystallization age of the MIU has been previously determined to be 1410 ± 16 Ma based on CA-TIMS U-Pb dating of zircon from a light grey layer (#04-395z; Dunning and Indares, 2010). This correlates well with the age bracket of a pre-Grenvillian metamorphic event in the PLV between 1408 ± 24 Ma and 1391 ± 33 (Lasalle et al., 2013) determined from zircon rims in two metapelite samples. This post-Pinwarian metamorphic event (including uncertainties) in the PLV was previously attributed to the emplacement of the mafic rocks in the adjacent MIU (Indares and Moukhsil, 2013; Lasalle et al., 2013), but can now also be related to the intrusion of the mafic sills in the PLV (this study), as the ages of the two units overlap, within uncertainties.

The PLV was metamorphosed during the Ottawan phase of the Grenvillian Orogeny, as revealed by: (i) monazite ages between ca. 1081-1038 Ma determined by TIMS (Dunning and Indares, 2010); (ii) ages of BSE-dark grains or cores of monazites between ca. 1082-1059 Ma determined by LA-ICP-MS analyses (Lasalle et al., 2014); and (iii) metamorphic zircon ages between ca. 1076-1044 Ma determined by LA-ICP-MS analyses (Lasalle et al., 2013). Modelling of *P-T* paths for several paragneiss samples in the PLV has provided an estimated peak Ottawan metamorphic conditions of 600-1100 MPa and 800-900 °C, with retrograde conditions of 600-800 MPa and 800-865 °C (Lasalle and Indares, 2014; Patrick and Indares, 2017).

The PLV was also affected by the Rigolet phase as supported by: (i) one concordant TIMS analysis of metamorphic monazite at 1001 ± 3 Ma (Dunning and Indares, 2010); and (ii) the ages between ca. 1014-980 Ma obtained from BSE-bright metamorphic rims of monazites from the matrix of aluminous paragneiss samples (Lasalle et al., 2014). In this study, the CL images of zircon from the mafic sills in the PLV (fig. 2.5, i and ii) reveal multiple metamorphic rims around prismatic igneous cores. Our data yield a lower intercept metamorphic age of $1029\ ^{+33}_{-47}$ Ma, overlapping within uncertainties with the previous results, but also allowing for the possibility that the PLV could have been affected by Rigolet metamorphism. In the Lac Okaopéo area to the south, a similar metamorphic age of 1027 ± 25 Ma for the main Pb-loss event in zircon was recorded from the ca. 1497 Ma Bardoux pluton, and a metamorphic zircon from the 1383.4 Ma metagabbronorite yielded an age of 1002 ± 2 Ma (Augland et al., 2015). The age of intrusion of the unmetamorphic Okaopéo plutonic suite at 1014.6 ± 2.1 Ma within the PLV was interpreted to provide a minimum age for the metamorphism of the PLV in the Lac Okaopéo area (Augland et al., 2015).

The late-Grenvillian ages documented in the PLV and metagabbronorite were ascribed to the thermal and/or fluid effects of several small granitic pegmatite intrusions and/or fluid-assisted greenschist-facies metamorphism during the Rigolet phase (Lasalle et al., 2014; Augland et al., 2015). However, the ca. 996.7-1005.4 Ma magmatic monazite in REE-rich pegmatitic granite dykes derived from partial melting of Knob Lake Group paragneiss units at depth (Turlin et al., 2017) suggest that the Canyon domain and the Lac Okaopéo area were subjected to short-lived, high-grade Rigolet metamorphism, which could have overprinted the peak Ottawan metamorphism.

2.6.2 Significance of the Sm-Nd isotope data

The mafic sills emplaced into the PLV have low $\varepsilon Nd_{1.4Ga}$ values (-0.4) that are just below the CHUR evolution line (fig. 2.6), which could indicate derivation from an undepleted primitive mantle source. However, there is no evidence for such a mantle source at this time in rocks preserved in the Grenville Province. Therefore, depleted mantle modified by crustal components, or enriched mantle, seems a more plausible explanation for the observed isotopic compositions of the mafic sills. From ca. 1.65-1.13 Ga, magmas derived from the subcontinental lithospheric mantle (SCLM) to the southeast of the Superior Province were shown to be depleted suggesting the involvement of relatively young depleted mantle and crust with very short crustal residence time (Emslie and Hegner, 1993). Such depleted mantle-derived melts could have interacted with enriched crustal components to produce the observed isotopic composition in the mafic sills. In this context, it is noteworthy that Emslie et al. (1997) postulated a role for either melting of, or contamination by, depleted Labradorian SCLM to explain the source characteristics of the Michael Gabbro (1426 ± 6 Ma; Schärer et al., 1986) and the Shabogamo Gabbro (1445 ± 4 Ma; Krogh, 1993), which were subsequently interpreted to have been emplaced in a back-arc setting inboard from, and parallel to, the Laurentian margin (Rivers and Corrigan, 2000). Although comparable in terms of T_{DM} ages, these gabbroic dykes exhibit more negative εNd values (-4.0 to -6.0) than the mafic sills in the PLV (εNd -0.4).

Two other analyses, one from the light grey sample dated at 1.41 Ga from the MIU and a mafic sample from the QFU, yielded εNd values of +0.0 to +0.9 at 1.4 Ga with model T_{DM} ages of 2.02-2.25 Ga (fig. 2.6; table 2.3) that were interpreted to

indicate derivation from depleted mantle followed by crustal contamination (Valverde Cardenas et al., 2012).

The study area in the Manicouagan lies immediately to the north of the Quebecia terrane (fig. 2.1b; Nd model age of 1.55 Ga; Dickin and Higgins, 1992; Dickin, 2000), and is located within their Makkovikian model-age crust (Nd model ages range from 1.7-2.0 Ga), which was suggested to have been reworked during the Labradorian Orogeny in a continental margin arc setting (Thomson et al., 2011; Vautour, 2015). The Nd data of the mafic rocks in our study correlate well with the data from the Makkovikian and older model-age crust (Dickin and Higgins, 1992; Thomson et al., 2011; Vautour, 2015), supporting the interpretation of Thomson et al. (2011) that the Geon 14 arc-related rocks in the Canyon domain were formed on older crust that had Laurentian affinity, and that they are not part of an accreted terrane (Quebecia?) such as the Montauban arc located farther southwest in Portneuf – St. Maurice domain (Corrigan and van Breemen, 1997; Sappin et al., 2009).

2.6.3 Petrogenesis

It is necessary to assess the possible effects of magmatic petrogenetic processes such as fractional crystallization, Fe-Ti enrichment, and degrees of crustal contamination before discussing the likely petrotectonic affinities of the mafic rocks in our study. The operating premise of this part of the study is that critical use of isotope, major, and trace element (REE, and HFSE) data from the samples in the PLV and MIU that are inferred to be least altered and most closely represent their original protolith chemistry can provide insights into the petrogenetic processes, origin, and tectonic setting of the mafic units.

2.6.3.1 Fractional crystallization and Fe-Ti-P enrichment

The high-grade mafic rocks of both the PLV and MIU have major and trace elements suggesting their protoliths were tholeiitic basalt. They exhibit low MgO, Mg#, Ni, Cr, and –ve Eu anomalies that are indicative of derivation from evolved magmas after early fractional crystallization of olivine, clinopyroxene, and plagioclase at source. The least altered mafic rocks in the PLV and the dark and intermediate grey rocks in the MIU display high TiO_2, $FeO_{(total)}$, and P_2O_5 at very low contents of SiO_2, characterizing them as high Fe-Ti (and -P) mafic tholeiites, formally known as "ferrobasalt" or "high Fe-Ti basalt" (Byerly et al., 1976), which in the terrestrial record is now well-known to be spatially restricted to extensional tectonic settings in both oceanic and continental environments. Peng et al. (2013) discussed the different processes suggested by various authors to be responsible for the enrichment of Fe-Ti content in mantle-derived mafic magmas. In both oceanic and continental extensional settings, the mechanism of Fe-Ti-P enrichment in tholeiitic basalt has been explained by a combination of high degrees (up to 74%) of plagioclase, clinopyroxene, and olivine fractionation and accumulation of Fe-Ti oxides and apatite in a closed system under low oxygen fugacity (f_{O2}) conditions, suggesting generation of such basalt in a shallow level (spinel-peridotite) extensional setting (Clague and Bunch, 1976; Byerly et al., 1976; Brooks and Nielsen, 1978; Sinton et al., 1983; Juster et al., 1989; Brooks et al., 1991). The high Fe-Ti-P mafic rocks in our study indicate early olivine, clinopyroxene, and plagioclase fractionation with decreasing MgO along a tholeiitic trend. They are rich in Fe-, Ti-, and P-bearing phases such as ilmenite, titanite, and apatite. Moreover, they exhibit high REE contents with marked negative Eu anomalies, features characteristic of ferrobasalts that have experienced up to 90% fractional crystallization

in the Lau Basin back-arc spreading centres (Pearce et al., 1994). In summary, we postulate that the mafic rocks in this study have experienced significant early olivine, clinopyroxene, and plagioclase fractionation coupled with Fe-Ti oxide and apatite saturation following the "Fenner" trend under low f_{O2} conditions (Morse, 1980) in a shallow level closed-system magma chamber. This is compatible with the generation of high Fe-Ti-P mafic rocks in an extensional setting.

In modern oceanic environments, high Fe-Ti-P basalts have been documented at the propagating tips of spreading centres along many mid-ocean ridges e.g., Galapagos spreading centre (Byerly et al., 1976; Juster et al., 1989) and East Pacific Rise (Clague and Bunch, 1976; Pearce et al., 1986), in oceanic back-arc basins e.g., Lau Basin (Pearce et al., 1994), and along spreading centres propagating into an island arc crust e.g., Josephine Ophiolite (Harper, 2003). In continental settings, such magmas are documented in modern continental rifts e.g., Afar Rift (Barberi et al., 1974) and the Red Sea (Cocherie et al., 1994), ancient plume-related continental rifts e.g., the Mesoproterozoic high Fe-Ti-P rocks of western Shandon in the North China Craton (Peng et al., 2013), in ancient intra-cratonic rifts e.g., Broken Hill Block of Australia (Rutherford et al., 2006; Raveggi et al., 2007), and in almost all major Proterozoic anorthosites or AMCG complexes worldwide (Ashwal, 1978, 1982; Philpotts, 1981; also for examples relevant to SE Laurentian margin see Duchesne, 1990; Owens and Dymek, 1992; McLelland et al., 1994; Dymek and Owens, 2001; Hébert et al., 2005; Charlier et al., 2006, 2008). Considering the active continental margin setting at 1.4 Ga along the southeastern margin of Laurentia, we infer that the high Fe-Ti-P mafic rocks in our study were formed in a continental margin back-arc or intra-arc extensional setting as has also been suggested for the Renzy terrane in the western Grenville

Province that has an inferred minimum age of ca. 1.40 Ga (Montreuil and Constantin, 2010).

2.6.3.2 Crustal contamination

In the PLV, the mafic sills exhibit major and trace element compositions, e.g., HFSE depletion relative to REE (fig. 2.9), low to moderate LREE enrichment, and relatively higher SiO_2 compared to other Fe-Ti-P metabasalts from the study area, and slightly negative εNd values, all of which suggest that their source was variably modified by crustal components, either in a subduction-related process or by crustal assimilation. Th is considered to be a reliable indicator of crustal input when compared with other incompatible elements such as Nb (Pearce and Peat, 1995; Pearce, 2008). On the Th/Yb vs. Nb/Yb diagram (fig. 2.11a; Pearce and Peat, 1995; Pearce, 2008), the mafic sills from the PLV plot on the mantle array between N-MORB and E-MORB precluding significant input from felsic upper crust or substantial melting of subducted sediments in an arc source. Therefore, their mantle source could have been modified by minor input from subduction-related fluids possibly derived from Th-depleted detritus causing the low Th and variable enrichments in the LILE (e.g., Woodhead et al., 2001). Melts derived from such fluid-metasomatized mantle were probably subjected to contamination by old mafic granulitic lower crust during ascent through attenuated continental crust prior to emplacement within the PLV sequence. The low Th in these samples and the presence of xenocrystic zircon also support the involvement of attenuated continental lower mafic crust (e.g., Peng et al., 2013).

The least altered dark and intermediate grey rocks from the MIU exhibit very low SiO_2 and low to moderate LREE enrichment, precluding significant contamination by upper crust or subduction components (Zheng and Hermann, 2014; Dai et al. 2015).

Their chondrite-normalized REE patterns and small –ve Nb anomalies suggest an enriched E-MORB-type source similar to the source for the PLV samples. Although the light grey rocks display a higher proportion of SiO_2 and LREE enrichment at low positive εNd values, assimilation and fractional crystallization (AFC; DePaolo, 1981a) processes involving upper crust would significantly increase SiO_2 content and decrease εNd values, which is not the case for these rocks. Therefore, a Paleoproterozoic juvenile mafic crust is probably a more suitable candidate as a potential contaminant of the mafic rocks in the MIU, as suggested by several authors for other mafic rocks of this age elsewhere in the Grenville Province (e.g., Dickin and Higgins, 1992; Sappin et al., 2009). The mafic samples from the QFU, however, exhibit higher SiO_2 contents (~53%) at εNd of 0.0. Moreover, their variably enriched Th contents (in table 2.3 and fig. 2.9f) suggest increased crustal input through subduction-processes and/or crustal contamination. All these mafic samples from the MIU and QFU exhibit variable SiO_2 contents, depletions in HFSE compared to REE, and variably depleted to enriched Th contents in the primitive mantle-normalized multi-element plots (fig. 2.9), and exhibit a trend from an enriched MORB-like mantle towards continental arc or lower crust (fig. 2.11a). These observations suggest variable degrees of addition of subduction components and/or contamination by juvenile mafic crust in their mantle sources. As such, the mingling of mafic magmas derived from heterogeneous mantle sources in a shallow magma chamber, while undergoing variable degrees of contamination by heterogeneous crustal components, is considered to be the most plausible interpretation for the mixed intrusive nature of the MIU.

2.6.4 Tectonic setting

The least altered mafic rocks from the PLV and the dark grey samples from the MIU exhibit values of Zr/Y (2-3), Zr/Yb (21-30), Zr/Hf (34-38), Ti/Y (245-297), and Ti/Zr (93-129) (table 2.3) that are comparable to those of average N-MORB (2.6, 24, 36, 272 and 103, respectively; average N-MORB values from Sun and McDonough, 1989). The intermediate grey sample exhibits somewhat higher values in Ti/Y (457) and Ti/Zr (187). The light grey rocks (except RS395A2) from the MIU and the mafic rocks from QFU exhibit a slightly wider range of values in Zr/Y (2-5), Zr/Yb (19-46), Zr/Hf (29-39), Ti/Y (201-314), and lower Ti/Zr (47-99).

On the Th/Yb–Nb/Yb diagram (fig. 2.11a) of Pearce (2008), the samples from the PLV and the dark and intermediate grey sample from the MIU plot along the mantle array, whereas the light grey rocks show a trend of increasing Th/Yb towards continental arc or crust. When considered together, the mafic components (dark, intermediate and light grey) from the MIU, along with the mafic rocks from QFU, exhibit a trend (grey shaded area in fig. 2.11a) from ocean floor basalt to continental margin arc basalt, suggesting a range of melt sources present at this time. In order to further constrain the tectonic setting(s) of their formation, the mafic samples in our study have been plotted on several REE- and HFSE-based tectonic discrimination diagrams (fig. 2.11 b-d), in which the mafic sills intruding the PLV straddle the depleted to enriched MORB fields with a weak trend towards arc, whereas the mafic rocks from the MIU and QFU define a clear trend from MORB to calc-alkaline arc basalt, a result of variable enrichment from crustal components. The moderately altered samples are slightly scattered due to alteration biases for the elements used in these diagrams, which shift the positions of the samples away from the Hf and Zr corners with a slight bias

towards the Nb, Y, and Th corners; however, this has not affected the plots significantly and less weight is given to these moderately altered samples.

Therefore, we infer that the high Fe-Ti-P mafic sills in the PLV exhibit evidence for a variably depleted to enriched MORB source that formed in an extensional setting on an active continental margin, with minor input from subduction components and contamination by older mafic granulitic lower crust. Considered collectively with the geochronological data, this is most compatible with continental intra-arc or back-arc rifting at or before $1439\ ^{+76}_{-68}$ Ma.

In the MIU, the mafic rocks formed at ca. 1410 Ma, and the mafic rocks in the QFU with an inferred age of 1.4 Ga, were both derived from mantle sources with a range of tectonic affinities from enriched MORB to continental arc, and were further variably modified by subduction and/or crustal contamination by Paleoproterozoic juvenile mafic crust. Such diverse geochemical signatures are characteristic of many modern and ancient active continental margin back-arc basins, and have recently been reported for post-Pinwarian mafic rocks in the western Grenville Province (e.g., Renzy terrane with an inferred minimum age of 1.40 Ga; Montreuil and Constantin, 2010). The increasing influence of arc or crustal components in the MIU and QFU suggests that the margin evolved from continental intra-arc or back-arc extension to crustal shortening before ca. 1410 Ma, resulting in increasing proximity of the back-arc source to the arc itself.

2.6.5 Tectonic Model and Implications

Recent studies by several workers in the central Grenville Province have led to the availability of a large amount of high-quality data enabling a refinement of the

Mesoproterozoic tectonic evolution of the study area. Of particular importance are the following observations:

1. The ages obtained from the fragmental igneous cores of detrital zircon in the aluminous paragneisses and quartzite of the PLV range between ~1.5-2.7 Ga, with the dominant peak at ~1.7-1.9 Ga, and subsidiary peaks at ~1.5 Ga and ~2.5-2.7 Ga, indicating the major supply of the detritus was derived from the nearby Labradorian and Makkovikian crust (Lasalle et al., 2013; Moukhsil et al., 2013a). This age distribution is very similar to that of the eastern part of the Wakeham Group (WG; Wodicka et al., 2003; van Breemen and Corriveau, 2005), suggesting that the provenance of detritus in both basins was from the Laurentian margin. This is difficult to reconcile with the accretion model of the Labradoria terrane at 1.65 Ga and the Quebecia terrane at 1.45 Ga (Dickin and Higgins, 1992; Martin and Dickin, 2005), because the older model age of the WG do not correlate with the younger detrital zircon ages derived from it.

2. The similar ages of detrital clastic sources in the PLV and WG, together with their similar depositional ages of ≥ 1.5 Ga, support the previously proposed back-arc or intra-arc settings for the WG related to an early phase of the accretionary Pinwarian Orogeny (Rivers and Corrigan, 2000; van Breemen and Corriveau, 2005; Corriveau and Bonnet, 2005; Rivers et al., 2012; Lasalle et al., 2013; Augland et al., 2015).

3. The presence of ~1500 Ma detrital zircon in both the PLV and the WG suggests that part of the detritus in both basins was derived from early-Pinwarian crust of felsic composition, which was most probably part of the continental-margin arc. Intra-arc volcanism of that age has been well documented farther east in both the

Musquaro sector of the Wakeham Group and in the La Romaine supracrustal belt, a southeastern extension of the Wakeham Group (fig. 2.1a; Corriveau and Bonnet, 2005; Bonnet et al., 2005).

4. The PLV and its proposed correlatives have been recognized over a large area in the central Grenville Province (Manicouagan area) and extend accross the Makkovikia, and Quebecia terranes, whereas the WG is restricted to the Labradoria terrane in the east (fig. 2.1).

5. The Bardoux Plutonic Suite, emplaced at ca. 1497 Ma within the PLV, also covers a wide area stitching the Makkovikia and the Quebecia Nd model-age terranes, and is suggested to have formed in a continental margin arc setting (Augland et al., 2015). The documentation of several felsic to mafic metavolcanic rocks, subvolcanic plutons, and pillow lavas in the western WG with evolved geochemical signatures (Martignole et al., 1994), together with evidence for associated syn-volcanic hydrothermal activity, suggests development of a continental back-arc to intra-arc basin related to the early Pinwarian arc (Corriveau and Bonnet, 2005). Metavolcanic rocks of comparable age to the Bardoux Plutonic Suite have also been reported from the eastern WG (Lac Musquaro area; fig. 2.1a), for which a depositional age between ca. 1.52-1.50 Ga has been determined (van Breemen and Corriveau, 2005). These metavolcanic rocks formed between 1511 ± 13 and 1491 ± 7 Ma (van Breemen and Corriveau, 2005), and were approximately coeval with several granitic orthogneisses emplaced between 1505 ± 12 and 1494 ± 12 Ma (SHRIMP U-Pb zircon; O. van Breemen and L. Corriveau, unpublished, cited in Corriveau and Bonnet, 2005) that exhibit evolving geochemical signatures suggestive of within-plate to

continental margin arc settings (Corriveau and Bonnet, 2005). Moreover, the earlier 1.53 Ga tonalitic intrusions (SHRIMP U-Pb zircon; O. van Breemen and L. Corriveau, unpublished, cited in Corriveau et al., 2003) that have volcanic arc granite or syn-collisional granite geochemical signatures were interpreted to be representative of an early Pinwarian intra-arc setting in the La Romaine supracrustal belt (Corriveau and Bonnet, 2005; Bonnet et al., 2005) farther east (fig. 2.1a).

The above observations suggest that there is compelling temporal and tectonic correlation between the PLV in the central Grenville Province and the WG in the eastern Grenville Province. As suggested previously by Augland et al. (2015) for the Lake Okaopéo area immediately south of the Manic 5 reservoir, it is reasonable to interpret that the PLV formed in an early Pinwarian active margin arc/back-arc setting similar to that of the WG, and that these terranes were not accreted to the continental margin. Indeed, although preserved as physically separate entities over ~200 km apart and lying on substrates with different model ages, both the PLV and WG are extensive units (figs. 2.1 and 2.2), and it appears feasible that they may be remnants of a single elongate back-arc basin or two coeval back-arc basins. Therefore, based on the above observations and integrating our results with those of Augland et al. (2015) from the nearby Lac Okaopéo area located immediately south of the Manic 5 reservoir, and also taking into account the conclusions of Schellart (2008a, b) on back-arc extension and trench migration in active arc systems, the following evolution of the study area in the central Grenville Province is proposed:

1. Ca. 1500 Ma: The early-Pinwarian (> 1500 Ma) continental-margin arc undergoes back-arc or intra-arc extension, forming a short-lived basin in which the PLV was

deposited within a short time interval at ca. 1500 Ma (fig. 2.12a; Lasalle et al., 2013). Back-arc extension gives way to compression and possible inversion (?) of the back-arc basin (fig. 2.12b), leading to intrusion of the Bardoux Plutonic Suite within the PLV at 1497 ± 5 Ma (Augland et al., 2015). The dominantly volcanic arc to subordinate within-plate type geochemical signatures and positive εHf values (4.7-2.3) of the granitoids composing this suite have been interpreted to indicate contamination of juvenile mantle-derived felsic magma with older Makkovikian model-age crust, as indicated by their T_{DM} model ages (1.9-2.05 Ga; Augland et al., 2015). Although we do not see any direct evidence of an early-Pinwarian arc in the study area, remnants of it have been reported from farther east in the Grenville Province in Labrador and Québec (Tucker and Gower, 1994; Gower and Krogh, 2002; Corriveau and Bonnet, 2005; Wodicka et al., 2003). Furthermore, the close temporal (fig. 2.10) and spatial relationships between the youngest age of deposition of the PLV and the intrusion of the arc-related Bardoux granitoids into the PLV supports the interpretation that the PLV was deposited in an arc-related setting. We further suggest that the within-plate character and juvenile mantle signature exhibited by some samples from the Bardoux Plutonic Suite provide cryptic evidence of earlier extension within the early-Pinwarian (> 1.5 Ga) arc through which the granitoid magmas were intruded. These geochemical features are widespread in the Wakeham group, where an evolution of geochemical signatures from within-plate to continental margin arc has been reported (Corriveau and Bonnet, 2005).

2. Ca. 1440-1430 Ma: Limited back-arc extension coeval with Geon 14 arc formation was postulated to have occurred along much of the length of the

Grenville Province by Rivers and Corrigan (2000). This is compatible with our data from the central Grenville Province in which the 1439 $^{+76}_{-68}$ Ma high Fe-Ti-P mafic sills in the PLV with variably depleted to enriched MORB signatures were contaminated by minor subduction components and old mafic granulitic lower crust as they intruded the sequence in an extensional back-arc rift setting (fig. 2.12c). The source for these mafic rocks must have evolved in a shallow magma chamber before being emplaced within the PLV. This interpretation is compatible with the geochemical signature of the coeval 'older tonalites' of the Hulot Complex, which intruded the PLV at 1434 $^{+7}_{-11}$ Ma farther south in Lac Okaopéo area, (Augland et al., 2015). These were interpreted to have been derived from juvenile mantle-derived magma (εHf = +8 to +10) contaminated by Labradorian (~1.6 Ga) crust in a distal arc or microcontinent-arc setting (Augland et al., 2015). Some of their samples of the 'older tonalites' plot in the within-plate field in the Rb-(Ta+Yb) diagram (fig. 2.3 in Augland et al., 2015; Moukhsil et al., 2013b) and show a trend towards peralkaline granite (Lars Augland, personal communication, 2016), which suggest the influence of an extensional setting farther inboard, possibly related to thinning of the Labradorian arc crust. Rims of detrital zircon in the PLV dated at ~1450 Ma (Lasalle et al., 2013) and the cores of metamorphic monazite in the PLV dated at ~1445 Ma (Lasalle et al., 2014) may record these igneous events.

3. Ca. 1410 Ma: The mafic rocks from the MIU emplaced at 1410 ± 16 Ma (Valverde Cardenas et al., 2012) and the inferred ca. 1.4 Ga mafic rocks from the QFU, both of which indicate enriched MORB and arc sources that developed in an inboard back-arc environment and were variably modified by subduction

components and/or contamination by Paleoproterozoic crust (fig. 2.12d). The geochemical and isotopic characters displayed by the arc to transitional-arc and non-arc compositions of these rocks support the presence of multiple sources that are typical of a back-arc setting developed inboard from, but in close proximity to, the continental-margin arc. Farther south from the Canyon domain in the Lac Okaopeó area, the 'younger tonalites' of the Hulot Complex, dated at 1413 ± 12 Ma and exhibiting more radiogenic Hf isotopic signatures (εHf = +6.27 to +8.04), were inferred to have formed in an arc setting as a result of increased proximity of the arc source due to shortening (and thickening?) of the Laurentian margin (Augland et al., 2015). Therefore, considering the ages with their uncertainties, and the probable proximity of the MIU and the 'younger tonalites', a tectonic setting possibly reflecting processes such as roll-forward (slab advance) of the subducting slab, or shortening of the proximal (outboard) part of the back-arc basin, and coeval extension within the distal part of the basin seems most plausible. Both this igneous activity and the associated inferred tectonic activity could explain the growth of zircon in the PLV as metamorphic grains and rims between ~1391-1408 Ma (Lasalle et al., 2013). This outboard shortening of the active margin could be temporally related to the post-Pinwarian island arc/back-arc accretion (e.g., the ca. 1.45-1.39 Ga Montauban Group and La Bostonnais complex; Nadeau and van Breemen, 1994; Sappin et al., 2009), and arc/back-arc development on the thin Laurentian margin (e.g., the ca. 1.40-1.35 Ga Bondy Gneiss Complex; Blein et al., 2003).

The end of the Pinwarian orogeny (1.52-1.46 Ga) in southeastern Laurentia was characterized by anorthosite-mangerite-charnockite-granite (AMCG) magmatism

(Gower and Krogh, 2002), with the granodiorite in the Banded Complex (1403 $^{+32}_{-25}$ Ma; Indares and Dunning, 2004) and the Renwick mangerite (1402 ± 72 Ma; Moukhsil et al., 2012, 2013a) possibly being local representatives of this suite. Both the mantle and crustal signatures of the component parts of these complexes are interpreted to have formed in a continental back-arc setting (Rivers and Corrigan, 2000; Rivers et al., 2012).

Most of the post-Pinwarian interval up to the onset of the Grenvillian Orogeny was characterized by short-lived compressional arc to extensional intra-arc or back-arc settings, involving both continental and oceanic arcs, and marginal basin settings. In the study area, we have documented two important magmatic events during Geon 14 that characterize the evolution from an extension to compression in a back-arc and related compressional arc developed on attenuated Laurentian margin. Such an oscillating structural evolution between extension and compression in continental margin arcs over time scales of a few 10s of Ma, and the associated isotopic 'pull-up' and 'pull-down' of εNd values, is typical of modern continental arcs (e.g., DeCelles et al., 2009).

An important feature of the Geon 14 magmatism in the central Grenville Province was the emplacement of mantle-derived high Fe-Ti-P mafic tholeiites that were variably contaminated by crustal sources. The repetitive intrusion of small volumes of high Fe-Ti-P magma is compatible with limited extension in a long-lived arc/back-arc regime (e.g., Montreuil and Constantin, 2010). Back-arc or intra-arc extension appears to have played an important role in the subduction-related processes on the southeastern margin of Laurentia during and after the Pinwarian Orogeny (e.g., Blein et al., 2003; Slagstad et al., 2004, 2009; Corriveau and Bonnet, 2005; Sappin et

al., 2009; Montreuil and Constantin, 2010), suggesting that a large part of the margin would have been dominated by thin, thermally weak, and rheologically soft crust that underwent repetitive arc formation and accretion followed by intra-arc or back-arc extension. This process of repetitive arc formation and accretion followed by intra-arc or back-arc extension appears to have continued throughout the remainder of the Mesoproterozoic up to the beginning of the Grenvillian Orogeny (Rivers and Corrigan, 2000).

2.7 Conclusions

The tectonomagmatic and related metamorphic events during Geon 14 in the central Grenville Province constitute an important part of the pre-Grenvillian evolution of the southeastern margin of Laurentia. In the last decade significant efforts have been directed to deciphering the details of these events that have been obscured by later high-grade metamorphism and associated deformation during the Grenvillian Orogeny. This study represents an attempt to see through this Grenvillian veil and interpret the geochemistry and tectonic significance of two suites of mafic rocks presently preserved as mid-pressure granulites. Specifically, analysis of the suite of mafic sills emplaced into the metasedimentary Complexe de la Plus Value (PLV), and of the mafic intrusive rocks comprising the Mafic to Intermediate Unit (MIU) has provided more detailed information about the pre-orogenic magmatism and hence the inferred architecture of this part of the Laurentian margin during Geon 14, and its possible implications for the pre-Grenvillian and Grenvillian orogenic evolution of SE Laurentia. The main conclusions of the study are:

1. The 1439 $^{+76}_{-68}$ Ma mafic sills intruded the PLV supracrustal sequence (> 1500 Ma) during limited extension of arc/back-arc crust, resulting in thinning of the Laurentian continental margin. These mafic sills were derived from variably depleted to enriched MORB-type mantle and were modified by minor subduction components and contamination by old mafic granulitic lower crust.
2. The mafic intrusive rocks in the MIU, characterized as arc to transitional-arc and non-arc types, were formed at ca. 1410 Ma in a back-arc setting where shortening of the Laurentian crust increased the proximity of the back-arc to the more outboard arc source as suggested by increased crustal input from subduction components and/or contamination. The various magmatic components in the unit were mingled in a shallow closed magma chamber before their final emplacement.
3. Repetitive intrusion of the high Fe-Ti-P mafic rocks during Geon 14 in the central Grenville Province suggests that arc/back-arc extension was an important process in an overall compressional arc regime on SE Laurentia during the Mesoproterozoic. Such a tectonic setting resulted in prolonged but limited extension of thin, hot, and ductile crust.

These conclusions are compatible with both the general model of an active margin on SE Laurentia during the Mesoproterozoic, suggested previously by others, and with more recent work in the central Grenville Province, but provide significant new details and refinements for the region.

2.8 Acknowledgements

This study is part of the Ph.D. project of B.M, supported by a Natural Sciences and Engineering Research Council of Canada Discovery Grant (A.I) and a Memorial

University School of Graduate Studies fellowships (B.M). Greg Dunning is thanked for carrying out the CA-TIMS U-Pb zircon analyses and for providing critical comments on an earlier draft of the manuscript. Pam King, Sherri Strong, and Anne Westhues are gratefully acknowledged for assisting with sample preparation and for carrying out the TIMS Sm-Nd isotope analyses in the TERRA Facility. We also thank Michael Shaffer, David Grant, and Dylan Goudie for assistance and advice with the SEM-MLA mapping and CL imaging at the Micro Analysis Facility (MAF-IIC) in the Bruneau Centre for Research and Innovation at Memorial University. Reviews by L. Corriveau and D. Corrigan greatly improved the quality of this manuscript. The authors also thank the journal editor Ali Polat, associate editor B. Murphy, and editorial assistant Debbie Regier for swift handling of the manuscript. Finally, BM would like to express his deepest gratitude to Toby Rivers for many long discussions, meticulously detailed, critical, and insightful comments on several versions of the manuscript, and for sharing his wealth of wisdom on Grenvillian geology.

2.9 References

Ashwal, L.D. 1978. Petrogenesis of massif-type anorthosites: crystallization history and liquid line of descent of the Adirondack and Morin complexes. PhD dissertation, Princeton University.

Ashwal, L.D. 1982. Mineralogy of mafic Fe-Ti oxide-rich differentiates of the Marcy anorthosite massif, Adirondacks, New York. American Mineralogist, 67: 14–27.

Augland, L.E., Moukhsil, A., Solgadi, F., Indares, A. 2015. Pinwarian to Grenvillian magmatic evolution in the central Grenville Province: new constraints from ID-TIMS U-Pb ages and coupled Lu-Hf S-MC-ICP-MS data. Canadian Journal of Earth Sciences, 52(9): 1–21. doi: 10.1139/cjes-2014-0232

Barbarin, B. 2005. Mafic magmatic enclaves and mafic rocks associated with some granitoids of the central Sierra Nevada batholith, California: nature, origin, and relations with the hosts. Lithos, 80: 155–177. doi:10.1016/j.lithos.2004.05.010

Barberi, F., Ferrara, G., Santacroce, R., Treuil, M., Varet, J. 1975. A transitional basalt-pantellerite sequence of fractional crystallization, the Boina centre (Afar Rift, Ethiopia). Journal of Petrology, 16: 22–56. doi:10.1093/petrology/16.1.22

Beaumont, C., Nguyen, M.H., Jamieson, R.A., Ellis, S. 2006. Crustal flow modes in large hot orogens. Geological Society of London Special Publications, 268: 91–145. doi:10.1144/GSL.SP.2006.268.01.05

Bouvier, A., Vervoort, J.D., Patchett, P.J. 2008. The Lu–Hf and Sm–Nd isotopic composition of CHUR: constraints from unequilibrated chondrites and implications for the bulk composition of terrestrial planets. Earth and Planetary Science Letters, 273: 48–57. https://doi.org/10.1016/j.epsl.2008.06.010

Blein, O., Laflèche, M.R., Corriveau, L. 2003. Geochemistry of the granulitic Bondy gneiss complex: A 1.4 Ga arc in the Central Metasedimentary Belt, Grenville Province, Canada. Precambrian Research, 120(3): 193–217. doi: 10.1016/S0301-9268(02)00112-2

Bonnet, A.-L., Corriveau, L., Laflèche, M. R., 2005. Chemical imprint of highly metamorphosed volcanic-hosted hydrothermal alterations in the La Romaine Supracrustal Belt, eastern Grenville Province, Quebec. Canadian Journal of Earth Sciences, 42(10): 1783–1814. https://doi.org/10.1139/e05-098

Brooks, C.K., Nielsen, T.F.D. 1978. Early stages in the differentiation of the Skaergaard magma as revealed by a closely related suite of dike rocks. Lithos, 11: 1–14. doi:10.1016/0024-4937(78)90027-0

Brooks, C.K., Larsen, L.M., Nielsen, T.F.D. 1991. Importance of iron-rich tholeiitic magmas at divergent plate margins: a reappraisal. Geology, 19(3): 269–272. doi:10.1130/0091-7613(1991)019<0269:ioirtm>2.3.co;2

Byerly, G.R., Melson, W.G., Vogt, P.R. 1976. Rhyodacites, andesites, ferro-basalts and ocean tholeiites from the Galapagos spreading center. Earth and Planetary Science Letters, 30(2): 215–221. doi:10.1016/0012-821X(76)90248-X

Cabanis, B., Lecolle, M. 1989. Le diagramme La/10-Y/15-Nb/8 : un outil pour la discrimination des séries volcaniques et la mise en évidence des processus de mélange et/ou de contamination crustale. Comptes Rendus de l'Académie des Sciences, Série 2, Mécanique, Physique, Chimie, Sciences de l'Univers, Sciences de la Terre, 309(20) : 2023–2029.

Castro, A., de la Rosa, J.D., Stephens, W.E. 1990. Magma mixing in the subvolcanic environment: petrology of the Gerena interaction zone near Seville, Spain.

Contributions to Mineralogy and Petrology, 106(1): 9–26. doi:10.1007/BF00306405

Cawood, P.A., Kroner, A., Collins, W.J., Kusky, T.M., Mooney, W.D., Windley, B.F. 2009. Accretionary orogens through Earth history. Geological Society of London Special Publications, 318: 1–36. doi:10.1144/SP318.1

Charlier, B., Duchesne, J.-C., Vander Auwera, J. 2006. Magma chamber processes in the Tellnes ilmenite deposit (Rogaland Anorthosite Province, SW Norway) and the formation of Fe-Ti ores in massif-type anorthosites. Chemical Geology, 234(3-4): 264–290. doi:10.1016/j.chemgeo.2006.05.007

Charlier, B., Sakoma, E., Sauvé, M., Stanaway, K., Vander Auwera, J., Duchesne, J.-C. 2008. The Grader layered intrusion (Havre-Saint-Pierre Anorthosite, Quebec) and genesis of nelsonite and other Fe–Ti–P ores. Lithos, 101(3): 359–378. doi:10.1016/j.lithos.2007.08.004

Clague, D.A., Bunch, T.E. 1976. Formation of ferrobasalt at East Pacific Midocean spreading centers. Journal of Geophysical Research, 81(23): 4247–4256. doi:10.1029/JB081i023p04247

Clift, P., Vannucchi, P. 2004. Controls on tectonic accretion versus erosion in subduction zones: implications for the origin and recycling of the continental crust. Reviews in Geophysics, 42, RG2001: 1–31. doi:10.1029/2003RG000127.1.INTRODUCTION

Cocherie, A., Calvez, J., Oudin-Dunlop, E. 1994. Hydrothermal activity as recorded by Red Sea sediments: Sr-Nd isotopes and REE signatures. Marine Geology, 118(3): 291–302. doi:10.1016/0025-3227(94)90089-2

Corrigan, D., Hajnal, Z., Németh, B., Lucas, S.B. 2005. Tectonic framework of a Paleoproterozoic arc–continent to continent–continent collisional zone, Trans-Hudson Orogen, from geological and seismic reflection studies. Canadian Journal of Earth Sciences, 42(4): 421–434. doi:10.1139/e05-025

Corriveau, L., Bonnet, A.L. 2005. Pinwarian (1.50 Ga) volcanism and hydrothermal activity at the eastern margin of the Wakeham Group, Grenville Province, Quebec. Canadian Journal of Earth Sciences, 42(10): 1749–1782. doi:10.1139/e05-086

Corriveau, L., Bonnet, A.L., van Breemen, O., Pilote, P. 2003. Tracking the Wakeham Group volcanic rocks and associated copper – iron oxide hydrothermal activity from La Romaine eastward, Eastern Grenville Province, Québec. Geological Survey of Canada, Paper 2003-C12, pp. 11.

Corriveau, L., Perreault, S., and Davidson, A., 2007. Prospective metallogenic settings of the Grenville Province. *In* Mineral deposits of Canada: A synthesis of major deposit-types, district metallogeny, the evolution of geological provinces and exploration methods. *Edited by* W.D. Goodfellow, Geological Association of Canada, Mineral Deposits Division, Special Publication 5, pp. 819–848.

Corriveau, L. and Spry, P., 2014. Metamorphosed hydrothermal ore deposits. *In* Treatise on Geochemistry, Second Edition. *Edited by* Holland, H.D. and Turekian, K.K., Oxford, Elsevier, Vol. 13, pp. 175–194. https://doi.org/10.1016/B978-0-08-095975-7.01107-4

Cox, R., Indares, A. 1999a. High-pressure and high-temperature metamorphism of the mafic and ultramafic Lac Espadon suite, Manicouagan Imbricate Zone, eastern Grenville Province, Quebec. Canadian Mineralogist, 37: 335–357.

Cox, R., Indares, A. 1999b. Transformation of Fe-Ti gabbro to coronite, eclogite and amphibolite in the Baie du Nord segment, Manicouagan Imbricate Zone, eastern Grenville Province. Journal of Metamorphic Geology, 17(5): 537–555. doi:10.1046/j.1525-1314.1999.00216.x

Cox, R., Dunning, G., Indares, A. 1998. Petrology and U–Pb geochronology of mafic, high-pressure, metamorphic coronites from the Tshenukutish domain, eastern Grenville Province. Precambrian Research, 90: 59–83. doi:10.1016/S0301-9268(98)00033-3

Dai, L.-Q., Zhao, Z.-F., Zheng, Y.-F., Zhang, J. 2015. Source and magma mixing processes in continental subduction factory: Geochemical evidence from postcollisional mafic igneous rocks in the Dabie orogen. Geochemistry, Geophysics, Geosystems, 16(3): 659–680. doi:10.1002/2014GC005620

DeCelles, P.G., Ducea, M.N., Kapp, P., Zandt, G. 2009. Cyclicity in Cordilleran orogenic systems. Nature Geoscience, 2(4): 251–257. doi:10.1038/ngeo469

DePaolo, D.J. 1981a. Trace element and isotopic effects of combined wallrock assimilation and fractional crystallization. Earth and Planetary Science Letters, 53(2): 189–202. doi:10.1016/0012-821X(81)90153-9

DePaolo, D.J. 1981b. Neodymiun isotopes in the Colorado Front Range and crust-mantle evolution in the Proterozoic. Nature, 291: 193–196. doi: 10.1038/291193a0

Dickin, A.P. 2000. Crustal formation in the Grenville Province: Nd-isotope evidence. Canadian Journal of Earth Sciences, 37: 165–181. doi:10.1139/e99-039

Dickin, A.P., Higgins, M.D. 1992. Sm/Nd evidence for a major 1.5 Ga crust-forming event in the central Grenville province. Geology, 20(2): 137–140. doi:10.1130/0091-7613(1992)020<0137:SNEFAM>2.3.CO;2

Dickin, A. P., McNutt, R.H. 2007. The Central Metasedimentary Belt (Grenville Province) as a failed back-arc rift zone: Nd isotope evidence. Earth and Planetary Science Letters, 259(1-2): 97–106. doi: 10.1016/j.epsl.2007.04.031

Duchesne, J.-C. 1990. Origin and evolution of monzonorites related to anorthosites. Schweizerische Mineralogische und Petrographische Mitteilungen, 70: 189–198.

Dunning, G., Indares, A. 2010. New insights on the 1.7-1.0 Ga crustal evolution of the central Grenville Province from the Manicouagan-Baie Comeau transect. Precambrian Research, 180(3): 204–226. doi:10.1016/j.precamres.2010.04.005

Dymek, R.F., Owens, B.E. 2001. Petrogenesis of apatite-rich rocks (nelsonites and oxide-apatite gabbronorites) associated with massif anorthosites. Economic Geology, 96(4): 797–815. doi:10.2113/gsecongeo.96.4.797

Emslie, R.F., Hamilton, M.A., Gower, C.F. 1997. The Michael Gabbro and other Mesoproterozoic lithospheric probes in southern and central Labrador. Canadian Journal of Earth Sciences, 34(12): 1566–1580. doi:10.1139/e17-127

Emslie, R.F., Hegner, E. 1993. Reconnaissance isotopic geochemistry of anorthosite-mangerite-charnockite-granite (AMCG) complexes, Grenville Province, Canada. Chemical Geology, 106: 279–298. https://doi.org/10.1016/0009-2541(93)90032-E

Gobeil, A., Hébert, C., Clark, C., Beaumier, M., Perreault, S. 2002. Géologie de la région du lac De La Blache (22K03/22K04). Ministère des Ressources naturelles du Québec, Québec, RG2002-01.

Gobeil, A., Hébert, C., Clark, T., David, J., Davis, D. 2005. Nouvelles données géochronologiques dans l'est du Grenville: précisions sur l'évolution

magmatique. *In* Ministère Des Ressources naturelles du Québec, Résumé Des Conférences et de L'exposition Géoscientifique. Congrès de Québec Exploration. pp. 2003–2005.

Goldstein, S., O'Nions, R.K., Hamilton, P.J. 1984. A Sm-Nd isotopic study of atmospheric dusts and particulates from major river systems. Earth and Planetary Science Letters, 70(2): 221–236. https://doi.org/10.1016/0012-821X(84)90007-4

Gower, C.F. 1996. The evolution of the Grenville Province in eastern Labrador, Canada. Geological Society of London Special Publication, 112: 197–218. doi:10.1144/GSL.SP.1996.112.01.11

Gower, C.F., Krogh, T.E. 2002. A U-Pb geochronological review of the Proterozoic history of the eastern Grenville Province. Canadian Journal of Earth Sciences, 39(5): 795–829. doi:10.1139/e01-090

Gower, C.F., Tucker, R.D. 1994. Distribution of pre-1400 Ma crust in the Grenville province: Implications for rifting in Laurentia-Baltica during geon 14. Geology, 22(9): 827–830. doi: 10.1130/0091-7613(1994)022<0827:DOPMCI>2.3.CO;2

Gower, C.F., Ryan, A.B., Rivers, T. 1990. Mid-Proterozoic Laurentia-Baltica: an overview of its geological evolution and a summary of the contributions made by this volume. *In* Mid-Proterozoic Laurentia-Baltica. *Edited by* C.F. Gower, T. Rivers, and A.B. Ryan. Geological Association of Canada, Special Paper 38, pp. 1–20.

Hanmer, S., Corrigan, D., Pehrsson, S., Nadeau, L. 2000. SW Grenville Province, Canada: the case against post–1.4 Ga accretionary tectonics. Tectonophysics, 319: 33–51. doi:10.1016/S0040-1951(99)00317-0

Harper, G.D. 2003. Fe-Ti basalts and propagating-rift tectonics in the Josephine Ophiolite. Geological Society of America Bulletin, 115(7): 771–787. doi: 10.1130/0016-7606(2003)115<0771:FBAPTI>2.0.CO;2

Hartel, T.H.D., Pattison, D.R.M. 2003. Genesis of the Kapuskasing (Ontario) migmatitic mafic granulites by dehydration melting of amphibolite: the importance of quartz to reaction progress. Journal of Metamorphic Geology, 14: 591–611. doi:10.1046/j.1525-1314.1996.00404.x

Hébert, C., Cadieux, A.-M., van Breemen, O. 2005. Temporal evolution and nature of Ti–Fe–P mineralization in the anorthosite–mangerite– charnockite–granite (AMCG) suites of the south- central Grenville Province, Saguenay – Lac St. Jean area, Quebec, Canada. Canadian Journal of Earth Sciences, 42(10): 1865–1880. doi:10.1139/e05-050

Hibbard, M.J. 1981. The magma mixing origin of mantled feldspars. Contributions to Mineralogy and Petrology, 76(2): 158–170. doi:10.1007/BF00371956

Hoffman, P.F. 1988. United Plates of America, the birth of a craton: early Proterozoic assembly and growth of Laurentia. Annual Review of Earth and Planetary Sciences, 16(1): 543–603. doi:10.1146/annurev.ea.16.050188.002551

Hynes, A., Rivers, T. 2010. Protracted continental collision – evidence from the Grenville Orogen. Canadian Journal of Earth Sciences, 47(5): 591–620. doi:10.1139/E10-003

Hynes, A., Indares, A., Rivers, T., Gobeil, A. 2000. Lithoprobe line 55: integration of out-of-plane seismic results with surface structure, metamorphism, and geochronology, and the tectonic evolution of the eastern Grenville Province. Canadian Journal of Earth Sciences, 37(2-3): 341–358. doi:10.1139/e99-076

Indares, A. 1997. Garnet-kyanite clinopvroxenites and garnet-kyanite restites from the manicouagan imbricate zone: A case of high-P - High-T metamorphism in the Grenville Province. Canadian Mineralogist, 35: 1161–1171.

Indares, A.D. 2003. Metamorphic textures and P-T evolution of high-P granulites from the Lelukuau terrane, NE Grenville Province. Journal of Metamorphic Geology, 21: 35–48. doi: 10.1046/j.1525-1314.2003.00414.x

Indares, A., Dunning, G. 2004. Crustal architecture above the high-pressure belt of the Grenville Province in the Manicouagan area: New structural, petrologic and U-Pb age constraints. Precambrian Research, 130: 199–228. doi: 10.1016/j.precamres.2003.11.005

Indares, A., Dunning, G., Cox, R., Gale, D., Connelly, J. 1998. High-pressure, high-temperature rocks from the base of thick continental crust: Geology and age constraints from the Manicouagan Imbricate Zone, eastern Grenville Province. Tectonics, 17(3): 426–440. doi: 10.1029/98TC00373

Indares, A., Dunning, G., Cox, R. 2000. Tectono-thermal evolution of deep crust in a Mesoproterozoic continental collision setting: the Manicouagan example. Canadian Journal of Earth Sciences, 37(2-3): 325–340. doi: 10.1139/cjes-37-2-3-325

Ishikawa, Y., Sawaguchi, T., Iwaya, S., and Horiuchi, M. 1976. Delineation of prospecting targets for Kuroko deposits based on modes of volcanism of underlying dacite and alteration halos. Mining Geology, 26: 105–117 (in Japanese with English abs.) https://doi.org/10.11456/shigenchishitsu1951.26.105

Jamieson, R.A., Beaumont, C., Nguyen, M.H., Lee, B. 2002. Interaction of metamorphism, deformation and exhumation in large convergent orogens. Journal of Metamorphic Geology, 20: 9–24. doi:10.1046/j.0263-4929.2001.00357.x

Jenner, G.A. 1996. Trace element geochemistry of igneous rocks: geochemical nomenclature and analytical geochemistry. *In* Trace Element Geochemistry of Volcanic Rocks: Applications for Massive Sulphide Exploration. *Edited by* D.A. Wyman. Geological Association of Canada, Short Course Notes, Vol. 12, pp. 51–77.

Jensen, L.S., Pyke, D.R. 1982. Komatiites in the Ontario portion of the Abitibi belt. *In* Komatiites. *Edited by* N.T. Arndt and E.G. Nesbitt. Allen and Unwin, London. pp. 147–157.

Jiang, S.-Y., Wang, R.-C., Xu, X.-S., Zhao, K.-D. 2005. Mobility of high field strength elements (HFSE) in magmatic-, metamorphic-, and submarine-hydrothermal systems. Physics and Chemistry of the Earth, Parts A/B/C, 30(17-18): 1020–1029. https://doi.org/10.1016/j.pce.2004.11.004

Juster, T.C., Grove, T.L., Perfit, M.R. 1989. Experimental constraints on the generation of FeTi basalts, andesites, and rhyodacites at the Galapagos Spreading Center, 85°W and 95°W. Journal of Geophysical Research, 94(B7): 9251–9274. doi: 10.1029/JB094iB07p09251

Kamber, B.S., Anthony, Ewart, A., Collerson, K.D., Bruce, M.C., Mcdonald, G.D. 2002. Fluid-mobile trace element constraints on the role of slab melting and implications for Archaean crustal growth models. Contributions to Mineralogy and Petrology, 144: 38–56. doi:10.1007/s00410-002-0374-5

Kelemen, P.B., Hanghøj, K., Greene, A.R. 2014. One view of the geochemistry of subduction-related magmatic arcs, with an emphasis on primitive andesite and

lower crust. *In* Treatise on Geochemistry (Second Edition), Vol. 4. The Crust. *Edited by* Heinrich D. Holland and Karl K. Turekian, Elsevier, Amsterdam. pp. 749–806. doi: 10.1016/B978-0-08-095975-7.00323-5

Koyaguchi, T. 1986. Textural and compositional evidence for magma mixing and its mechanism, Abu volcano group, southwestern Japan. Contribution to Mineralogy and Petrology, 93: 33–45. doi: 10.1007/BF00963583

Kuno, H. 1950. Petrology of Hakone volcano and the adjacent areas, Japan. Geological Society of America Bulletin, 61(9): 957–1020. doi:10.1130/0016-7606(1950)61[957:POHVAT]2.0.CO;2

Laflèche, M.R., Dupuy, C., Bougault, H. 1992. Geochemistry and petrogenesis of Archean mafic volcanic rocks of the southern Abitibi Belt, Québec. Precambrian Research, 57(3-4): 207–241. doi:10.1016/0301-9268(92)90003-7

Larbi, Y., Stevenson, R., Verpaelst, P., Brisebois D., and Madore, L. 2003. Caractérisations isotopique (Sm–Nd) et géochimique du Groupe de Wakeham: un bassin sédimentaire protérozoïque dans la Province de Grenville. *In* Synthèse géologique et métallogénique de la partie est de la Province de Grenville. *Edited by* D. Brisebois and T. Clark. Ministère des Ressources naturelles, de la Faune et des Parcs, Québec, DV 2002-03, pp. 247–268.

Large, R.R., Gemmell, J.B., Paulick H., Huston, D.L. 2001. The alteration box plot: a simple approach to understanding the relationship between alteration mineralogy and lithogeochemistry associated with volcanic-hosted massive sulfide deposits. Economic Geology, 96(5): 957–971. 10.2113/gsecongeo.96.5.957

Lasalle, S., Indares, A. 2014. Anatectic record and contrasting P–T paths of aluminous gneisses from the central Grenville Province. Journal of Metamorphic Geology, 32(6): 626–646. doi:10.1111/jmg.12083

Lasalle, S., Fisher, C.M., Indares, A., Dunning, G. 2013. Contrasting types of Grenvillian granulite facies aluminous gneisses: Insights on protoliths and metamorphic events from zircon morphologies and ages. Precambrian Research, 228: 117–130. http://dx.doi.org/10.1016/j.precamres.2013.01.014

Lasalle, S., Dunning, G.R., Indares, A. 2014. In situ laser ablation–ICPMS dating of monazite from aluminous gneisses: Insights on the tectono-metamorphic history of a granulite-facies domain in the central Grenville Province. Canadian Journal of Earth Sciences, 51(6): 558-572. doi:10.1139/cjes-2013-0170

Lindline, J., Crawford, W.A., Crawford, M.L. 2004. A bimodal volcanic--plutonic system: the Zarembo Island extrusive suite and the Burnett Inlet intrusive complex. Canadian Journal of Earth Sciences, 41(4): 355–375. doi:10.1139/E04-009

Ludden, J., Gélinas, L., Trudel, P. 1982. Archean metavolcanics from the Rouyn–Noranda district, Abitibi Greenstone Belt, Quebec. 2. Mobility of trace elements and petrogenetic constraints. Canadian Journal of Earth Sciences, 19(12): 2276–2287. doi:10.1139/e82-200

Martin, C., Dickin, A.P. 2005. Styles of Proterozoic crustal growth on the southeast margin of Laurentia: evidence from the central Grenville Province northwest of Lac St.-Jean, Quebec. Canadian Journal of Earth Sciences, 42(10): 1643–1652. doi:10.1139/e05-052

Mattinson, J.M. 2005. Zircon U–Pb chemical abrasion (CA-TIMS) method; combined annealing and multi-step partial dissolution analysis for improved precision and

accuracy of zircon ages. Chemical Geology, 220(1-2): 47–66. doi:10.1016/j.chemgeo.2005.03.011

McLelland, J., Ashwal, L., Moore, L. 1994. Composition and petrogenesis of oxide-, apatite-rich gabbronorites associated with Proterozoic anorthosite massifs: examples from the Adirondack Mountains, New York. Contributions to Mineralogy and Petrology, 116: 225–238. doi: 10.1007/BF00310702

Meschede, M., 1986. A method of discriminating between different types of mid-ocean ridge basalts and continental tholeiites with the Nb–Sr–Y diagram. Chemical Geology, 56(3-4): 207-218. https://doi.org/10.1016/0009-2541(86)90004-5

Montreuil, J.F., Constantin, M. 2010. The geochemistry of mafic gneisses from the Renzy terrane, western Grenville Province, Quebec: implications for the geodynamic setting of the early Mesoproterozoic Laurentian margin. Precambrian Research, 181: 150–166. doi: 10.1016/j.precamres.2010.06.001

Morse, S.A. 1980. Kiglapait mineralogy II: Fe-Ti oxide minerals and the activities of oxygen and silica. Journal of Petrology, 21: 685–719. doi:10.1093/petrology/21.4.685.

Moukhsil, A., Solgadi, F., Lacoste, P., Gagnon, M., David, J. 2012. Géologie de la région du lac du Milieu (SNRC 22O03, 22O04, 22O06, 22J13 et 22J14). Ministère des Ressources naturelles, Québec. RG 2012-01.

Moukhsil, A., Solgadi, F., Thomas, C., Séverine, B., Indares, A., Davis, D.W. 2013a. Géologie du nord-ouest de la région du barrage Daniel-Johnson (Manic 5), Côte-Nord. Ministère des Ressources naturelles, Québec. RG 2013-01.

Moukhsil, A., Solgadi, F., Indares, A., Belkacim, S. 2013b. Géologie de la région septentrionale du réservoir aux Outardes 4, Côte-Nord. Ministère des Ressources naturelles, Québec. RG 2013-03.

Nadeau, L., van Breemen, O. 1994. Do the 1.45–1.39 Ga Montauban Group and the La Bostonnais complex constitute a Grenvillian accreted terrane? Geological Association of Canada–Mineralogical Association of Canada, Annual Meeting, Program with Abstracts, 19: A81.

Nielsen, A.B., Thorkelson, D.J., Gibson, H.D., Marshall, D.D. 2013. The Wernecke igneous clasts in Yukon, Canada: Fragments of the Paleoproterozoic volcanic arc terrane Bonnetia. Precambrian Research, 238: 78–92. doi:10.1016/j.precamres.2013.09.017

Owens, B.E., Dymek, R.F. 1992. Fe-Ti-P-rich rocks and massif anorthosite; problems of interpretation illustrated from the Labrieville and St-Urbain plutons, Quebec. Canadian Mineralogist, 30: 163–190.

Pattison, D.R.M. 2003. Petrogenetic significance of orthopyroxene-free garnet + clinopyroxene + plagioclase ± quartz-bearing metabasites with respect to the amphibolite and granulite facies. Journal of Metamorphic Geology, 21: 21–34. doi:10.1046/j.1525-1314.2003.00415.x

Pattison, D.R.M., Chacko, T., Farquhar, J., McFarlane, C.R.M. 2003. Temperatures of granulite-facies metamorphism: constraints from experimental phase equilibria and thermobarometry corrected for retrograde exchange. Journal of Petrology, 44(5): 867–900. doi:10.1093/petrology/44.5.867

Pearce, J.A. 1983. Role of sub-continental lithosphere in magma genesis at active continental margins. *In* Continental Basalts and Mantle Xenoliths. *Edited by* C.J. Hawkesworth, M.J. Norry. Shiva, Nantwich, pp. 230–249.

Pearce, J.A. 1996. A user's guide to basalt discrimination diagrams. Trace element geochemistry of volcanic rocks: applications for massive sulphide exploration. Geological Association of Canada, Short Course Notes, Vol. 12 (79). pp 79–113.
Pearce, J.A. 2008. Geochemical fingerprinting of oceanic basalts with applications to ophiolite classification and the search for Archean oceanic crust. Lithos, 100(1-4): 14–48. doi: 10.1016/j.lithos.2007.06.016
Pearce, J.A., Cann, J.R. 1973. Tectonic setting of basic volcanic rocks determined using trace element analyses. Earth and Planetary Science Letters, 19(2): 290–300.
Pearce, J.A., Peat, D.W. 1995. Tectonic implications of the composition of volcanic arc magmas. Annual Review of Earth and Planetary Sciences, 23: 251–285. doi:10.1146/annurev.ea.23.050195.001343
Pearce, J.A., Rogers, N., Tindle, A.J., Watson, J.S. 1986. Geochemistry and petrogenesis of basalts from Deep Sea Drilling Project Leg 92, Eastern Pacific. Initial Reports Deep Sea Drilling Project, 92: 435–457. doi:10.2973/dsdp.proc.92.126.1986
Pearce, J.A., Ernewein, M., Bloomer, S.H., Parson, L.M., Murton, B.J., Johnson, L.E. 1994. Geochemistry of Lau Basin volcanic rocks: influence of ridge segmentation and arc proximity. Geological Society of London Special Publications, 81: 53–75. doi:10.1144/GSL.SP.1994.081.01.04
Peng, T., Wilde, S.A., Fan, W., Peng, B., Mao, Y. 2013. Mesoproterozoic high Fe–Ti mafic magmatism in western Shandong, North China Craton: petrogenesis and implications for the final breakup of the Columbia supercontinent. Precambrian Research, 235: 190–207. doi: 10.1016/j.precamres.2013.06.013
Philpotts, A.R. 1981. A model for the generation of massif-type anorthosites. Canadian Mineralogist, 19: 233–253.
Piercey, S.J., Murphy, D.C., Creaser, R.A. 2012. Lithosphere-asthenosphere mixing in a transform-dominated late Paleozoic backarc basin: implications for northern Cordilleran crustal growth and assembly. Geosphere, 8(3): 716–739. doi:10.1130/GES00757.1
Pinet, N. 2016. Southern continuation of the Wakeham Group and Robe-Noire mafic suite (eastern Grenville Province) from hydrocarbon-targeted seismic reflection data on Anticosti Island, Quebec, Canada. Canadian Journal of Earth Sciences, 53(9): 875–882. doi:10.1139/cjes-2016-0011
Raveggi, M., Giles, D., Foden, J., Raetz, M. 2007. High Fe-Ti mafic magmatism and tectonic setting of the Paleoproterozoic Broken Hill Block, NSW, Australia. Precambrian Research, 156(1-2): 55–84. doi: 10.1016/j.precamres.2007.02.006
Rivers, T. 1997. Lithotectonic elements of the Grenville Province: review and tectonic implications. Precambrian Research, 86(3-4): 117–154. doi:10.1016/S0301-9268(97)00038-7
Rivers, T. 2008. Assembly and preservation of lower, mid, and upper orogenic crust in the Grenville Province—Implications for the evolution of large hot long-duration orogens. Precambrian Research, 167(3-4): 237–259. doi: 10.1016/j.precamres.2008.08.005
Rivers, T., Corrigan, D. 2000. Convergent margin on southeastern Laurentia during the Mesoproterozoic: tectonic implications. Canadian Journal of Earth Sciences, 37(2-3): 359–383. doi:10.1139/e99-067

Rivers, T., Martignole, J., Gower, C.F., Davidson, A. 1989. New tectonic divisions of the Grenville Province, Southeast Canadian Shield. Tectonics, 8(1): 63–84. doi:10.1029/TC008i001p00063

Rivers, T., Culshaw, N., Hynes, A., Indares, A., Jamieson, R., Martignole, J. 2012. The Grenville orogen–a post-Lithoprobe perspective. *In* Tectonic Styles in Canada: The Lithoprobe perspective. *Edited by* J.A. Percival, F.A. Cook, and R.M Clowes. Geological Association of Canada, Special Paper, 49: 97-236.

Rosing, M.T. 1990. The theoretical effect of metasomatism on Sm-Nd isotopic systems. Geochimica et Cosmochimica Acta, 54(5): 1337–1341. doi:10.1016/0016-7037(90)90158-H

Rubin, J.N., Henry, C.D., Price, J.G. 1993. The mobility of zirconium and other "immobile" elements during hydrothermal alteration. Chemical Geology, 110(1-3): 29–47. doi:10.1016/0009-2541(93)90246-F

Rudnick, R.L. 1992. Restites, Eu anomalies and the lower continental crust. Geochimica et Cosmochimica Acta, 56(3): 963–970. doi:10.1016/0016-7037(92)90040-P

Rudnick, R.L., Gao, S. 2014. Composition of the continental crust. *In* Treatise on Geochemistry (Second Edition), Vol. 4. The Crust. *Edited by* Heinrich D. Holland and Karl K. Turekian, Elsevier, Amsterdam. pp. 1–51. DOI: 10.1016/B978-0-08-095975-7.00301-6

Rudnick, R.L., McLennan, S.M., and Taylor, S.R. 1985. Large iron lithophile elements in rocks from high-pressure granulite facies terrains. Geochimica et Cosmochimica Acta, 49: 1645–1655. doi:10.1016/0016-7037(85)90268-6

Rutherford, L., Barovich, K., Hand, M., Foden, J. 2006. Continental ca. 1.7-1.69 Ga Fe-rich metatholeiites in the Curnamona Province, Australia: a record of melting of a heterogeneous, subduction-modified lithospheric mantle. Australian Journal of Earth Sciences, 53(3): 501–519. doi: 10.1080/08120090600632466

Sappin, A. A., Constantin, M., Clark, T., van Breemen, O. 2009. Geochemistry, geochronology, and geodynamic setting of Ni-Cu±PGE mineral prospects hosted by mafic and ultramafic intrusions in the Portneuf-Mauricie Domain, Grenville Province, Quebec. Géologie Québec Contribution 8439-2008-2009-5. Canadian Journal of Earth Sciences, 46(5): 331–353. doi:10.1139/E09-022

Sato, H. 1975. Diffusion coronas around quartz xenocrysts in andesite and basalt from Tertiary volcanic region in northeastern Shikoku, Japan. Contributions to Mineralogy and Petrology, 50(1): 49–64. doi:10.1007/BF00385221

Sawyer, E.W. 1991. Disequilibrium melting and the rate of melt-residuum separation during migmatisation of mafic rocks from the Grenville Front, Québec. Journal of Petrology, 32(4): 701-738. https://doi.org/10.1093/petrology/32.4.701

Schärer, U., Krogh, T.E., and Gower, C.F. 1986. Age and evolution of the Grenville Province in Eastern Labrador from U-Pb systematics in accessory minerals. Contributions to Mineralogy and Petrology, 94: 438 -451. https://doi.org/10.1007/BF00376337

Schellart, W.P. 2008a. Overriding plate shortening and extension above subduction zones: a parametric study to explain formation of the Andes Mountains. Geological Society of America Bulletin, 120(11-12): 1441–1454. doi:10.1130/B26360.1

Schellart, W.P. 2008b. Subduction zone trench migration: slab driven or overriding-plate driven? Physics of the Earth and Planetary Interiors, 170(1-2): 73–88. doi:10.1016/j.pepi.2008.07.040

Shaw, D.M. 1968. A review of K/Rb fractionation trends to covariance analysis. Geochimica Cosmochimica Acta, 32(6): 573-602. https://doi.org/10.1016/0016-7037(68)90050-1

Sinton, J.M., Wilson, D.S., Christie, D.M., Hey, R.N., Delaney, J.R. 1983. Petrological consequences of rift propagation on oceanic spreading ridges. Earth and Planetary Science Letters, 62: 193–207. doi:10.1016/0012-821X(83)90083-3

Slagstad, T., Culshaw, N.G., Jamieson, R.A., Ketchum, J.W. 2004. Early Mesoproterozoic tectonic history of the southwestern Grenville Province, Ontario: constraints from geochemistry and geochronology of high-grade gneisses. Geological Society of America Memoirs, 197: 209–241. doi:10.1130/0-8137-1197-5.209

Slagstad, T., Culshaw, N.G., Daly, J.S., Jamieson, R.A. 2009. Western Grenville Province holds key to midcontinental Granite-Rhyolite Province enigma. Terra Nova, 21: 181–187. doi:10.1111/j.1365-3121.2009.00871.x

Smith, T.E., Harris, M.J., Huang, C.H., Holm, P.E. 2001. The geochemical nature of the igneous rocks of the Sharbot Lake domain, Central Metasedimentary Belt, Ontario. Canadian Journal of Earth Sciences, 38(7): 1037–1057. doi:10.1139/cjes-38-7-1037

Sorensen, S.S., Grossman, J.N. 1989. Enrichment of trace elements in garnet amphibolites from a paleo-subduction zone: Catalina Schist, southern California. Geochimica Cosmochimica Acta, 53(12): 3155–3177. doi:10.1016/0016-7037(89)90096-3

Spitz, G., Darling, R. 1978. Major and minor element lithogeochemical anomalies surrounding the Louvem copper deposit, Val d'Or, Quebec. Canadian Journal of Earth Sciences, 15(7): 1161–1169. doi:10.1139/e78-122

Stacey, J.S., Kramers, J.D., 1975. Approximation of terrestrial lead isotope evolution by a two stage model. Earth and Planetary Science Letters. 26(2): 207–221. https://doi.org/10.1016/0012-821X(75)90088-6

Sun, S., McDonough, W. 1989. Chemical and isotopic systematics of oceanic basalts: implications for mantle composition and processes. Geological Society of London Special Publications, 42(1): 313-345. https://doi.org/10.1144/GSL.SP.1989.042.01.19

Sutcliffe, R.H. 1989. Magma mixing in late Archean tonalitic and mafic rocks of the Lac des Iles area, western Superior province. Precambrian Research, 44(2): 81–101. doi:10.1016/0301-9268(89)90077-6

Sutcliffe, R.H., Sweeny, J.M., Edgar, A.D. 1989. The Lac des Iles Complex, Ontario: petrology and platinum-group-elements mineralization in an Archean mafic intrusion. Canadian Journal of Earth Sciences, 26(7): 1408–1427. doi:10.1139/e89-120

Taylor, B., Martinez, F. 2003. Back-arc basin basalt systematics. Earth and Planetary Science Letters, 210: 481–497. doi:10.1016/S0012-821X(03)00167-5

Tanaka, T., Togashi, S., Kamioka, H., Amakawa, H., Kagami, H., Hamamoto, T., Yuhara, M., Orihashi, Y., Yoneda, S., Shimizu, H., Kunimaru, T., Takahashi, K., Yanagi, T., Nakano, T., Fujimaki, H., Shinjo, R., Asahara, Y., Tanimizu, M., Dragusanu, C. 2000. JNdi-1: A neodymium isotopic reference in consistency with

LaJolla neodymium. Chemical Geology, 168: 279–281. doi:10.1016/S0009-2541(00)00198-4

Tatsumi, Y., Hamilton, D.L., Nesbitt, R.W. 1986. Chemical characteristics of a fluid phase from a subducted lithosphere and origin of arc magmas: evidence from high pressure studies and natural rocks. Journal of Geophysical Research, 29(1-4): 293-309. https://doi.org/10.1016/0377-0273(86)90049-1

Thompson, A.B., Schulmann, K., Jezek, J., Tolar, V. 2001. Thermally softened continental extensional zones (arcs and rifts) as precursors to thickened orogenic belts. Tectonophysics, 332(1-2): 115–141. doi:10.1016/S0040-1951(00)00252-3

Thomson, S.D., Dickin, A.P., Spray, J.G. 2011. Nd isotope mapping of Grenvillian crustal terranes in the vicinity of the Manicouagan Impact Structure. Precambrian Research, 191: 184–193. doi:10.1016/j.precamres.2011.08.006

Tucker, R.D., Gower, C.F. 1994. A U-Pb geochronological framework for the Pinware Terrane, Grenville Province, Southeast Labrador. The Journal of Geology, 102(1): 67–78. https://doi.org/10.1086/629648 (Available from http://www.jstor.org/stable/30065711)

Valverde Cardenas Cardenas, C., Indares, A., Jenner, G. 2012. Mafic and ultrapotassic rocks from the Canyon domain (central Grenville Province): geochemistry and tectonic implications. Canadian Journal of Earth Sciences, 49(2): 412–433. doi:10.1139/e11-065

van Breemen, O., Corriveau, L. 2005. U-Pb age constraints on arenaceous and volcanic rocks of the Wakeham Group, eastern Grenville Province. Canadian Journal of Earth Sciences, 42(10): 1677–1697. doi:10.1139/e05-079

van Breemen, O., Davidson, A. 1988. Northeast extension of Proterozoic terranes of mid-continental North America. Geological Society of America Bulletin, 100(5): 630–638. doi:10.1130/0016-7606(1988)100<0630:NEOPTO>2.3.CO;2

Vautour, S. 2015. A new model for the Quebecia terrane in the Grenville Province as a Composite Arc Belt: Sm-Nd evidence. M.Sc. dissertation, Earth and Environmental Sciences, Macmaster University, Hamilton, Ontario. Available from http://hdl.handle.net/11375/18231

Vernon, R.H. 1990. Crystallization and hybridism in microgranitoid enclave magmas: Microstructural evidence. Journal of Geophysical Research, 95 (B11): 17849-17859. doi:10.1016/0024-4937(88)90024-2

Vernon, R.H., Etheridge, M. A., Wall, V.J. 1988. Shape and microstructure of microgranitoid enclaves: Indicators of magma mingling and flow. Lithos, 22: 1–11. doi:10.1016/0024-4937(88)90024-2

Vielzeuf, D., Clemens, J.D., Pin, C., and Moinet, E. 1990. Granites, granulites and crustal differentiation. *In* Granulites and crustal evolution. *Edited by* D. Vielzeuf and Ph. Vidal. Nato Advanced Study Institutes Series, Series C, Mathematical and Physical Sciences, No. 311, pp. 59–85.

Winchester, J.A., Floyd,P.A., 1976. Geochemical magma type discrimination: application to altered and metamorphosed basic igneous rocks. Earth and Planetary Science Letters. 28 (3), 459–469. https://doi.org/10.1016/0012-821X(76)90207-7

Wodicka, N., David, J., Parent, M., Gobeil, A., Verpaelst, P. 2003. Géochronologie U-Pb et Pb-Pb de la région de Sept-Îles–Natashquan, Province de Grenville, Moyenne-Côte-Nord. *In* Synthèse géologique et métallogénique de la partie est de la Province de Grenville. *Edited by* D. Brisebois and T. Clark. Ministère des

Ressources naturelles, de la Faune et des Parcs, Québec, DV 2002-03, pp. 59–118.
Whitmeyer, S., Karlstrom, K.E. 2007. Tectonic model for the Proterozoic growth of North America. Geosphere, 3(4): 220–259. doi:10.1130/GES00055.1
Whitney, D.L., Evans, B.W. 2010. Abbreviations for names of rock-forming minerals. American Mineralogist, 95: 185–187. doi:10.2138/am.2010.3371
Wood, D. A. 1980. The application of a Th-Hf-Ta diagram to problems of tectonomagmatic classification and to establishing the nature of crustal contamination of basaltic lavas of the British Tertiary volcanic province. Earth and Planetary Science Letters, 50 (1): 11–30. https://doi.org/10.1016/0012-821X(80)90116-8
Woodhead, J.D., Hergt, J.M., Davidson, J.P., Eggins, S.M. 2001. Hafnium isotope evidence for 'conservative' element mobility during subduction zone processes. Earth and Planetary Science Letters, 192: 331–346. https://doi.org/10.1016/S0012-821X(01)00453-8
Yang, P., Indares, A.D. 2005. Mineral zoning, phase relations, and P-T evolution of high-pressure granulites from the Lelukuau Terrane, northeastern Grenville Province, Quebec. Canadian Mineralogist, 43: 443–462. doi:10.2113/gscanmin.43.1.443
Yardley, B.W.D., 2012. The chemical composition of metasomatic fluids in the crust. *In* Metasomatism and the chemical transformation of rock. *Edited by* D.E. Harlov and H. Austrheim, Lecture Notes in Earth System Sciences, pp. 17–52.
Zheng, Y.-F., Hermann, J. 2014. Geochemistry of continental subduction-zone fluids. Earth, Planets and Space, 66: 93. doi:10.1186/1880-5981-66-93

Table 2.1. U-Pb data for the mafic samples in Complexe de la Plus Value, Canyon domain.

Sample #383c	Weight (mg)[a]	Concentration U (ppm)	Concentration Pb rad (ppm)[b]	Measured Total common Pb (pg)	Measured $^{206}Pb/^{204}Pb$	Corrected atomic ratios[c] $^{208}Pb/^{206}Pb$	$^{206}Pb/^{238}U$	$2\sigma \pm$	$^{207}Pb/^{235}U$	$2\sigma \pm$	$^{207}Pb/^{206}Pb$	$2\sigma \pm$	Age [Ma] $^{206}Pb/^{238}U$	$^{207}Pb/^{235}U$	$^{207}Pb/^{206}Pb$
Fraction															
Z1 1 euh prm	0.002	303	57.4	5.6	996	0.0573	0.1938	78	2.1362	120	0.07994	36	1142	1161	1196
Z2 1 best prm	0.002	273	52.2	9.3	559	0.0536	0.1961	152	2.1664	202	0.08012	54	1154	1170	1200
Z3 1 euh prm	0.002	202	45.2	9.7	449	0.098	0.2196	140	2.5749	236	0.08504	66	1280	1294	1316
Z4 4 best euh prm	0.006	47	9.2	5.6	653	0.0589	0.1999	90	2.2271	184	0.08079	56	1175	1190	1216
Z5 3 clr euh prm	0.004	49	8.7	2.1	1228	0.0473	0.1838	100	1.9325	170	0.07628	58	1087	1092	1102

Note:

All zircon grains were chemically abraded (Mattinson, 2005) prior to dissolution. Z, zircon; 2, 4, number of grains in analysis; prm, prism; sml, small; euh, euhedral; clr, clear.

a . Weights of grains were estimated, with potential uncertainties of 50% for these small samples.
b . Radiogenic lead
c . Atomic ratios corrected for fractionation, spike, laboratory blank of 1-2 picograms (pg) common lead, and initial common lead at the age of the sample were calculated from the model of Stacey and Kramers (1975), and 0.3 pg U blank. Two sigma uncertainties are reported after the ratios and refer to the final digits.

Table 2.2. Sm-Nd data for the mafic rocks in Canyon domain.

Sample	Geol. Domain	Nd (ppm)	Sm (ppm)	Sm/Nd	$^{147}Sm/^{144}Nd_{calc}$	$^{143}Nd/^{144}Nd_{meas}$	2σ	$^{143}Nd/^{144}Nd_{ini}$	εNd_{0}	$\varepsilon Nd_{1.4\ Ga}$	T_{DM}	T_{DM} (DePaolo)	T_{CHUR}
RS383E^{++}	PLV	34.13	9.25	0.27	0.1638	0.512314	8	0.510807	-6.2	-0.4	2573	2206	1495
383c	PLV	30.64	8.58	0.28	0.1693	0.512362	7	0.510805	-5.2	-0.4	2723	2318	1526
395-d1	MIU	56.22	16.86	0.30	0.1813	0.512304	7	0.510637	-6.4	-3.7		3668	
395-dx	MIU	52.70	16.81	0.32	0.1928	0.512368	7	0.510595	-5.1	-4.6			
RS395$a_2$$^{+}$	MIU	44.38	9.856	0.22	0.1342	0.512106	3	0.510871	-10.2	0.9	2015	1777	1292
RS209-1^{+}	QFU	20.99	5.15	0.25	0.1482	0.512191	6	0.510828	-8.6	0.0	2247	1961	1399

Note:

1. calc = calculated, meas = measured, ini = initial, T_{DM} = depleted mantle model age.

2. T_{DM} values are calculated based on present day $(^{147}Sm/^{144}Nd)_{DM} = 0.2137$ and $(^{143}Nd/^{144}Nd)_{DM} = 0.513160$ (Goldstein et al., 1984) of depleted mantle based on the assumption that this mantle was separated from the CHUR at 4.55 Ga with a linear evolution, and present day εNd value of +10. T_{DM} (DePaolo) is calculated after DePaolo (1981a).

3. $T_{DM} = 1/\lambda \times \ln[1+\{(^{143}Nd/^{144}Nd)_{sample} - 0.513160\}/\{(^{147}Sm/^{144}Nd)_{sample} - 0.2137\}]$

4. εNd and T_{CHUR} values are calculated based on chondrite uniform reservoir (CHUR) values of $^{147}Sm/^{144}Nd = 0.1960 \pm 4$ and $^{143}Nd/^{144}Nd = 0.512630 \pm 11$ (2) (Bouvier et al., 2008), and $\lambda\ ^{147}Sm = 6.539\ (\pm 0.061) \times 10^{-12}\ Yr^{-1}$ (Begemann et al., 2001). 2 = 2 standard error of the mean x 10^{-6}.

5. $(^{147}Sm/^{144}Nd)_{calc} = Sm/Nd \times [0.53151+0.14252\ (^{143}Nd/^{144}Nd)_{meas}]$

6. The results of isotopic measurements for Nd reference material JNdi-1 (Nd) = 512098 ± 6 (2σ, n = 15).

7. Samples with superscript + are from Valverde Cardenas et al. (2012); superscript ++ indicates previously analyzed samples published here; all samples recalculated based on the values of CHUR and DM used here.

8. All model ages and εNd values are calculated using U-Pb crystallization ages (t) determined for the mafic sill in PLV (this study), the light grey rock in MIU (Dunning and Indares, 2010), and an estimated age of 1.4 Ga for the QFU (Valverde Cardenas et al., 2012; Indares and Moukhsil, 2013).

9. Sm and Nd concentrations were obtained by FUS-MS and have detection limits of 0.1 ppm.

Table 2.3. Major and trace element data for the mafic rocks in Canyon domain.

Suite	PLV	PLV	PLV	PLV	MIU	MIU	MIU	MIU	MIU	MIU	MIU	QFU	QFU
Sample	11-383c	RS383E^{++}	RS399^{++}	RS383E1^{++}	11-395dx	11-395d1	11-395d4	RS395A1	11-395	11-395g2	RS395A2^{+}	RS206C1^{+}	RS 209-1^{+}
SiO_2	46.21	45.03	43.76	44.36	40.55	40.36	40.38	42.58	46.55	46.54	46.08	53.38	52.95
Al_2O_3	13.35	13.14	14.01	12.69	13.53	12.30	14.07	12.56	19.05	20.34	18.09	14.55	15.83
$Fe_2O_{3\,(T)}$	19.44	20.30	19.75	20.72	23.75	25.44	22.01	21.85	13.26	13.06	13.35	14.34	12.83
MnO	0.30	0.30	0.28	0.32	0.41	0.45	0.33	0.27	0.18	0.16	0.19	0.22	0.19
MgO	5.72	6.03	6.53	6.6	5.86	6.04	5.96	7.08	4.64	3.56	4.82	4.73	8.13
CaO	9.60	10.05	10.27	10.08	10.63	11.49	10.71	10.72	8.83	8.56	9.08	8.15	8.15
Na_2O	1.66	1.17	1.00	1.54	0.95	0.59	1.32	1.14	3.01	3.00	3.02	0.78	0.74
K_2O	0.89	0.90	0.67	0.59	0.40	0.13	0.84	0.89	1.91	2.06	1.83	0.77	0.23
TiO_2	2.65	2.84	2.64	3.44	3.70	4.05	3.52	2.99	1.78	1.83	1.82	2.12	0.94
P_2O_5	0.48	0.49	0.44	0.32	0.45	0.70	0.45	0.27	0.52	0.78	0.50	0.45	0.07
LOI	-0.64	-0.87	-0.28	-0.6	-0.67	-0.96	-0.55	< 0.01	0.87	0.13	0.45	< 0.01	-0.02
Total	99.66	99.38	99.07	100.06	99.56	100.59	99.04	100.35	100.6	100.02	99.23	99.49	100.04
FeO_t	17.49	18.27	17.77	18.64	21.37	22.89	19.8	19.66	11.93	11.75	12.01	12.9	11.54
#Mg	0.37	0.37	0.40	0.39	0.33	0.32	0.35	0.39	0.41	0.35	0.42	0.40	0.56
Sc	50	52	50	58	63	66	60	60	29	19	34	43	37
V	460	446	435	742	616	470	623	803	282	134	302	260	229
Cr	50	52	71	—	< 20	< 20	< 20	60	< 20	< 20	< 20	40	288
Co	130	233	177	203	189	148	171	278	66	53	158	297	168
Ni	40	50	64	70	< 20	< 20	< 20	100	< 20	< 20	< 20	30	81
Cu	80	26	45	35	20	20	20	70	20	< 10	< 10	10	34
Zn	130	158	133	209	130	170	180	210	90	140	190	180	161
Y	58	57	49	70	91	104	86	39	34	31	43	60	28
Zr	170	183	154	50	152	216	164	96	112	425	135	272	57
Hf	4.5	5.1	4.5	2.0	4.1	5.2	4.8	2.9	3.1	8.5	4.0	6.9	2.0
Ga	19	19	23	18	18	15	28	21	24	25	25	21	21
Ge	2	—	—	—	4	3	3	2	2	2	1	2	—
Nb	14	13	9	27	34	27	27	9	9	10	11	14	4
Ta	2.0	1.0	0.5	1.5	3.7	2.5	3.4	0.8	1.0	1.0	0.5	0.9	0.3
Rb	48	40	17	9	11	2	9	29	64	62	101	40	10
Ba	310	269	141	198	111	22	115	147	1000	1085	614	556	63
Sr	134	122	221	156	110	73	163	149	897	949	606	212	132
Pb	< 5	—	—	—	< 5	< 5	< 5	7	< 5	7	21	8	—
Th	0.5	0.6	0.4	1.0	1.1	1.1	2.4	0.6	1.0	2.8	1.6	3.2	3.2
U	0.5	0.5	0.3	0.7	0.6	0.6	1.2	0.3	0.4	0.6	0.7	1.3	1.6
Cs	0.6	—	—	—	< 0.5	< 0.5	< 0.5	0.4	0.5	0.6	1.3	0.4	—
La	16.7	17.4	19.1	16.0	23.2	27.1	39.2	19.3	25.2	32.5	29.4	41.3	12.6
Ce	45.4	49.1	51.2	48.8	68.0	75.8	112.0	54.5	60.7	78.0	73.4	91.5	34.2
Pr	6.8	7.1	6.9	7.9	11.1	11.6	16.8	7.5	8.6	9.7	10.2	11.8	4.7
Nd	32.8	33.1	32.0	41.6	55.6	57.9	76.1	31.7	40.3	42.7	45.3	49.7	20.8
Sm	9.3	9.2	8.5	13.7	18.4	18.1	19.1	7.5	9.4	9.0	10.2	10.9	5.4
Eu	2.08	2.28	2.48	1.78	1.90	1.95	3.47	2.19	2.33	2.41	2.85	2.71	1.10
Gd	9.6	10.1	9.1	14.8	20.5	19.6	17.4	7.6	7.9	8.3	9.6	10.7	5.4
Tb	1.7	1.9	1.7	2.7	3.3	3.3	2.7	1.3	1.2	1.3	1.5	1.9	1.0
Dy	10.7	10.8	9.5	14.5	18.4	19.3	15.3	7.0	6.8	6.8	7.7	10.6	5.5
Ho	2.2	2.2	1.9	2.6	3.5	3.8	3.0	1.3	1.4	1.3	1.4	2.0	1.1
Er	6.3	6.7	5.8	7.4	9.9	10.9	8.8	3.9	3.8	3.6	4.2	6.2	3.3
Tm	0.93	1.02	0.87	1.05	1.42	1.61	1.28	0.61	0.55	0.54	0.62	0.94	0.50
Yb	5.9	6.2	5.4	6.2	8.9	10.3	8.0	3.8	3.6	3.3	3.8	5.9	3.0
Lu	0.97	0.88	0.79	0.84	1.36	1.59	1.26	0.56	0.55	0.53	0.55	0.85	0.40
∑REE	151.4	158.0	155.2	179.9	245.5	262.9	324.4	148.9	172.4	200.0	200.8	247.0	98.9
Eu/Eu*	0.67	0.72	0.86	0.38	0.30	0.32	0.58	0.89	0.83	0.85	0.88	0.77	0.62
Ti/Eu	7638	7467	6382	11586	11674	12451	6081	8185	4580	4552	3828	4690	5123
Zr/Hf	38	36	34	26	37	42	34	33	36	50	34	39	29
Ti/Y	274	297	321	293	244	233	245	457	314	354	251	210	201
Zr/Y	3	3	3	1	2	2	2	2	3	14	3	5	2
Ti/Zr	93	93	103	412	146	112	129	187	95	26	81	47	99
Zr/Yb	29	30	29	8	17	21	21	25	31	129	35	46	19
$(La/Nb)_{PM}$	1.2	1.3	2.2	0.6	0.7	1.0	1.5	2.3	2.9	3.4	2.7	3.1	3.5
$(Nb/Th)_{PM}$	3.3	2.7	2.9	3.2	3.7	2.9	1.3	1.9	1.1	0.4	0.8	0.5	0.1
$(La/Yb)_{CN}$	2.0	2.0	2.6	1.8	1.9	1.9	3.5	3.6	5.0	7.1	5.5	5.1	3.0
$(Gd/Yb)_{CN}$	1.3	1.3	1.4	2.0	1.9	1.6	1.8	1.6	1.8	2.1	2.1	1.5	1.5
$(La/Sm)_{CN}$	1.2	1.2	1.4	0.8	0.8	1.0	1.3	1.7	1.7	2.3	1.9	2.4	1.5
A.I	37.0	38.0	39.0	38.0	35.0	34.0	36.0	40.0	36.0	33.0	35.0	38.0	48.0
CCPI	91	93	94	93	96	98	93	93	78	77	79	92	96
P.I	0.63	0.62	0.67	0.59	0.63	0.56	0.62	0.56	0..83	0.89	0.77	0.52	0.57
K_2O/Na_2O	0.5	0.8	0.7	0.4	0.4	0.2	0.6	0.8	0.6	0.7	0.6	1.0	0.3
Al_2O_3/Na_2O	8.0	11.2	14.0	8.2	14.2	20.8	10.7	11.0	6.3	6.8	6.0	18.7	21.4

Note:

1. The oxide concentrations are reported in wt%, whereas trace element concentrations are reported in ppm.
2. The deviation of Eu from the rest of the REE can be expressed as Eu anomaly (Eu/Eu*), where Eu* refers to the value obtained by linear interpolation between adjacent elements.
3. $FeO_t = 0.8998 \times Fe_2O_3$; $Ti = 5995 \times TiO_2$
4. #Mg is calculated as #Mg = MgO/(MgO + $Fe_2O_{3\,total}$) in moles.
5. Superscript + indicates 1.41 Ga arc rocks from Valverde Cardenas et al. (2012). QFU, Quartzofeldspathic unit (see Indares and Moukhsil, 2013 for definitions).
6. Superscript ++ indicates previously analyzed unpublished data.
7. Subscript 'PM' indicates primitive mantle-normalized and 'CN' indicates chondrite-normalized values of Sun and McDonough (1989).
8. A.I, alteration index; P.I, peraluminous index; CCPI, chlorite-carbonate-pyrite index; see text for details.

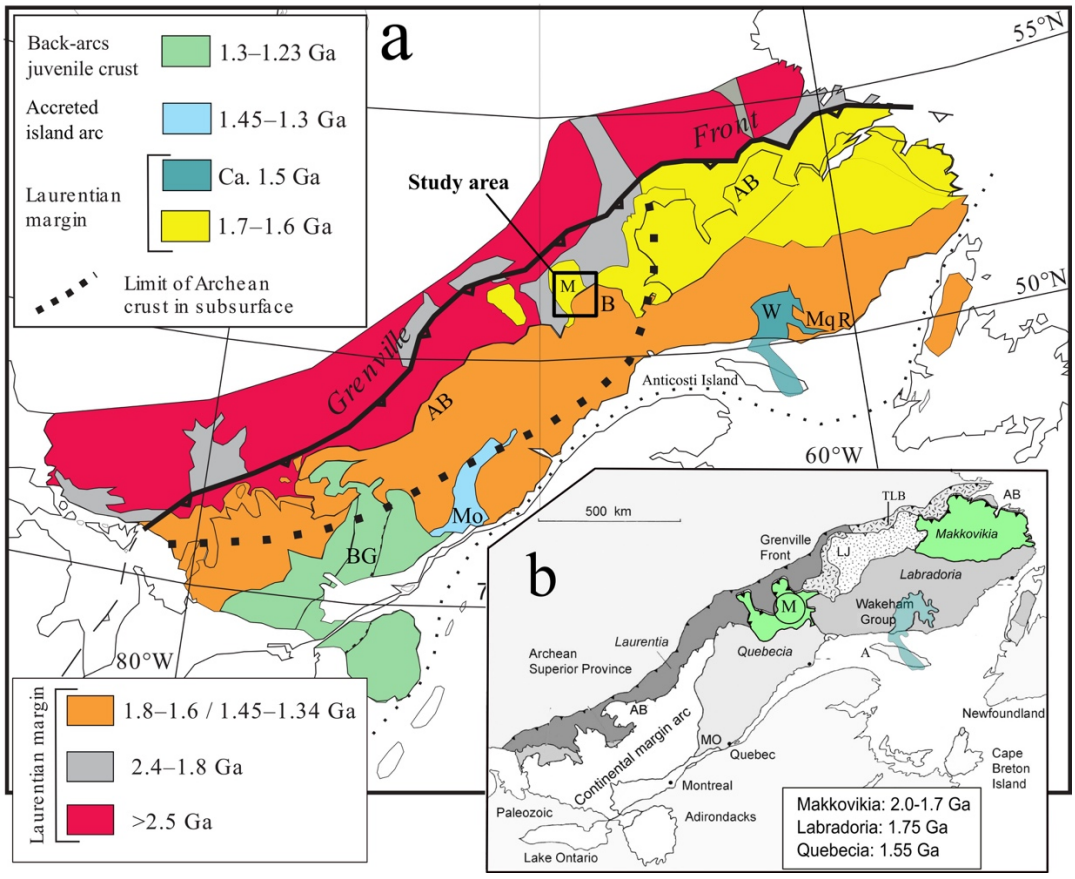

Figure 2.1. (a) Schematic map of the Grenville Province showing principal crustal age (U-Pb) domains in the pre-Grenvillian Laurentian crust (simplified from Rivers et al., 2012), with the southern continuation of the Wakeham Group under Paleozoic rocks on Anticosti Island after Pinet (2016); (b) Schematic map of the Grenville Province showing principal crustal domains or terranes based on crustal formation ages (Nd model ages; modified from Thomson et al., 2011 and Vautour, 2015). A, Anticosti Island; AB, Allochthon Boundary; BG, Bondy Gneiss Complex; B, Bardoux Plutonic Suite; LJ, Lac Joseph allochthon, largely composed of metasedimentary rocks with a Makkovikian model age; M, Manicouagan Impact Crater; Mo, Montauban; Mq, Lac Masquaro; R, Musquaro-La Romaine extension; TLB, Trans-Labrador batholith; W, Wakeham Group.

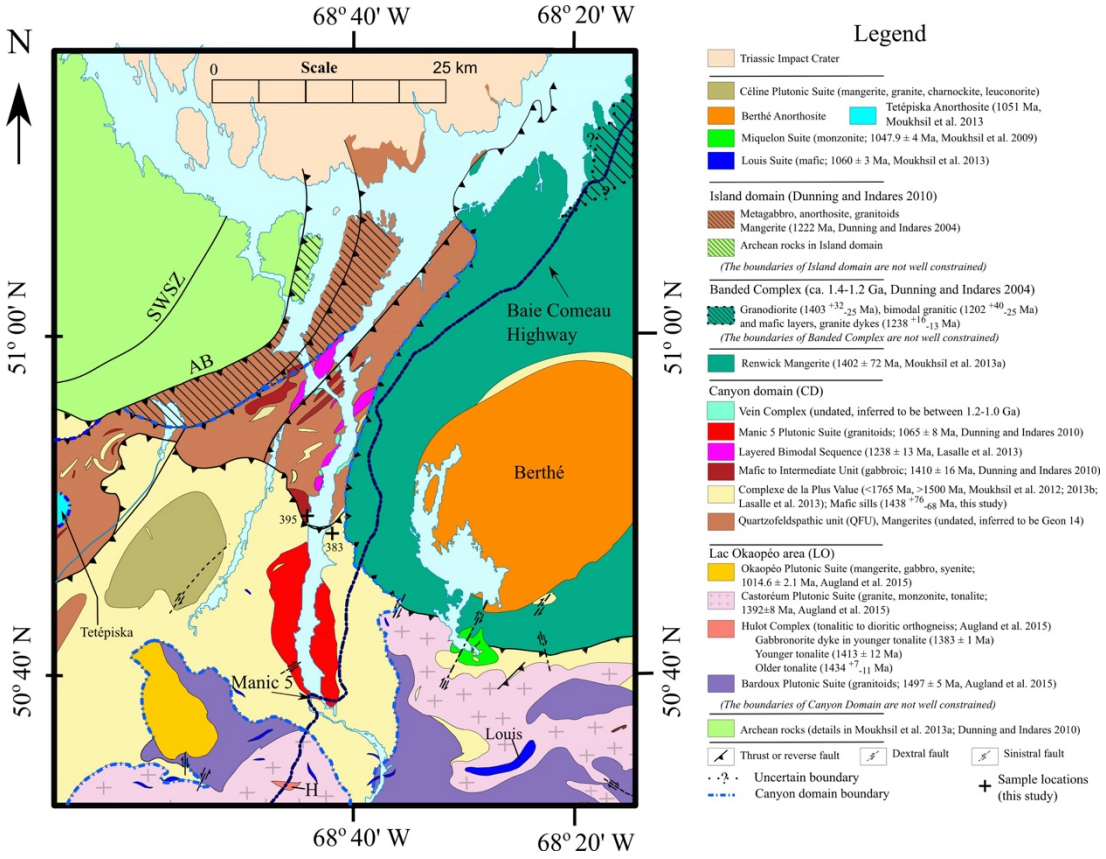

Figure 2.2. Simplified geological map of the study area in the Canyon domain located to the south of Manicouagan Impact Crater (compiled after Indares and Dunning, 2004; Dunning and Indares, 2010; Moukhsil et al., 2013a, b; and Augland et al., 2015). Note that the boundaries of the Banded Complex, Canyon domain, and the Island domain (Dunning and Indares, 2010) are not well defined. AB, Allochthon Boundary; H, Hulot Complex; SWSZ, Southwest Shear Zone.

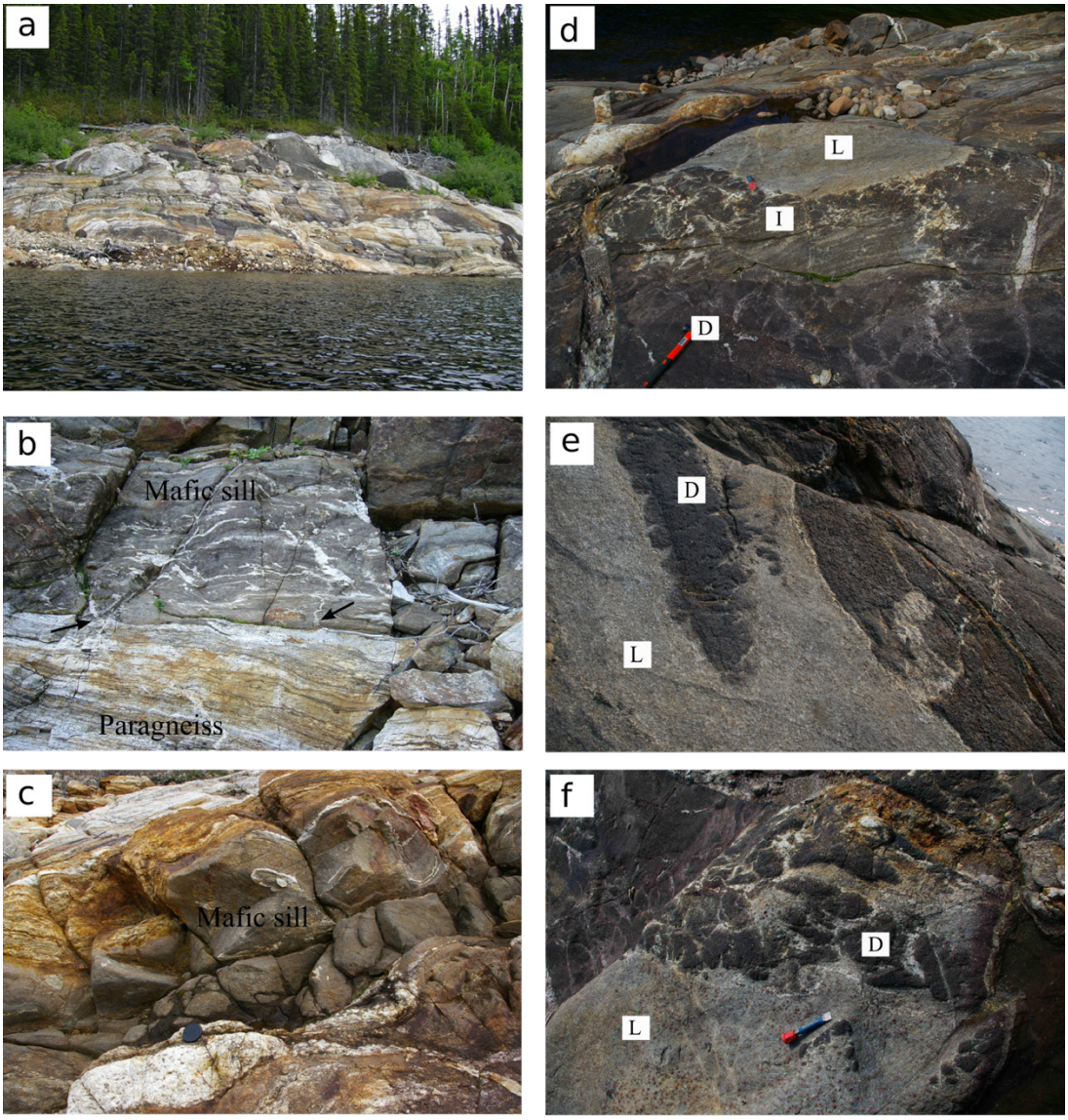

Figure 2.3. Field photographs of the mafic rocks in the Complexe de la Plus Value (PLV; a-c) and the intrusive rocks of the Mafic to Intermediate Unit (MIU; d-f). (a) A typical outcrop (#11-383c) of PLV showing mafic layers interpreted as intrusive sills within the paragneiss; (b) Close up of a mafic sill in the PLV showing contact with layered paragneiss and injection of leucocratic veins (partial melts from the paragneiss indicated by arrows) that are oriented parallel and transverse to paragneiss layering; (c) Outcrop of a homogeneous mafic sill interlayered with paragneiss but mostly free from injected leucocratic veins; (d) Outcrop of MIU showing different mafic components ranging from dark (D) to intermediate (I) to light grey (L) along with leucocratic films and pods; (e) Light grey component intruding and mingling with the dark grey component within the MIU showing a sharp to diffuse cuspate-lobate contact between them, and some parts of the dark grey component are partially disaggregated within the light grey component indicating contemporaneity of, and mingling between, the two phases; (f) Disintegration of rounded to sub-rounded fragments of the more mafic dark and intermediate grey components within the less mafic light grey component, indicative of the effects of magma mingling.

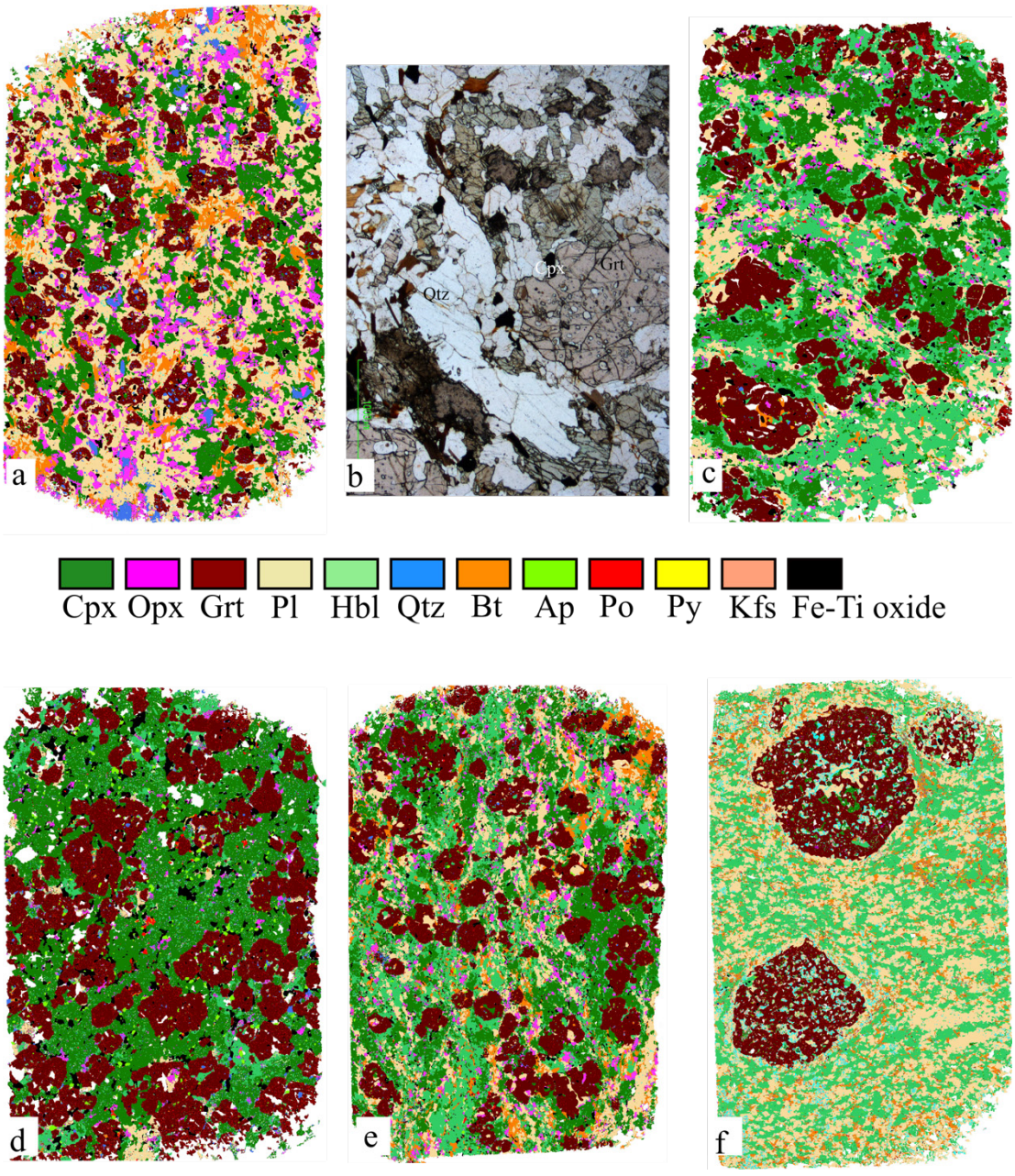

Figure 2.4. SEM-MLA mineralogical maps and photomicrograph of mafic rocks in the Complexe de la Plus Value (PLV; a-c) and the intrusive rocks of the Mafic to Intermediate Unit (MIU; d-f) from the Canyon domain. (a) Type-I texture in sample #11-383c in the PLV showing poikiloblastic garnet in a heterogeneous matrix composed of plagioclase, orthopyroxene, clinopyroxene, biotite, ilmenite, and quartz. Note the presence of large quartz grains and their association with orthopyroxene in the matrix; (b) Photomicrograph in plane-polarized light showing large ribbon shaped quartz xenocryst partially mantled partially by pyroxenes and plagioclase observed in Type-I; (c) Type-II texture in sample #11-383E1 in the PLV showing large garnet porphyroblasts in a matrix of plagioclase, hornblende, clinopyroxene, ilmenite and minor biotite (note the abundance of hornblende, larger garnet, and absence of large quartz grains in this sample); (d) Dark grey component of MIU (#11-395d1) with large

subidiomorphic garnet and clinopyroxene with ubiquitous ilmenite, apatite, orthopyroxene, and minor hornblende and plagioclase; (e) Intermediate grey component of MIU (#11-395a1) with medium grained garnet porphyroblasts in a matrix of hornblende, plagioclase, clinopyroxene, orthopyroxene, biotite and ilmenite; (f) Light grey component of MIU (#11-395) showing large poikiloblastic garnet porphyroblasts rimmed by plagioclase with subordinate amount of hornblende and biotite; matrix composed of plagioclase, hornblende, and biotite that wraps around garnet. Each MLA map is ~4cm in length (standard size of a thin section).

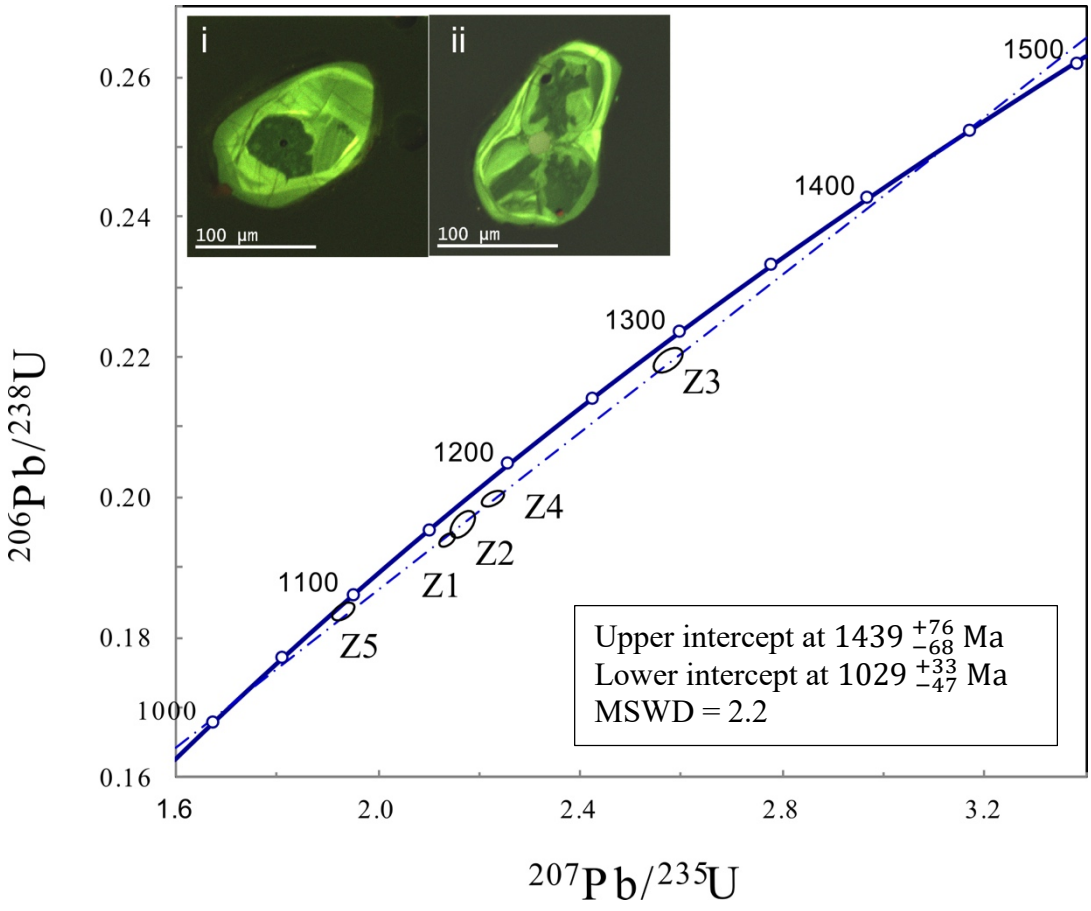

Figure 2.5. U-Pb concordia diagram with CL images of representative prismatic zircon from mafic sill #11-383c in the Complexe de la Plus Value (PLV).

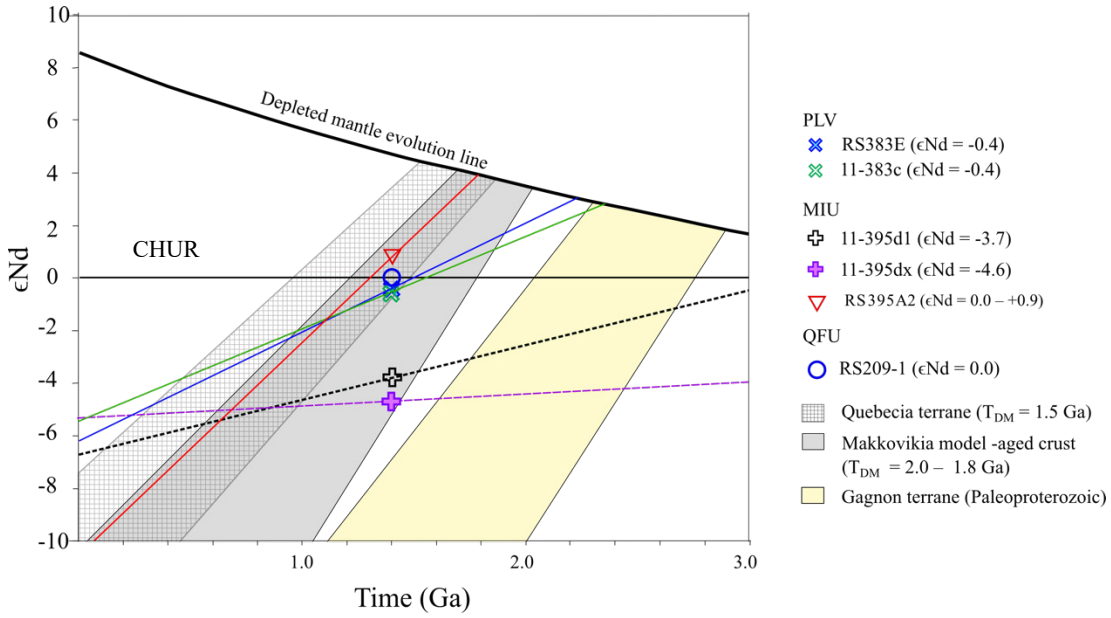

Figure 2.6. εNd vs. time plot showing the mafic sills in the Complexe de la Plus Value (PLV) and the intrusive rocks of the Mafic to Intermediate Unit (MIU) in the Canyon domain (this study) plotted at 1.4 Ga. Data for the mafic rocks from the QFU with an inferred ~1.4 Ga age are from Valverde Cardenas et al. (2012); evolution lines and fields for Quebecia, Makkovikia, and the Gagnon terrane are from Thomson et al. (2011); depleted mantle evolution line after DePaolo (1981b).

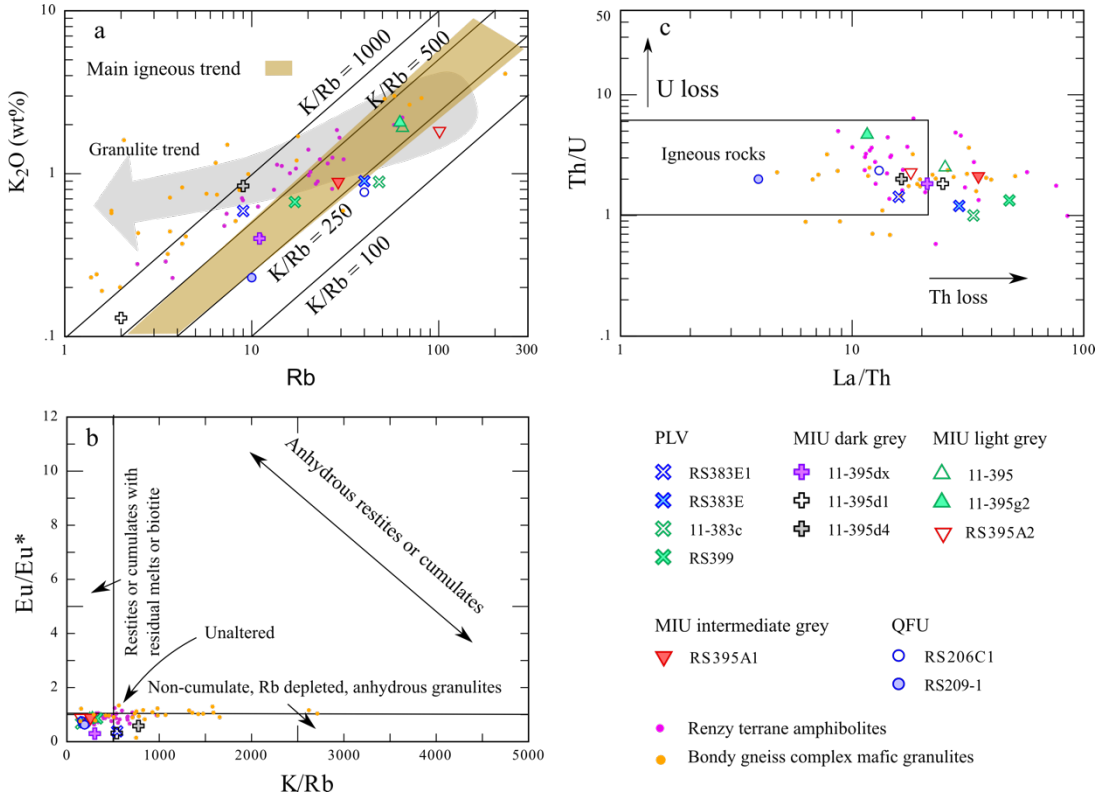

Figure 2.7. (a) K_2O vs. Rb plot (modified after Rudnick et al., 1985); (b) Eu/Eu* vs. K/Rb plot (modified after Rudnick, 1992) and (c) Th/U vs. La/Th plot (modified after Rudnick et al., 1985); for the mafic rocks from the Complexe de la Plus Value (PLV) and the intrusive rocks of the Mafic to Intermediate Unit (MIU) in the Canyon domain. Data for the mafic gneisses from the Bondy gneiss complex (Blein et al., 2003), mafic rocks from the QFU (Valverde Cardenas et al., 2012), and the Renzy terrane amphibolites (Montreuil and Constantin, 2010), all with a known or inferred age of ~1.4 Ga are also shown.

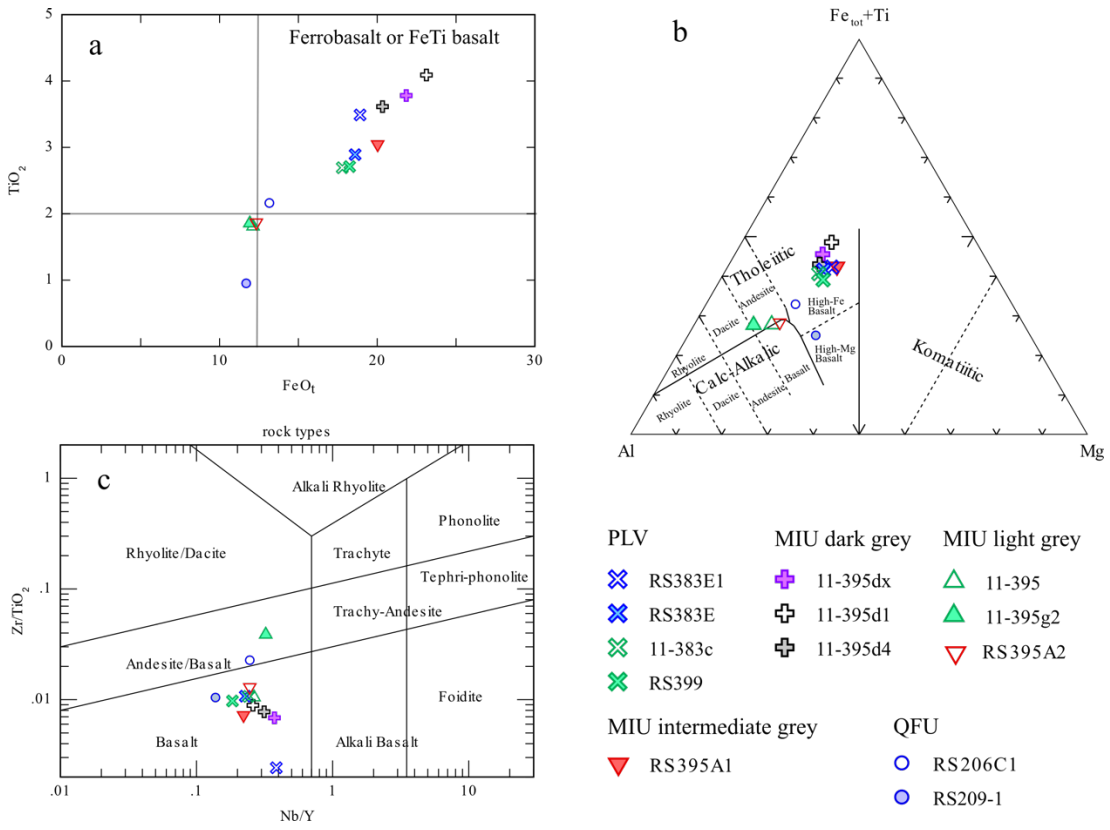

Figure 2.8. Rock-type classification diagrams for mafic samples from the Complexe de la Plus Value (PLV) and the intrusive rocks of the Mafic to Intermediate Unit (MIU) in the Canyon domain. (a) FeO_t vs. TiO_2 diagram showing high Fe-Ti basalt fields (after Byerly et al., 1976); (b) Al- Fe_{tot}+Ti- Mg diagram (after Jensen and Pyke, 1982); (c) Zr/TiO_2 vs. Nb/Y diagram (after Winchester and Floyed, 1976; modified by Pearce, 1996).

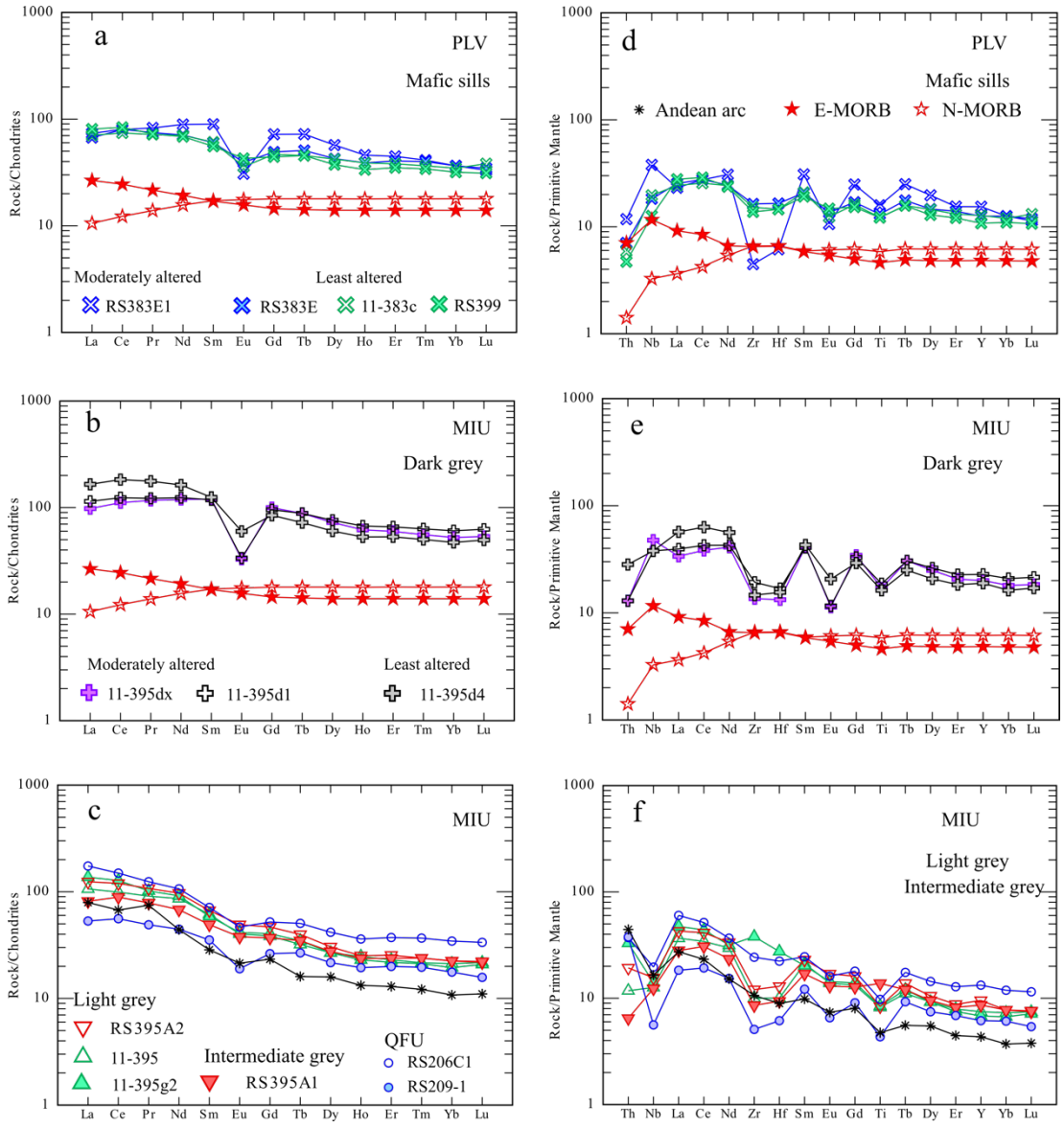

Figure 2.9. Chondrite-normalized REE (a-c) and primitive mantle-normalized REE and HFSE (d-f) patterns for the mafic samples in the Complexe de la Plus Value (PLV) and for the intrusive rocks in the Mafic to Intermediate Unit (MIU). (a) Mafic sills in the PLV; (b) Dark grey rocks, and (c) Intermediate and light grey rocks in the MIU. Multi-element (REE and HFSE) diagrams for the mafic rocks in (d) PLV; (e) Dark grey rocks, and (f) Intermediate and light grey rocks in the MIU. Normalizing values for chondrite and primitive mantle are from Sun and McDonough (1989). Also shown for comparison the patterns of N-MORB and E-MORB (Sun and McDonough, 1989), average Andean arc (Kelemen et al., 2014), and the inferred ~1.4 Ga mafic rocks from the QFU (Valverde Cardenas et al., 2012).

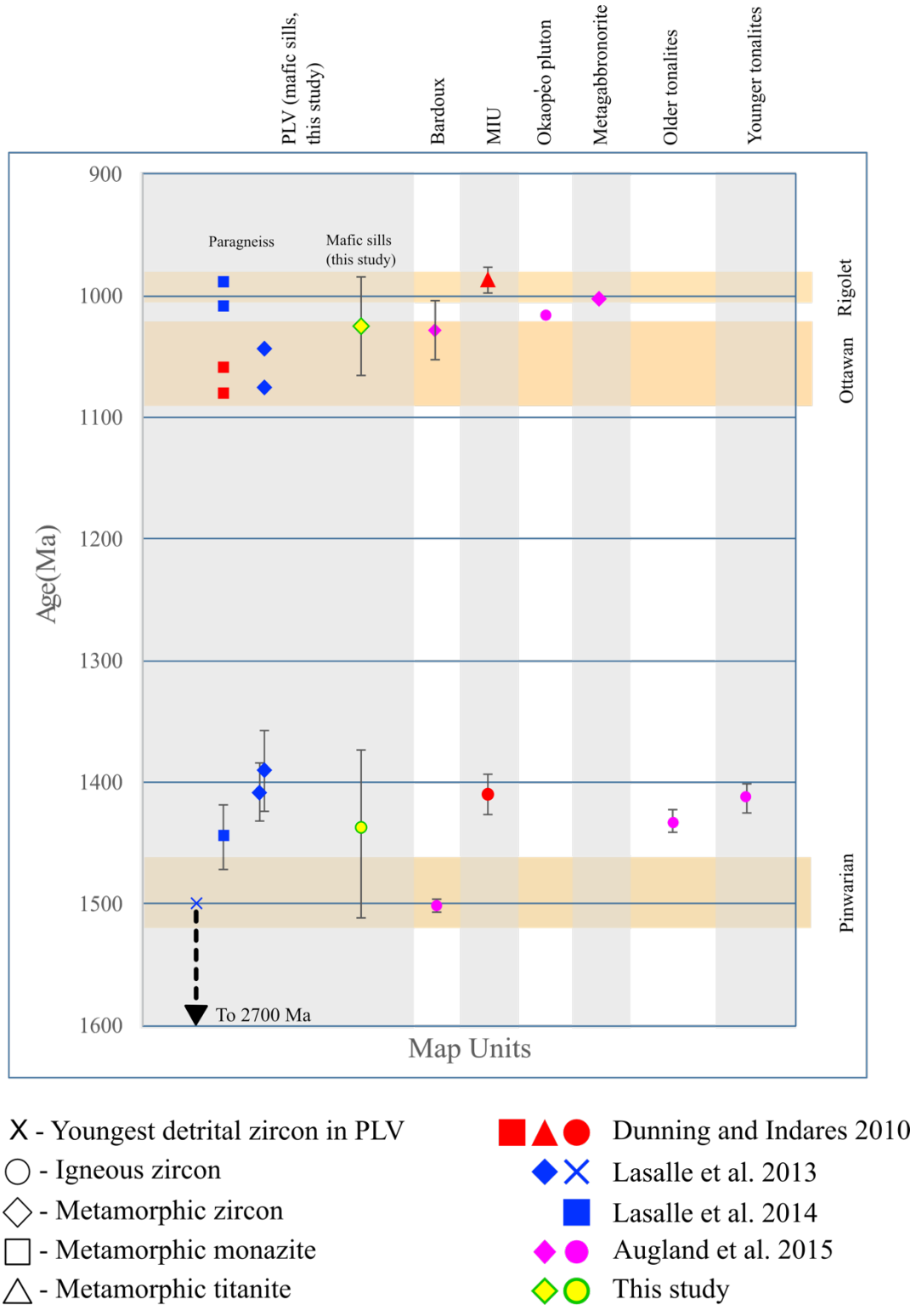

Figure 2.10. Summary of U-Pb ages from the Canyon domain and the Lac Okaopéo area. Data points are colour coded and sources are mentioned on the figure. Vertical error bars indicate uncertainties associated with ages; the upper age limit of detrital zircon from the PLV is ~1500 Ma and the downward-pointing arrow indicates the oldest detrital grain at ~2700 Ma (from Lasalle et al., 2013).

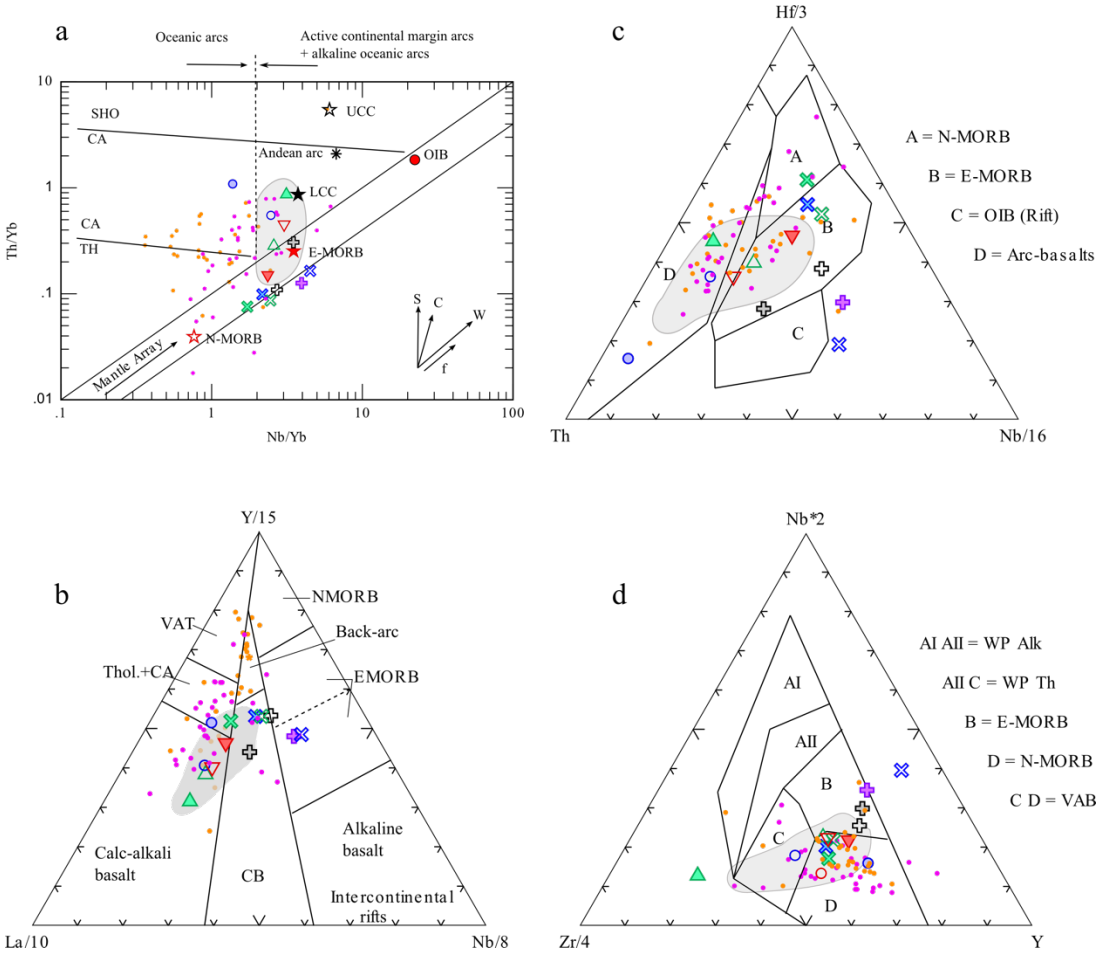

Figure 2.11. (a) Th/Yb vs. Nb/Yb (after Pearce 2008); (b) La/10–Y/15–Nb/8 (after Cabanis and Lecolle, 1989); (c) Th–Hf/3–Nb/16 (after Wood, 1980); and (d) Zr/4–Nb*2–Y (after Meschede, 1986) diagrams showing data plots for the mafic sills in the Complexe de la Plus Value (PLV) and the intrusive rocks of the Mafic to Intermediate Unit (MIU) in the Canyon domain. Data for the average lower and upper continental crust (LCC and UCC) after (Rudnick and Gao, 2014), remaining data sources and symbols are as in fig. 2.7 and 2.9. Vectors at bottom right in (a) indicate trends of subduction zone enrichment (S), crustal contamination (C), within-plate enrichment (W), and fractional crystallization (f).

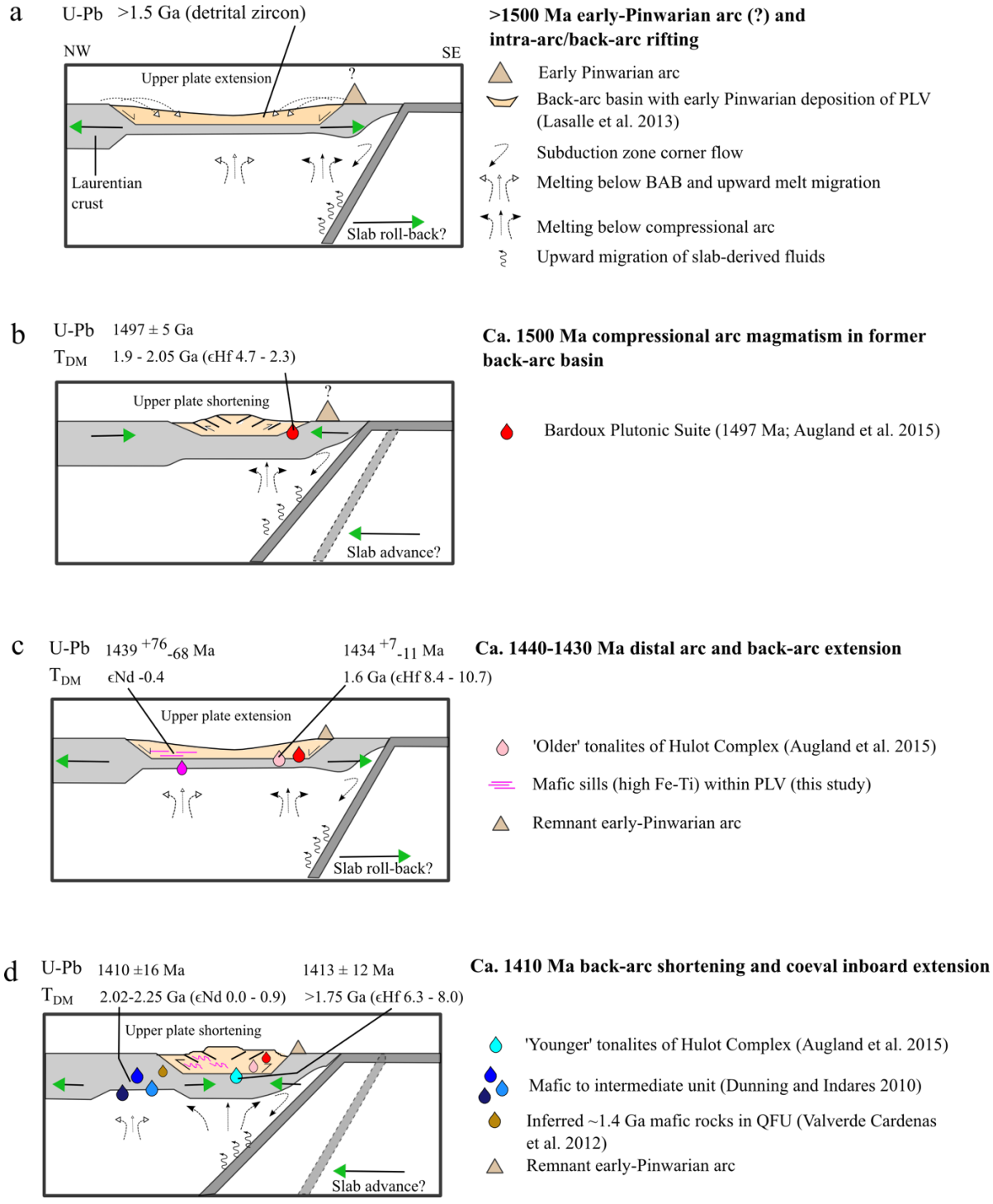

Figure 2.12. Schematic cross-sections illustrating the proposed tectonic model for the Geon 14 evolution of the southeastern Laurentian margin in the Canyon domain of the central Grenville Province (modified from Hanmer et al., 2000; Blein et al., 2003). Data compiled from Dunning and Indares (2010); Moukhsil et al. (2012, 2013a, b); Lasalle et al. (2013); and Augland et al. (2015).

3 Late-orogenic mafic magmatism in the hinterland, central Grenville Province: lithospheric extension in the evolution of a large hot orogen

3.1 Abstract:

Geochronological, geochemical and isotopic data for two late-orogenic suites of metamorphosed mafic dykes and sills provide new constraints on the nature of mantle sources and the tectonic evolution during the waning stages of the Grenvillian Orogeny (ca. 1090-980 Ma), which is divided into the Ottawan (~1090-1020 Ma), post-Ottawan (~1020-1005 Ma), and Rigolet (~1005-980 Ma) orogenic phases. U-Pb dating of zircon of the two suites of mafic granulites in the hinterland of the central Grenville Province has yielded ages of 1007.7 ± 2.0 Ma for the syn-metamorphic emplacement of dykes in the Vein Complex (VC), and of 997.0 ± 3.8 Ma for the emplacement of the sills in the Layered Bimodal Suite (LBS). The major and trace element chemistry and Sr-Nd isotopic compositions of the two tholeiitic suites indicate they are intraplate basalts derived from ~4-10% melting of asthenospheric mantle, followed by ~4-20% contamination by crust or SCLM and low-pressure fractionation-differentiation.

Previous studies have reported the post-Ottawan emplacement of several within plate-type, alkalic mafic to felsic plutons and anorthosite-mangerite-charnockite-granite (AMCG) suites followed by Rigolet emplacement of crust-derived pegmatite granite dykes in the study area. Taken together with the results of this study, the post-Ottawan tectonic setting is proposed to have involved a brief phase of lithospheric extension followed by the Rigolet convergence. Lithospheric extension gave rise to

asthenospheric upwelling resulting in melting of the extended SCLM and lower crust, thereby producing the wide range of small-volume, alkaline syenite-granite intrusions and AMCG suites. Continued extension and local lithospheric thinning led to decompression-melting of rising asthenosphere at shallow depth, and production of the earlier batches of small-volume tholeiitic intraplate mafic dykes and sills of the VC and LBS at ca. 1008 Ma. The younger ca. 997 Ma mafic sills in the LBS were derived from relatively deeper melting of asthenosphere within the transitional garnet-spinel-peridotite field, during the compressive Rigolet phase. It is thus suggested that there were two distinct episodes and styles of orogenic collapse associated with the Grenvillian Orogeny: the syn-Ottawan phase at ~1060-1040 Ma proposed by others, driven by delamination of the base of the overthickened lithosphere; and the post-Ottawan phase from ~1020-1005 Ma, driven by the extension of the previously thinned lithosphere.

3.2 Introduction

Mantle-derived rocks can provide crucial information about both the nature of the underlying mantle during orogeny and the petrogenetic processes in their formation (e.g., Bonin, 2004; Zhao et al., 2005). In modern large and hot long-duration collisional orogens (LHOs), such as the Himalaya-Tibet Orogen (Beaumont et al., 2006), mantle-derived magmatism is diverse in volume, distribution, timing, and composition, signifying its derivation from a variety of sources such as upwelling asthenospheric mantle, subcontinental lithospheric mantle (SCLM) that may have been metasomatically enriched in incompatible elements during previous subduction events, and mixing of melts from different sources, including inputs from the crust (Bonin, 2004; Dai et al., 2015). In post-collisional settings, these diverse magmatic expressions

have been ascribed to a variety of tectonic processes including thinning of the overthickened crust and lithospheric mantle root by delamination (Bird, 1979; Kay and Kay, 1993); convective thinning of the lithosphere (Houseman et al., 1981; England and Houseman, 1988, 1989); or post-collisional slab break-off (Davies and von Blanckenburg, 1995).

The Grenville Orogen (ca. 1090-980 Ma; *sensu stricto* of Rivers et al., 2008), part of which is preserved within the Grenville Province in North America (fig. 3.1), is widely considered to be an ancient analogue of the modern Himalaya-Tibet Orogen (e.g., Carr et al., 2000; Jamieson et al., 2007; Rivers, 2008; Rivers et al., 2012). The Grenvillian Orogeny has been empirically subdivided into two phases: the ca. 1090-1020 Ma Ottawan phase for which evidence is preserved in allochthonous rocks in the orogenic hinterland; and the ca. 1005-980 Ma Rigolet phase for which evidence is mainly preserved in the parautochthonous foreland (Rivers et al. 2012). Recent work in the Grenville Province has documented the distribution and compositional diversity of post-collisional suites with mantle signatures, as deduced from their trace element and isotopic characteristics, that include: (i) within-plate tholeiitic and alkaline mafic intrusions ascribed to asthenospheric mantle with variable degrees of contamination by orogenic crust and/or lithospheric mantle (e.g., McLelland and Chiarenzelli, 1990; Gower et al., 1994; Corriveau et al., 2003; Indares and Dunning, 2004; Heaman et al., 2004; Augland et al., 2015, 2017); and (ii) small-volume, alkaline intrusions with arc to within-plate signatures that originated from melting of metasomatized SCLM (e.g., Corriveau et al., 1990; Corriveau and Gorton, 1993; Corrigan and Hanmer, 1997; Owens and Tomascak, 2002; Morin et al., 2005; Valverde Cardenas et al., 2012; Augland et al., 2017; Côté et al., 2018).

In the late-orogenic setting (<1020 Ma; i.e., post-Ottawan phase) of the Grenville Orogen, the topic of this contribution, the thermal core of the orogenic hinterland, termed the Interior Magmatic Belt (IMB; Owen and Erdmer, 1990; Gower et al., 1991; fig. 3.2), was intruded by a variety of dispersed, post-collisional, crust- and mantle-derived, alkalic mafic to felsic plutons and the AMCG suites with arc- to within plate-type geochemical signatures between ca. 1020-1005 Ma that were attributed to melting in the SCLM and orogenic lower crust in an extensional setting (Owens et al., 1994; Gower et al., 1994; Higgins and van Breemen, 1996; Icenhower et al., 1998; Indares et al., 1998; Gower and Krogh, 2002; Gobeil et al., 2002; Owens and Tomascak, 2002; Corriveau et al., 2003; Indares and Dunning, 2004; Hébert et al., 2005, 2009; Bédard, 2009; Moukhsil et al., 2009, 2014; Owens and Dymek, 2016; Augland et al., 2015, 2017; Turlin et al., 2017, 2019; Côté et al., 2018). In the central Grenville Province, this period was also coeval with the gravitational collapse and crustal extension of the hinterland at ca. 1017-1007 Ma (Indares et al., 1998). However, some recently proposed tectonic models for the Grenville Province suggest the derivation of late-orogenic alkalic mafic-syenitic-AMCG suites from supra-subduction zone mantle, which was interpreted to have evolved from the Ottawan continental margin accretionary arc and back-arc setting to a post-Ottawan extension, which was related to slab break-off or retreat (Augland et al., 2015, 2017; Côté et al., 2018; Turlin et al., 2019). Subsequent renewed convergence during the Rigolet phase (~1005-980 Ma; Rivers, 2008) was inferred to be the propagation of the orogenic front from hinterland into the foreland of the Grenville Province (Rivers et al., 2012), although recent studies from the central Grenville Province presented evidence in favour of the kinematically

equivalent interpretation involving underthrusting of the orogenic foreland beneath the hinterland at ca. 1008-1002 Ma (Jannin et al., 2018a, b; Turlin et al., 2019).

This paper presents the petrography, major and trace element geochemistry, Sr-Nd isotopes, and CA-TIMS U-Pb ages of two suites of late-orogenic, meta-mafic rocks from the Canyon domain in the hinterland of the central Grenville Province in Quebec, in order to investigate their sources and tectonic setting, and evaluate their significance for the late-orogenic evolution. Combined with recently published data, these two mafic suites allow us to: (i) identify the evidence for a post-Ottawan amphibolite- to granulite-facies metamorphism in the hinterland; and (ii) constrain the late-orogenic lithospheric extension that resulted in local thinning and melting in the SCLM prior to the Rigolet compression and crustal thickening.

3.3 Geological setting

The Manicouagan area (fig. 3.3) in the central Grenville Province exposes two of the first-order tectonic divisions of the Grenville Orogen, the Parautochthonous Belt in the north separated by the gently SE-dipping Allochthon Boundary (AB; which recorded both reverse- and normal-sense movements) from the structurally overlying Allochthonous Belt in the south (fig. 3.1). In this area, the Parautochthonous Belt is represented by the Gagnon terrane, a polydeformed and metamorphosed early Paleoproterozoic continental-margin sequence and its underlying Archaean basement. Both the supracrustal sequence and its basement were deformed into a metamorphic fold-thrust belt during the terminal Rigolet phase of the Grenvillian Orogeny at ca. 1005-980 Ma, with the grade of metamorphism increasing from greenschist-facies near the Grenville Front to amphibolite-, high-pressure (H*P*) granulite-, and eclogite-facies

conditions farther southeast (peak conditions of 1250-1300 MPa, 815-830 °C) (Rivers 1983a, 1983b; Indares, 1995; Jordan et al., 2006; van Gool et al., 2008; Indares et al., 2008; Dunning and Indares, 2010; Jannin et al., 2018a, b).

In the central Grenville Province, the Gagnon terrane is tectonically overlain by the Manicouagan Imbricate Zone (MIZ; Indares et al., 1998; Cox et al., 1998; located to the north of the area in fig. 3.3), which mainly consists of remnants of a Labradorian (~1.65 Ga) AMCG suite, Pinwarian (~1.52-1.46 Ga; Tucker and Gower, 1994; Gower and Krogh, 2002) granitoid plutons, Shawinigan (ca. 1170 Ma) gabbro sills (Cox et al., 1998), and several Ottawan gabbroic stocks and dykes emplaced between ca. 1026-1038 Ma (Indares et al., 1998; Indares and Dunning, 2004). The MIZ was metamorphosed under eclogite- to H*P* granulite-facies conditions of 750–920 ºC and 1700–1900 MPa during the Ottawan phase of the Grenvillian Orogeny at ~1060–1030 Ma (Cox and Indares, 1999a, 1999b; Indares and Dunning, 2001; Indares, 2003; Yang and Indares, 2005; Indares et al., 2008) and is part of the Allochthonous H*P* belt (aH*P* Belt) of Rivers (2008). In the MIZ, the syn-Ottawan Gabriel dykes (undated), the high Fe-Ti gabbroic Themines dykes (>1026 Ma; Dunning and Indares, 2010), the 1039 ± 2 Ma gabbroic stocks (Indares and Dunning, 2004), and the slightly younger fine-grained gabbroic dykes (undated) were interpreted to have been derived by decompression melting of upwelling asthenosphere following partial or complete removal of SCLM by convective thinning or delamination (Indares and Dunning, 2004).

In contrast, the large area to the south, southeast and east of the MIZ, known as Berthé terrane (Hynes et al., 2000) was metamorphosed under Ottawan medium-*P* (M*P*) granulite-facies conditions (Indares and Dunning, 2004; Dunning and Indares, 2010; Lasalle et al., 2014), and is part of the Allochthonous M*P* belt (aM*P* Belt) of

Rivers (2008). This belt is composed of tectonically imbricated domains, with different protoliths and ages, including gabbro, anorthosite, and megacrystic granitoids of Labradorian age (ca. 1694 Ma gabbro; Dunning and Indares, 2010) in the Island domain; felsic migmatites of unknown age in the Gabriel Complex (which yielded inherited monazite age of ca. 1478 Ma; Indares and Dunning, 2004); Pinwarian to post-Pinwarian (ca. 1.5-1.4 Ga) intrusions in the Canyon domain in the south (Dunning and Indares, 2010; Lasalle et al., 2014; Maity and Indares, 2018); and Elzevirian granite (ca. 1238-1202 Ma; Indares and Dunning, 2004) in the Banded Complex and the mafic Toulnustouk sills (ca. 1228 Ma; Indares and Dunning, 2004) in the Hart Jaune Terrane. Additionally, the mafic granulites of the Hart Jaune terrane (HJT), which have yielded a Pinwarian (ca. 1470 Ma; Hynes et al., 2000) age of metamorphism, escaped the Ottawan high-grade events and represent a high-level crustal segment, the Ottawan Orogenic Lid (Rivers, 2012), preserved between the antiforms of the aH*P* MIZ and the aM*P* Gabriel Complex. The study area for this research is part of the Canyon domain, which is described in more detail below.

3.3.1 Geology of the study area- The Canyon domain

The Canyon Domain (fig. 3.3), first defined in the vicinity of the Manicouagan Reservoir by Hynes et al. (2000), structurally overlies aM*P* and aH*P* units of Labradorian age in the Island domain to the northwest and the MIZ to the north, respectively (Indares et al. 2000; Dunning and Indares 2010), and is characterized by a package of supracrustal units and associated plutonic rocks metamorphosed under M*P* granulite-facies conditions (Dunning and Indares, 2010; Indares and Moukhsil, 2012; Lasalle and Indares, 2014). In this study, the Canyon domain is informally divided into northern and southern parts located on opposite sides of the prominent thrust-sense

shear zone with an overall east-west-trend. In the hanging wall of this thrust, the oldest unit in the southern Canyon domain is the ca. 1.5 Ga paragneiss sequence of the Complexe de la Plus Value (PLV; Lasalle et al., 2013), which was deposited in a back-arc setting (Augland et al., 2015; Maity and Indares, 2018), and was intruded by 1439 $^{+76}_{-68}$ Ma high Fe-Ti-P mafic sills in a period of limited extension within the arc or back-arc (Maity and Indares, 2018).

In the footwall to the north of this thrust, large parts of the Canyon domain (Canyon Complex of Moukhsil et al., 2013a) consist of: (i) the 1416 ± 10 Ma Mafic to Intermediate Unit (MIU) formed in a mature continental arc (Valverde Cardenas et al., 2012), or a compressional back-arc to arc setting (Maity and Indares, 2018); (ii) the supracrustal Quartzofeldspathic Unit (QFU), inferred to have been deposited in the Geon 14 arc setting (Indares and Moukhsil, 2013); (iii) remnants of a volcanic belt termed the Layered Bimodal Suite (LBS; Indares and Mouksil, 2013), formed at 1238 ± 13 Ma (Lasalle et al., 2013) in an extensional setting (Dunning and Indates, 2010; Indares and Mouksil, 2013; Hindemith et al., 2017); and (iv) the Vein Complex (VC; Indares and Mouksil, 2013) of unknown age and tectonic setting. In low-strain outcrops, the VC exhibits an intricate anastomosing "vein-like" pattern of felsic and mafic layers (fig. 2c in Indares & Moukhsil, 2013) that grade into more strained layering that locally forms "straight gneisses" (figs. 2c and 2e, respectively, in Indares and Moukhsil, 2013), indicative of high-strain ductile deformation. This suite also contains coherent, homogeneous metagabbroic layers that lack visible evidence for high-strain ductile deformation, and variably strained mafic dykes, boudins and rafts (fig. 3.4a & b), that are analyzed further in this study. The metagabbroic layers exhibit sharp to diffuse boundaries, but their original relationship to the surrounding felsic gneisses is unclear.

The hydrothermally altered, supracrustal Layered Bimodal Suite (LBS) consists of alternating felsic and mafic layers (fig. 3 in Indares and Moukhsil, 2013), with the former comprising fine-grained pink or white gneiss (including nodular aluminous gneiss, garnetite and impure quartzite) with thin compositional layering devoid of ferromagnesian minerals, and the latter ranging from homogeneous to heterogeneous composition (Indares and Dunning, 2010; Indares and Moukhsil, 2013; Hindemith and Indares, 2013; Hindemith et al., 2017). Quartzofeldspathic veins of anatectic origin occur within the felsic and mafic units suggesting they have undergone deformation under high-grade metamorphic conditions. The LBS was initially interpreted to have formed in an intracontinental rift setting (Dunning and Indares, 2010; Valverde Cardenas et al., 2012; Indares and Moukhsil, 2013), but the predominantly arc to subordinate within plate geochemical signatures in the ca. 1238-1202 Ma mafic and granitic intrusions (Indares and Dunning, 2004; Valverde et al., 2012; Moukhsil et al., 2014; Hindemith et al., 2017; Moukhsil and Solgadi, 2017), coupled with the lack of coarse clastics and alkaline mafic magmas, suggest that the LBS was most likely formed in a subduction setting, related to an extensional back-arc or intra-arc comparable to the Elzivirian back-arc in the western Grenville Province (Rivers and Corrigan, 2000). The LBS also includes several massive and variably deformed mafic layers, rafts, and attenuated dykes (fig. 3.4c & d) that also cross-cut the QFU and VC in the northern Canyon domain (Indares and Mouksil, 2013).

The Canyon domain is cross-cut by several felsic intrusions including: (i) the 1004.2 ± 2.3 to 1001.9 ± 3.9 Ma rare-earth element (REE)-rich, pegmatitic granite dykes (PGDs) in the PLV in the southern Canyon domain (Turlin et al., 2017); (ii) the 995 ± 3.5 Ma undeformed granite pegmatites (Dunning and Indares, 2010); and (iii) the

986 ± 0.5 Ma pink leucogranite dyke swarms in the northern Canyon domain (Jannin et al., 2018b). The older PGDs and the younger dyke swarms were inferred to have been derived from partial melting of paragneiss in the Paleoproterozoic Knob Lake Group (KLG) in the Gagnon terrane as a result of its underthrusting beneath the hinterland during the Rigolet convergence (Jannin et al., 2018b; Turlin et al., 2019).

Finally, the central and southern parts of the Canyon domain are intruded by a suite of 980 ± 3 Ma potassic to ultrapotassic dykes that are undeformed to variably deformed and recrystallized (Dunning and Indares, 2010; Valverde Cardenas et al., 2012).

3.3.2 Metamorphism in Canyon domain

All rocks in the Canyon domain except the Rigolet pegmatites and potassic to ultrapotassic dykes noted above have a high-grade metamorphic signature, and the dominant metamorphic sub-assemblages are Pl + Grt + Cpx + Opx + Hbl in mafic rocks and Grt + Sill + Kfs ± Bt + Liq (mineral abbreviations from Whitney and Evans, 2010) in aluminous quartzofeldspathic rocks, indicative of Ottawan (ca. 1080-1050 Ma, see below) M*P* granulite-facies metamorphism (Dunning and Indares, 2010; Lasalle and Indares, 2014). The Ottawan metamorphic evolution in the PLV, as determined from sillimanite-bearing paragneiss samples from the southern Canyon domain and from the Lac du Milieu area to the southeast of fig. 3.3, followed a prograde *P-T* path with a moderate d*P*/d*T* and an elevated temperature gradient at pressures below the kyanite-sillimanite boundary, reaching peak suprasolidus conditions of ~800-1100 MPa and 840-965 °C, followed by moderate decompression and re-crossing of the solidus at ~600-820 MPa and 820-840 °C (Lasalle and Indares, 2014; Patrick and Indares, 2017). For the LBS in the northern Canyon domain, the Ottawan *P-T* evolution was broadly

similar, with a moderate prograde d*P*/d*T* and attainment of suprasolidus metamorphic conditions at ~780-1100 MPa and 830-875 °C, followed by retrograde decompression and cooling to the solidus at 650-800 MPa and 825-857 °C (Lasalle and Indares, 2014; Patrick and Indares, 2017). The moderate d*P*/d*T* of the prograde *P-T* paths yielded by these M*P* rocks in the Grenvillian hinterland are compatible with an elevated thermal regime beneath a long-duration orogenic plateau. More recent work has revealed evidence for retrograde cooling of the LBS from peak-Ottawan suprasolidus metamorphic conditions in the kyanite stability field (i.e., at higher pressure) following NW-directed thrusting (Da1 of Jannin et al., 2018b).

Most metamorphic rims on zircon from the PLV and LBS in the Canyon domain have yielded ages between 1081 ± 5 Ma and 1044 ± 15 Ma (TIMS; Dunning and Indares, 2010; LA-ICP-MS; Lasalle et al., 2013), which were inferred by these authors to represent the time of the peak-Ottawan M*P* granulite-facies conditions. This interpretation was supported by metamorphic monazite ages between 1080-1020 Ma, with a significant cluster between 1070-1050 Ma (TIMS; Dunning and Indares, 2010; LA-ICP-MS; Lasalle et al., 2014). These age ranges, coupled with *P-T* modelling suggest a protracted thermal evolution in the Grenvillian hinterland during the Ottawan phase. However, some younger, post-Ottawan ages have also been determined, including monazite ages of 1020 ± 2 Ma and 1001 ± 3 Ma for two samples from the LBS (TIMS; Dunning and Indares, 2010), and an imprecise U-Pb zircon age of 1002 ± 42 Ma determined from a wide (~20-80 µm), homogeneous, low-U metamorphic rim from the same sample (LA-ICP-MS; Lasalle et al., 2014). In addition, BSE-bright, Th-enriched rims of matrix monazite grains from the PLV and LBS have yielded ages of 988 ± 28 Ma and 1014 ± 31 to 980 ± 31 Ma, respectively (LA-ICP-MS; Lasalle et al.,

2014). The latter authors tentatively associated these late Grenvillian ages with a fluid influx that caused a greenschist- to sub-greenschist-facies metamorphic overprint, and/or with the late intrusions of granitic pegmatites and ultrapotassic dykes between ca. 995-980 Ma. However, based on field relations of the ca. 1004-1002 Ma REE-rich PGDs with their host PLV, Turlin et al. (2017, 2018) proposed that the PLV was near its wet solidus temperature during the emplacement of the PGDs. Recently, Jannin et al. (2018b) showed that the LBS was metamorphosed under lower-pressure suprasolidus conditions in the field of sillimanite stability during a Rigolet SE-directed, normal-sense, shearing event (their D2), the timing of which was constrained by the age of syn-D2 pink leucogranite dyke swarms at 986 ± 2 Ma.

3.4 Field Relations and Petrography

The mafic rocks in the VC are fine- to coarse-grained, dark grey, massive, metagabbros that range from continuous coherent layers parallel to the regional gneissosity (fig. 3.4a) to attenuated dykes with evidence for stretching and boudinage on the meter scale (fig. 3.4b). These latter features provide clear evidence that the mafic rocks are intrusive, and that they are deformed, but they lack the pervasive ductile fabrics of the country rocks, suggesting they were intruded into previously deformed rocks as sills and dykes. Overall, the field relations in the VC suggest that the generally well preserved mafic sills and dykes were subjected to relatively lower strain conditions than their hosts, and that they intruded into the gneisses after formation of the ductile high-strain gneissic layering, but before complete cessation of deformation and metamorphism. Most of the mafic rocks from the VC are crudely foliated to non-foliated, and display fine- to medium-grained, granoblastic assemblages consisting of

Pl + Hbl + Cpx + Grt ± Opx ± Ttn ± Bt ± Ilm (fig. 3.5a) attesting to recrystallization under granulite-facies conditions (e.g., Pattison, 2003).

The mafic rocks in the LBS range from dark to light grey, homogeneous to heterogeneous, medium- to coarse-grained layers that are either massive or locally deformed into boudins and pinch and swell structures (fig. 3.4c and d). The mafic layers in the LBS are distinct from those in the VC in that they exhibit significant compositional and textural variations, including: (i) granoblastic Hbl + Pl (fig. 3.5b); (ii) large garnet porphyroblasts in a matrix composed of Pl + Hbl + Bt + Opx, in which garnet is variably replaced at its margins by hornblende, biotite, plagioclase, orthopyroxene, and quartz (fig. 3.5c); and (iii) garnet porphyroblasts in a matrix rich in Pl + Opx + Cpx + Bt ± Hbl (fig. 3.5d), in which garnet is partially replaced by symplectic Opx + Pl coronas. Additionally, trace amounts of zircon, allanite, thorite, barite, monazite and sulphides have been documented. The peak assemblage of Hbl + Pl in one sample is indicative of amphibolite-facies conditions, whereas the breakdown of garnet to Pl + Hbl + Bt in most samples suggests retrogression or decompression. The general assemblage of Grt + Pl + Hbl + Bt + Opx is indicative of L*P* granulite-facies conditions, and some of these samples exhibit the development of Pl + Opx coronas around garnet, suggesting heating or decompression under L*P* granulite-facies conditions (Pattison, 2003), prior to variable, post-peak retrogression under hydrous conditions (formation of hornblende and biotite at the expense of clinopyroxene and garnet). In the samples with corona texture, clinopyroxene is restricted to the matrix and rare alteration zones, and is associated with quartz, hornblende, biotite, and opaque phases. The large, irregular, partially resorbed, quartz grains present in some samples are xenocrystic and rimmed by pyroxene, biotite, and an opaque phase (fig. 3.5e). The

microstructural domains of hydrothermal alteration contain variable proportions of secondary sericite and chlorite with the sample 11-331b being the most altered. In addition, sample 11-317a contains a thin vein composed of K-feldspar and biotite.

In summary, the mafic rocks from the VC exhibit metamorphic textures and mineral assemblages suggestive of peak granulite-facies metamorphism, whereas those from the LBS are suggestive of decompression or heating to peak L*P* granulite-facies conditions before partial post-peak retrogression to amphibolite-facies assemblages.

3.5 Analytical Methods

Six samples from the VC and five samples from the LBS were taken from the least altered and freshest parts of outcrops of the dykes and sills in the study area for whole-rock major and trace element analysis. Selected samples were crushed and powdered using standard clean laboratory protocols at Memorial University of Newfoundland (MUN), and were analyzed for whole-rock major and trace element concentrations at the Activation Laboratories (Actlabs) Ltd. in Ontario, Canada. The standard analytical protocol involved fusing a measured weight of rock powder with lithium metaborate/ tetraborate to produce homogeneous glass beads that were analyzed using combination of simultaneous/sequential Thermo Jarrell-Ash ENVIRO II or a Varian Vista 735 inductively coupled plasma (ICP) for all major elements and selected trace elements (Ba, Be, Sc, Sr, V, Y, Zr), and by using Perkin Elmer Sciex ELAN 6000, 6100, or 9000 fusion inductively coupled plasma mass spectrometry (FUS-ICP/MS) for the remaining trace elements (appendix A). The details of their analytical protocols can be found on the Actlabs website (www.actlabs.com). The detection limits for the analyses are typically in the range of 0.01-0.001 % for major elements and 1-30 ppm

for trace elements. For tracer isotopes of two samples each from the VC and LBS, Sr was separated followed by Sm and Nd from whole-rock powders following an in-house protocol at MUN, and isotope ratios were measured using a multi-collector Finnigan Mat 262 mass spectrometer in static and dynamic modes. U-Pb zircon dating for two samples from the VC and LBS was carried out by chemical abrasion thermal ion mass spectrometry (CA-TIMS) using a Finnigan Mat 262 mass spectrometer at MUN following the procedure described in Sparkes and Dunning (2014). Details of all the isotope analytical procedures are described in appendix A.

3.6 Results

3.6.1 U-Pb Geochronology

One sample from the VC and one from the LBS were chosen for U-Pb zircon dating by CA-TIMS to determine the timing of crystallization and metamorphism of the mafic rocks. Zircon were extracted from both samples using standard crushing and separation techniques. Zircon grains from both samples are clear, colourless to yellowish, with a few exhibiting inclusions and fractures. The grains mainly consisted of two morphological types: euhedral to subhedral prisms that are interpreted to have formed during igneous crystallization, and rounded, multi-faceted 'soccer ball' grains inferred to have formed during high-grade metamorphism (see Corfu et al., 2003; and references therein). The isotopic data are presented in table 3.1 and plotted on a Concordia diagram in fig. 3.6 using Isoplot 3.0 (Ludwig, 2003).

Sample #11-208 is from a homogeneous metagabbroic dyke in the Vein Complex. Of the prisms, one single-grain (Z1) and two multi-grain analyses (Z3, 4) are concordant and yield a weighted average age of 1007.1 ± 3.0 Ma (MSWD = 0.36) (fig.

3.6a). The prism fraction Z2 yields a significantly older age of 1021.9 ± 4.9 Ma (MSWD = 0.92), and possibly represents a xenocryst or mixing with a xenocrystic core. Three multi-grain analyses (Z5, 6, 7) of small, clear, round grains yield a weighted average age of 1008.0 ± 2.5 Ma (MSWD = 0.22), which overlaps within uncertainty with the weighted average age of the three prisms. Several interpretations of the data are possible, but considering that the prisms and round grains overlap with each other rather than defining a chord, a weighted average age 1007.7 ± 2.0 Ma (MSWD = 0.0018), calculated for all the concordant grains (except Z2), is interpreted to be the best estimate for the age of syn-metamorphic emplacement of this sample.

Sample #11-331b comes from a homogeneous mafic layer in the Layered Bimodal Suite. Two populations of zircon were recovered: euhedral to subhedral clear prisms with medium (1:2) to high (1:4) aspect ratios, and more rounded stubby grains with low (~1:1) aspect ratios, which are interpreted to be relict prisms modified during granulite-facies metamorphism (e.g., Corfu et al., 2003). Four fractions of the best zircon prisms were analyzed. Z1 is a multigrain fraction consisting of two euhedral grains, whereas Z2, Z3, and Z4 are analyses of single euhedral grains, all of which are concordant and overlap with a weighted average age of 997.0 ± 3.8 Ma (MSWD = 0.96) (fig. 3.6b). There is no spread of ages on the Concordia diagram, as would be expected for prisms with older xenocrystic cores, or for igneous grains overprinted by a younger granulite-facies event, suggesting this is the zircon crystallization age of the mafic sill in the LBS. The zircon could have been metamorphosed either during their emplacement at ca. 997 Ma since there is evidence for a high thermal gradient at this time in the structurally overlying PLV to the south (e.g., Turlin et al., 2017, 2018), or during a younger suprasolidus metamorphic condition at ca. 990 Ma related to mid-

crustal channel flow in the northern Canyon domain (Jannin et al., 2018b). The concordant and overlapping data in fig. 3.6b suggests that either the dated prisms in our study did not record younger metamorphic event(s), or their metamorphic rims were removed during the chemical abrasion procedure. A more detailed study is required to unambiguously link zircon growth events to late-Grenvillian metamorphism.

3.6.2 Major and trace element Geochemistry

The major and trace element geochemistry for the mafic rocks in VC and LBS is presented in table 3.2. Six additional samples that were previously thought to be related to ~1.2 Ga crustal extension (Valverde Cardenas et al., 2012), but are now recognized to be part of these two suites, are also included in the table.

Both the VC and LBS suites experienced late-Grenvillian granulite-facies metamorphism and low-grade hydrothermal alteration (Hindemith and Indares, 2013; Hindemith et al., 2017), which could have affected their major and trace element compositions. Therefore, the mafic rocks in our study were tested for element mobility by using appropriate geochemical screening methods (appendix B), before their major and trace element compositions were used to study their petrogenesis and tectonic setting. The screening process yielded evidence for hydrothermal alteration in a few samples, but most exhibit major and trace element features suggesting their protolith chemistry is largely preserved. As such, they are not restites and hydrothermal alteration has not changed their whole-rock immobile incompatible element concentrations and ratios, which are used in this study.

The mafic samples from the dykes and sills in both suites exhibit overlapping compositional ranges in SiO_2 (45-49 wt%), MgO (5.5-8.8 wt%), Al_2O_3 (12-17 wt%),

TiO_2 (0.9-3.8 wt%), and $Fe_2O_{3(tot)}$ (11.6-18.9 wt%). They are subalkaline tholeiitic basalt to basaltic andesite in composition (fig. 3.7), and exhibit variable Mg# (39-61) together with variable Ni and Cr (720 and 490 ppm to below detection limit, respectively) (fig. 3.8a and b). On plots against Zr as fractionation index, they exhibit positive correlations with $Fe_2O_{3(tot)}$ (not shown), TiO_2 (fig. 3.8c), P_2O_5 (fig. 8d), and Y (fig. 3.8e), and negative correlations with CaO/Al_2O_3 and TiO_2/P_2O_5 (not shown), Al_2O_3/TiO_2 (fig. 3.8f), and Sc/Yb (fig. 3.8g). Their Eu* anomalies ($Eu/Eu^* = Eu_{CN}/\sqrt{(Sm_{CN} \times Gd_{CN})}$; CN, chondrite normalized) (fig. 3.8h) are restricted to a narrow range between 0.8-1.2.

The mafic samples from both suites exhibit a range of trace element concentrations, and can be subdivided based on their normalized REE patterns and ratios, and the presence or absence of a negative Nb anomaly relative to both La and Th (fig. 3.9; table 3.3). Among the three groups in the VC, the samples in VC1 have moderate LREE enrichment (fig. 3.9a), low La/Nb, no Th enrichment relative to La or Nb, and no negative Nb anomaly (fig. 3.9f). Those in VC2 exhibit moderate LREE enrichment similar to VC1 (fig. 3.9b), but higher La/Nb, stronger Th enrichment relative to Nb [$(Th/La)_{PM} \cong 1$; PM, primitive mantle], and a symmetrical negative Nb anomaly (Whalen et al., 2006; fig. 3.9g). The samples in VC3 have the strongest LREE enrichment (fig. 3.9c), highest La/Nb, Th enrichment similar to those in VC2 [but $(Th/La)_{PM} < 1$], and an asymmetrical negative Nb anomaly (fig. 3.9h). The samples in VC3 also exhibit the strongest depletions in Zr, Hf, and Ti compared to the two other groups, and all the three groups have low MREE/HREE ratios [$(Dy/Yb)_{CN} = 1.1\text{-}1.3$] (fig. 3.9a-c).

The mafic samples in the LBS can be grouped into LBS1 with moderate LREE enrichment and low MREE/HREE ratios (fig. 3.9d), variable La/Nb, no Th enrichment relative to La or Nb, and no negative Nb anomaly (fig. 3.9i). In comparison, the samples in LBS2 exhibit stronger LREE enrichment and higher MREE/HREE ratios (fig. 3.9e), high La/Nb, variable Th enrichment relative to Nb [but $(Th/La)_{PM} < 1$], and no negative Nb anomaly except in sample 11-317b (fig. 3.9j). All the samples in the LBS exhibit variable to no depletion in Zr and Hf but a distinct positive anomaly in Ti.

In various tectonic discrimination diagrams (fig. 3.10 a-c), the mafic samples from both suites with non-arc signature (fig. 3.10d) plot in the ocean-floor or mid-ocean ridge basalt (OFB or MORB) to within-plate or ocean island basalt (WPB or OIB) fields, whereas those with arc signatures exhibit a trend from ocean-floor basalt to arc, variations that are consistent with their negative Nb anomalies and variable Th enrichments (fig. 3.10d). However, all the mafic rocks exhibit high Ti, Zr, and P contents and relatively higher Zr/Y (2.5 - 10) and Ti/V (21 - 96) ratios compared to arc rocks. In Zr/Y-Zr (fig. 3.10e) and Ti-V (fig. 3.10f) diagrams, two samples plot near the boundary between arc and MORB fields whereas the remaining samples exhibit MORB or back-arc basalt (BAB) to OIB signatures.

3.6.3 Whole rock Sm-Nd and Rb-Sr isotopes

Four samples, two each from the VC and LBS, were selected for whole-rock Sm-Nd and Rb-Sr isotopic analysis. The isotope analytical data including published data for three samples (one in VC and two in LBS) from Valverde Cardenas et al. (2012) are presented in table 3.3, and plotted in fig. 3.11. The initial isotope ratios are calculated at 1 Ga.

The samples from the VC yield $\varepsilon Nd_{1\ Ga}$ values between +2.8 and -3.6, with corresponding depleted mantle Nd model ages (T_{DM}, DePaolo, 1981a) between 1.46 and 1.92 Ga. They have low initial Sr [$I_{Sr} = (^{87}Sr/^{86}Sr)_{initial}$] isotopic ratios of 0.70394 and 0.70465, with induced errors less than 0.00010 suggesting insignificant element mobility (Jahn, 2004; see footnotes of table 3.3).

The samples from the LBS yield $Nd_{1\ Ga}$ values between -1.1 and +5.2, with corresponding depleted mantle T_{DM} model ages between 1.71 and 1.08 Ga. Two of these samples have relatively high I_{Sr} ratios of 0.70682 and 0.70973 with induced errors between 0.00013 to 0.00031. The higher error value in sample 11-331b is significantly above the accepted value of 0.00010 (table 3.3), suggesting variable mobility of Rb and increase in Rb/Sr ratio. This sample (11-331b) exhibits evidence for strong sericitization and chloritization suggesting low-grade hydrothermal alteration may have affected its Rb/Sr ratio. Alternatively, variable degrees of mixing with crustal melt or fluid could also have increased the I_{Sr} ratios and Rb contents.

3.7 Petrogenesis of the mafic rocks

The mafic rocks in our study display sub-alkaline tholeiitic composition and immobile major and trace element ratios that span arc to intraplate settings in several tectonic discrimination diagrams (fig. 3.10). The observed REE and HFSE patterns (fig. 3.9), Nb/Th ratios (fig. 3.10d), and the ranges of εNd and I_{Sr} values (fig. 3.11-3.13) suggest the potential involvement of multiple sources, including: (i) a depleted asthenospheric mantle source; (ii) a supra-subduction zone mantle (SSZM) or arc source; (iii) a subduction-modified subcontinental lithospheric mantle (SCLM) source; and (iv) an enrichment process such as a low degree of partial melting, fractional

crystallization (FC), and/or crustal assimilation and fractional crystallization (AFC; DePaolo, 1981b).

3.7.1 Fractional crystallization

Despite evidence for high-grade metamorphism and minor hydrothermal alteration in some samples, which may have altered the concentrations of some mobile elements, the compositions of the mafic rocks in both suites exhibit consistent variations in major and trace elements, and element ratios, suggestive of fractional crystallization (fig. 3.8). In particular, olivine, clinopyroxene, and plagioclase fractionation are suggested by the variable MgO (9.4-5.5 wt%), Mg# (39-61), Cr (<20-320 ppm), and Ni (<20-210 ppm) concentrations, and negative Eu anomaly (Eu/Eu* = 0.81-1.15). The positive covariation of Ni (fig. 3.8a) and Cr (fig. 3.8b) with MgO, and the negative covariation of Sc/Yb (fig. 3.8g) and TiO_2 (fig. 3.8c) with the fractionation index Zr, suggest variable degrees of olivine, clinopyroxene, and plagioclase fractionation (e.g., Pearce and Norry, 1979). The sample RS431 from LBS1 has much higher Cr (490 ppm) and Ni (720 ppm) at comparable MgO (~6 wt%) and Mg# (44) than other samples, indicating a different mantle source, or much higher Ni and Cr in the parental melt, or this sample possibly being a cumulate. The variation of Eu anomaly (Eu/Eu*) from slightly positive to negative values with increasing Zr (fig. 3.8h) (or decreasing MgO) suggests that plagioclase was an accumulating phase for the most primitive samples, but became a fractionating phase during the later stage of magmatic evolution. The systematic increase in Fe_2O_3 and TiO_2 (fig. 3.8c) and a sharp decrease in Al_2O_3/TiO_2 (fig. 3.8f) with fractionation preclude significant Fe-Ti oxide separation, and are thus indicative of low oxygen fugacity (f_{O2}) conditions. The increase in P_2O_5 and Y (figs. 3.8d and e) and decrease in TiO_2/P_2O_5 with Zr (not shown) suggest

apatite accumulation. At comparable Zr, four samples of the LBS comprise a high P_2O_5 cluster, suggesting either a different source or a different path of fractionation for these samples.

The differentiation of tholeiitic magma resulting in fractionation of early-formed olivine and clinopyroxene, plagioclase, and accumulation of Fe-Ti oxides (e.g., ilmenite, rutile, titanite) and apatite under low f_{O2} conditions is typical of low-pressure fractional crystallization of modern ferrobasalts in oceanic and continental rift environments (Barberi et al., 1975; Byerly et al., 1976). However, the mafic tholeiites exhibit variable degrees of LREE enrichment and HFSE depletion relative to the adjacent REE (fig. 3.9). Although the LREE enrichment can be explained by partial melting of a mantle peridotite source, the highly variable incompatible element ratios, depletions in HFSE and the range of εNd and I_{Sr} ratios observed in the mafic rocks cannot be explained by any combination of partial melting and fractionation-accumulation processes. Rather, these trace element and isotopic features must be inherited source features (e.g., an arc or SCLM source), or alternatively, be related to contamination of mantle melts by an incompatible element-enriched lithospheric source, e.g., the continental crust or SCLM.

3.7.2 Arc vs. lithospheric contamination

Although a depleted asthenospheric mantle source is obvious for the least contaminated samples with high Nb/Th (Nb/Th > 7 indicating a non-arc source; Swinden et al., 1989), the pronounced depletions in HFSE with low Nb/Th (< 5), and enrichments in LREE (and LILE), are characteristics of both arc rocks produced in supra-subduction zones (i.e., SSZM) and mantle-derived melts contaminated by

continental crust or a subduction-metasomatized SCLM (e.g., Whalen et al., 1996; Whalen et al., 2006).

The mafic samples with a negative Nb anomaly and Nb/Th < 7 (fig. 3.10d) plot in the volcanic arc or transitional field in tectonic discrimination diagrams involving Th, Nb, Zr, and Ti (fig. 3.10a-d). Two of these samples (11-349 and RS314) – with high MgO, low Nb/Th, low Y, and low HFSE abundances (fig. 3.9g and h) – plot near the boundary between arc and MORB fields on the Zr-Zr/Y and Ti-V discrimination diagrams (fig. 3.10e-f), suggesting a depleted arc-type signature (e.g., Tatsumi and Eggins, 1995; Ewart et al., 1998). The remaining samples have overall HFSE contents higher than volcanic arc basalts (fig. 3.9f-j), and they plot in the MORB or BAB to OIB fields on the Zr-Zr/Y and Ti-V diagrams (fig. 3.10e-f). In discriminating between arc and contaminated continental tholeiites, several authors have pointed out the high abundances of trace elements in the latter compared to those in the arc-related tholeiitic and calc-alkaline rocks (e.g., Xu et al., 2008; Xia et al., 2014; Xu et al., 2017; Xia and Li, 2019).

Typical arc tholeiites exhibit low Nb/Th, but over a range of positive εNd values that can range from depleted mantle to CHUR (~0.0 to +5.0 at ca. 1 Ga; fig. 3.12a) (e.g., Whalen et al., 1996, 2006; Swinden et al., 1997). In comparison, continental tholeiites contaminated by crust or SCLM exhibit a wider range of εNd, varying from positive (non-arc source) to highly negative (continental crust or SCLM) (e.g., Swinden et al., 1997). In the mafic rocks in LBS, εNd varies from +5.2 (close to the depleted mantle at ca. 1 Ga; DePaolo, 1981a) to -1.0 (T_{DM} 1.08-1.71 Ga), and in the VC from +2.9 to -3.6 (T_{DM} 1.46-1.92 Ga) (fig. 3.11a; table 3.3). In both VC and LBS, εNd correlates positively with Nb/Th, Nb/La, and Sm/Nd, and negatively with $(La/Yb)_{CN}$,

SiO_2, and K/Zr (fig. 3.12b-f), features that are characteristic of continental tholeiites contaminated by crust or subduction-metasomatized SCLM. However, as discussed above, a small number of samples with arc-type signature were likely to have been derived from a subduction-metasomatized SCLM.

3.7.3 Role of lithospheric contamination

For a quantitative evaluation of crustal components in the mafic rocks, calculations of AFC (DePaolo, 1981b; appendix C) involving depleted asthenospheric mantle-derived melt and Labradorian crust (ca. 1.65 Ga; Schärer, 1991; Kerr, 1989; Thomson et al., 2011) and Archean crust (ca. 2.65 Ga; Weaver and Tarney, 1984; Kerr et al., 1995; Thomson et al., 2011) as end members were performed using Nd and Sr isotope data (table 3.4; figs. 3.13a-c). The ratio of assimilation to crystallization rate (R) required to fit the data is high (0.7), which is consistent with the high temperature of mafic magmas (~1100-1200 °C) and the high thermal gradient of crust undergoing extension and high-grade metamorphism. Lower R values (e.g., 0.2) produce flatter curves and much higher degrees of fractionation before the required degree of contamination is reached (e.g., curve Ib), thereby resulting in more felsic melt compositions (e.g., Chen et al., 1994). The AFC calculations suggest that the sample from VC2 requires ~4% assimilation of an Rb-rich crustal melt (curve I), whereas the sample in VC3 can be modelled using ~15% assimilation of an Sr-rich crustal melt (curve II).

The AFC calculations for the sample 11-331a from LBS1 require ~10% assimilation of crustal melts derived from an Rb-rich granite or granodiorite (curve I; figs. 3.13a & b). The sample 11-331b from LBS2 exhibits an even higher I_{Sr} ratio that, coupled with its high $^{143}Nd/^{144}Nd$, cannot be modelled with any value of R in the AFC

calculation (e.g., curves Ia and b in fig. 3.13a-c). The closest match is obtained by the curve Ib, which requires a very high degree of fractional crystallization (~90%) before the required degree of contamination is reached. Although an upper crustal contamination is obvious for the sample, as indicated by the presence of large xenocrystic quartz grains, late hydrothermal alteration has also affected it, as indicated by the presence of abundant sericite and chlorite. This latter process could have increased its Rb content resulting in very high I_{Sr}, and a high induced error in the I_{Sr} calculation, without necessarily affecting its Nd isotopic composition (table 3.3).

The AFC calculations suggest that ~15% or less contamination by an Archean crust (Weaver and Tarney, 1984) or underlying SCLM could also produce the observed Sr-Nd isotopic signatures of the mafic rocks, (curve III, fig. 3.13a and d, table 3.4). However, an Archean lithospheric contaminant produces much steeper AFC curves, resulting in lower Nd contents, and thus requiring much higher degrees (~60%) of fractional crystallization to reach the required level of Nd in the sample 11-351 in VC3 (fig. 3.13c). Further, for the modelled composition of the Archean crust (Weaver and Tarney, 1984), more than 30% contamination is required to reach the Sr content and Sr isotopic ratio for sample 11-351 (fig. 3.13c). Although a higher Sr content in the Archean contaminant would lower the required contamination level, the Sr values used in the modelled Archean crust (Sr = 350-580 ppm; Weaver and Tarney, 1984) is appropriate and comparable to that of the Archean crust from the Ashuanipi Complex (Sr = 318-758 ppm; Percival et al., 2003). Overall, our mafic dataset is best fit with AFC models using Proterozoic crust (or SCLM) as contaminants.

The calculated degrees of AFC in the mafic rocks cannot, however, explain the observed Nd contents (Nd = 18.7-40.6 ppm; fig. 3.13c), which are higher than the

relatively low Nd contents in the contaminant Labradorian or Archean crust (table 3.4). The high Nd coupled with high Zr, Ti, and moderate to low MgO and Mg# suggest that most of the contaminated samples in the VC and LBS were also variably fractionally crystallized. This is further supported by the observation that the contaminated samples with high Zr (~100-260 ppm) are generally more differentiated, with higher REE contents and negative Eu anomalies, but without significant increase in La/Yb ratios (fig. 3.13d), indicating the role of crystal fractionation (especially plagioclase) in a shallow magma chamber. These observations imply that the parental melts of the mafic rocks could have been contaminated before differentiation in an intermediate to shallow-level chamber, from which both the primitive and differentiated magmas with variable degrees of contamination were released and intruded the crust in the form of dykes and sills (e.g., Nykänen et al., 1994).

3.7.4 Depths of melting

The partition coefficients of REEs vary markedly with the mantle source mineralogy, i.e., MREEs show moderate and HREEs high compatibility in garnet but are incompatible in spinel (e.g., Halliday et al., 1995). As a result, the LREE/MREE and MREE/HREE ratios can be elevated in small-degree melts derived from garnet-peridotite, whereas melts of spinel-peridotite will produce MREE/HREE ratios similar to the mantle source and LREE/MREE ratios will increase with decreasing degree of melting (McKenzie and O'nions, 1991; Aldanmaz et al., 2000) or increasing source enrichment. Moreover, garnet is a stable phase in the mantle above ~80 km whereas spinel is stable below ~60 km and the depth between 60-80 km is considered to be transitional where both garnet and spinel can coexist (Ellam, 1992; Robinson and Wood, 1998). Therefore, the REE data that are strongly dependent on the spinel- vs.

garnet-peridotite can offer a sensitive means to infer the nature of source, degree of partial melting, and the depth of melt generation in the mantle source region.

The relatively high SiO_2 and low Fe_2O_3-TiO_2 contents in the least contaminated tholeiitic samples with highest MgO suggest that they were derived from partial melting of mantle peridotite at shallow depth (e.g., Klein and Langmuir, 1987). A shallow depth is also supported by the flat to slightly fractionated HREE patterns (fig. 3.9a-d) and HREE contents (~10-20 times chondritic) of the most primitive samples in VC and LBS1 – indicating partial melting took place mostly at shallow depth. Those in LBS2 exhibit greater fractionation in HREE (fig. 3.9e) and high Ti/Y, which is suggestive of greater depth of melt generation for these samples. The depth of melt generation can be semi-qualitatively assessed using $(Tb/Yb)_{PM}$ ratios as a proxy (Wang et al., 2002). In the $(Tb/Yb)_{PM}$ vs. $(La/Sm)_{PM}$ diagram (fig. 3.14a), most of the mafic rocks plot within the spinel-peridotite field corresponding to < 2.8 GPa or < 85 km depth. At comparable $(La/Sm)_{PM}$ ratios, two samples from LBS2 (11-317b, 11-331b) exhibit higher $(Tb/Yb)_{PM}$, which crosses the spinel-garnet boundary, indicating a higher proportion of garnet in their source, whereas the third sample (11-216c) exhibits much higher $(La/Sm)_{PM}$ ratio comparable to those from VC3. Increasing La/Sm in the mafic samples indicates increasing degree of crustal contamination, as discussed above. In the Ce/Sm vs. Sm/Yb diagram (fig. 3.14b), the modelled (non-modal batch melting, appendix C) partial melting curves for a primitive mantle composition within the shallow spinel-peridotite and deeper garnet-peridotite are shown. The least contaminated mafic samples with Nb/Th > 5 and MgO > 5 wt% indicate between ~4-10% melting of peridotite, and garnet: spinel-peridotite ratios of up to ~40:60. The sample in LBS2 exhibits ~5% melting and garnet: spinel peridotite ratios of ~70:30.

In summarizing the petrogenesis of the mafic rocks, their geochemical and isotopic features are best explained by partial melting of a predominantly depleted asthenospheric source contaminated by Paleoproterozoic crust or SCLM, and a subordinate arc-type SCLM source. The least contaminated samples suggest derivation from 4-10% partial melting of peridotite with a maximum garnet: spinel peridotite ratio of ~40:60 for the samples in VC and LBS1, and ~5% partial melting of mantle peridotite with garnet: spinel peridotite ratio of ~70:30 for the samples in LBS2. The degree of crustal contamination was relatively greater for the VC (~4-20%) compared to that in the LBS (~4-10%), which is compatible with the MORB to arc-type signatures of the former, and the MORB to WPB-type signatures of the latter (fig. 3.10). Parental melts of the mafic rocks were contaminated before differentiation in an intermediate to shallow level chamber, where both primitive and differentiated magmas with variable degrees of contamination evolved together. Fractionation of early-formed olivine and clinopyroxene, plagioclase, and accumulation of Fe-Ti oxides (e.g., ilmenite, rutile, titanite) and apatite took place under low f_{O2} condition, suggesting low-pressure fractional crystallization.

3.8 Discussion

3.8.1 Late-orogenic magmatic events in the hinterland

The available age data for late-Grenvillian (ca. 1020-980 Ma) igneous and metamorphic events in the Canyon domain, Grenville hinterland, are summarized in fig. 3.15. The emplacement ages for the mafic rocks in the VC and LBS at 1007.7 ± 2.0 Ma and 997 ± 3.8 Ma, respectively, span the post-Ottawan to early-Rigolet phases of the Grenvillian orogeny. This part of the central Grenville Province also records several

post-Ottawan to early-Rigolet intrusions: (i) ca. 1017-1015 Ma Sabot and Okaopéo plutonic suite consisting mangerite and gabbronorite (Gobeil et al., 2002; Moukhsil et al., 2013b, 2014; Augland et al., 2015); (ii) the ca. 1017-1007 Ma granite veins and sheets (e.g., 1015 Ma Hart Jaune granite; Indares et al., 1998) in the in aH*P* MIZ; (iii) the ca. 1004-1002 Ma REE-rich pegmatite granite dykes (PGDs) in the southern Canyon domain and in the Lac Okaopéo area (Turlin et al., 2017, 2019); (iv) the ca. 995 Ma undeformed pegmatite granite dyke in the Canyon domain (Dunning and Indares, 2010); and (v) the syn-tectonic (syn-D2) pegmatite granite dykes and coeval ca. 986 Ma pink leucogranite dyke swarm in the northern Canyon domain (Jannin et al., 2018).

Elsewhere in the southwestern Grenville Province, several post-Ottawan alkalic syenite to granite and AMCG suites have been reported, e.g., the ca. 1020.6 Ma Wemotaci and ca. 1019 Ma Rheaume syenites (Côté et al., 2018); the ca. 1014 Ma Core and ca. 1009 Ma Bouvreuil syenite (Augland et al., 2017); and the ca. 1020-1008 Ma Valin Anorthositic suite (Emslie and Hunt, 1990; Owens et al., 1994; Higgins and van Breemen, 1996; Hébert et al., 2005).

Among these, the post-Ottawan magmatic intrusions (ca. 1020-1005 Ma) are interpreted by the above authors to have been derived from melting of upwelling asthenosphere, lithospheric mantle, and lower crust, and emplaced in an extensional setting. They provide important geochemical, tectonic, and temporal constraints on the post-Ottawan evolution of the Grenville hinterland that are discussed in section 3.8.4. On the other hand, the Rigolet pegmatitic granite intrusions (ca. 1005-986 Ma) are interpreted to have been derived from partial melting of allochthonous PLV paragneiss and/or parautochthonous paragneiss from the Gagnon terrane at depth, which was

interpreted to have been underthrust beneath the hinterland in the beginning of Rigolet convergence (Turlin et al., 2017, 2019; Jannin et al., 2018b).

3.8.2 Late-orogenic metamorphism in the hinterland

3.8.2.1 Zircon and monazite ages

On the *hanging wall* (southeast) side of the AB, the post-Ottawan thermal events in aM*P* and aH*P* domains in the central Grenville Province are constrained by metamorphic zircon and monazite ages. The metamorphic zircon age of ca. 1008 Ma for the mafic dyke in the VC and the inferred ≤ 997 Ma age of metamorphism for mafic sills in the LBS in northern Canyon domain (this study) correlate with other post-Ottawan zircon ages in the aM*P* belt in the study area that range from ca. 1013-996 Ma (Indares et al., 1998; Cox et al., 2002; Indares and Dunning, 2004; Dunning and Indares, 2010; Lasalle et al., 2013; Augland et al., 2015), and a relatively wider range of monazite ages between ca. 1020-980 Ma, determined from aluminous paragneiss samples in the LBS and PLV (Dunning and Indares, 2010; Lasalle et al., 2014). As noted previously, these zircon and monazite ages were collectively interpreted to represent one or more thermal pulses related to late-tectonic igneous intrusions (i.e., of the granite pegmatites and ultrapotassic dykes), and/or to zircon and monazite growth during a fluid-present, greenschist-facies metamorphic overprint (Indares and Dunning, 2004; Dunning and Indares, 2010; Lasalle et al., 2013, 2014).

In the aH*P* MIZ, the post-Ottawan metamorphic zircon (~1026-1007 Ma; Cox et al., 2002) and monazite ages (~1020-1006 Ma; Indares and Dunning, 2001; Lasalle et al., 2014) were correlated with northwest-directed tectonic extrusion of deep crustal levels either followed by, or coeval with, southeast-directed extension at the structural

top (Indares et al., 1998; Indares, et al., 2000; Cox et al., 2002). The extension in the Boundary Zone (structural top of the MIZ) was constrained by several granite intrusions between ca. 1017-1007 Ma (Indares et al., 1998) along steeply southeast-dipping shear zones to the north of Hart Jaune terrane (HJT; orogenic lid). A distinctly younger metamorphic monazite age of 989 ± 2 Ma (Scott and Hynes, 1994) at the base of the HJT was inferred to indicate Rigolet crustal thickening and lower amphibolite-facies metamorphism in the overlying MIZ (Hynes et al., 2000; Indares et al., 2000).

On the *footwall* (northwest) side of the AB, zircon ages come from the early Paleoproterozoic KLG metapelites in the Gagnon terrane that recorded zircon growth episodes between ca. 1002 and 961 Ma (Jannin et al. 2018a, b), and metamorphic monazite development at ca. 995 Ma and ca. 988-985 Ma (Jordan et al., 2006). These zircon and monazite ages were correlated with multiple stages of reverse and normal shearing and high-grade metamorphism (in both the kyanite and sillimanite fields) during underthrusting of the footwall Gagnon terrane in the Parautochthonous Belt beneath the hinterland during the Rigolet orogenic phase (Jordan et al., 2006; Indares et al., 2008; Jannin et al., 2018a, b). Among these, the ca. 993-986 Ma normal-sense shear zones developed in the allochthonous and underlying parautochthonous rocks were interpreted as parts of a crustal-scale channel named the Thachic Shear Zone (Jannin et al., 2018b).

3.8.2.2 Titanite ages

In the aM*P* belt, the range of titanite ages in the Canyon domain and the Banded Complex to the northeast is essentially identical (ca. 995-987 Ma and ca. 993-987 Ma, respectively; Indares and Dunning, 2004), and were interpreted to indicate post-

deformation thermal disturbances related to pegmatite intrusion coeval with localized shearing (Indares and Dunning, 2010).

In the MIZ, the post-Ottawan titanite ages between ca. 1007-989 Ma were interpreted to indicate retrograde amphibolite-facies metamorphism and Rigolet crustal shortening (Indares et al., 1998; Indares et al., 2000).

3.8.3 Summary and tectonic context of igneous and metamorphic ages

i. The post-Ottawan crustal extension and amphibolite-facies metamorphism between ca. 1020-1007 Ma in the aH*P* MIZ are broadly coeval with the high-grade metamorphism at ca. 1020-1000 Ma in the structurally overlying aM*P* Canyon domain. These ages also overlap with the crystallization ages of the alkalic arc to intraplate type Sabot and Okaopéo AMCG suites at ca. 1017-1015 Ma, and that of the intrusion of arc to intraplate type mafic tholeiitic dykes of VC at ca. 1008 Ma, collectively suggesting that large areas of the hinterland comprising different Ottawan pressure domains were under extension at this time (fig. 3.16a, b).

ii. The post-Ottawan metamorphic zircon (~1013-996 Ma) and monazite ages (~1020-980 Ma) in the aM-L*P* belt in the hinterland were collectively interpreted to represent thermal pulses related to late-tectonic igneous intrusions and greenschist-facies metamorphism (Indares and Dunning, 2004; Dunning and Indares, 2010; Lasalle et al., 2013, 2014). However, the ca. 1004-1002 Ma REE-rich PGDs, with igneous monazite ages formed between ca. 1005-997 Ma, were interpreted to have been derived by partial melting of parautochthonous paragneiss units deeper in orogenic crust, (Turlin et al., 2017, 2018, 2019; see

Côté et al., 2018 for an alternative interpretation). These data suggest high-grade metamorphism and partial melting in the deep parautochthonous crust as a result of its underthrusting beneath the hinterland at this time. Moreover, based on field evidence, these PGDs were inferred to have intruded the migmatitic paragneisses of the PLV when the latter was close to their wet solidus condition (Turlin et al., 2018), implying the aM*P* crust was at higher temperature in the post-Ottawan than previously interpreted.

iii. Post-Ottawan high-grade metamorphism in the aM*P* belt is further supported by the petrographic evidence of granulite- to amphibolite-facies assemblages in the mafic rocks, for which an age of ca. 1008 Ma in the VC and ≤ 997 Ma in the LBS are determined (this study).

iv. The REE-rich PGDs in the southern Canyon domain and in Lac Okaopéo area were interpreted to have been derived from partial melting of the underlying parautochthonous KLG paragneiss, as a result of underthrusting of Gagnon terrane beneath the southern Canyon domain (fig. 3.16c). However, the PGDs have not been reported from the northern Canyon domain where the ca. 1008-997 Ma mafic dykes and sills of VC and LBS occur (fig. 3.3). This may indicate that the southern Canyon domain and the Lac Okaopéo area were more proximal to the AB and the underlying parautochthonous crust compared to the northern Canyon domain at the beginning of the Rigolet orogenic phase (fig. 3.16c; discussed further below).

v. Rigolet underthrusting of the Gagnon terrane led to the development of ca. 990 Ma mid-crustal channel along the newly recognized Thachic Shear Zone (TSZ)

in the northern Canyon domain and adjacent Gagnon terrane (Jannin et al., 2018b).

vi. A younger age limit for high-grade metamorphism in the northern Canyon domain is constrained by the ca. 986 Ma pink leucogranite dyke swarm and syn-kinematic pegmatites that intruded during the normal-sense shearing along the TSZ in the northern Canyon domain, which was in the immediate hanging wall of AB at that time (Da2 of Jannin et al., 2018b). The leucogranite dyke swarm was inferred to have been derived by partial melting of paragneiss in the parautochthonous Gagnon terrane that was transported beneath the study area by Rigolet underthrusting (during Dp1 of Jannin et al., 2018a, 2018b). The inference implies that the parautochthonous crust was below the northern Canyon domain by ca. 986 Ma, and strongly suggests that the northern Canyon domain was extruded along the AB between ca. 997-990 Ma (fig. 3.16d), and was subsequently incorporated into the ca. 990 Ma TSZ channel (fig. 3.16e).

vii. The Rigolet amphibolite-facies metamorphism and deformation in the TSZ and the development of the ca. 990 Ma channel in the northern Canyon domain were coeval with metamorphism and related pegmatite intrusions between ca. 995-987 Ma (U-Pb titanite ages; Dunning and Indares, 2010) in the MIU and PLV in the hanging wall of the TSZ (subdomains 3a and 3b of Jannin et al., 2018b; fig. 3.3b). Moreover, the formation of the Rigolet channel was also coeval with the ca. 989 Ma L*P* amphibolite-facies metamorphism at the base of HJT during assembly of the aM-L*P* units (Banded and Gabriel Complexes to the north of Canyon domain) into a Rigolet fold-thrust stack that was thrust over the aH*P*

MIZ (Scott and Hynes, 1994; Hynes et al., 2000; Indares et al., 2000; Indares and Dunning, 2004).

3.8.4 Late-orogenic tectonic setting of the hinterland: geochemical constraints

The post-Ottawan to early Rigolet (ca. 1020-995 Ma) record of mantle-derived intrusions in the interior magmatic belt (orogenic core) in the Grenvillian hinterland is relatively sparse (fig. 3.2), and hence not much has been known about its tectonic setting (Rivers, 2015). However, several recently reported magmatic suites, including the alkaline syenitic to gabbroic complexes, granitic pegmatites, and mangerite suites, noted previously, together with the previously known AMCG complexes and the tholeiitic mafic dykes and sills in our study, provide the basis for an improved understanding.

In the central Grenville Province, the metaluminous ca. 1017-1015 Ma Okaopéo and Sabot mangerite suite exhibit an A-type geochemical signature, whereas their mafic tholeiitic, Fe-Ti-P oxide-rich gabbronoritic components exhibit a tholeiitic intraplate character (Gobeil et al., 2002; Moukhsil et al., 2013b, 2014; Augland et al., 2015). The Okaopéo mangerite has an alkalic arc granitoid signature with low negative zircon εHf values (-1.01 to -1.73) and Makkovikian model ages (~1.9 Ga) (Moukhsil et al., 2014; Augland et al., 2015). These authors suggested that both the Okaopéo and Sabot suites were components of late-orogenic AMCG suites, and compared them to other, mostly small-volume, late-Grenvillian AMCG suites, such as the ca. 1020-1008 Ma Valin suite (part of the CRUML belt; Owens et al. 1994; Hébert et al., 2009), and the undated Berthé anorthosite (inferred to be ca. 1 Ga; Moukhsil et al., 2013a) (figs. 3.2 and 3.3).

Many of the syn-Grenvillian andesine anorthosites are small, highly alkalic bodies (e.g., Owens et al., 1994; Icenhower et al., 1998; Owens and Dymek, 2001), thereby contrasting with the much larger pre-Grenvillian sub-alkaline labradorite anorthosite suites in the Grenville Province, suggesting they were derived from different source(s). For example, the ca. 1010-1008 Ma alkalic Labrieville anorthosite, part of the Valin AMCG suite, exhibits low I_{Sr} (~0.7032-0.7034), low positive εNd values (+0.8 to +2.5), a young model age (T_{DM} 1.26-1.36 Ga), and contains high Ba and Sr (Owens et al., 1994). These late-orogenic AMCG suites were interpreted to have been derived from melting of a young lower crustal component, with the heat source supplied by rising asthenosphere associated with an upwelling mantle plume, or as a result of lithospheric delamination, in a manner similar to that envisaged for other Grenvillian AMCG suites (e.g., Owens et al., 1994; Higgins and van Breemen, 1994). However, trace element modelling on the late-Grenvillian alkalic AMCG suites is suggestive of their derivation from an incompatible element-enriched and subduction-metasomatized lithospheric mantle source (Greenough and Owen, 1995; Owens and Tomascak, 2002; Bédard, 2009), similar to that proposed for the ca. 1060 Ma Saint Urbain suite (Icenhower et al., 1998). Similarly, the Okaopéo mangerite suite with high Ba and Sr contents and an A-type volcanic arc granitoid signature with homogeneous Hf isotope composition also suggests a subduction-modified, incompatible element-enriched, lithospheric mantle source, possibly mixed with melts of Paleoproterozoic lower crust (Augland et al., 2015). The intraplate-type mafic components of the Okaopéo suite suggest asthenospheric melt contaminated by SCLM and/or crust. On an orogen-scale, the late- to post-Ottawan alkalic AMCG suites were interpreted to have been emplaced in an extensional setting following Ottawan crustal thickening (Owens

and Dymek, 2016), and this extensional setting with thinned orogenic lithosphere has been compared with the Basin and Range Province (Greenough and Owen, 1995; Rivers, 2015).

Elsewhere in the western Grenville Province, post-Ottawan alkalic suites from the Haut-Saint-Maurice area include several small-volume, arc to within-plate-type, syenodiorite to granite suites that were emplaced between ca. 1021-1009 Ma (Augland et al., 2017; Côté et al., 2018). Among these, the Core syenite (ca. 1014 Ma) exhibits low positive εHf values (+1.4 to +3.0) and a post-Pinwarian model age (ca. 1.4 Ga), whereas the Bouvreuil syenite (1009 Ma) exhibits high negative εHf values (-2.0 to -3.1) and a Labradorian model age (ca. 1.6 Ga) (Augland et al., 2017). In a recently proposed tectonic model, the mid- to post-Ottawan alkalic mafic to felsic suites were interpreted to have been derived from supra-subduction zone mantle that evolved from a ca. 1040-1015 Ma accretionary arc and associated back-arc to a ca. 1015-1000 Ma extensional setting related to slab break-off or retreat (Augland et al., 2017; Côté et al., 2018), which they correlated with late-Grenvillian orogenic collapse in the crust. In this model, the Ottawan phase was compared with an Andean accretionary orogeny (Augland et al., 2017; Côté et al., 2018). However, the lack of tholeiitic to calc-alkaline basalt-andesites and calcic to calc-alkalic to alkali-calcic arc granitoids (Gill, 1981; Brown et al., 1984; Tatsumi et al., 1986; Kelemen et al., 2014), derived from subduction-modified depleted mantle, followed by their differentiation under high P_{H2O} and high f_{O2} conditions, typical of modern arc settings (Ballhaus et al., 1990; Arculus, 1994), are inconsistent with this model. The absence of evidence for a rapid progression of high-volume magmatism from an early arc-type to non-arc-type mafic and then WPG and VAG magmatism along a linear belt, typical of slab break-off model (e.g., Turner

et al., 1999; Whalen et al., 2006; Xu et al., 2008), argues against the post-Ottawan slab break-off model. LILE- and HFSE-enriched alkalic suites with arc geochemical signatures, although characteristic of modern, metasomatized SSZM (e.g., Varne and Foden, 1986; Stolz et al., 1998), are also well known to occur in many post-collisional suites derived from previously metasomatized SCLM (e.g., Brown et al., 1984; DeCelles et al., 2002; Chung et al., 2005; Jiang et al., 2012; and references therein), but their characteristic Nd or Hf isotopic signatures are very different (e.g., the Kohistan arc vs. the French Massif Central; Moyen et al., 2017). For example, the modern day Andean Cordillera exhibits isotopic "pull-ups" and "pull-downs" (DeCelles et al., 2009), which are comparable to its ancient analogue, the southeastern margin of Laurentia during the Mesoproterozoic (Augland et al., 2015; Maity and Indares, 2018; Groulier et al., 2018a), but not to the Grenvillian Orogen, for which enriched Nd isotopic signatures of orogenic mantle-derived suites are linked with its enriched lithospheric mantle sources (fig. 3.11b) that were metasomatized during the long-lived Paleoproterozoic to Mesoproterozoic subduction events along the SE margin of Laurentia. On the other hand, incompatible element-enrichment in SCLM-derived post-collisional intrusions in the Variscan (Gutiérrez-Alonso et al., 2011; Dostal et al., 2019) or Himalaya-Tibet Orogen (Jiang et al., 2012; Liu et al., 2014) is widely interpreted to be largely a result of pre- to syn-collisional subduction events, which could have predated the timing of magmatism by several 10s to 100s of million years. In the case of Grenville Province, the radiogenic isotope data available from the Ottawan and post-Ottawan magmatic suites support older SCLM and asthenospheric sources in a collisional setting, rather than a continental margin accretionary arc and back-arc setting. The Grenvillian incompatible element-enriched SCLM could have developed

during the long-lived Mesoproterozoic subduction-related events along the southeastern Laurentian margin preceding the Grenvillian Orogeny (Rivers and Corrigan, 2000; Chiarenzelli et al., 2010).

On the other hand, the ensuing Rigolet phase (ca. 1005-980 Ma) is mostly recognized as a renewed phase of continental convergence, when the orogenic front moved from the Grenvillian hinterland to the foreland in the Parautochthonous Belt (Rivers, 2008; 2015 Rivers et al., 2012). As noted, the ca. 1004-1002 Ma REE-rich PGDs and the ca. 984 Ma pink leucogranite dyke swarms, intrusive within the aM*P* belt, were interpreted to have been derived from partial melting of Paleoproterozoic (KLG) and/or Archean paragneiss in the Gagnon terrane that was underthrust beneath the hinterland during the onset of the Rigolet phase at ca. 1005 Ma (Jannin et al., 2018a, b; Turlin et al., 2017, 2019). The ca. 980 Ma ultrapotassic dykes in the Canyon domain (Dunning and Indares, 2010) were also interpreted to have been derived from an Archean SCLM (Valverde Cardenas et al., 2012). These data strongly suggest that the post-Ottawan extensional setting was followed by early-Rigolet convergence and underthrusting of the Parautochthonous Belt beneath the Allochthonous Belt. The tectonic significance of the ultrapotassic dykes in relation to the Rigolet orogenic phase is discussed in Chapter 4.

3.8.5 Tectonic setting of the mafic rocks in the study area

Based on the discussion in the preceding section, we propose that a short-lived, lithospheric-scale extension took place during the post-Ottawan period in the hinterland in the central Grenville Province. Lithospheric extension, even with a small stretching factor, can cause melting in the SCLM under a potential mantle temperature as low as ca. 1280 °C and a lithospheric thickness of 80-100 km or less (e.g., McKenzie and

Bickle, 1988; Gallagher and Hawkesworth, 1992). Hence, lithospheric extension at the beginning of the post-Ottawan period (fig. 3.16a) could have caused melting in the previously-metasomatized SCLM to produce the mafic alkaline plutons and AMCG suites with arc to within plate geochemical signatures that were emplaced between ca. 1017-1015 Ma in the study area and between ca. 1021-1000 Ma in the western Grenville Province.

Continued extension would have allowed asthenospheric upwelling to relatively shallow levels, where decompression melting produced the mafic tholeiitic magmas with arc to MORB and WPB-type geochemical signatures that intruded the VC at ca. 1008 Ma (fig. 3.16b). The samples from LBS1 with a MORB-type signature could also have been emplaced at this time. The combined trace element and isotopic data for the VC and LBS1 (figs. 3.11-3.13) indicate mainly spinel-facies (<80 km depth) melting of the depleted asthenospheric mantle followed by crustal contamination. Melting of spinel-peridotite also provides an approximate estimate of the decreased lithospheric thickness under continental extension at this time compared to that of the early- and mid-Ottawan period reported from the western Grenville Province (based on mineral geothermobarometry data; Corriveau and Morin, 2000; Côté et al., 2018). The LBS2 samples exhibit MORB (or BAB) to OIB-type signatures and one sample yields high positive εNd value, implying melting had progressed to deeper levels of the upwelling asthenosphere, within the garnet-stability field, by ca. 997 Ma. This indicates lithospheric thickening at this time, which is compatible with Rigolet crustal shortening in the study area.

However, given the coeval emplacement of the mafic tholeiites in the northern Canyon domain and the REE-rich PGDs of Turlin et al. (2017, 2019) in the southern

Canyon domain/Lac Okaopéo area, the contrasting deductions of melting of an upwelled asthenospheric mantle in an extensional setting, and melting of the PLV and KLG paragneisses in a compressional setting, respectively, yield an apparent contradiction regarding the post-Ottawan tectonic setting. Moreover, the REE-rich PGDs do not occur in the northern Canyon domain, where the coeval mafic rocks of the VC and the LBC and the younger ca. 986 Ma pink leucogranite dyke swarms are pervasive. These observations suggest that before ca. 1005 Ma the structurally lower northern Canyon domain (subdomains 2a and 3a of Jannin et al., 2018b; fig. 3.3b) was in a more distal (southeasterly) location with respect to the AB such that it had access to upwelling asthenospheric melts in the hinterland (fig. 3.16b); whereas the structurally higher PLV in the southern Canyon domain (subdomain 3b of Jannin et al., 2018b) and the Lac Okaopéo area were in a more proximal (northwesterly) location with respect to the AB and the underlying parautochthonous Gagnon terrane in the foreland, and to melts derived from it (fig. 3.16b-c). In this setting, perhaps a thin sliver of previously upwelled asthenosphere was sandwiched between the underthrust Archean lithosphere and the overlying Grenvillian hinterland. The ca. 1005-1002 Ma REE-rich PGDs, derived from underthrust Paleoproterozoic (KLG) to Archean paragneiss of the Gagnon terrane, were intruded in the PLV and in the Lac Okaopéo area, whereas the ca. 1008-997 Ma mafic dykes and sills, derived from asthenospheric mantle, were emplaced within the VC and LBS in the structurally lower crustal panel of the northern Canyon domain. This arrangement was then followed by ductile extrusion of the northern Canyon domain to the northwest along the AB (fig. 3.16d), such that its original position relative to the southern Canyon domain and Lac Okaopéo

area was reversed, after which it became incorporated into the ca. 990 Ma channel flow regime within the TSZ as described by Jannin et al. (2018b) (their domain 2a; fig. 3.3b).

This scenario is compatible with two independent observations. Firstly, it is compatible with intrusion of the ca. 986 Ma pink leucogranite dyke swarm in the northern Canyon domain, but the absence of the ca. 1005-1002 Ma REE-rich PGDs, both presumably being derived from the underlying parautochthonous crust (Jannin et al., 2018b; Turlin et al., 2019). Secondly, it provides a metamorphic context for the petrographic evidence for decompression and/or heating in the mafic samples from the LBS, and for the interpretation that the dykes and sills in the VC and LBS were emplaced into high-grade metamorphic rocks.

In conclusion, the mafic rocks of this study were intruded within the aM*P* crust in a tectonic setting that progressed from post-Ottawan extensional to Rigolet compressional regimes. Overall, the tectonic setting of the Grenville Orogen evolved from a large, hot, long-duration continental collisional phase in the Ottawan to a short-duration, post-Ottawan lithospheric extensional phase that was shortly followed by the Rigolet phase of renewed convergence. The interval between the Ottawan and Rigolet phases, previously referred to as a "hiatus", is now well constrained as a period of lithospheric extension and resulting orogenic collapse, which is distinct from the Ottawan orogenic collapse that resulted from lithospheric delamination of the overthickened orogenic root.

3.9 Summary and conclusions

Based on field observations, petrography, major and trace element geochemistry, Sr-Nd isotopes, and U-Pb zircon geochronology, the following conclusions are reached:

i. The mafic dykes and sills in the VC and in the LBS, both with amphibolite- to granulite-facies mineral assemblages, were emplaced during the post-Ottawan period, with the age of syn-metamorphic emplacement of the former being constrained at ca. 1008 Ma and an emplacement age of ca. 997 Ma for the latter.

ii. The dykes in the VC record evidence for granulite-facies metamorphism (assemblage Grt + Opx + Cpx + Pl + Hbl) at ca. 1008 Ma, whereas the sills in the LBS record decompression and/or heating to L*P* amphibolite- and granulite-facies assemblages (Grt + Pl + Opx ± Hbl ± Bt) at ≤ 997 Ma. This implies that this part of the orogenic hinterland experienced two regional high-grade metamorphisms during the Grenvillian Orogeny: an earlier, high-strain, M*P* granulite-facies event in the early- to mid-Ottawan (~1080-1040 Ma) that was associated with crustal thickening and widespread partial melting; and a later, short-duration, lower-strain, post-Ottawan amphibolite- to granulite-facies event from ca. 1008 to ≤ 997 Ma that was driven by lithospheric extension and crustal thinning followed by Rigolet convergence, for which evidence is best preserved in the northern Canyon domain. This late-orogenic high-grade metamorphism is only readily recognized in small post-Ottawan units that were emplaced after the earlier Ottawan high-grade metamorphism, and its extent remains poorly constrained in the Allochthonous Belt.

iii. The dykes and sills in the VC and LBS are small-volume, mafic tholeiites that were emplaced in a transitional setting varying from extensional to compressional tectonic regimes. They were derived predominantly from an isotopically depleted asthenospheric mantle source with REE composition broadly similar to the primitive mantle. The most primitive samples from VC and LBS1 indicate ~4-10% melting of a spinel-peridotite source at shallow depth (<80 km), with a maximum garnet: spinel peridotite ratio of ~40:60, but samples in the LBS2 also indicate melting in a slightly deeper transitional garnet-spinel-peridotite source (~60-100 km depth), or mixing between melts derived from garnet- and spinel-peridotite, which is consistent with higher garnet: spinel peridotite ratio of ~70:30.

iv. Melts thus derived were subjected to variable degrees of contamination by lithospheric melts in intermediate to shallow magma chambers, and simultaneous low-pressure fractional crystallization of olivine-clinopyroxene-plagioclase and accumulation of Fe-Ti oxides and apatite under low f_{O2} conditions. The AFC calculations suggest that the degree of mixing with crustal melts was between ~4-20% in the VC and ~4-10% in the LBS.

v. When integrated with other studies, the results of this study suggest that the post-Ottawan lithospheric extension and asthenospheric upwelling gave rise to melting in the extended SCLM and lower crust, thereby producing a wide range of alkaline syenite-granite bodies, alkalic AMCG suites, and granite pegmatite intrusions. Continued extension allowed decompression-melting of rising asthenosphere at shallow depth (≤60 km), thereby producing the small-volume tholeiitic intraplate mafic dykes and sills of the VC and LBS. A small number

of samples in the LBS2 were derived from relatively deeper (≥65 km) melting within the asthenosphere during the early-Rigolet phase of shortening and crustal thickening, which also resulted in underthrusting of the orogenic foreland beneath the hinterland.

vi. The presence of several post-Ottawan to early-Rigolet leucogranite bodies in the Grenville hinterland, presumably derived from lower levels of allochthonous crust and the underthrust parautochthonous crust, indicates that crustal melting was important during this interval. Their widespread distribution over hundreds of km^2 implies the existence of an elevated regional geotherm, which is compatible with the evidence for a second high-grade metamorphic event in the aM*P* crust at this time. Moreover, an elevated geotherm may also explain the well-known signature of very slow cooling of the high-grade hinterland after the Ottawan metamorphic peak, recorded in many $^{40}Ar/^{39}Ar$ hornblende and biotite dating studies (Rivers, 2012).

vii. During the post-Ottawan period, the northern Canyon domain was in a more distal position with respect to the Allochthon Boundary and the Parautochthonous Belt, and was laterally extruded to the northwest along the base of the Allochthon Boundary before being incorporated into the Rigolet mid-crustal channel.

In conclusion, the magmatic products derived from melting of orogenic crust and its underlying heterogeneous mantle sources provide unique constraints on the multi-stage tectonic evolution of the ancient Grenvillian LHO, permitting significant refinement to existing tectonic models and offering an opportunity for comparison with tectonic processes in modern LHOs.

3.10 Acknowledgement

This research is part of the Ph.D. project of B.M. and was supported by a NSERC Discovery Grant to A.I. Sherri Strong, Anne Westhues, Pam King, Amanda Langille, Michael Shaffer, David Grant, and Dylan Goudie are acknowledged for help with sample preparation and analyses at Memorial University. Toby Rivers is gratefully acknowledged for informal discussions and thought-provoking reviews of several versions of the manuscript, and Graham Layne is thanked for sharing his insights on geochemistry. Constructive criticism on an earlier version of this manuscript from Hamish Sandemann and an anonymous reviewer are gratefully acknowledged.

3.11 References

Aldanmaz, E., Pearce, J., Thirlwall, M., Mitchell, J. 2000. Petrogenetic evolution of late Cenozoic, post-collision volcanism in western Anatolia, Turkey. Journal of Volcanology and Geothermal Research, 102: 67–95. doi:10.1016/S0377-0273(00)00182-7

Arculus, R.J. 1994. Aspects of magma genesis in arcs. Lithos, 33: 189–208. doi:10.1016/0024-4937(94)90060-4.

Augland, L.E., Moukhsil, A., Solgadi, F. 2017. Mantle influence of syn- to late-Grenvillian alkaline magmatism in the Grenville Province: causes and implications. Canadian Journal of Earth Sciences, 15: 1–15. doi:dx.doi.org/10.1139/cjes-2016-0135

Augland, L.E., Moukhsil, A., Solgadi, F., Indares, A., McFarlane, C. 2015. Pinwarian to Grenvillian magmatic evolution in the central Grenville Province: new constraints from ID–TIMS U–Pb ages and coupled Lu–Hf S–MC–ICP–MS data. Canadian Journal of Earth Sciences, 52: 701–721. doi:10.1139/cjes-2014-0232

Ballhaus, C., Berry, R.F., Green, D.H. 1990. Oxygen fugacity controls in the Earth's upper mantle. Nature, 348: 437–440. doi:10.1038/348437a0

Barberi, F., Ferrara, G., Santacroce, R., Treuil, M., Varet, J. 1975. A transitional basalt-pantellerite sequence of fractional crystallization, the Boina Centre (Afar Rift, Ethiopia). Journal of Petrology, 16: 22–56. doi:10.1093/petrology/16.1.22

Beaumont, C., Nguyen, M.H., Jamieson, R. A., Ellis, S. 2006. Crustal flow modes in large hot orogens. Geological Society London Special Publication, 268: 91–145. doi:10.1144/GSL.SP.2006.268.01.05

Bédard, J.H. 2009. Parental magmas of Grenville Province massif-type anorthosites, and conjectures about why massif anorthosites are restricted to the Proterozoic. Earth and Environmental Science Transactions of the Royal Society of Edinburgh, 100: 77–103. doi:10.1017/S1755691009016016

Begemann, F., Ludwig, K.R., Lugmair, G.W., Min, K., Nyquist, L.E., Patchett, P.J., Renne, P.R., Shih, C.-Y., Villa, I.M., Walker, R.J. 2001. Call for an improved set of decay constants for geochronological use. Geochimica Cosmochimica Acta, 65: 111–121. doi:10.1016/S0016-7037(00)00512-3

Bird, P. 1979. Continental delamination and the Colorado Plateau. Journal of Geophysical Research: Solid Earth, 84(B13): 7561–7571. doi:10.1029/JB084iB13p07561

Bonin, B. 2004. Do coeval mafic and felsic magmas in post-collisional to within-plate regimes necessarily imply two contrasting, mantle and crustal, sources? A review. Lithos, 78: 1–24. doi:10.1016/j.lithos.2004.04.042

Bouvier, A., Vervoort, J.D., Patchett, P.J. 2008. The Lu–Hf and Sm–Nd isotopic composition of CHUR: constraints from unequilibrated chondrites and implications for the bulk composition of terrestrial planets. Earth and Planetary Science Letters, 273: 48–57. doi:10.1016/j.epsl.2008.06.010

Brown, G.C., Thorpe, R.S., Webb, P.C. 1984. The geochemical characteristics of granitoids in contrasting arcs and comments on magma sources. Journal of Geological Society London, 141: 413–426. doi:10.1144/gsjgs.141.3.0413

Byerly, G.R., Melson, W.G., Vogt, P.R. 1976. Rhyodacites, andesites, ferro-basalts and ocean tholeiites from the Galapagos spreading center. Earth and Planetary Science Letters, 30: 215–221. doi:10.1016/0012-821X(76)90248-X

Carr, S.D., Easton, R.M., Jamieson, R.A., Culshaw, N.G. 2000. Geologic transect across the Grenville orogen of Ontario and New York. Canadian Journal of Earth Sciences, 37: 193–216. doi:10.1139/e99-074

Chen, J., Henderson, C.M.B., Foland, K.A. 1994. Open-system, sub-volcanic magmatic evolution: constraints on the petrogenesis of the Mount Brome alkaline complex, Canada. Journal of Petrology, 35: 1127–1153. doi:10.1093/petrology/35.4.1127

Chiarenzelli, J., Lupulescu, M., Cousens, B., Thern, E., Coffin, L., Regan, S. 2010. Enriched Grenvillian lithospheric mantle as a consequence of long-lived subduction beneath Laurentia. Geology, 38: 151–154. doi:10.1130/G30342.1

Chung, S.L., Chu, M.F., Zhang, Y., Xie, Y., Lo, C.H., Lee, T.Y., Lan, C.Y., Li, X., Zhang, Q., Wang, Y. 2005. Tibetan tectonic evolution inferred from spatial and temporal variations in post-collisional magmatism. Earth-Science Reviews, 68: 173–196. doi:10.1016/j.earscirev.2004.05.001

Corfu, F., Hanchar, J.M., Hoskin, P.W.O., Kinny, P. 2003. Atlas of zircon textures. Reviews in Mineralogy and Geochemistry, 53(1): 469–500. doi:10.2113/0530469

Corrigan, D., Hanmer, S. 1997. Anorthosites and related granitoids in the Grenville Orogen: a product of convective thinning of the lithosphere? Geology, 25: 61–64. doi:10.1130/0091-7613(1997)025<0061:AARGIT>2.3.CO;2

Corriveau, L., and Morin, D. 2000. Modelling 3D architecture of western Grenville from surface geology, xenoliths, styles of magma emplacement, and Lithoprobe reflectors. Canadian Journal of Earth Sciences, 37: 235–251. doi:10.1139/e99-121.

Corriveau L., Tellier, M.L., Morin, D. 1996. Le dyke de minette de Rivard et le complexe gneissique cuprifère de Bondy; implications tectoniques et métallogéniques pour la région de Mont-Laurier, Québec. Commission géologique du Canada, Dossier public, 3078: 70. Available at: https://doi.org/10.4095/210924.

Corriveau, L., Amelin, Y. 1994. Sources of Proterozoic K-rich alkaline and shoshonitic magmatism in the SW Grenville Province, Quebec: Nd-Sr-Pb isotopic study. *In* Abstracts of the Eighth International Conference on Geochronology, Cosmochronology and Isotope Geology. *Edited by* Lanphere, M.A., Dalrymple, G.B., Turrin, B.D., pp. 68.

Corriveau, L., Bonnet, A.-L., van Breemen, O., Pilote, P. 2003. Tracking the Wakeham Group volcanic rocks and associated copper-iron oxide hydrothermal activity from La Romaine eastward, eastern Grenville Province, Quebec. Geological Survey of Canada, Current Research, C12: 11. Available at: http://publications.gc.ca/Collection/GSC-CGC/M44-2003/Articles/c12.pdf

Corriveau, L., Gorton, M.P. 1993. Coexisting K-rich alkaline and shoshonitic magmatism of arc affinities in the Proterozoic: a reassessment of syenitic stocks in the southwestern Grenville Province. Contribution to Mineralogy and Petrology, 113: 262–279. doi:10.1007/BF00283233

Corriveau, L., Heaman, L.M., Marcantonio, F., van Breemen, O. 1990. 1.1 Ga K-rich alkaline plutonism in the SW Grenville Province. Contribution to Mineralogy and Petrology, 105: 473–485. doi:10.1007/BF00286834

Côté, G., Moukhsil, A., Constantin, M., David, J. 2018. Geochemical characterization, geochronology, and geodynamic implications of Grenville rare earths bearing syenites, Haut-Saint-Maurice, QC, Canada. Minerals, 8: 336. doi:10.3390/min8080336

Cox, R., Indares, A., Dunning, G. 2002. Temperature–time paths in the high-P Manicouagan Imbricate zone, eastern Grenville Province: evidence for two metamorphic events. Precambrian Research, 117: 225–250. doi:10.1016/S0301-9268(02)00059-1

Cox, R.A., Dunning, G.R., Indares, A.D. 1998. Petrology and U–Pb geochronology of mafic, high-pressure, metamorphic coronites from the Tshenukutish domain, eastern Grenville Province. Precambrian Research, 90: 59–83. doi:10.1016/S0301-9268(98)00033-3

Cox, R.A., Indares, A. 1999a. High-pressure and high-temperature metamorphism of the mafic and ultramafic Lac Espadon suite, Manicouagan Imbricate Zone, eastern Grenville Province, Quebec. Canadian Mineralogist, 37: 335–357.

Cox, R.A., Indares, A. 1999b. Transformation of Fe-Ti gabbro to coronite, eclogite and amphibolite in the Baie du Nord segment, Manicouagan Imbricate Zone, eastern Grenville Province. Journal of Metamorphic Geology, 17: 537–555. doi:10.1046/j.1525-1314.1999.00216.x

Dai, L.-Q., Zhao, Z.-F., Zheng, Y.-F., Zhang, J. 2015. Source and magma mixing processes in continental subduction factory: geochemical evidence from postcollisional mafic igneous rocks in the Dabie orogen. Geochemistry, Geophysics, Geosystems, 16: 659–680. doi:10.1002/2014GC005620

Davies, J.H., von Blanckenburg, F. 1995. Slab breakoff: a model of lithosphere detachment and its test in the magmatism and deformation of collisional orogens. Earth and Planetary Science Letters, 129: 85–102. doi:10.1016/0012-821X(94)00237-S

Dostal, J., Murphy, J.B., and Shellnutt, J.G. 2019. Secular isotopic variation in lithospheric mantle through the Variscan orogen: Neoproterozoic to Cenozoic magmatism in continental Europe. Geology, 47: 637–640. doi:10.1130/G46067.1.

DeCelles, P.G., Ducea, M.N., Kapp, P., Zandt, G. 2009. Cyclicity in Cordilleran orogenic systems. Nature Geoscience, 2: 251–257. doi:10.1038/ngeo469
DeCelles, P.G., Robinson, D.M., Zandt, G. 2002. Implications of shortening in the Himalayan fold-thrust belt for uplift of the Tibetan Plateau. Tectonics, 21: 12-1–12-25. doi:10.1029/2001TC001322
DePaolo, D.J. 1981a. Neodymium isotopes in the Colorado Front Range and crust-mantle evolution in the Proterozoic. Nature, 291: 193–196. doi:10.1038/291193a0
DePaolo, D.J. 1981b. Trace element and isotopic effects of combined wallrock assimilation and fractional crystallization. Earth and Planetary Science Letters, 53: 189–202. doi:10.1016/0012-821X(81)90153-9
Dickin, A.P. 2000. Crustal formation in the Grenville Province: Nd-isotope evidence. Canadian Journal of Earth Sciences, 37: 165–181. doi:10.1139/e99-039
Dickin, A.P., Higgins, M.D. 1992. Sm/Nd evidence for a major 1.5 Ga crust-forming event in the central Grenville province. Geology, 20: 137–140. doi:10.1130/0091-7613(1992)020<0137:SNEFAM>2.3.CO;2
Dostal, J., Murphy, J.B., and Shellnutt, J.G. 2019. Secular isotopic variation in lithospheric mantle through the Variscan orogen: Neoproterozoic to Cenozoic magmatism in continental Europe. Geology, 47: 637–640. doi:10.1130/G46067.1.
Dunning, G., Indares, A. 2010. New insights on the 1.7–1.0 Ga crustal evolution of the central Grenville Province from the Manicouagan – Baie Comeau transect. Precambrian Research, 180: 204–226. doi:10.1016/j.precamres.2010.04.005
Ellam, R.M. 1992. Lithospheric thickness as a control on basalt geochemistry. Geology, 20: 153–156. Doi:10.1130/0091-7613(1992)020<0153:LTAACO>2.3.CO;2
Emslie, R.F., Hunt, P.A. 1990. Ages and petrogenetic significance of igneous mangerite-charnockite suites associated with massif anorthosites, Grenville Province. Journal of Geology, 98: 213–231. doi:10.1086/629394
England, P.C., Houseman, G.A. 1988. The mechanics of the Tibetan Plateau. Philosophical Transactions of the Royal Society of London, 326: 301–320. doi:10.1098/rsta.1988.0089
England, P.C., Houseman, G.A. 1989. Extension during continental convergence, with application to the Tibetan Plateau. Journal of Geophysical Research, 94: 17561–17579. doi:10.1029/JB094iB12p17561
Ewart, A., Collerson, K.D., Regelous, M., Wendt, J.I., Niu, Y. 1998. Geochemical evolution within the Tonga-Kermadec-Lau arc-back-arc systems: the role of varying mantle wedge composition in space and time. Journal of Petrology, 39: 331–368. doi:10.1093/petroj/39.3.331
Gallagher, K., Hawkesworth, C. 1992. Dehydration melting and the generation of continental flood basalts. Nature, 358: 57–59. doi:10.1038/358057a0
Gill, J.B., 1981. Orogenic andesites and plate tectonics. Springer-Verlag, Berlin, Heidelberg. Vol. 16. pp. 390. doi:10.1007/978-3-642-68012-0
Gobeil, A., Hébert, C., Clarck, C., Beaumier, M., Perreault, S. 2002. Géologie de la région du lac De La Blache (22K03/22K04). Ministère des Ressources Naturelles Québec, Qué RG2002-01, 50p.
Goldstein, S.L., O'Nions, R.K., Hamilton, P.J. 1984. A Sm-Nd isotopic study of atmospheric dusts and particulates from major river systems. Earth and Planetary Science Letters, 70: 221–236. doi:10.1016/0012-821X(84)90007-4

Gower, C.F., Heaman, L.M., Loveridge, W.D., Schärer, U., Tucker, R.D. 1991. Grenvillian magmatism in the eastern Grenville Province, Canada. Precambrian Research, 51: 315–336. doi:10.1016/0301-9268(91)90106-K

Gower, C.F., Krogh, T.E. 2002. A U-Pb geochronological review of the Proterozoic history of the eastern Grenville Province. Canadian Journal of Earth Sciences, 39: 795. doi:10.1139/e01-090

Gower, C.F., van Nostrand, T., Evans-Lanswood, D. 1994. Geology of the Pinware region, southeast Labrador. Current Research, Newfoundland and Labrador Department of Natural Resources, Geological Survey Branch, Report, 94–1: 347–369.

Gutiérrez-Alonso, G., Murphy, J.B., Fernandez-Suarez, J., Weil, A.B., Franco, M.P., and Gonzalo, J.C. 2011. Lithospheric delamination in the core of Pangea: Sm-Nd insights from the Iberian mantle. Geology, 39: 155–158. doi:10.1130/G31468.1.

Greenough, J.D., and Owen, J. V. 1995. The role of subcontinental lithospheric mantle in massif-type petrogenesis: evidence from the Red Bay pluton, Labrador. Schweizerische Mineralogische und Petrographische Mitteilungen, 75: 1–15. Available from: http://dx.doi.org/10.5169/seals-57141.

Groulier, P.-A., Indares, A., Dunning, G., Moukhsil, A., and Wälle, M. 2018a. Peri-Laurentian, Pinwarian-age oceanic arc crust preserved in the Grenville Province: insights from the Escoumins supracrustal belt. Precambrian Research, 311: 37–64. doi:10.1016/J.PRECAMRES.2018.04.001.

Groulier, P.-A., Indares, A., Dunning, G., Moukhsil, A., Wälle, M. 2018b. Peri-Laurentian, Pinwarian-age oceanic arc crust preserved in the Grenville Province: insights from the Escoumins supracrustal belt. Precambrian Research, 311: 37–64. doi:10.1016/J.PRECAMRES.2018.04.001.

Gutierrez-Alonso, G., Murphy, J.B., Fernandez-Suarez, J., Weil, A.B., Franco, M.P., and Gonzalo, J.C. 2011. Lithospheric delamination in the core of Pangea: Sm-Nd insights from the Iberian mantle. Geology, 39: 155–158. doi:10.1130/G31468.1.

Halliday, A.N., Lee, D.-C., Tommasini, S., Davies, G.R., Paslick, C.R., Godfrey Fitton, J., James, D.E. 1995. Incompatible trace elements in OIB and MORB and source enrichment in the sub-oceanic mantle. Earth and Planetary Science Letters, 133: 379–395. doi:10.1016/0012-821X(95)00097-V

Heaman, L.M., Gower, C.F., Perreault, S. 2004. The timing of Proterozoic magmatism in the Pinware terrane of southeast Labrador, easternmost Quebec and northwest Newfoundland. Canadian Journal of Earth Sciences, 41: 127–150. doi:10.1139/e03-088

Hébert, C., Cadieux, A.-M., van Breemen, O. 2005. Temporal evolution and nature of Ti–Fe–P mineralization in the anorthosite-mangerite–charnockite–granite (AMCG) suites of the south-central Grenville Province, Saguenay – Lac St. Jean area, Quebec, Canada. Canadian Journal of Earth Sciences, 42: 1865–1880. doi:10.1139/e05-050

Hébert, C., Cadieux, A.-M., van Breemen, O. 2009. Région du réservoir Pipmuacan (SNRC 22E): Ministére des Ressources naturelles et de la Faune, Quebec. Synthèse Géologique: RG2009-01, 1-56. Available from: http://collections.banq.qc.ca/ark:/52327/bs1940773

Higgins, M.D., van Breemen, O. 1996. Three generations of anorthosite-mangerite-charnockite-granite (AMCG) magmatism, contact metamorphism and tectonism

in the Saguenay-Lac-Saint-Jean region of the Grenville Province, Canada. Precambrian Research, 79: 327–346. doi:10.1016/0301-9268(95)00102-6

Hindemith, M., Indares, A., Piercey, S. 2017. Hydrothermally altered volcanic rocks metamorphosed at granulite-facies conditions: an example from the Grenville Province. Canadian Journal of Earth Sciences, 54: 622–638. doi:10.1139/cjes-2016-0146

Hindemith, M., Indares, A.D. 2013. The petrographic and geochemical study of hydrothermally altered metavolcanics, metamorphosed at granulite-facies conditions from the Canyon domain in the central Grenville Province of Quebec, Canada. Geological Association of Canada-Mineralogical Association of Canada Annual Meeting, Winnipeg, Abstract, vol. 36, pp. 1.

Houseman, G.A., McKenzie, D.P., Molnar, P. 1981. Convective instability of a thickened boundary layer and its relevance for the thermal evolution of continental convergent belts. Journal of Geophysical Research: Solid Earth, 86: 6115–6132. doi:10.1029/JB086iB07p06115

Hynes, A., Indares, A., Rivers, T., Gobeil, A. 2000. Lithoprobe line 55: integration of out-of-plane seismic results with surface structure, metamorphism, and geochronology, and the tectonic evolution of the eastern Grenville Province. Canadian Journal of Earth Sciences, 37: 341–358. doi:10.1139/e99-076

Icenhower, J.P., Dymek, R.F., Weaver, B.L. 1998. Evidence for an enriched mantle source for jøtunite (orthopyroxene monzodiorite) associated with the St. Urbain anorthosite, Quebec. Lithos, 42: 191–212. doi:10.1016/S0024-4937(97)00042-X

Indares, A. 1995. Metamorphic interpretation of high-pressure-temperature metapelites with preserved growth zoning in garnet, eastern Grenville Province, Canadian Shield. Journal of Metamorphic Geology, 13: 475–486. doi:10.1111/j.1525-1314.1995.tb00235.x

Indares, A. 2003. Metamorphic textures and P-T evolution of high-P granulites from the Lelukuau terrane, NE Grenville Province. Journal of Metamorphic Geology, 21: 35–48. doi:10.1046/j.1525-1314.2003.00414.x

Indares, A., Dunning, G. 2001. Partial melting of high-P–T metapelites from the Tshenukutish terrane (Grenville Province): petrography and U–Pb geochronology. Journal of Petrology, 42: 1547–1565. doi:10.1093/petrology/42.8.1547

Indares, A., Dunning, G. 2004. Crustal architecture above the high-pressure belt of the Grenville Province in the Manicouagan area: new structural, petrologic and U-Pb age constraints. Precambrian Research, 130: 199–228. doi:10.1016/j.precamres.2003.11.005

Indares, A., Dunning, G., Cox, R. 2000. Tectono-thermal evolution of deep crust in a Mesoproterozoic continental collision setting: the Manicouagan example. Canadian Journal of Earth Sciences, 37: 325–340. doi:10.1139/cjes-37-2-3-325

Indares, A., Dunning, G., Cox, R., Gale, D., Connelly, J. 1998. High-pressure, high-temperature rocks from the base of thick continental crust: geology and age constraints from the Manicouagan Imbricate Zone, eastern Grenville Province. Tectonics, 17: 426–440. doi:10.1029/98TC00373

Indares, A., Moukhsil, A. 2013. Geon 12 crustal extension in the central Grenville Province, implications for the orogenic architecture, and potential influence on the emplacement of anorthosites. Canadian Journal of Earth Sciences, 50: 955–966. doi:10.1139/cjes-2012-0161

Indares, A., White, R.W., Powell, R. 2008. Phase equilibria modelling of kyanite-bearing anatectic paragneisses from the central Grenville Province. Journal of Metamorphic Geology, 26: 815–836. doi:10.1111/j.1525-1314.2008.00788.x

Jahn, B.M. 2004. The Central Asian Orogenic Belt and growth of the continental crust in the Phanerozoic. Geological Society London, Special Publication, 226: 73–100. doi:10.1144/GSL.SP.2004.226.01.05

Jamieson, R.A., Beaumont, C., Nguyen, M.H., Culshaw, N.G. 2007. Synconvergent ductile flow in variable-strength continental crust: numerical models with application to the western Grenville orogen. Tectonics, 26: 1–23. doi:10.1029/2006TC002036

Jannin, S., Gervais, F., Moukhsil, A., Augland, L.E. 2018a. Late-Grenvillian channel flow in the central Grenville Province (Manicouagan Reservoir area): new constraints from a structural and geochronological study of the Allochthon Boundary Thrust. Journal of Structural Geology, 115: 132–151. doi:10.1016/j.jsg.2018.07.019.

Jannin, S., Gervais, F., Moukhsil, A., Augland, L.E., Crowley, J.L. 2018b. Déformations tardi-Grenvilliennes dans la ceinture parautochthone (Province de Grenville centrale) : contraintes géochronologiques par couplage de méthodes U–Pb de haute résolution spatiale et de haute précision. Canadian Journal of Earth Sciences, 55: 406–435. doi:10.1139/cjes-2017-0129.

Jensen, L.S., Pyke, D.R. 1982. Komatiites in the Ontario Portion of the Abitibi Belt. *In* Komatiites. *Edited by* N.T. Arndt, E.G. Nisbet. Allen & Unwin, London, pp. 147–157.

Jiang, Y.-H., Liu, Z., Jia, R.-Y., Liao, S.-Y., Zhou, Q., Zhao, P. 2012. Miocene potassic granite–syenite association in western Tibetan Plateau: implications for shoshonitic and high Ba–Sr granite genesis. Lithos, 134–135: 146–162. doi:10.1016/J.LITHOS.2011.12.012

Jordan, S.L., Indares, A., Dunning, G. 2006. Partial melting of metapelites in the Gagnon terrane below the high-pressure belt in the Manicouagan area (Grenville Province): pressure–temperature (P–T) and U–Pb age constraints and implications. Canadian Journal of Earth Sciences, 43: 1309–1329. doi:10.1139/e06-038

Kay, R.W., Mahlburg Kay, S. 1993. Delamination and delamination magmatism. Tectonophysics, 219: 177–189. doi:10.1016/0040-1951(93)90295-U

Kelemen, P.B., Hanghøj, K., Greene, A.R. 2014. 4.21 – One view of the geochemistry of subduction-related magmatic arcs, with an emphasis on primitive andesite and lower crust. *In* Treatise on Geochemistry. pp. 749–806. doi:10.1016/B978-0-08-095975-7.00323-5

Kerr, A. 1989. Geochemistry of the Trans-Labrador granitoid belt, Canada. A quantitative comparative study of a Proterozoic batholith and possible Phanerozoic counterparts. Precambrian Research, 45: 1–17. doi:10.1016/0301-9268(89)90027-2

Kerr, A.C., Kempton, P.D., and Thompson, R.N. 1995. Crustal assimilation during turbulent magma ascent (ATA); new isotopic evidence from the Mull Tertiary lava succession, N. W. Scotland. Contributions to Mineralogy and Petrology, 119: 142–154. Springer-Verlag. doi:10.1007/BF00307277.

Kinzler, R.J. 1997. Melting of mantle peridotite at pressures approaching the spinel to garnet transition: application to mid-ocean ridge basalt petrogenesis. Journal of Geophysical Research: Solid Earth, 102: 853–874. doi:10.1029/96JB00988

Klein, E.M., Langmuir, C.H. 1987. Global correlations of ocean ridge basalt chemistry with axial depth and crustal thickness. Journal of Geophysical Research, 92: 8089. doi:10.1029/JB092iB08p08089

Konopelko, D., Klemd, R. 2016. Deciphering protoliths of the (U)HP rocks in the Makbal metamorphic complex, Kyrgyzstan: geochemistry and SHRIMP zircon geochronology. European Journal of Mineralogy, 28: 1233–1253. doi:10.1127/ejm/2016/0028-2602

Lasalle, S., Dunning, G., Indares, A., McFarlane, C. 2014. In situ LA–ICP–MS dating of monazite from aluminous gneisses: insights on the tectono-metamorphic history of a granulite-facies domain in the central Grenville Province. Canadian Journal of Earth Sciences, 51: 558–572. doi:10.1139/cjes-2013-0170

Lasalle, S., Fisher, C.M., Indares, A., Dunning, G. 2013. Contrasting types of Grenvillian granulite facies aluminous gneisses: insights on protoliths and metamorphic events from zircon morphologies and ages. Precambrian Research, 228: 117–130. doi:10.1016/j.precamres.2013.01.014

Lasalle, S., Indares, A. 2014. Anatectic record and contrasting P–T paths of aluminous gneisses from the central Grenville Province. Journal of Metamorphic Geology, 32: 627–646. doi:10.1111/jmg.12083

Liu, D., Zhao, Z., Zhu, D.-C., Niu, Y., DePaolo, D.J., Harrison, T.M., Mo, X., Dong, G., Zhou, S., Sun, C., Zhang, Z., and Liu, J. 2014. Postcollisional potassic and ultrapotassic rocks in southern Tibet: mantle and crustal origins in response to India–Asia collision and convergence. Geochimica et Cosmochimica Acta, 143: 207–231. doi:10.1016/j.gca.2014.03.031.

Ludwig, K.R. 2003. ISOPLOT 3.0: a geochronological toolkit for Microsoft Excel. Berkeley Geochronology Center. Special publication, 4: 1–71.

Maity, B., Indares, A. 2018. The Geon 14 arc-related mafic rocks from the Central Grenville Province. Canadian Journal of Earth Sciences, 55(6): 545-570. doi:10.1139/cjes-2017-0197

Mattinson, J.M. 2005. Zircon U–Pb chemical abrasion ("CA-TIMS") method: combined annealing and multi-step partial dissolution analysis for improved precision and accuracy of zircon ages. Chemical Geology, 220(1-2): 47–66. doi:10.1016/j.chemgeo.2005.03.011

McKenzie, D., Bickle, M.J. 1988. The volume and composition of melt generated by extension of the lithosphere. Journal of Petrology, 29: 625–679. doi:10.1093/petrology/29.3.625

McKenzie, D., and O'Nions, R.K. 1991. Partial melt distributions from inversion of rare earth element concentrations. Journal of Petrology, 32: 1021–1091. doi:10.1093/petrology/32.5.1021.

McLelland, J., Chiarenzelli, J.R. 1990. Geochronological studies in the Adirondack Mountains and the implications of a Middle Proterozoic tonalite suite. *In* Mid-Proterozoic Laurentia-Baltica. *Edited by* C.F. Gower, T. Rivers, and A.B. Ryan. Geological Association of Canada, pp. 175–194.

Morin, D., Hébert, R., Corriveau, L. 2005. Mesoproterozoic deep K-magmatism recorded in a megacryst- and xenolith-bearing minette dyke, western Grenville

Province. Canadian Journal of Earth Sciences, 42: 1881–1906. doi:10.1139/e05-083

Moukhsil, A., Lacoste, P., Gobeil, A., David, J. 2009. Synthèse géologique de la région de Baie-Comeau (SNRC 22F). Ministère des Ressources Naturelles la Faune, Québec, RG2009-03. Available from: http://collections.banq.qc.ca/ark:/52327/bs1947450.

Moukhsil, A., Solgadi, F., Thomas, C., Séverine, B., Indares, A., Davis, D.W. 2013a. Géologie du nord-ouest de la région du barrage Daniel-Johnson (Manic 5), Côte-Nord. Ministère des Ressources naturelles, Québec. RG 2013-01. Available from: http://gq.mines.gouv.qc.ca/documents/examine/RG201301/RG201301.pdf.

Moukhsil, A., Solgadi, F., Indares, A., Belkacim, S. 2013b. Géologie de la région septentrionale du réservoir aux Outardes 4, Côte-Nord. Ministère des Ressources Naturelles, Québec RG 2013-03: 31. Available from: http://gq.mines.gouv.qc.ca/documents/EXAMINE/RG201303/.

Moukhsil, A., Solgadi, F., Belkacim, S., Elbasbas, A., and Augland, L.E. 2014. Géologie de la région du lac Okaopéo, Côte-Nord. Ministère des Ressources Naturelles la Faune, Québec, RG 2014-03. Available from: ftp://ftp.mrn.gouv.qc.ca/Public/Geologie/Sigeom_Internet_FICHIERS/RG%202014-03.pdf.

Moukhsil, A., Solgadi, F. 2017. Géologie, potentiel minéral et cadre géodynamique des roches de la région du réservoir Daniel-Johnson (Manicouagan), partie centrale de la Province de Grenville. *In* Géologie, potentiel minéral et cadre géodynamique des roches de la région du réservoir Daniel-Johnson (Manicouagan), partie centrale de la Province de Grenville. Moukhsil, A. *coordonnateur*. Ministère de l'Énergie et des Ressources naturelles, Québec, MM 2017-1: 7-92. Available from: http://gq.mines.gouv.qc.ca/documents/EXAMINE/MM201701/MM201701.pdf.

Moyen, J.-F., Laurent, O., Chelle-Michou, C., Couzinié, S., Vanderhaeghe, O., Zeh, A., Villaros, A., Gardien, V. 2017. Collision vs. subduction-related magmatism: two contrasting ways of granite formation and implications for crustal growth. Lithos, 277: 154–177. doi:10.1016/j.lithos.2016.09.018

Nykänen, V.M., Vuollo, J.I., Liipo, J.P., Piirainen, T.A. 1994. Transitional (2.1 Ga) Fe-tholeiitic-tholeiitic magmatism in the Fennoscandian Shield signifying lithospheric thinning during Paleoproterozoic extensional tectonics. Precambrian Research, 70: 45–65. doi:10.1016/0301-9268(94)90020-5

Owen, J. V, Erdmer, P. 1990. Middle Proterozoic geology of the Long Range Inlier, Newfoundland: regional significance and tectonic implications. *In* Mid-Proterozoic Laurentia-Baltica. *Edited by* C.F. Gower, T. Rivers, and A.B.Ryan. Geological Association of Canada, Special Paper 38: 215–231.

Owens, B.E., and Dymek, R.F. 2001. Petrogenesis of the Labrieville alkalic anorthosite massif, Grenville Province, Quebec. Journal of Petrology, 42: 1519–1546. doi:10.1093/petrology/42.8.1519

Owens, B.E., Dymek, R.F. 2016. Comparative petrology of the Montpelier and Roseland potassic anorthosites, Virginia. Canadian Mineralogist, 54: 1563–1593. doi:10.3749/canmin.1600002

Owens, B.E., Dymek, R.F., Tucker, R.D., Brannon, J.C., Podosek, F.A. 1994. Age and radiogenic isotopic composition of a late- to post-tectonic anorthosite in the

Grenville Province: the Labrieville massif, Quebec. Lithos, 31: 189–206. doi:10.1016/0024-4937(94)90009-4
Owens, B.E., and Tomascak, P.B. 2002. Mesoproterozoic lamprophyres in the Labrieville Massif, Quebec: clues to the origin of alkalic anorthosites? Canadian Journal of Earth Sciences, 39: 983–997. doi:10.1139/e02-010.
Patrick, M.E., Indares, A. 2017. Petrography and phase equilibria modeling of mid-P aluminous gneisses derived from hydrothermally altered protoliths, Grenville Province. Canadian Journal of Earth Sciences, 54: 1103–1118. doi:10.1139/cjes-2016-0162
Pattison, D.R.M. 2003. Petrogenetic significance of orthopyroxene-free garnet + clinopyroxene + plagioclase ± quartz-bearing metabasites with respect to the amphibolite and granulite facies. Journal of Metamorphic Geology, 21: 21–34. doi:10.1046/j.1525-1314.2003.00415.x
Pearce, J. 1996. Sources and settings of granitic rocks. Episodes, 19: 120–125.
Pearce, J.A., Cann, J.R. 1973. Tectonic setting of basic volcanic rocks determined using trace element analyses. Earth and Planetary Science Letters, 19: 290–300. doi:10.1016/0012-821X(73)90129-5
Pearce, J.A., Norry, M.J. 1979. Petrogenetic implications of Ti, Zr, Y, and Nb variations in volcanic rocks. Contribution to Mineralogy and Petrology, 69: 33–47. doi:10.1007/BF00375192
Pearce, J.A., Parkinson, I.J. 1993. Trace element models for mantle melting: application to volcanic arc petrogenesis. Geological Society London, Special Publication, 76: 373–403. doi:10.1144/GSL.SP.1993.076.01.19
Percival, J.A., Stern, R.A., and Rayner, N. 2003. Archean adakites from the Ashuanipi complex, eastern Superior Province, Canada: geochemistry, geochronology and tectonic significance. Contributions to Mineralogy and Petrology, 145: 265–280. doi:10.1007/s00410-003-0450-5.
Rivers, T. 1983a. The northern margin of the Grenville Province in western Labrador – anatomy of an ancient orogenic front. Precambrian Research, 22: 41–73. doi:10.1016/0301-9268(83)90058-X
Rivers, T. 1983b. Progressive metamorphism of pelitic and quartzofeldspathic rocks in the Grenville Province of western Labrador – tectonic implications of bathozone 6 assemblages. Canadian Journal of Earth Sciences, 20: 1791–1804. doi:10.1139/e83-171
Rivers, T. 2008. Assembly and preservation of lower, mid, and upper orogenic crust in the Grenville Province—implications for the evolution of large hot long-duration orogens. Precambrian Research, 167: 237–259. doi:10.1016/j.precamres.2008.08.005
Rivers, T. 2012. Upper-crustal orogenic lid and mid-crustal core complexes: signature of a collapsed orogenic plateau in the hinterland of the Grenville Province. Canadian Journal of Earth Sciences, 49: 1–42. doi:10.1139/e11-014.
Rivers, T. 2015. Tectonic Setting and Evolution of the Grenville Orogen: An Assessment of Progress Over the Last 40 Years. Geoscience Canada, 42: 77–124. doi:10.12789/geocanj.2014.41.057.
Rivers, T., Corrigan, D. 2000. Convergent margin on southeastern Laurentia during the Mesoproterozoic: tectonic implications. Canadian Journal of Earth Sciences, 37: 359–383. doi:10.1139/e99-067

Rivers, T., Culshaw, N., Hynes, A., Indares, A., Jamieson, R., Martignole, J. 2012. The Grenville Orogen–a post-Lithoprobe perspective, *In* Tectonic Styles in Canada: the Lithoprobe Perspective. *Edited by* J.A. Percival, F.A. Cook, and R.M. Clowes. Geological Association of Canada, Special Paper, pp. 97–236.

Robinson, J.A.C., Wood, B.J. 1998. The depth of the spinel to garnet transition at the peridotite solidus. Earth and Planetary Science Letters, 164: 277–284. doi:10.1016/S0012-821X(98)00213-1

Rollinson, H. 1993. Using geochemical data. 352 pp., Longman, London.

Rudnick, R.L., Gao, S. 2014. 4.1 – Composition of the continental crust. *In* Treatise on Geochemistry. pp. 1–51. doi:10.1016/B978-0-08-095975-7.00301-6

Schärer, U. 1991. Rapid continental crust formation at 1.7 Ga from a reservoir with chondritic isotope signatures, eastern Labrador. Earth and Planetary Science Letters, 102: 110–133. doi:10.1016/0012-821X(91)90002-Y

Schmitz, M.D., Schoene, B. 2007. Derivation of isotope ratios, errors, and error correlations for U-Pb geochronology using ^{205}Pb-^{235}U-(^{233}U)-spiked isotope dilution thermal ionization mass spectrometric data. Geochemistry, Geophysics, Geosystems, 8: 1–20. doi:10.1029/2006GC001492

Scott, D.J., Hynes, A. 1994. U-Pb geochronology along the Manicouagan corridor, preliminary results: evidence for ca. 1.47 Ga metamorphism. Lithoprobe Abitibi-Grenville Transect. Lithoprobe Report, 41: 109–110.

Shaw, D.M. 1970. Trace element fractionation during anatexis. Geochimica Cosmochimica Acta, 34: 237–243. doi:10.1016/0016-7037(70)90009-8

Shervais, J.W. 1982. Ti-V plots and the petrogenesis of modern and ophiolitic lavas. Earth and Planetary Science Letters, 59: 101–118. doi:10.1016/0012-821X(82)90120-0

Sparkes, G.W., Dunning, G.R. 2014. Late Neoproterozoic epithermal alteration and mineralization in the western Avalon zone: a summary of mineralogical investigations and new U/Pb geochronological results. Current Research, Newfoundland and Labrador Department of Natural Resources, Geological Survey, Report 14-1: 99–128. Available from: https://www.nr.gov.nl.ca/nr/mines/geoscience/publications/currentresearch/2014/Sparkes-2014.pdf.

Stacey, J.S., Kramers, J.D. 1975. Approximation of terrestrial lead isotope evolution by a two-stage model. Earth and Planetary Science Letters, 26: 207–221. doi:10.1016/0012-821X(75)90088-6.

Stolz, A.J., Varne, R., Wheller, G.E., Foden, J.D., Abbott, M.J. 1988. The geochemistry and petrogenesis of K-rich alkaline volcanics from the Batu Tara volcano, eastern Sunda arc. Contribution to Mineralogy and Petrology, 98: 374–389. doi:10.1007/BF00375187

Sun, S. -s., McDonough, W.F. 1989. Chemical and isotopic systematics of oceanic basalts: implications for mantle composition and processes. Geological Society London, Special Publication, 42: 313–345. doi:10.1144/GSL.SP.1989.042.01.19

Swinden, H.S., Jenner, G.A., Kean, B.F., Evans, D.T.W. 1989. Volcanic rock geochemistry as a guide for massive sulphide exploration in central Newfoundland. Current Research, Newfoundland and Labrador Department of Natural Resources, Geological Survey Branch, Report, 89: 201–219. Available from:https://www.nr.gov.nl.ca/mines&en/geosurvey/publications/cr1989/Swinden.pdf.

Swinden, H.S., Jenner, G.A., Szybinski, Z.A. 1997. Magmatic and tectonic evolution of the Cambrian-Ordovician Laurentian margin of Iapetus: geochemical and isotopic constraints from the Notre Dame subzone, Newfoundland. *In* The Nature of Magmatism in the Appalachian Orogen. *Edited by* A.K. Sinha, J.B. Whalen, J.P. Hogan. Geological Society of America Memoir, Boulder, Colorado, pp. 337–365.

Tatsumi, Y., Eggins, S.M. 1995. Subduction Zone Magmatism. Blackwell Science, Cambridge, pp. 211.

Tatsumi, Y., Hamilton, D.L., Nesbitt, R.W. 1986. Chemical characteristics of fluid phase released from a subducted lithosphere and origin of arc magmas: evidence from high-pressure experiments and natural rocks. Journal of Volcanology and Geothermal Research, 29: 293–309. doi:10.1016/0377-0273(86)90049-1

Thomson, S.D., Dickin, A.P., Spray, J.G. 2011. Nd isotope mapping of Grenvillian crustal terranes in the vicinity of the Manicouagan Impact Structure. Precambrian Research, 191: 184–193. doi:10.1016/j.precamres.2011.08.006

Tollo, R., Corriveau, L., McLelland, J., Bartholomew, M. 2004. Proterozoic tectonic evolution of the Grenville orogen in North America: an introduction. *In* Proterozoic tectonic evolution of the Grenville Orogen in North America. *Edited by* R.P. Tollo, L. Corriveau, J. McLelland, and M.J. Bartholomew. GSA Memoirs, 197(03): 1-18.

Tucker, R.D., Gower, C.F. 1994. A U-Pb geochronological framework for the Pinware Terrane, Grenville Province, Southeast Labrador. Journal of Geology, 102: 67–78. doi:10.1086/629648

Turlin, F., André-Mayer, A.-S., Moukhsil, A., Vanderhaeghe, O., Gervais, F., Solgadi, F., Groulier, P.-A., Poujol, M. 2017. Unusual LREE-rich, peraluminous, monazite- or allanite-bearing pegmatitic granite in the central Grenville Province, Québec. Ore Geology Reviews, 89: 627–667. doi:10.1016/j.oregeorev.2017.04.019

Turlin, F., Deruy, C., Eglinger, A., Vanderhaeghe, O., André-Mayer, A.-S., Poujol, M., Moukhsil, A., Solgadi, F. 2018. A 70 Ma record of suprasolidus conditions in the large, hot, long-duration Grenville Orogen. Terra Nova, 30: 233–243. doi:10.1111/ter.12330

Turlin, F., Vanderhaeghe, O., Gervais, F., André-Mayer, A.-S., Moukhsil, A., Zeh, A., Solgadi, F., I.P.T.N. 2019. Petrogenesis of LREE-rich pegmatitic granite dykes in the central Grenville Province by partial melting of Paleoproterozoic-Archean metasedimentary rocks: evidence from zircon U-Pb-Hf-O isotope and trace element analyses. Precambrian Research, 327: 327-360. doi:10.1016/j.precamres.2019.02.009.

Turner, S.P., Platt, J.P., George, R.M.M., Kelley, S.P., Pearson, D.G., Nowell, G.M. 1999. Magmatism associated with orogenic collapse of the Betic-Alboran domain, SE Spain. Journal of Petrology, 40: 1011–1036. doi:10.1093/petroj/40.6.1011.

Valverde Cardenas, C., Indares, A., Jenner, G. 2012. Mafic and ultrapotassic rocks from the Canyon domain (central Grenville Province): geochemistry and tectonic implications. Canadian Journal of Earth Sciences, 49: 412–433. doi:10.1139/e11-065.

van Gool, J.A.M., Rivers, T., Calon, T. 2008. Grenville Front zone, Gagnon terrane, southwestern Labrador: configuration of a midcrustal foreland fold-thrust belt. Tectonics, 27: 1–35. doi:10.1029/2006TC002095.
Varne, R., Foden, J.D. 1986. Geochemical and isotopic systematics of eastern Sunda arc volcanics: implications for mantle sources and mantle mixing processes. Developments in Geotectonics, 21: 159–189. doi:10.1016/B978-0-444-42688-8.50013-8.
Vermeesch, P. 2006. Tectonic discrimination diagrams revisited. Geochemistry, Geophysics, Geosystems, 7: Q06017. doi:10.1029/2005GC001092
Vervoort, J.D., Blichert-Toft, J. 1999. Evolution of the depleted mantle: Hf isotope evidence from juvenile rocks through time. Geochimica Cosmochimica Acta, 63: 533–556. doi:10.1016/S0016-7037(98)00274-9
Villemant, B., Jaffrezic, H., Joron, J.-L., Treuil, M. 1981. Distribution coefficients of major and trace elements; fractional crystallization in the alkali basalt series of Chaîne des Puys (Massif Central, France). Geochimica Cosmochimica Acta, 45: 1997–2016. doi:10.1016/0016-7037(81)90055-7
Walter, M.J. 1998. Melting of garnet peridotite and the origin of komatiite and depleted lithosphere. Journal of Petrology, 39: 29–60. doi:10.1093/petroj/39.1.29
Wang, K., Plank, T., Walker, J.D., Smith, E.I. 2002. A mantle melting profile across the Basin and Range, SW USA. Journal of Geophysical Research: Solid Earth, 107: ECV 5-1-ECV 5-21. doi:10.1029/2001JB000209
Weaver, B.L., Tarney, J. 1984. Empirical approach to estimating the composition of the continental crust. Nature, 310: 575–577. doi:10.1038/310575a0.
Whalen, J.B., Jenner, G.A., Longstaffe, F.J., Robert, F., Gariépy, C. 1996. Geochemical and isotopic (O, Nd, Pb and Sr) constraints on A-type granite petrogenesis based on the Topsails igneous suite, Newfoundland Appalachians. Journal of Petrology, 37: 1463–1489. doi:10.1093/petrology/37.6.1463
Whalen, J.B., McNicoll, V.J., van Staal, C.R., Lissenberg, C.J., Longstaffe, F.J., Jenner, G.A., van Breeman, O., 2006. Spatial, temporal and geochemical characteristics of Silurian collision-zone magmatism, Newfoundland Appalachians: An example of a rapidly evolving magmatic system related to slab break-off. Lithos, 89: 377–404. doi:10.1016/j.lithos.2005.12.011
Whitney, D.L., Evans, B.W. 2010. Abbreviations for names of rock-forming minerals. American Mineralogist, 95: 185–187. doi:10.2138/am.2010.3371
Wood, D.A. 1980. The Application of a Th-Hf-Ta diagrams to problems of tectonomagmatic classification and to establish the nature of crustal contaminants of basaltic lavas of the British Tertiary volcanic province. Earth and Planetary Science Letters, 50: 11–30. doi:10.1016/0012-821X(80)90116-8
Workman, R.K., Hart, S.R. 2005. Major and trace element composition of the depleted MORB mantle (DMM). Earth and Planetary Science Letters, 231: 53–72. doi:10.1016/j.epsl.2004.12.005
Xia, L.-Q. 2014. The geochemical criteria to distinguish continental basalts from arc related ones. Earth-Science Reviews, 139: 195–212. doi:10.1016/J.EARSCIREV.2014.09.006
Xia, L., Li, X. 2019. Basalt geochemistry as a diagnostic indicator of tectonic setting. Gondwana Research, 65: 43–67. doi:10.1016/J.GR.2018.08.006
Xu, W., Xu, X., Zeng, G. 2017. Crustal contamination versus an enriched mantle source for intracontinental mafic rocks: insights from early Paleozoic mafic rocks of the

South China Block. Lithos, 286–287: 388–395. doi:10.1016/J.LITHOS.2017.06.023

Xu, Y.G., Lan, J.B., Yang, Q.J., Huang, X.L., Qiu, H.N. 2008. Eocene break-off of the Neo-Tethyan slab as inferred from intraplate-type mafic dykes in the Gaoligong orogenic belt, eastern Tibet. Chemical Geology, 255: 439–453. doi:10.1016/j.chemgeo.2008.07.016

Yang, P., Indares, A.D. 2005. Mineral zoning, phase relations, and P-T evolution of high-pressure granulites from the Lelukuau terrane, northeastern Grenville Province, Quebec. Canadian Mineralogist, 43: 443–462. doi:10.2113/gscanmin.43.1.443.

Zhao, Z.F., Zheng, Y.F., Wei, C.S., Wu, Y.B., Chen, F., Jahn, B.M. 2005. Zircon U-Pb age, element and C-O isotope geochemistry of post-collisional mafic-ultramafic rocks from the Dabie orogen in east-central China. Lithos, 83: 1–28. doi:10.1016/j.lithos.2004.12.014.

Table 3.1. U-Pb isotope data for the Vein Complex and the Layered Bimodal Suite.

			Concentration		Measured		Corrected Atomic Ratios[c]								Age [Ma]						
Fraction	Description	Weight [a] (mg)	U (ppm)	Pb (ppm)[b]	Total common Pb (pg)	$^{206}Pb/^{204}Pb$	$^{208}Pb/^{206}Pb$	$^{206}Pb/^{238}U$	2	±	$^{207}Pb/^{235}U$	2	±	$^{207}Pb/^{206}Pb$	2	±	Rho[d]	$^{206}Pb/^{238}U$	2	±	$^{207}Pb/^{235}U$	2	±	$^{207}Pb/^{206}Pb$	2	±	Disc %[e]
11-208																										
Z1	1 large prism	0.002	508	88.6	4.6	1780	0.1295	0.16858	112		1.6883	124		0.07264	28		0.85	1004.3	6.2		1004.1	4.7		1003.9	9.3		-0.02
Z2	1 large prism	0.002	286	51.8	2.6	1784	0.1493	0.17205	98		1.7331	134		0.07306	40		0.71	1023.4	5.4		1020.9	5.0		1015.6	12.1		-0.24
Z3	2 large prism	0.003	302	52.8	2.4	4060	0.1302	0.16892	104		1.6967	104		0.07285	20		0.90	1006.2	5.7		1007.3	3.9		1009.8	7.4		0.11
Z4	2 large prism	0.003	387	67.2	5.2	2400	0.1190	0.16956	156		1.7054	160		0.07295	34		0.87	1009.7	8.6		1010.6	5.8		1012.6	10.7		0.09
Z5	3 small clear round balls	0.003	202	35.0	2.9	2284	0.1115	0.16969	68		1.7043	88		0.07284	26		0.72	1010.4	3.7		1010.1	3.3		1009.5	8.8		-0.03
Z6	3 small clear round balls	0.003	165	28.1	4	1339	0.0977	0.16869	84		1.6900	100		0.07266	32		0.69	1004.9	4.6		1004.8	3.8		1004.5	10.2		-0.01
Z7	2 small clear round balls	0.002	48	8.3	1.5	678	0.1195	0.16980	138		1.6930	202		0.07231	78		0.47	1011.0	7.6		1005.9	7.6		994.7	22.5		-0.51
11-331b																										
Z1	2 prism	0.003	115	18.4	2.9	1280	0.0426	0.16684	94		1.6577	96		0.07206	36		0.62	994.7	5.2		992.5	3.7		987.6	11.3		-0.22
Z2	1 prism	0.002	337	53.9	3.6	1482	0.0398	0.16730	76		1.6744	82		0.07259	28		0.65	997.2	4.2		998.9	3.0		1002.5	9.3		0.16
Z3	1 prism	0.002	1946	310.7	18	1682	0.0397	0.16691	124		1.6724	134		0.07267	24		0.91	995.1	6.8		998.1	5.1		1004.8	8.3		0.30
Z4	1 prism	0.003	160	25.7	30	186	0.0423	0.16772	104		1.6739	232		0.07238	90		0.44	999.5	5.7		998.7	8.8		996.6	25.7		-0.09

Notes:
All zircon was chemically abraded (Mattinson, 2005) prior to dissolution. Z, zircon; 2, 4 number of grains in analysis.
(a) Weights of grains were estimated, with potential uncertainties of 50% for these small samples.
(b) Radiogenic lead
(c) Atomic ratios corrected for fractionation, spike, laboratory blank of 1- 2 picograms (pg) common lead, and initial common lead at the age of the sample calculated from the model of Stacey & Kramers (1975), and 0.3 pg U blank.
(d) Rho valuea were calculated after Schmitz & Schoene, 2007.
(e) Discordance = $[((^{207}Pb/^{235}U)/(^{206}Pb/^{238}U))-1] \times 100$
Two sigma uncertainties are reported after the ratios and refer to the final digits.

Table 3.2. Major and trace element geochemistry of mafic rocks from the Vein Complex and Layered Bimodal Suite.

Sample no	RS430+	RS431+	11-317a	11-331a	11-317b	11-331b	11-216-2c	RS314+	11-208	11-356-1	RS356+	11-215-1	11-215-5	RS457+	11-349	11-351	RS207b+
Layer type	mafic layer	mafic layer	mafic layer	mafic layer	mafic layer	mafic layer	mafic layer	mafic dyke	mafic dyke	mafic dyke	mafic dyke	mafic dyke	mafic dyke	mafic dyke	mafic dyke	mafic dyke	mafic body
Geol. Domain	Layered Bimodal Suite (ca. 997 Ma)							Vein Complex (ca. 1008 Ma)									
Group	LBS1				LBS2			VC1				VC2			VC3		
SiO2	47.01	45.26	45.21	48.81	44.67	47.89	46.77	47.42	45.71	47.72	46.25	47.13	47.32	45.80	46.97	48.80	50.34
TiO2	1.29	2.21	2.45	2.16	2.36	3.79	1.741	0.859	2.74	2.32	2.89	1.57	1.43	3.14	1.10	2.12	1.33
Al2O3	16.79	14.43	17.26	15.89	16.23	16.63	16.61	14.57	15.97	14.94	12.02	17.35	16.42	15.40	15.67	14.32	14.95
Fe2O3	11.75	16.1	15.45	13.14	14.12	15.47	13.51	11.78	16.79	16.54	18.89	12.41	12.28	17.16	11.55	14.28	11.79
MnO	0.172	0.248	0.264	0.216	0.187	0.231	0.217	0.171	0.227	0.23	0.213	0.172	0.167	0.224	0.19	0.227	0.18
MgO	8.80	6.34	7.86	6.29	7.65	5.63	6.79	9.4	6.20	6.02	6.52	8.32	8.07	5.54	7.47	5.51	6.89
CaO	10.81	8.02	8.11	7.41	8.75	5.22	8.82	9.29	8.59	9.15	9.37	10.28	10.30	7.70	11.59	8.42	9.29
Na2O	2.35	3.12	1.34	2.51	2.84	2.06	3.81	3.21	2.97	2.54	0.43	2.56	2.55	3.07	2.8	3.15	2.73
K2O	0.25	1.14	0.75	1.37	1.34	1.5	1.49	0.56	0.76	0.79	1.04	0.40	0.37	1.02	1.18	0.94	1.31
P2O5	0.13	0.50	0.46	0.43	0.51	0.40	0.21	0.05	0.34	0.22	0.31	0.16	0.14	0.52	0.09	0.20	0.34
LOI	0.6	1.47	-0.04	0.29	0.39	0.08	0.41	1.77	0.41	0.05	1.67	-0.02	0.18	0.29	0.66	0.91	0.24
Total	99.94	98.84	99.11	98.51	99.05	98.92	100.4	99.09	100.7	100.5	99.61	100.3	99.23	99.88	99.29	98.88	99.38
#Mg	0.60	0.44	0.50	0.49	0.52	0.42	0.50	0.61	0.42	0.42	0.41	0.57	0.57	0.39	0.56	0.43	0.54
FeOt	10.57	14.49	13.90	11.82	12.71	13.92	12.16	10.60	15.11	14.88	17.00	11.17	11.05	15.44	10.39	12.85	10.61
Sc	34	33	30	26	27	26	27	31	31	39	55	26	31	29	41	37	34
V	212	254	301	270	248	276	284	209	248	332	815	220	231	195	278	306	205
Cr	180	490	70	70	60	80	40	320	90	140	10	70	160	70	260	130	140
Co	131	101	139	119	75	127	79	93	91	101	318	93	92	211	109	86	118
Ni	170	720	150	90	70	10	60	210	70	60	120	140	160	10	100	40	40
Cu	50	30	30	5	5	5	50	60	50	70	60	30	30	40	140	40	10
Zn	70	160	160	90	110	120	140	110	120	110	290	50	50	160	60	120	110
Ga	18	21	18	19	18	24	22	19	24	23	28	19	19	22	18	23	18
Rb	5	26	33	44	34	72	29	9	19	10	82	8	10	18	21	8	39
Cs	0.25	1.5	0.8	0.25	3.9	0.6	0.25	0.25	0.25	0.25	1.3	0.25	0.25	0.25	0.25	0.25	0.6
Sr	231	351	228	288	295	193	544	245	218	183	63	310	227	275	402	724	314
Ba	72	518	176	212	240	548	368	147	253	180	233	113	94	423	227	406	427
Ti	7746	13225	14670	12937	14166	22733	10437	5150	16432	13914	17350	9436	8567	18806	6618	12685	7943
Zr	77	110	127	113	113	261	103	49	206	159	167	87	108	222	56	158	182
Hf	2.2	3.1	3.1	3	3.1	6.1	2.7	1.4	5.3	4.4	4.5	2.2	2.8	6	1.7	4.5	4.6
Nb	6.12	8.4	6	7	7	14	8	3	8	5	7.1	8	9	16.44	3	8	8.2
Ta	0.4	0.3	1.1	1.6	1.0	2.8	0.8	0.1	1.1	1.2	0.57	1.3	1.5	1.1	1.5	1.1	0.44
Th	0.60	0.90	0.70	0.60	1.30	0.70	0.80	0.6	1.50	1.70	1.97	0.80	1.10	1.50	0.90	1.20	1.85
U	0.2	0.4	0.4	0.5	0.6	1.1	0.3	0.2	0.6	0.5	1.71	0.3	0.4	0.4	0.3	0.6	0.61
Pb	5	11	6	8	10	2.5	9	2.5	8	5	2.5	2.5	2.5	2.5	8	11	11
Y	20	34	31	27	25	26	20	20	41	42	50.4	18	23	48	21	47	37.6
La	5.5	10.3	14.8	15.3	15.9	17.8	26.4	5.5	14.7	14.1	20.5	8.4	9.8	20.5	18.8	31.7	27.9
Ce	14.1	27.1	33.1	34	38.4	46.7	56.7	12.3	35.1	32.3	51.4	19.2	22.2	49.6	34.2	70.5	60
Pr	2	4.07	4.55	4.48	5.02	6.81	6.64	1.68	5.12	4.49	6.93	2.71	2.95	6.81	4.09	9.44	7.24
Nd	9.6	18.7	21.7	21.1	23	31.9	27.4	8.1	25.4	21.8	29.8	13	14.1	29.6	16.9	40.6	29.2
Sm	2.7	5.2	5.3	4.9	5.9	7.9	5.7	2.4	7.1	6.5	7.4	3.4	3.8	7.6	3.9	9.3	6.18
Eu	1.10	2.01	1.71	1.80	1.89	2.13	1.90	1.02	2.13	1.98	2.32	1.21	1.21	2.66	1.24	2.39	1.95
Gd	3.20	5.70	5.50	4.90	5.70	7.10	5.0	3.1	7.60	7.30	8.23	3.4	4.0	8.4	3.8	8.7	6.41
Tb	0.60	1.00	0.90	0.80	0.90	1.10	0.70	0.6	1.3	1.3	1.4	0.6	0.7	1.4	0.7	1.5	1.1
Dy	3.40	5.80	5.90	5.20	5.00	5.90	4.30	3.4	7.80	8.20	8.32	3.5	4.3	8.3	4.1	9.3	6.51
Ho	0.70	1.20	1.20	1.10	0.90	1.10	0.80	0.7	1.60	1.60	1.66	0.7	0.9	1.7	0.8	1.8	1.31
Er	2.0	3.40	3.40	3.30	2.60	2.90	2.20	2	4.70	4.70	4.99	1.9	2.6	4.8	2.5	5.3	3.88
Tm	0.29	0.50	0.50	0.51	0.35	0.38	0.32	0.3	0.68	0.72	0.76	0.28	0.40	0.70	0.37	0.79	0.591
Yb	1.90	3.20	3.30	3.40	2.30	2.40	2.10	1.9	4.50	4.60	4.74	1.80	2.60	4.40	2.40	5.10	3.72
Lu	0.28	0.48	0.53	0.57	0.37	0.36	0.31	0.26	0.70	0.76	0.69	0.28	0.41	0.69	0.38	0.81	0.547

Notes:

1. The oxide concentrations are reported in weight percentages (wt%), whereas trace element concentrations are reported in parts per million (ppm).
2. The deviation of Eu from the rest of REE can be expressed as Eu anomaly (Eu/Eu*) where * refers to the value obtained by linear interpolation between adjacent elements.
3. $FeO_t = 0.8998 \times Fe_2O_3$; $Ti = 5995 \times TiO_2$
4. $\#Mg = MgO/(MgO+Fe_2O_{3\ total})$ in moles.
5. + sign indicates samples from Valverde Cardenas et al., 2012.

Table 3.3. Whole-rock Sr and Nd isotopic data of the mafic rocks from the Vein Complex and Layered Bimodal Suite.

Sample	Geological suites	Nd (ppm)	Sm (ppm)	Sm/Nd	$(^{147}Sm/^{144}Nd)_{calc}$	$(^{143}Nd/^{144}Nd)_{meas}$	2s	$(^{143}Nd/^{144}Nd)_{ini}$	$\varepsilon Nd_{0.0}$	$\varepsilon Nd_{1.0}$	T_{CR}	T_{DM}	Rb (ppm)	Sr (ppm)	$(^{87}Sr/^{86}Sr)_{meas.}$	2	$(^{87}Rb/^{86}Sr)_{calc.}$	$(^{87}Sr/^{86}Sr)_{ini}$	Induced error in $(^{87}Sr/^{86}Sr)_{ini}$
RS457[+]	VC1	31.71	7.90	0.25	0.1506	0.512410	7	0.511422	-4.3	1.5	1807	1503							
11-208	VC2	23.08	6.42	0.28	0.1682	0.512596	7	0.511493	-0.7	2.9	1883	1459	19	218	0.707573	11	0.25225	0.70397	0.00007
11-351	VC3	36.71	8.24	0.22	0.1357	0.512050	7	0.511160	-11.3	-3.6	2161	1921	8	724	0.705110	10	0.03197	0.70465	0.00001
RS430[+]	LBS1	10.26	2.88	0.28	0.1697	0.512723	5	0.511610	1.8	5.2	1512	1082							
RS431[+]	LBS1	27.30	5.35	0.20	0.1184	0.512248	4	0.511471	-7.5	2.5	1458	1258							
11-331-a	LBS1	19.29	4.50	0.23	0.1410	0.512217	7	0.511292	-8.1	-1.0	1971	1709	44	288	0.713150	34	0.44242	0.70682	0.00013
															[0.712921]	[10]	[0.442424]	[0.706594]	[0.00013]
11-331-b	LBS2	29.48	7.15	0.24	0.1466	0.512545	7	0.511583	-1.7	4.7	1396	1114	72	193	0.725198	14	1.08160	0.70973	0.00031
															[0.725208]	26	[1.0816]	[0.709740]	[0.00031]

Note:

1. Rb, Sr, Sm and Nd concentrations were obtained by ICP-MS and have precision less than ± 2%.
2. calc = calculated, meas = measured, ini = initial; replicate analyses are within parentheses [].
3. Crustal residence ages (T_{CR}) are calculated based on the present day $^{147}Sm/^{144}Nd = 0.2137$ and $^{143}Nd/^{144}Nd = 0.51316$ of depleted mantle with εNd value of +10, assuming a linear evolution from 4 Ga to the present (Goldstein et al., 1994); depleted mantle model ages (T_{DM}) are calculated based on the quadratic equation by DePaolo (1981a).
4. εNd values are calculated based on Chondrite uniform reservoir (CHUR) values of $^{147}Sm/^{144}Nd = 0.1960 \pm 4$ and $^{143}Nd/^{144}Nd = 0.512613 \pm 11$ (2) (Bouvier et al., 2008), and $\lambda\ ^{147}Sm = 6.539\ (\pm 0.061) \times 10^{-12}\ Yr^{-1}$ (Begemann et al., 2001). 2 = 2 standard error of the mean × 10^{-6}.
5. $(^{147}Sm/^{144}Nd)_{calc} = Sm/Nd \times [0.53151 + 0.14252\ (^{143}Nd/^{144}Nd)_{meas}]$.
6. $\lambda\ ^{87}Rb = 1.42 \times 10^{-11}\ Yr^{-1}$ (Begemann et al., 2001).
7. $(^{87}Rb/^{86}Sr)_{calc} = Rb/Sr \times [2.6939 + 0.2832(^{87}Sr/^{86}Sr)_{meas}]$.
8. Induced error in $(^{87}Sr/^{86}Sr)_{initial} = {}^{87}Rb/^{86}Sr \times$ (% error assigned) × $(e^{\lambda t}-1)$ (Jahn 2004).
9. The results of isotopic measurements for Sr and Nd reference materials are: NBS-987 (Sr) = 0.710245 ± 19 (2σ). JNdi-1 (Nd) = 512098 ± 6 (2σ).
10. All model ages and εNd values are calculated at 1 Ga.

Table 3.4. Parameters used for assimilation-fractional crystallization (AFC) calculations.

AFC Curve No.	Sample No.	Rock type	Nd (ppm)	Sm (ppm)	Sr (ppm)	$^{143}Nd/^{144}Nd$	$^{87}Sr/^{86}Sr$	D_{Sr}	D_{Nd}	R
I	CG-554	Granodiorite	25.2	4.86	218	0.510974	0.723492	0.4	0.12	0.7
Ia								1.5	0.12	0.7
Ib								1.5	0.12	0.1
II	CG-172A	Quartz-diorite	28.9	6.78	1391	0.510753	0.703897	0.4	0.12	0.7
III	ALC	Archean lower crust	18.5	3.30	569	0.510416	0.705000	0.4	0.12	0.7

Note: Labradorian crust (CG-554 and CG-172A; Schärer, 1991); ALC (Weaver and Tarney, 1984), Sr isotope ratio estimated from Lewisian lower crust (Kerr et al., 1995); Nd isotope ratios from average of Gagnon terrane orthogneiss (Thomson et al., 2011). D_{Sr} value of 1.5 for the curves Ia and Ib are assumed; for remaining D values see fig. 3.13.

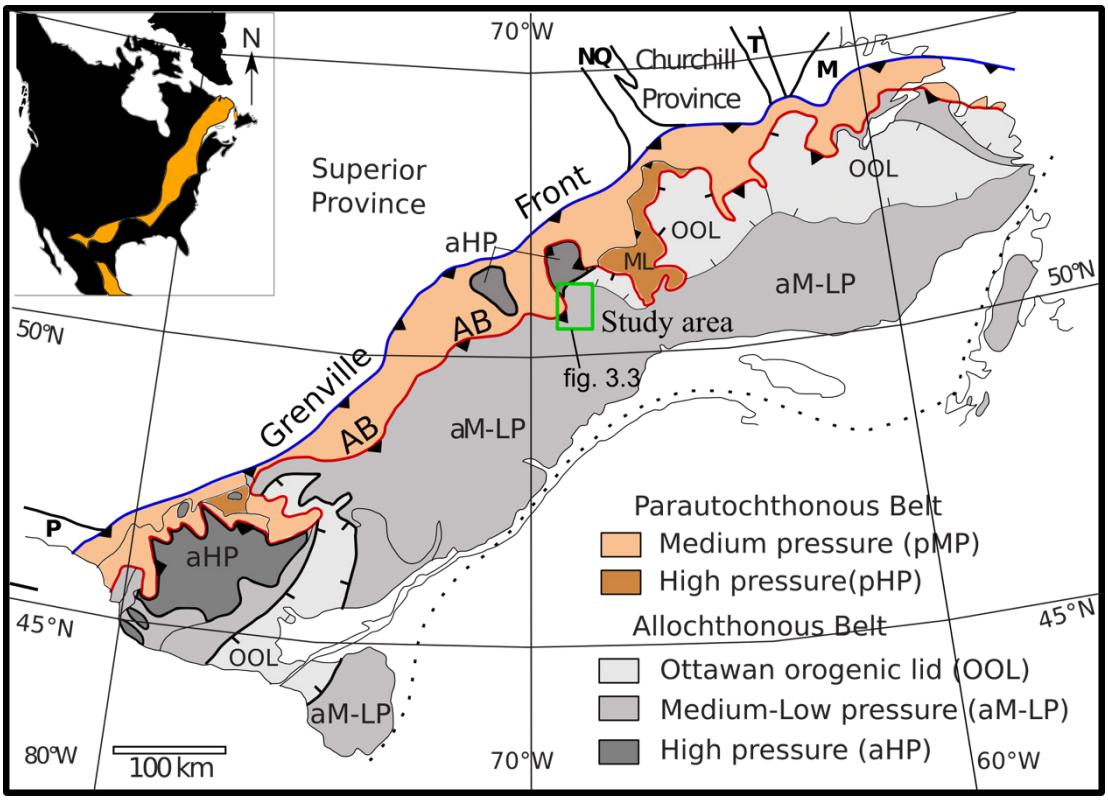

Figure 3.1. Schematic map showing tectonic division of the Grenville Province into belts on the basis of timing and pressure of peak metamorphism and tectonic character (simplified from Rivers et al., 2012). AB: Allochthon Boundary; aHP, allochthon high pressure; aMP, allochthon medium pressure; aLP, allochthon low pressure; pHP, parautochthonous high pressure; pMP; parautochthonous medium pressure; OOL, Ottawan orogenic lid; NQ, New Quebec Orogen; T, Torngat Orogen; M, Makkovik Orogen; P, Penokean Orogen; ML, Molson Lake Terrane; square box shows the location of the study area in fig. 3.3. Inset figure shows the extent of the Grenville orogenic belt in North America, modified after Tollo et al. (2004).

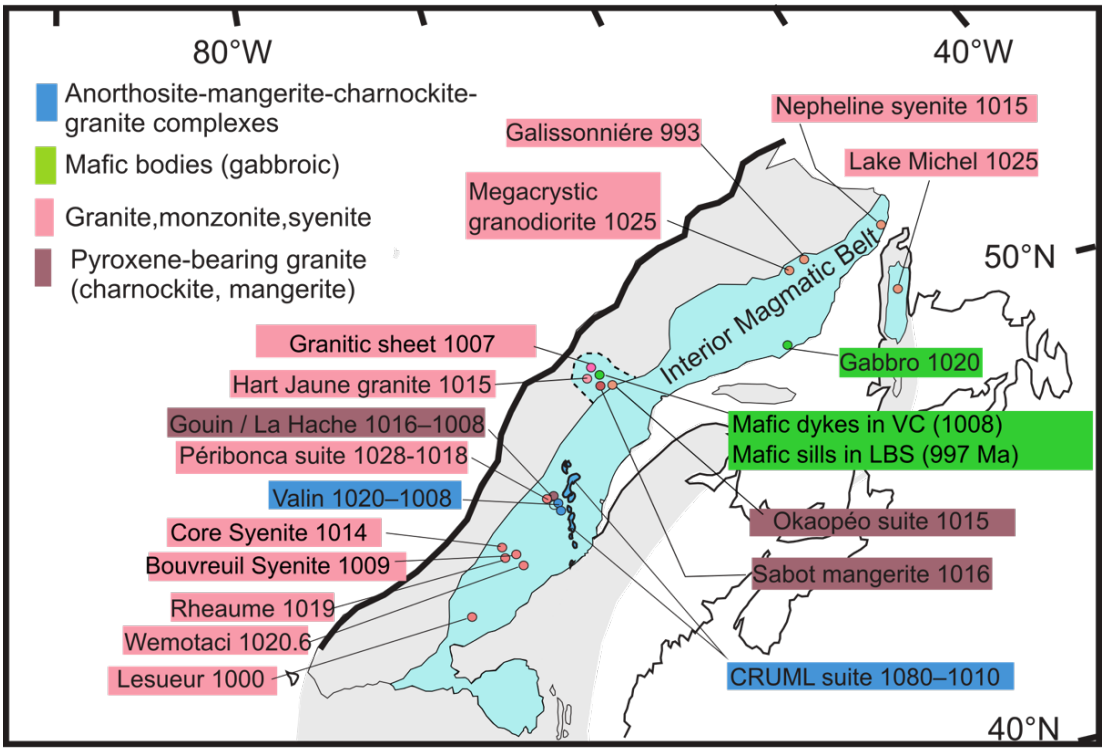

Figure 3.2. Simplified sketch map of the Grenville Orogen (after Rivers et al., 2012) showing locations and compositions of post-Ottawan (1020-980 Ma) magmatism with respect to the Interior Magmatic Belt. Uncertainties in crystallization ages are either indicated or are < 5 Ma. Data source: Rivers et al. (2012), with additional data on Okaopéo plutonic suite (Augland et al., 2015); Bourguet, Bouvreuil, and Core syenite (Augland et al., 2017); Rheaume and Wematoci syenites (Côté et al., 2018); Lesueur alkaline suite (Davis and Nantel, 2016), and Labrieville lamprophyres (Owens & Tomascak, 2002); CRUML, Château-Richer, St-Urban, Mattawa, and Labrieville AMCG complexes (Hébert et al., 2009); VC, Vein Complex, LBS, Layered Bimodal Suite (this study).

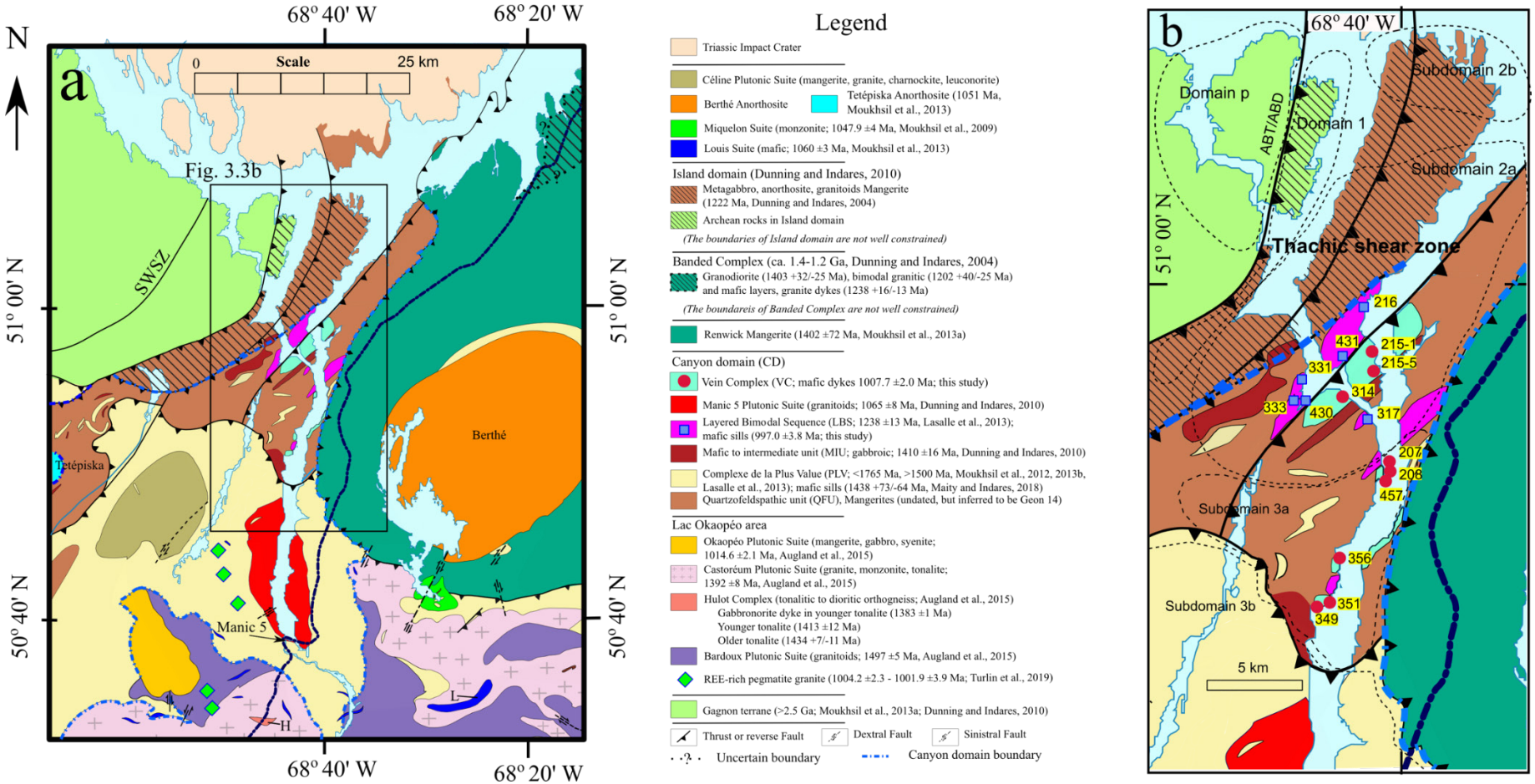
a
b
N
68° 40' W
68° 20' W
51° 00' N
50° 40' N
0
Scale
25 km
Fig. 3.3b
SWSZ
Tetépiska
Berthé
Manic 5
L
H
Legend
Triassic Impact Crater
Céline Plutonic Suite (mangerite, granite, charnockite, leuconorite)
Berthé Anorthosite
Tetépiska Anorthosite (1051 Ma, Moukhsil et al., 2013)
Miquelon Suite (monzonite; 1047.9 ±4 Ma, Moukhsil et al., 2009)
Louis Suite (mafic; 1060 ±3 Ma, Moukhsil et al., 2013)
Island domain (Dunning and Indares, 2010)
Metagabbro, anorthosite, granitoids Mangerite (1222 Ma, Dunning and Indares, 2004)
Archean rocks in Island domain
(The boundaries of Island domain are not well constrained)
Banded Complex (ca. 1.4-1.2 Ga, Dunning and Indares, 2004)
Granodiorite (1403 +32/-25 Ma), bimodal granitic (1202 +40/-25 Ma) and mafic layers, granite dykes (1238 +16/-13 Ma)
(The boundareis of Banded Complex are not well constrained)
Renwick Mangerite (1402 ±72 Ma, Moukhsil et al., 2013a)
Canyon domain (CD)
Vein Complex (VC; mafic dykes 1007.7 ±2.0 Ma; this study)
Manic 5 Plutonic Suite (granitoids; 1065 ±8 Ma, Dunning and Indares, 2010)
Layered Bimodal Sequence (LBS; 1238 ±13 Ma, Lasalle et al., 2013); mafic sills (997.0 ±3.8 Ma; this study)
Mafic to intermediate unit (MIU; gabbroic; 1410 ±16 Ma, Dunning and Indares, 2010)
Complexe de la Plus Value (PLV; <1765 Ma, >1500 Ma, Moukhsil et al., 2012, 2013b, Lasalle et al., 2013); mafic sills (1438 +73/-64 Ma, Maity and Indares, 2018)
Quartzofeldspathic unit (QFU), Mangerites (undated, but inferred to be Geon 14)
Lac Okaopéo area
Okaopéo Plutonic Suite (mangerite, gabbro, syenite; 1014.6 ±2.1 Ma, Augland et al., 2015)
Castorêum Plutonic Suite (granite, monzonite, tonalite; 1392 ±8 Ma, Augland et al., 2015)
Hulot Complex (tonalitic to dioritic orthogneiss; Augland et al., 2015)
Gabbronorite dyke in younger tonalite (1383 ±1 Ma)
Younger tonalite (1413 ±12 Ma)
Older tonalite (1434 +7/-11 Ma)
Bardoux Plutonic Suite (granitoids; 1497 ±5 Ma, Augland et al., 2015)
REE-rich pegmatite granite (1004.2 ±2.3 - 1001.9 ±3.9 Ma; Turlin et al., 2019)
Gagnon terrane (>2.5 Ga; Moukhsil et al., 2013a; Dunning and Indares, 2010)
Thrust or reverse Fault
Dextral Fault
Sinistral Fault
Uncertain boundary
Canyon domain boundary
Domain p
ABT/ABD
Domain 1
Subdomain 2b
Subdomain 2a
Thachic shear zone
Subdomain 3a
Subdomain 3b
5 km
216
431
215-1
215-5
331
314
333
430
317
207
208
457
356
351
349

Figure 3.3. (a) Geological map of the study area in the Canyon domain located to the south of the Manicouagan Impact Crater (modified from Maity and Indares, 2018); (b) Close-up of the study area showing locations of the mafic samples from the VC and LBS, along with structural domains and shear zones from Jannin et al. (2018b). Sample location 333 from Lasalle et al. (2013, 2014).

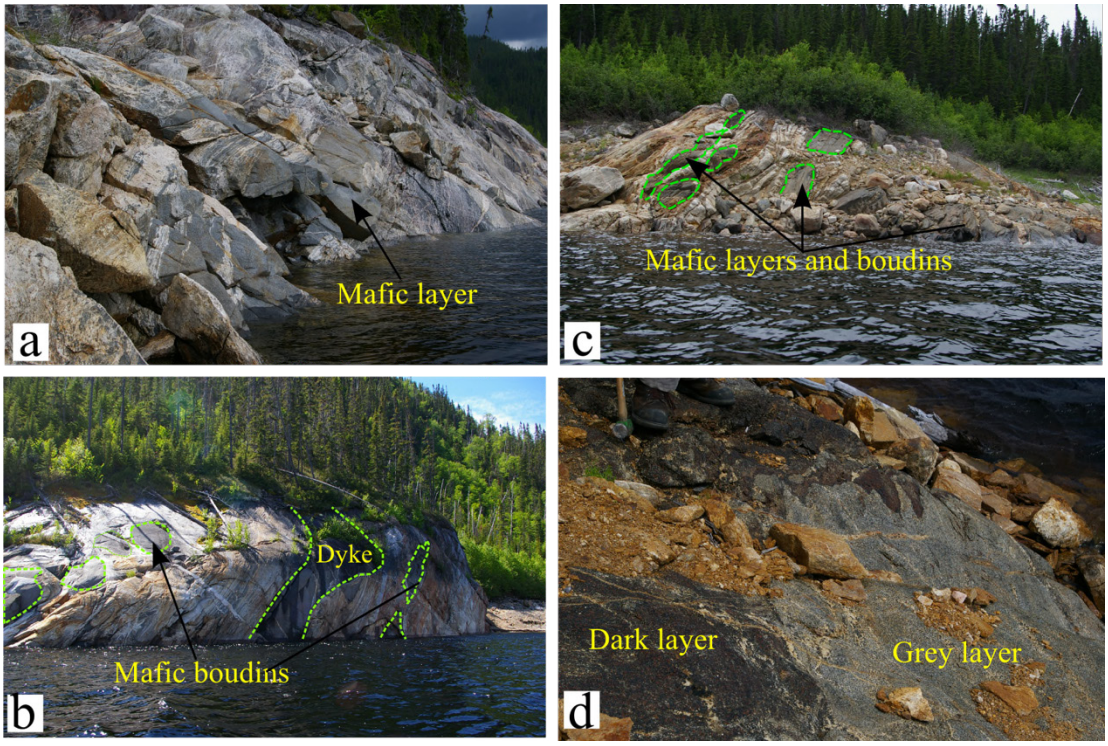

Figure 3.4. Field photographs of the mafic rocks, (a-b) dykes in the VC, (c-d) sills in the LBS. (a) Mafic dyke cross-cutting the VC; (b) mafic dykes in the VC deformed into isolated boudins; (c) mafic sill within felsic gneiss in the LBS, with sills showing pinch-and-swell and boudinage structure; (d) heterogeneous light and dark grey mafic sills in the LBS.

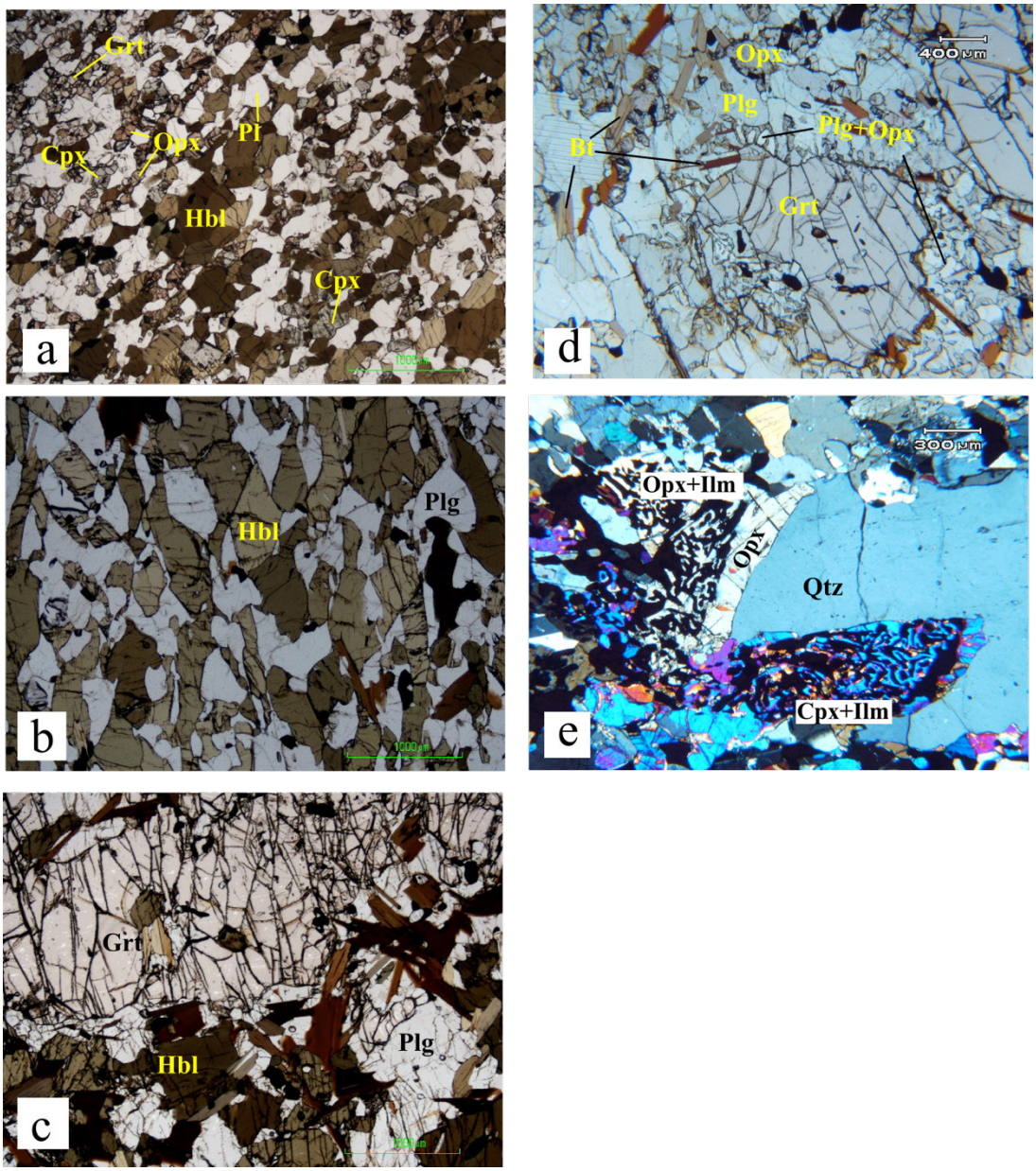

Figure 3.5. Photomicrographs of (a) mafic dykes in the VC, (b-e) mafic sills in the LBS. (a) granoblastic hornblende, clinopyroxene, orthopyroxene, plagioclase, and garnet indicative of MP granulite-facies metamorphism; (b) plagioclase and hornblende in amphibolite; (c) garnet porphyroblast corroded by plagioclase and hornblende; (d) garnet porphyroblast corroded by plagioclase + orthopyroxene corona and biotite; (e) large quartz xenocryst rimmed by pyroxene and pyroxene + ilmenite symplectite.

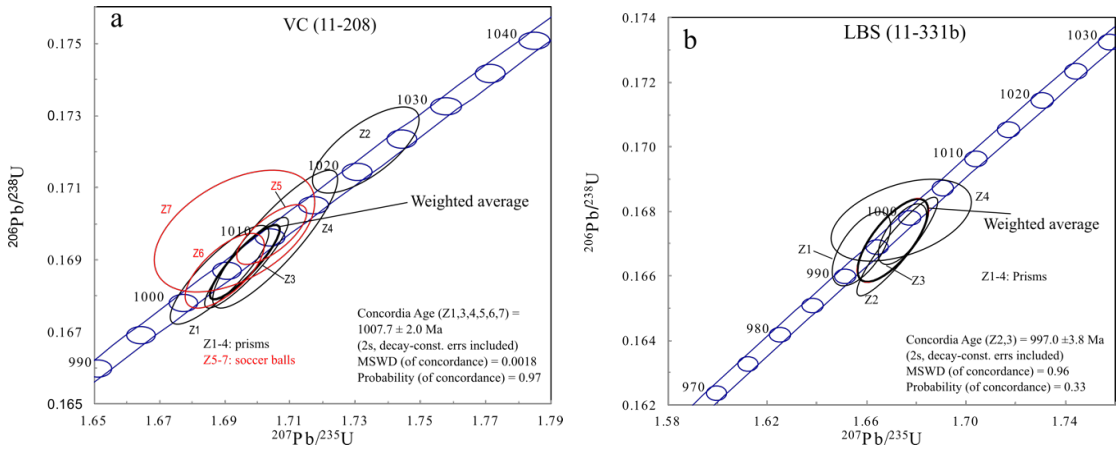

Figure 3.6. U-Pb (zircon) Concordia diagrams for: (a) mafic dyke (#11-208) in the VC; (b) mafic sill (#11-331b) in the LBS. All analyses are plotted with 2σ absolute errors and the reported ages include decay constant errors. Analysis numbers are given in table 3.1 and are indicated next to the corresponding error ellipses on the Concordia diagram. Black ellipses are igneous prisms, red ellipses are metamorphic soccer balls, thick black ellipses are weighted averages.

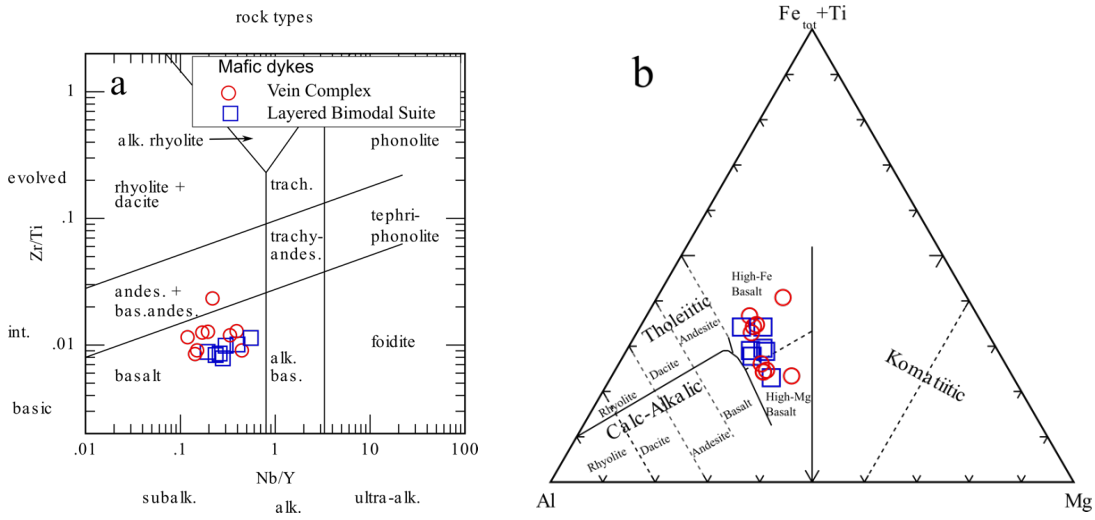

Figure 3.7. Rock-type classification diagrams for the mafic samples from the VC and the LBS. (a) Zr/Ti vs. Nb/Y diagram (Pearce, 1996); (b) Al-(Fe_t+Ti)-Mg cation plot (Jensen and Pyke, 1982).

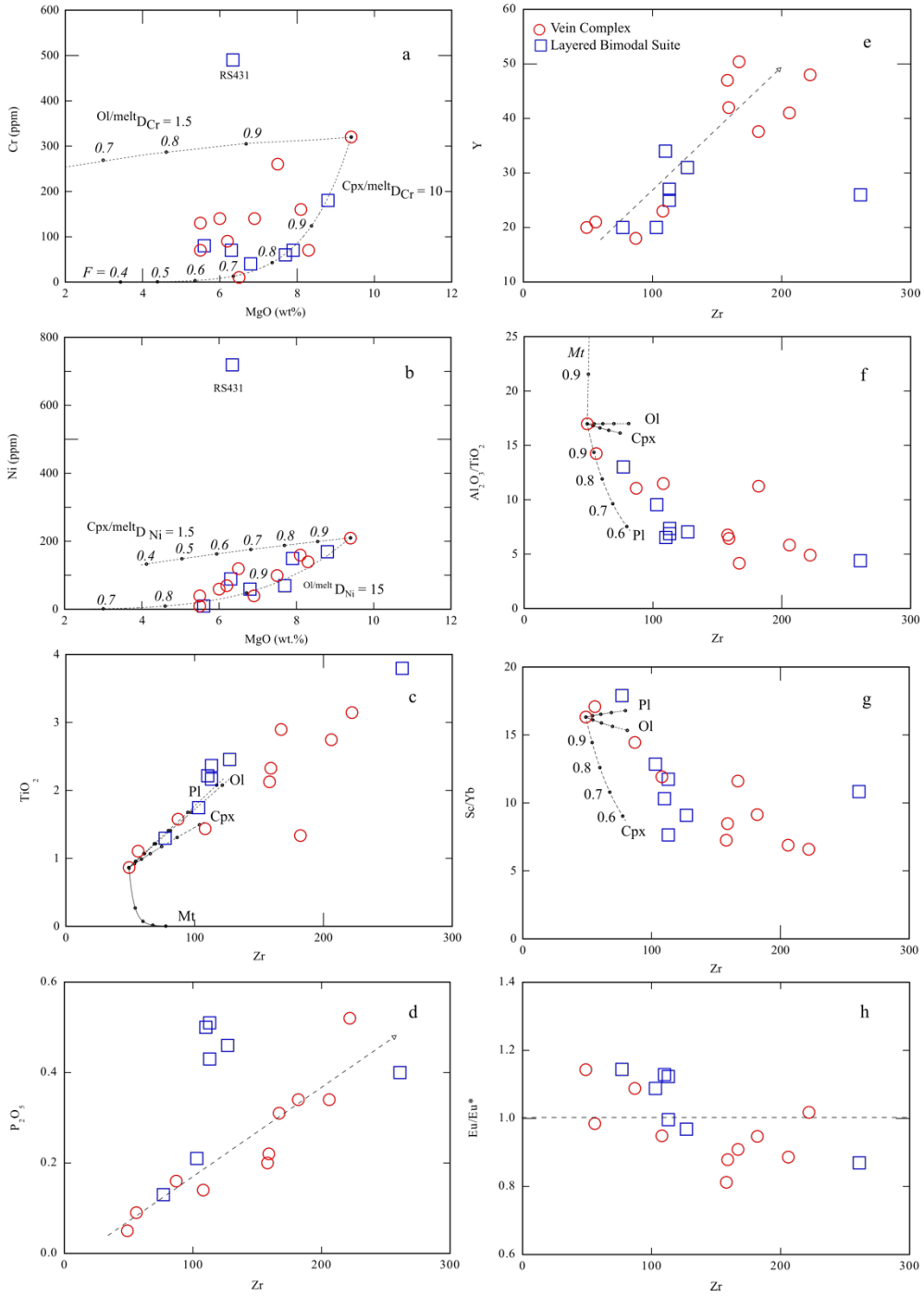

Figure 3.8. Plots of (a) Cr (ppm); and (b) Ni (ppm) vs. MgO (wt. %); (c) TiO_2 (ppm); (d) P_2O_5 (ppm); (e) Y (ppm); (f) Al_2O_3/TiO_2; (g) Sc/Yb; (h) Eu/Eu* vs. Zr (ppm) for the mafic rocks from the VC and LBS. $Eu/Eu^* = Eu_{CN} / \sqrt{(Sm_{CN} \times Gd_{CN})}$; CN, chondrite normalized. The dashed curves indicate fractional crystallization from the high MgO sample RS314, small dots on the curves and the numbers in italics indicate the value of F = remaining melt fraction after crystal fractionation; partition coefficients are after Rollinson (1993), Villemant et al. (1981), and Pearce and Parkinson (1993).

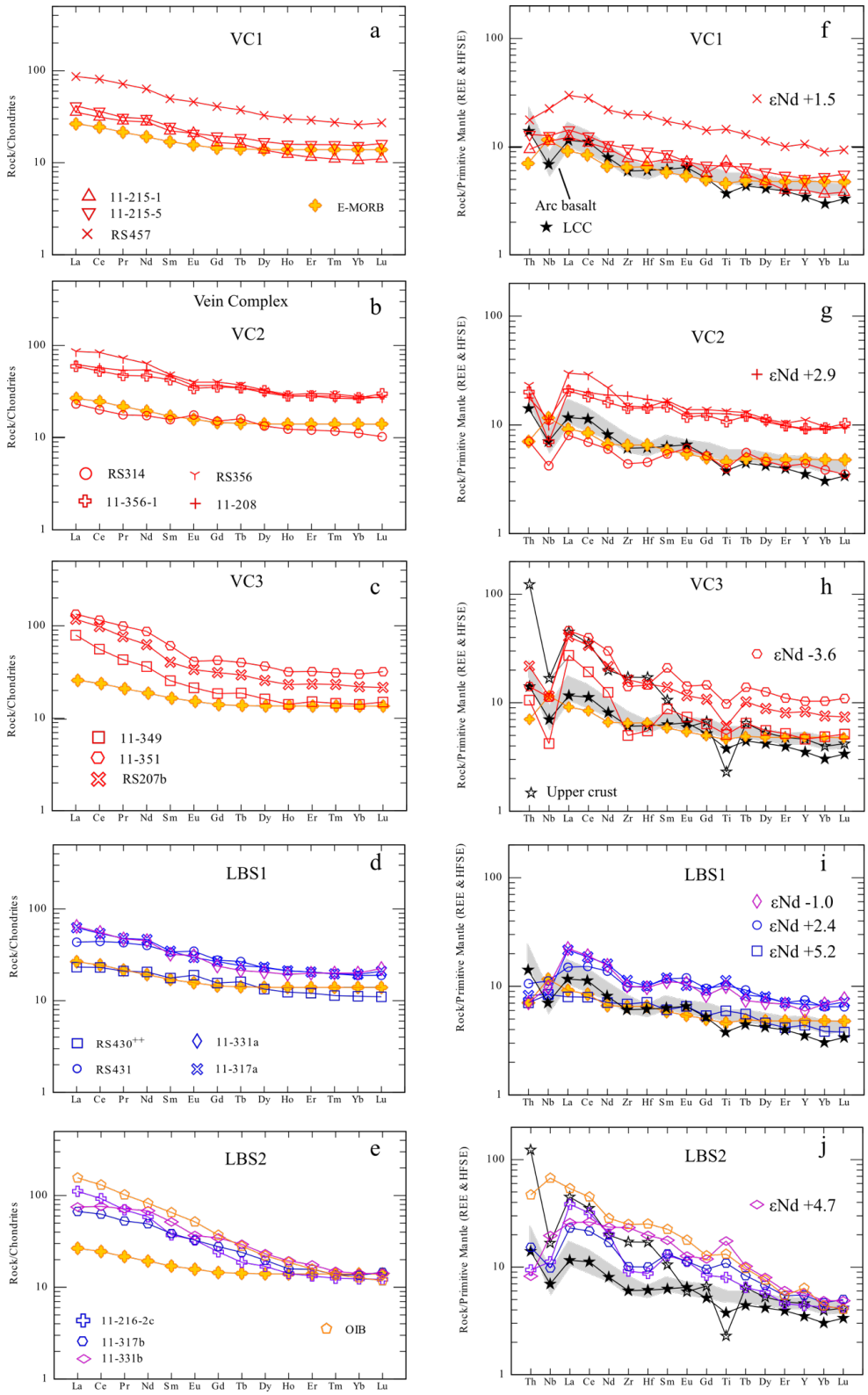

Figure 3.9. (a-e) Chondrite-normalized REE patterns, and (f-j) primitive mantle-normalized trace element patterns for the mafic rocks in the VC and LBS. Normalizing values are from Sun and McDonough (1989), LCC, lower continental crust, and UCC, upper continental crust (Rudnick and Gao, 2014); arc basalts (Kelemen et al., 2014).

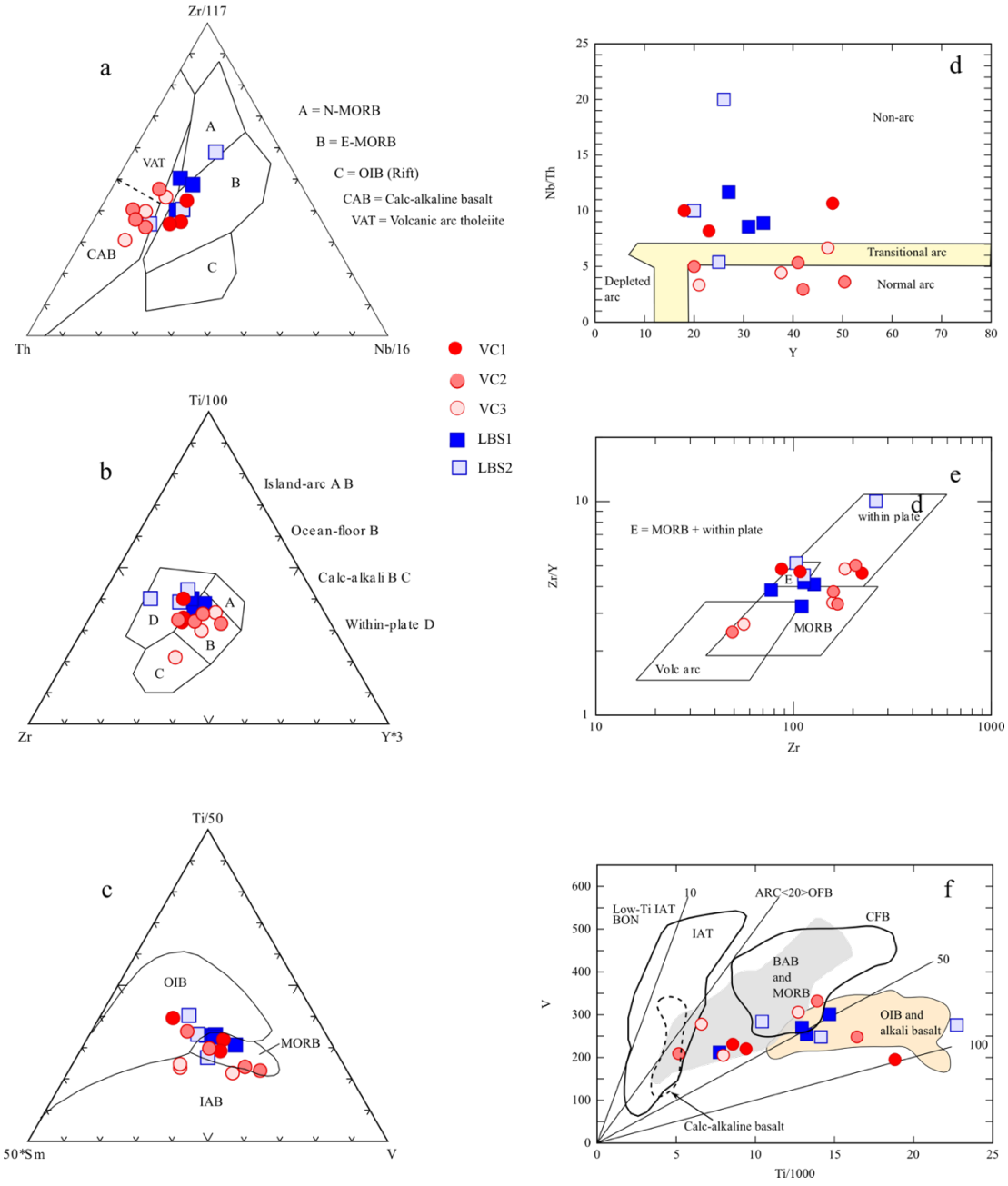

Figure 3.10. Tectonic discrimination diagrams (a) Th-Zr/117-Nb/16 (Wood, 1980); (b) Zr-Ti/100-Y*3 (Pearce & Cann, 1973); (c) Ti/50-50*Sm-V (Vermeesch, 2006); (d) Nb/Th vs. Y (Swinden et al., 1989); (e) Zr/Y-Y (Pearce and Norry, 1979) ; (f) Ti-V (Shervais, 1982; modified by Rollinson, 1993) showing plots for the mafic rocks of the VC and LBS.

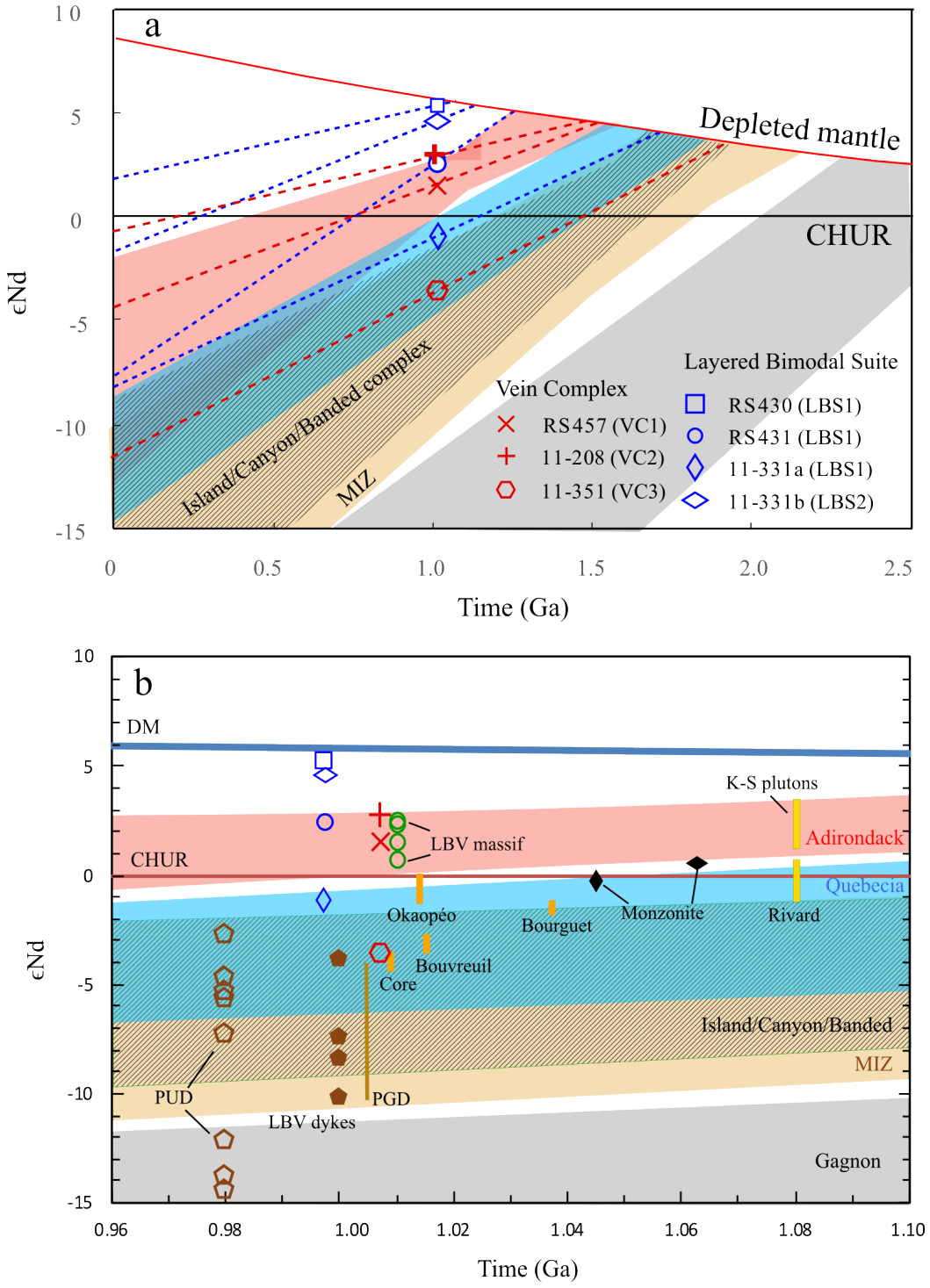

Figure 3.11. Plots for εNd vs. time (Ga). εNd values are calculated at 1 Ga. Data source: Mesoproterozoic orthogneisses from the Canyon domain, Island domain, Banded Complex (thin black diagonal lines), the Labradorian crust in MIZ (light yellow), and Archean Gagnon terrane (grey) (Thomson et al., 2011); Adirondack crust (light red; derived from Grenvillian SCLM; Chiarenzelli et al., 2010; and references therein); Quebecia (light blue; Dickin, 2000; Dickin and Higgins, 1992), Labrieville (LBV) massif anorthosite (Owens et al., 1994); Labrieville lamprophyre dykes (Owens and

Tomascak, 2002); Monzonite (Groulier et al., 2018b); Rivard minette dyke (Corriveau et al., 1996); Kensington-Schoottamatta plutons (K-S) (Corriveau and Amelin, 1994); εNd values for the pegmatite granite dyke (PGD; Turlin et al., 2019), Okaopéo mangerite (Augland et al., 2015), syenite plutons from Bourguet, Bouvreuil, and Core (Augland et al., 2017) are estimated from their zircon εHf values following Vervoort and Blichert-Toft; 1999); DM, depleted mantle (DePaolo, 1981a); CHUR, chondritic uniform reservoir (Bouvier et al., 2008).

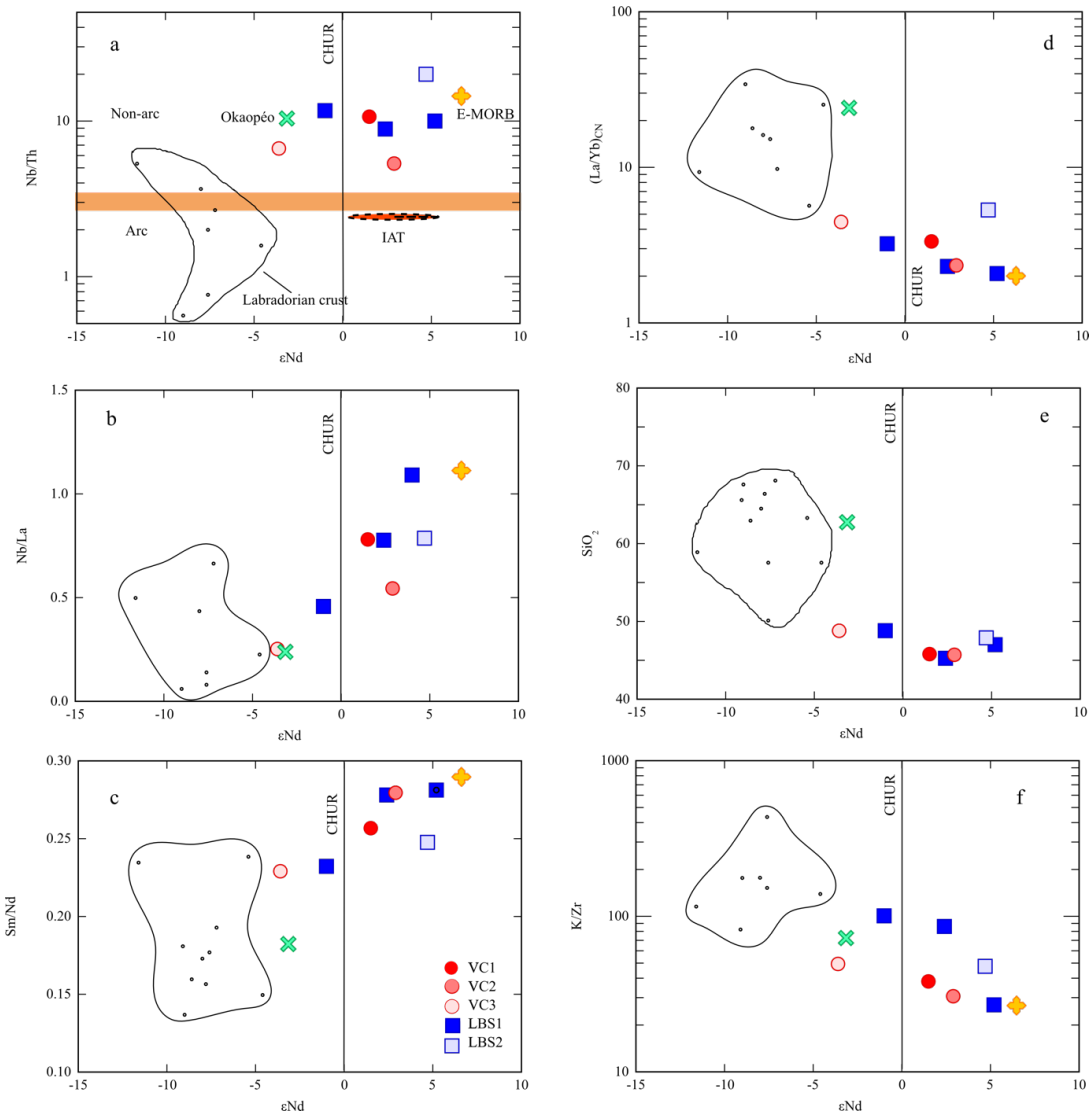

Figure 3.12. Plots for εNd vs. (a) Nb/Th; (b) Nb/La; (c) Sm/Nd; (d) $(La/Yb)_{CN}$; (e) SiO_2; and (f) K/Zr. Black points bound by black solid line indicates Labradorian crust (Kerr, 1989; Schärer, 1991); Okaopéo mangerite is shown for comparison with its εNd value estimated from the published zircon εHf value (Augland et al., 2015) following Vervoort and Blichert-Toft (1999). Arc vs. non-arc fields shown by the horizontal light brown bar (Whalen et al., 2006); IAT, Island arc tholeiite derived from supra-

subduction zone mantle (SSZM; Whalen et al., 2006); E-MORB, enriched MORB mantle (Sun and McDonough, 1989).

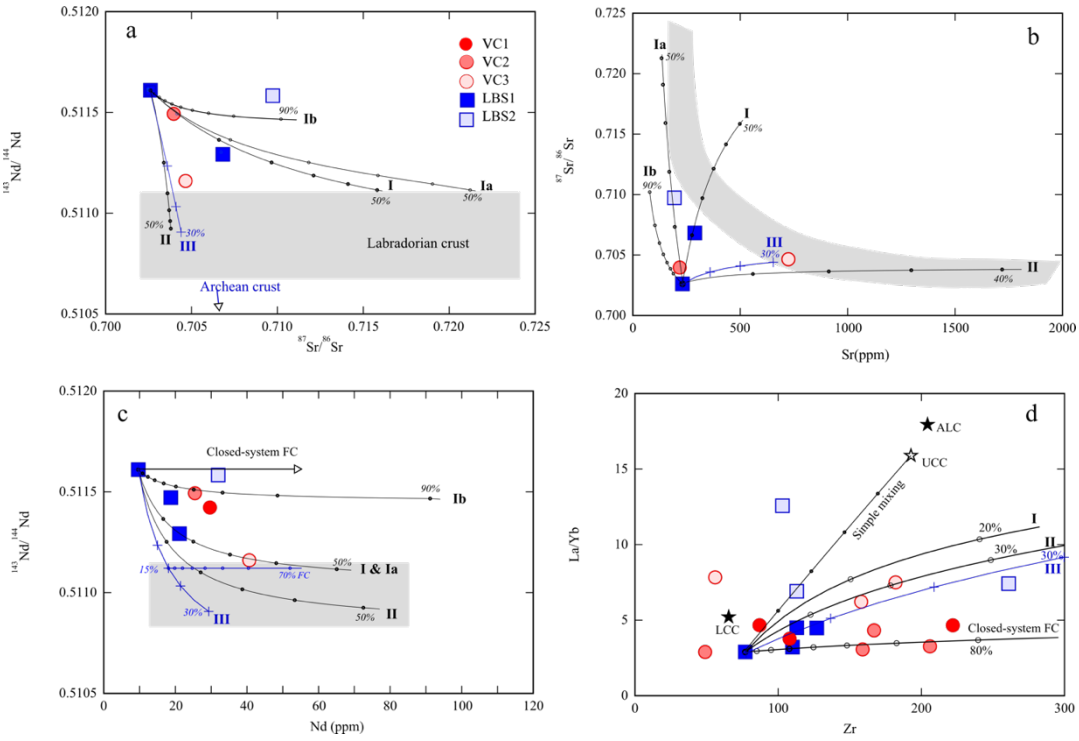

Figure 3.13. (a) $^{143}Nd/^{144}Nd$ vs. $^{87}Sr/^{86}Sr$; (b) $^{87}Sr/^{86}Sr$ vs. Sr (ppm); (c) $^{143}Nd/^{144}Nd$ vs. Nd (ppm); and (d) La/Yb vs. Zr (ppm) diagrams for LBS and VC. The AFC curves between RS430 and different crustal components are labeled with specific parameters given in table 3.4; black solid curves (I-II) indicate AFC for Labradorian crust and blue curves (III) for Archean crust; each small dot on the AFC curves indicate percentage of crustal assimilation as indicated by the numbers in italics; D values (table 3.4) were calculated assuming fractional crystallization of 20% olivine, 45% clinopyroxene, and 20% plagioclase; using the same partition coefficients as in fig. 3.8; for the curves Ia and b, higher D_{Sr} values were assumed; horizontal dashed blue line from the curve III indicates 70% pure fractional crystallization after 15% AFC with an Archean crust; simple mixing line between upper crust and asthenospheric melt with each dot indicating 20% mixing. Data source: Labradorian crust (Kerr, 1989; Schärer, 1991); UCC, Upper continental crust (Rudnick and Gao, 2014); ALC, Archean lower crust (Weaver and Tarney, 1984; Kerr et al., 1995; Thomson et al., 2011); The initian Sr isotope value for RS430 is recalculated from that of the E-DMM (Workman and Hart, 2005).

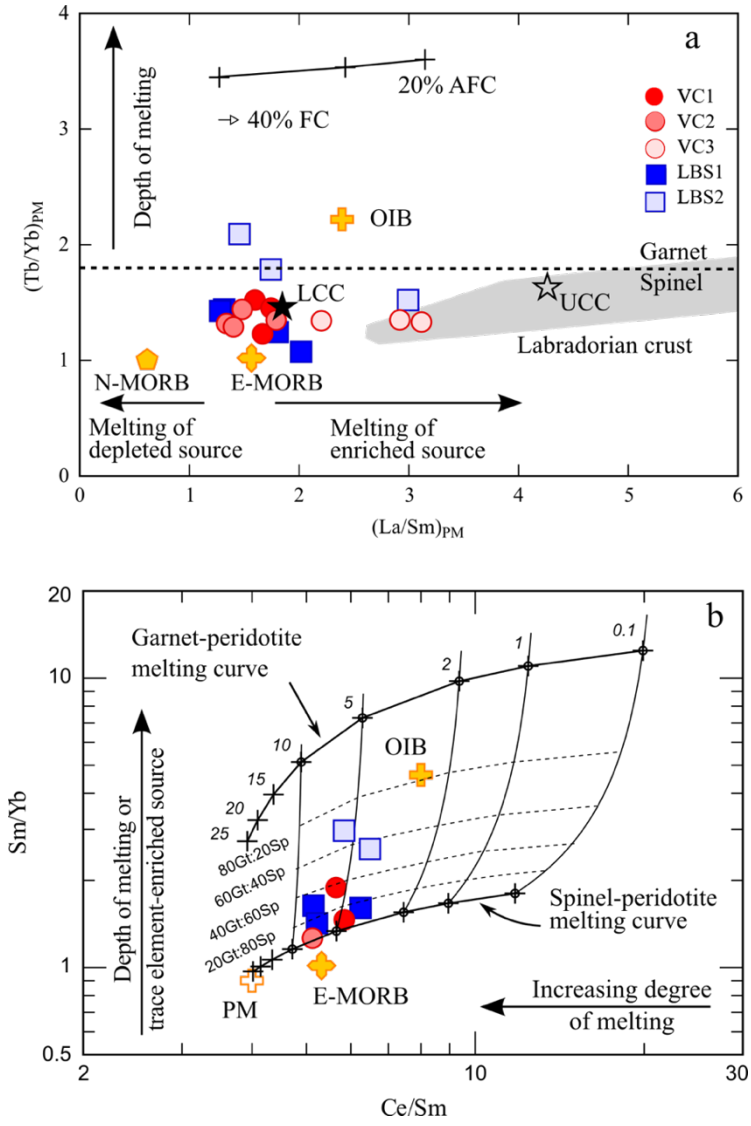

Figure 3.14. Plots for (a) $(Tb/Yb)_{PM}$ vs. $(La/Sm)_{PM}$ (modified after Konopelko & Klemd, 2016) diagram with the dashed horizontal line indicating the spinel-garnet melting boundary at $(Tb/Yb)_{PM}$ = 1.8 corresponding to 2.8 GPa (Wang et al., 2002); curve indicating 20% AFC of upper crust in N-MORB and vector indicating 40% closed-system fractional crystallization are shown; E-MORB, N-MORB, OIB (Sun and McDonough, 1989); upper and lower continental crust (UCC, LCC) (Rudnick and Gao, 2014); (b) Sm/Yb vs Ce/Sm diagram; partial melting curves (black thick solid lines) for model spinel- and garnet-peridotite of primitive mantle composition (PM; Sun and McDonough, 1989) using non-modal batch melting (Shaw, 1970) of spinel-peridotite ($Ol_{0.53}$ + $Opx_{0.27}$ + $Cpx_{0.17}$ + $Sp_{0.03}$) that melts in the proportions ($Ol_{0.06}$ + $Opx_{0.28}$ + $Cpx_{0.67}$ + $Sp_{0.11}$) (Kinzler, 1997), and garnet peridotite ($Ol_{0.60}$ + $Opx_{0.20}$ + $Cpx_{0.10}$ + $Gt_{0.10}$) that melts in the proportions ($Ol_{0.03}$ + $Opx_{0.16}$ + $Cpx_{0.88}$ + $Gt_{0.09}$) (Walter, 1998); numbers on curves indicate degrees of melting in percentage; dashed lines indicate mixing between spinel- and garnet-peridotite; mineral partition coefficients are from Halliday et al. (1995).

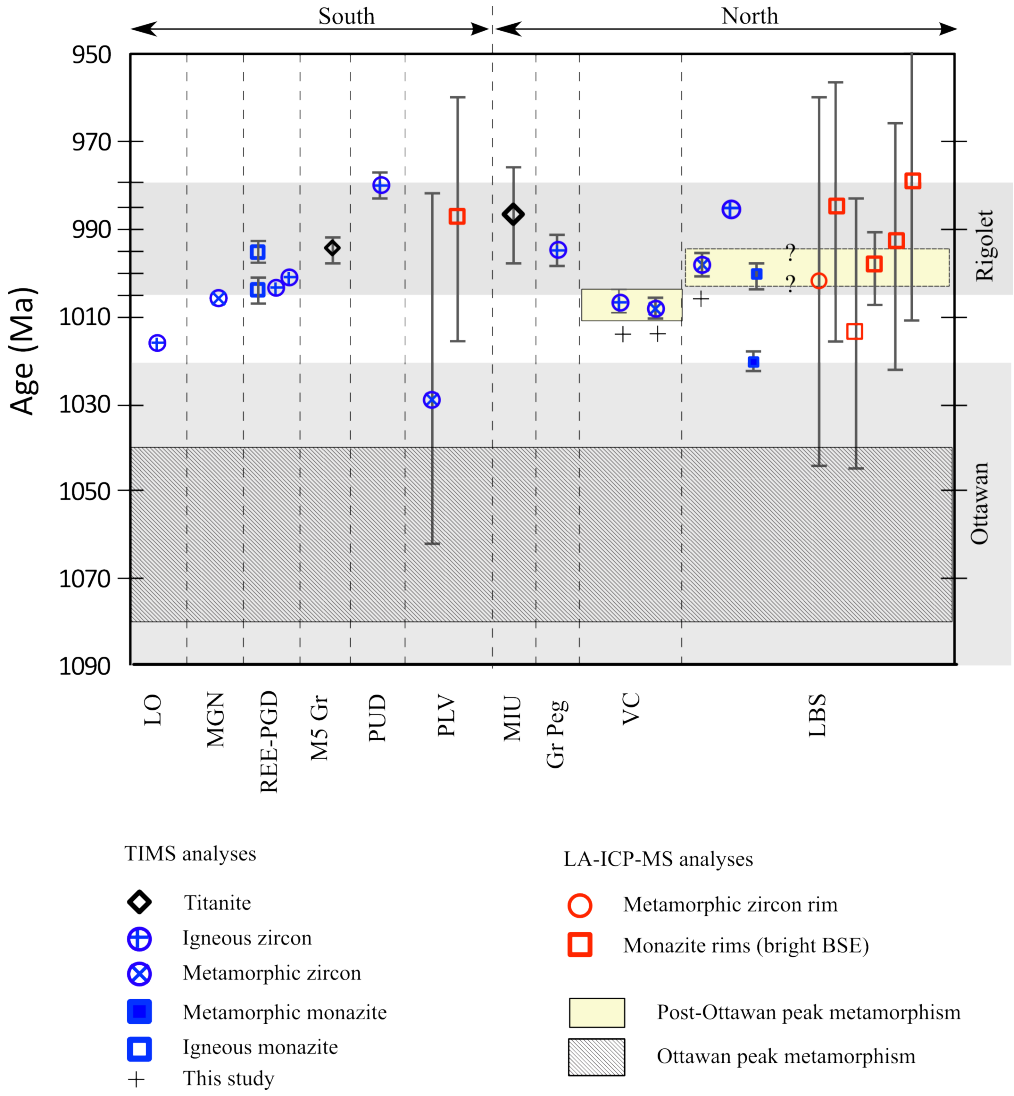

Figure 3.15. Plot of rock units vs. ages of igneous and metamorphic events in the Canyon domain and part of the Lac Okaopéo area to the south, arranged from left to right according to their field occurrence from south to north, with tentative division between the southern and northern Canyon domains at the contact between the PLV and MIU (see fig. 3.3). Light yellow boxes indicate durations of granulite-facies metamorphism in VC and LBS; diagonal striped box indicates main Ottawan granulite-facies metamorphism (Dunning & Indares, 2010; Lasalle et al., 2013, 2014); the durations of Ottawan and Rigolet phases of the Grenvillian Orogeny indicated in grey are from Rivers et al., 2012. Gr Peg, granitic pegmatite dyke, and M5 Gr, Granite in Manic 5 area in the southern Canyon domain (Dunning & Indares, 2010); LO, Lac Okaopéo mangerite, MGN, metagabbronorite (Augland et al., 2015); MIU, Mafic to Intermediate Unit, and PLV, Complexe de la Plus Value (Maity & Indares, 2018); REE-Peg, REE-rich pegmatitic granite dykes (Turlin et al., 2017, 2019); PUD, potassic to ultrapotassic dykes (Valverde Cardenas et al., 2012); VC, Vein Complex; and LBS, Layered Bimodal Suite (this study, indicated by + signs). LA-ICP-MS analyses (in red) are from Lasalle et al. (2013, 2014); TIMS ages (in blue) are from Dunning & Indares (2010), Jannin et al. (2018b), and Turlin et al. (2017, 2019).

a. ca. 1020-1010 Ma: Lithospheric extension and SCLM melting

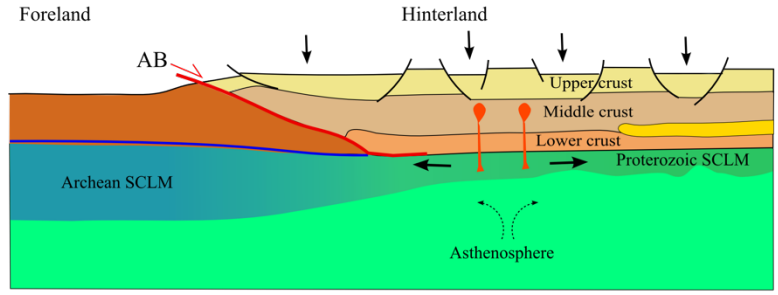

b. 1008 Ma: Lithospheric extension and decompression melting

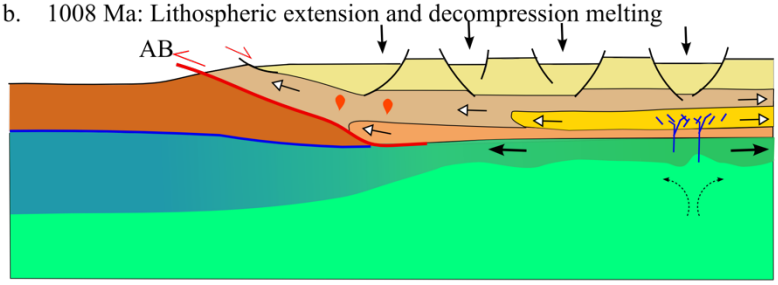

c. 1005-997 Ma: Rigolet underthrusting of foreland

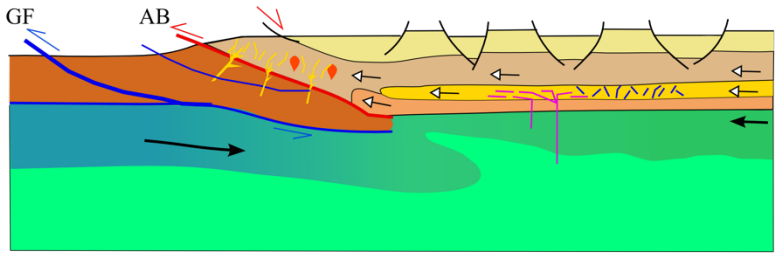

d. 997-993 Ma: Thrusting or extrusion of aMP crust (northern CD)

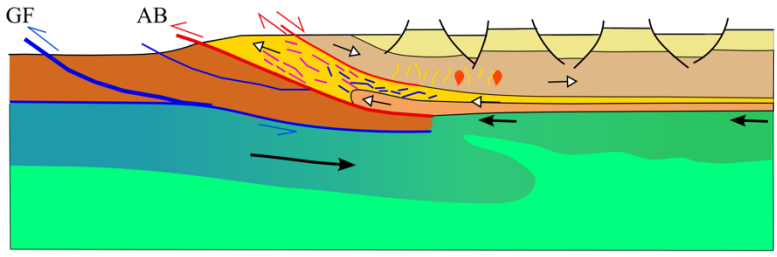

e. ca. 993-986 Ma: Development of channel

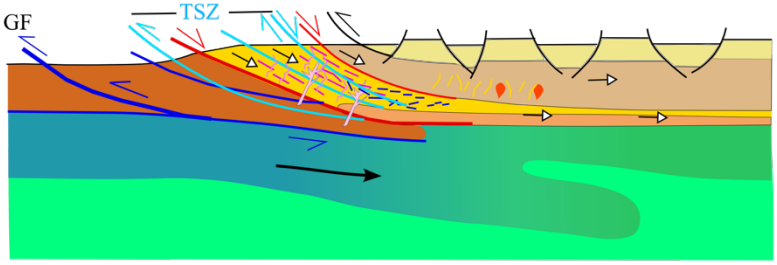

Okaopéo and Sabot AMCG suites (ca. 1017-1015 Ma)
/// Mafic dykes in VC (ca. 1008 Ma)
Mafic sills in LBS (ca. 997 Ma)
REE-rich PGD (ca. 1005-997 Ma)
Pink leucogranite (ca. 986 Ma)

Gravitational force
Thrust fault
Normal fault
Crustal flow (channel?)
Northern Canyon domain and Island domain
Southern Canyon domain

Figure 3.16. Schematic diagram showing the post-Ottawan tectonic evolution of the Grenvillian hinterland in the Canyon domain; inspired by Rivers (2008, 2012) and Jannin et al. (2018b). (a) Lithospheric extension, normal-sense displacement on AB, and orogenic collapse of the structural top in the hinterland at ca. 1020-1010 Ma (Indares et al., 1998), partial melting of stretched SCLM resulting in the coeval emplacement of the Okaopéo plutonic suite (Augland et al., 2015); note the thin Proterozoic SCLM under extension; (b) continued extension in the lower and mid-crust, whereas the upper parts of the mid-crust containing the Okaopéo suite are extruded to the northwest; asthenospheric upwelling and decompression melting at shallow depth, and the emplacement of mafic dykes in the VC in northern Canyon domain (in yellow) at ca. 1008 Ma; (c) Rigolet underthrusting of foreland beneath hinterland (Jannin et al., 2018a, 2018b), emplacement of the REE-rich granite pegmatite dykes (PGD) in the southern Canyon domain and in Lac Okaopéo area (Turlin et al., 2017, 2019), and coeval intrusion of mafic sills in the LBS in the northern Canyon domain (this study); (d) thrusting or extrusion of the northern Canyon domain along the Allochthon Boundary; (e) development of Rigolet crustal channel and the normal-sense Thachic Shear Zone (Jannin et al., 2018a, 2018b).

4 Late-orogenic potassic to ultrapotassic dykes from the central Grenvillian hinterland: trace element and Sr-Nd-Pb-O isotopic perspective

4.1 Abstract

New whole-rock Sr-Nd-Pb-O isotope data, combined with previously published data are used to examine the origins of a group of ca. 980 Ma potassic to ultrapotassic dykes (PUD) from the Canyon domain, central Grenville Province. The PUD suite can be divided into two groups that are geochemically distinct, and exhibit characteristic source mineralogy, depth of partial melting, and multi-stage metasomatism of heterogeneous sources within the Laurentian subcontinental lithospheric mantle. Major and trace element data suggest involvement of both fertile and depleted peridotite sources, whereas trace element and isotope data indicate long-term LREE and LILE enrichment and HFSE depletion in a subduction setting. Low time-integrated Rb/Sr, Sm/Nd, and U/Pb ratios suggest late-Archean and Paleoproterozoic, enriched EM-I mantle sources (Superior and Proterozoic SCLM, respectively), metasomatized by late-Archean to Proterozoic subduction of carbonate, phosphate, and pelagic sediments. Sr-O isotope correlation further indicates a latest phase of fluid metasomatism that is attributed to a combination of asthenospheric upwelling related to lithospheric extension and late-Grenvillian continental subduction.

The tectonic setting of the Rigolet phase is proposed to have been characterized by shallow-angle or flat subduction of the Superior lithosphere beneath the Grenvillian

hinterland. The intracontinental subduction was short-lived and probably terminated because of the inability to subduct buoyant and refractory Archean lithospheric mantle.

4.2 Introduction

Recent work in the Grenville Province has led to significant advances in understanding the evolution of the Grenvillian Orogeny, and to recognize it as a remnant of a large hot long-duration orogen (LHO; Beaumont et al., 2006; Jamieson et al., 2011; Rivers, 2008; Rivers et al., 2012; and references therein), comparable in scale and tectonic styles to its ancient analogue such as the Paleoproterozoic Trans-Hudson Orogen (Darbyshire et al., 2017), or its modern analogue such as the Himalaya-Tibet Orogen (Carr et al., 2000; Jamieson et al., 2007; Rivers, 2008, 2009; Rivers et al., 2012).

The Grenvillian Orogeny has been empirically subdivided into two orogenic phases, the ca. 1090-1020 Ma Ottawan phase for which evidence is preserved in allochthonous rocks in the orogenic hinterland, and the ca. 1005-980 Ma Rigolet phase for which evidence is mainly preserved in the parautochthonous foreland (Rivers et al. 2012). The Rigolet phase and the formation of the Parautochthonous Belt situated in the hanging wall of the Grenville Front (GF) (Rivers, 2008), has been interpreted to have resulted either from propagation of the orogen over its foreland (van Gool et al., 2008; Hynes and Rivers, 2010; Rivers, 2015; Rivers et al., 2012), or from underthrusting of the foreland beneath the hinterland (Jordan et al., 2006), in both cases leading to extrusion of the parautochthonous rocks from progressively deep crustal levels along the hanging wall of the GF (van Gool et al., 2008). Although kinematically

equivalent, these interpretations of the Rigolet phase differ in their implications for the petrogenetic involvement of crustal and mantle sources, as discussed herein.

Seismic reflection imaging in the western Grenville Province has shown that the GF there forms the base of a wide (9~30 km), moderately SE-dipping, crustal-scale shear zone that extends at progressively greater depth beneath much of the exposed Grenville Province (Green et al., 1988; Culshaw et al., 1997; Rivers, 1997). On the other hand, in the central and eastern parts of the province, metamorphic, geochronological, and structural features documented within the Parautochthonous Belt, especially in the Gagnon terrane in the eastern Quebec and western Labrador (Rivers, 1983a, 1983b; Jordan et al., 2006; van Gool et al., 2008), provide convincing geological evidence that an orogenic wedge, composed of foreland-derived crust (van Gool et al., 2008), developed during intracontinental subduction during the Rigolet phase. This latter setting is similar to the recently reported ca. 980 Ma underthrusting of the Eastern Segment, composed of Baltica crust, beneath the western Sveconorwegian terranes (Möller and Andersson, 2018), or to the underthrusting of the Indian mantle lithosphere beneath the southern Tibetan plateau (DeCelles et al., 2002; Chung et al., 2005). Such interpretations in the Grenville Province are corroborated by geophysical evidence supporting the presence of imbricated foreland crust and its underlying subcontinental lithospheric mantle (SCLM) along the southeastern margin of the Superior craton that extends up to ~250 km beneath the hinterland (Hynes et al., 2000; Adetunji et al., 2014; Boyce et al., 2016; Petrescu et al., 2016). However, the magmatic, geochemical, and isotopic signatures of a perceived late-Grenvillian intracontinental subduction event that extended under the Grenvillian hinterland remain little investigated and poorly understood.

Potassic and ultrapotassic rocks have long been considered to offer significant insights into the nature and composition of the mantle lithosphere beneath the modern LHOs (e.g., Miller et al., 1999; Prelević et al., 2012). Occurrences of such rock types in the Grenville Province are volumetrically small compared to sub-alkaline rocks during early- to mid- and post-Ottawan periods (ca. 1089-980 Ma) (Corriveau, 1990; Corriveau et al., 1990; Corriveau and Gorton, 1993; Owens and Tomascak, 2002; Gower and Krogh, 2002; Morin et al., 2005; Augland et al., 2015, 2017; Côté et al., 2018). However, unlike most of the Ottawan and post-Ottawan suites, the Rigolet lamprophyric and potassic to ultrapotassic dykes (PUD) were shown to exhibit geochemical and isotopic signatures that suggest long-term mantle enrichment - either during ancient long-lived subduction events or from ancient low-density melts that had migrated from the asthenosphere and metasomatized the lithospheric mantle (Owens and Tomascak, 2002; Valverde Cardenas et al., 2012). Valverde Cardenas et al. (2012) suggested that upwelling hot asthenosphere caused melting in an old, metasomatized Archean subcontinental lithospheric mantle (SCLM), which was introduced beneath the Grenville hinterland as a result of northwest-directed thrusting of the latter over its Archean foreland.

This paper presents new whole-rock Sr-Nd-Pb-O isotope data, which has been integrated with lithogeochemical and Sr-Nd isotope data from Valverde Cardenas et al. (2012) to show that the two types of PUDs were derived from both Proterozoic and Archean SCLM - with distinct depletion and multi-stage metasomatic enrichment histories – which, coupled with their syn-tectonic vs. post-tectonic characters, are used to develop a tectonic model for the Rigolet period of the Grenvillian orogeny. Integrating these results for units intruded into the orogenic hinterland with published

structural and geochronological data from subjacent parautochthonous foreland terranes (e.g., the Gagnon terrane; Jordan et al., 2006; van Gool et al., 2008; Jannin et al., 2018a; Turlin et al., 2019), it is inferred that gently SE-dipping or flat subduction beginning at ca. 1005 Ma brought the southeastern margin of the Superior craton and its Paleoproterozoic cover in the orogenic foreland beneath the study area in the hinterland. This late-orogenic intracontinental flat subduction event appears to have been comparable in many ways to other modern (DeCelles et al., 2002; Chung et al., 2005) and ancient (Cousens et al., 2001; Darbyshire et al., 2017; Möller and Andersson, 2018) LHOs - further suggesting that subduction of continental lithosphere has remained an important tectonic process in crustal evolution since at least the late Paleoproterozoic.

4.3 Geology of the study area

The Grenville Province consists of two distinct tectonometamorphic belts (Rivers et al., 1989): the Allochthonous Belt in the hinterland largely composed of the late-Paleoproterozoic to Mesoproterozoic pericratonic domains derived from the Laurentian-margin arc, back-arc, and accreted terranes; and the Parautochthonous Belt in the foreland, principally composed of the Archean Superior Province basement and its Paleoproterozoic cover sequences developed on the Laurentian continental margin (fig. 4.1). The Allochthonous and Parautochthonous Belts are separated by the Allochthon Boundary (AB), a southeast-dipping high-grade shear zone that locally records both thrust-sense and normal-sense displacements (Rivers, 2008). The Parautochthonous Belt is separated from the interior, reworked part of the Superior craton by the Grenville Front (GF), a moderately southeast-dipping crustal-scale shear

zone with compressional and transpressional structures that marks the northern limit of the penetrative Grenville deformation (Rivers, 2008).

4.3.1 Parautochthonous Belt units

In the northwestern part of the study area (fig. 4.2), this belt is represented by the Gagnon terrane, comprising the Archean Ulamen Complex (Moukhsil et al., 2013) and the Paleoproterozoic Knob Lake Group (KLG; Rivers, 1980; Gagnon Group of Clarke 1977). The Ulamen Complex consists of late-Archean basement tonalitic gneiss (ca. 2681-2685 Ma; Jordan et al., 2006; Davis and Dion, 2012 a, b; Moukhsil et al., 2013), dioritic gneiss (ca. 2693 Ma; Jordan et al., 2006), gneissic granite and gabbro, whereas the overlying Paleoproterozoic KLG, a ca. 1900 Ma continental margin sequence consists of metapelite, quartzite, marble, and iron formations that are continuous into the New Quebec Orogen to the northeast (Rivers, 1983a).

Both the Archean basement and its cover sequences in the Grenville Province were intensely metamorphosed and deformed during the Rigolet orogenic phase thereby obliterating most pre-existing structures (Jannin et al., 2018a). The grade of metamorphism in the Gagnon terrane ranges from greenschist-facies near the GF to high-*P* granulite- and eclogite-facies near the Allochthon Boundary (Jordan et al., 2006; Rivers, 2008). A kyanite-bearing paragneiss in the southern part of the Gagnon Group records a clockwise hair-pin shaped P-T path with peak conditions in the range of 1250-1300 MPa and 815-830 °C (Indares et al., 2008), the deepest and hottest conditions recorded within the orogenic wedge. U-Pb zircon crystallization ages of leucosomes comprising part of the high-grade assemblage related to the peak metamorphic conditions are ca. 995-985 Ma, whereas U-Pb titanite cooling ages are ca. 961-956 Ma (Jordan et al., 2006). These age ranges are compatible with the two-stage thrusting

documented in the Gagnon terrane (Jannin et al., 2018a). Their study reported an earlier set of SSE-trending lineations related to Rigolet phase D1 that formed the inner overgrowths on zircon (in syn-D2 leucosome) dated at 1002 ± 2 Ma (ID-TIMS), and the second stage of SSW-trending lineations related to D2 that formed the outer overgrowths in zircon (in syn-D2 leucosome) dated at ca. 986 ± 4 Ma (ID-TIMS). Other ages (by LA-ICP-MS) related to D2 include an older age of 995 ± 21 Ma from the outer overgrowths in zircon (in syn-D2 leucosome) and a younger age of 961 ± 22 Ma in a late-D2 pegmatite, although these ages overlap within uncertainties.

4.3.2 Allochthonous Belt units

This Belt structurally overlies the Gagnon terrane along the AB, and mainly consists of Paleoproterozoic to Mesoproterozoic rocks that were metamorphosed during the peak Ottawan high-grade event between ca. 1080-1040 Ma (Dunning and Indares, 2010). The HP Manicouagan Imbricate Zone (MIZ) north of the study area consists of a Labradorian (~1.65 Ga) anorthosite-mangerite-charnockite-granite complex and Pinwarian (~1.45 Ga) granitoids that have yielded peak metamorphic conditions of 1700-1900 MPa and 750-920 ˚C followed by strong decompression with high pressure gradient over short temperature interval (Cox and Indares, 1999a, 1999b; Cox, 1999; Cox et al., 1998; Indares, 1997; Indares et al., 1998; Yang and Indares, 2005). The peak metamorphic conditions are of comparable intensity to, but ~50 M.y older than, those recorded in the underlying Parautochthonous Belt in the foreland (see above), which coupled with the difference in their P-T-t path suggest a different evolution pattern for the MIZ versus the underlying Gagnon terrane.

The medium-pressure (M*P*) units of the Island domain, Canyon domain, Gabriel Complex, and Banded Complex consist of the late-Paleoproterozoic to mid-

Mesoproterozoic supracrustal and plutonic rocks that were metamorphosed at 800-900 °C and 600-1100 MPa from ca. 1080-1040 Ma (Indares and Dunning, 2004; Dunning and Indares, 2010; Lasalle et al., 2014; Lasalle and Indares, 2014; Patrick and Indares, 2017), and were subsequently affected by a short period of post-Ottawan (ca. 1008-997 Ma) upper amphibolite to granulite-facies metamorphism (Maity, *in prep.*). In addition, the Hart Jaune terrane to the southeast of the MIZ consists of ca. 1.47 Ga mafic granulites (Scott and Hynes, 1994; Hynes et al., 2000) that lack the evidence for penetrative Ottawan metamorphism (Indares and Dunning 2004), and constitutes part of the Ottawan Orogenic Lid (OOL; Rivers, 2008) in the study area.

4.3.3 The Canyon domain

The Canyon domain consists of Mesoproterozoic supracrustal rocks, plutonic units, and several dyke and sill complexes that were emplaced along the Laurentian margin between ca. 1.5 -1.2 Ga in continental arc to intermittent back-arc setting (Hynes et al., 2000; Gobeil et al., 2002, 2005; Dunning and Indares, 2010; Indares and Moukhsil, 2013; Moukhsil et al., 2012, 2013; Maity and Indares, 2018). The oldest unit from the southern part of the domain is the supracrustal Plus Value Complex (PLV), a predominantly metaclastic unit inferred to have been deposited in an active margin arc to back-arc setting at ~1.5 Ga (Moukhsil et al., 2012; Lasalle et al., 2013; Augland et al., 2015), and was subsequently intruded by several plutons (orthogneisses) of felsic to intermediate composition and mafic dykes and sill between ca. 1497-1015 Ma (Gobeil et al., 2005, 2002; Moukhsil et al., 2012, 2013; Augland et al., 2015; Maity and Indares, 2018).

The Mafic to Intermediate Unit (MIU) in the central part of the domain consists of 1410 ± 16 Ma plutonic rocks that were formed in a transitional arc to a back-arc

setting (Dunning and Indares, 2010; Maity and Indares, 2018). The northern part of the Canyon domain consists of – (i) the Quartzofeldspathic Unit, a supracrustal sequence inferred to have been deposited at ~1.4 Ga (Indares and Moukhsil, 2013) and intruded by ca. 1.4 Ga mafic rocks correlative with the MIU (Valverde Cardenas et al., 2012; Maity and Indares, 2018); (ii) the 1238±13 Ma supracrustal Layered Bimodal Sequence (LBS) formed in an extensional setting (Indares and Moukhsil, 2013; Lasalle et al., 2013); and (iii) an apparently younger magmatic suite of the Vein Complex of unknown age and origin. The LBS has been intruded by MORB to OIB-type mafic sills (ca. 1008-997 Ma; Maity, *in prep.*) and the Vein Complex by arc to MORB-type mafic dykes and sills (ca. 1008 Ma; *op. cit.*) during the post-Ottawan (ca. 1020-1005 Ma) lithospheric extension and orogenic collapse in the study area (*op. cit.*).

Finally, the Canyon domain has been intruded by several ca. 1005-995 Ma granitic pegmatite dykes (Dunning and Indares, 2010; Turlin et al., 2017) and the 980 ± 3.5 Ma potassic to ultrapotassic dykes (Dunning and Indares, 2010; Valverde Cardenas et al., 2012) during the younger Rigolet orogenic phase. They are the focus of this study.

4.3.4 The potassic to ultrapotassic dykes (PUD)

The field relations and petrography of the PUD in the Canyon domain have been described in detail previously (Valverde Cardenas, 2009; Valverde Cardenas et al., 2012), and only brief descriptions are given here. The dykes intrude the structures and compositional layering of their gneissic hosts at high angles. Based on their degree of deformation, the dykes in the PUD suite are subdivided into – a) foliated, and b) mildly foliated to non-foliated groups. The foliated dykes are ~10-20 cm wide and are commonly associated with a rim of felsic pegmatite. They contain large clinopyroxene

megacrysts or aggregates and occasional K-feldspar megacrysts with quartz inclusions, and the foliations in the matrix are defined by the preferred orientation of biotite along with plagioclase ± K-feldspar ± quartz ± hornblende. Feldspar is commonly sericitized, and clinopyroxene is generally corroded by hornblende. The mildly foliated to non-foliated dykes are mainly composed of biotite + K-feldspar + quartz ± amphibole defining a porphyritic texture, contain only minor to trace plagioclase, and lack pyroxene, except the massive textured sample 408 that contains both orthopyroxene and clinopyroxene. All the dykes are rich in biotite and apatite. Accessory phases include allanite, monazite, zircon, titanite, rutile, Fe-Ti oxides, and calcite.

4.4 Analytical Methods

Selected samples were crushed and powdered using standard clean laboratory protocols at Memorial University of Newfoundland (MUN). Whole-rock major and trace element concentrations were measured at the Activation Laboratories (Actlabs) Ltd. in Ontario, Canada. Their standard analytical protocols are available from Actlabs website (www.actlabs.com) and are briefly described in appendix A. For radiogenic tracer isotopes, Sr followed by Sm and Nd were separated from whole-rock powders following an in-house protocol at MUN, and isotope compositions were measures by Finnigan Mat 262 mass spectrometer in static and dynamic modes. Pb was separated from whole-rock powders and isotope compositions were measured in Finnigan Mat 262 mass spectrometer in static mode at MUN. Whole-rock oxygen isotope measurements were conducted using a dual-inlet, triple-collecting Thermo Scientific Delta Plus XL IRMS at the Western University, Ontario, Canada. All the isotope analytical procedures, uncertainties, precision and accuracy of data are reported in appendix A.

4.5 Results

4.5.1 Whole-rock major and trace elements

The whole-rock major and trace elements and Sr-Nd-Pb-O isotope ratios are presented in table 4.1. Based on major elements, the PUD samples are divided into PUD1 group, which includes all strongly foliated and one massive sample (408), and PUD2 group, which includes massive to mildly foliated samples (PUD1a and PUD1b subdivisions are based on Pb isotopes, see below). The PUD1 has a lower range in SiO_2, K_2O, P_2O_5, and Mg# and a higher range in Al_2O_3, Fe_2O_3, MnO, CaO, and Na_2O compared to the PUD2 group. In the total alkalis vs. silica diagram (fig. 4.3a), the PUD1 samples range from basalt to basaltic andesite and trachy-andesite, whereas PUD2 samples range from basaltic trachy-andesite to trachyte. In the K_2O vs. Na_2O diagram (fig. 4.3b), the three samples from PUD1 with highest Na_2O fall in the non-potassic to potassic or shoshonitic fields, whereas the remaining PUD1 samples, and all PUD2 samples, fall in the ultrapotassic field. In K_2O vs. SiO_2 diagram (not shown) all samples plot in the shoshonitic field except one (11-416) that plots in the high-K calc-alkaline field. According to the classification of Foley et al. (1987), the seven samples from the PUD with $K_2O/Na_2O > 2$ and MgO and $K_2O > 3$ wt% are ultrapotassic, and in the discrimination diagrams for ultrapotassic rocks they plot between the fields for Group I (lamproitic) and Group III (orogenic, lamprophyric) (fig. 4.3c, d).

Differences between the two groups of PUD also exist for other trace elements, e.g., the PUD1 samples are higher than PUD2 in Sc (14-22 vs. 4-11 ppm) and V (121-193 vs. 34-65 ppm), and lower in Rb (65-216 vs. 193-263 ppm), Sr (936-4301vs. 2701-6521 ppm), Th (2.1-6.1 vs. 10.8-16.2 ppm), and U (0.8-3.4 vs. 2.5-5.2 ppm) (table 4.1).

The PUD2 samples exhibit higher Ni (82-139 ppm) and Cr (151-270 ppm), whereas in PUD1 these elements are highly variable, with sample 398A (high MgO) exhibiting the highest values (230 and 638 ppm, respectively) compared to the remaining samples, which exhibit the lowest ranges (below detection limit to 102 ppm and 145 ppm, respectively). The two groups exhibit very high and overlapping concentrations in Ba (2098-7621 ppm) and Zr (191-911 ppm).

All the PUD samples are strongly enriched in LREE (La 200-1100 times chondrite) with no significant Eu anomalies and are relatively depleted in HREE (8-25 times chondrite) (fig. 4.4a-c). Sample 403 in PUD2 exhibit a distinct concave upward HREE pattern (fig. 4.4c). In the primitive mantle-normalized multi-element diagram (fig. 4.4e-g), PUD samples show strong negative anomalies in Nb and Ta, and variable anomalies in Ti and P. PUD1 samples also exhibit distinct patterns between its subgroups PUD1a and PUD1b. For example, Zr and Hf are less depleted in PUD1a compared to PUD1b and are variably depleted in PUD2. Ti and P are less depleted in PUD1a compared to PUD1b, whereas Ti is strongly depleted in PUD2 without depletion in P. Rb is depleted relative to Ba in all samples, and K is variable compared to La. PUD2 exhibits highest abundances in Rb and Sr whereas PUD1b has the highest Ba abundance. Th exhibits a negative anomaly compared to adjacent Ba and U in PUD1a, whereas it is variable relative to Ba and U in the two other groups with PUD2 having the highest Th and U abundances. Only two samples in PUD1a, for which Pb concentrations were measured, exhibit a positive Pb anomaly. The overall incompatible element abundances increase from PUD1a to PUD2.

4.5.2 Sr-Nd isotopes

The Sr-Nd isotope data are reported in table 4.1 and plotted in fig. 4.5a-c. The PUD1a samples exhibit relatively less unradiogenic Nd isotopic signatures and younger depleted mantle model ages (εNd = -2.8 to -5.1) compared to PUD1b (εNd = -4.5 to -7.1) and the strongly unradiogenic PUD2 samples (εNd = -12.1 to -14.4). The samples from the PUD1 exhibit Paleoproterozoic to Mesoproterozoic Nd model ages (T_{DM} 1.55-1.78 Ga, DePaolo, 1981; T_{CR} 1.70-1.97 Ga, Goldstein et al., 1984), and they plot slightly above, but parallel to, the regression lines for the other Proterozoic crust groupings in the study area (e.g., parallel to the MIZ, Island and Canyon domains, Banded complex, and below the Quebecia crust; Thompson et al., 2011; fig. 5a-b). The PUD1 yields intial εNd values older than the ca. 1.7-1.9 Ga K-rich suites from the western Grenville Province (e.g., the Kensington-Scoottamatta and the Rivard minette dykes; Corriveau and Amelin, 1994; Amelin et al., 1994; Corriveau et al., 1996), although they overlap with the calculated intial εNd values of the post-Ottawan K-rich suites (e.g., the ca. 1014-1009 Ma Core and Bouvreuil syenite plutons, the ca. 1000 Ma Labrieville lamprophyre dykes; Owens and Tomascak, 2002; Augland et al., 2017; fig. 5b). The PUD2 samples exhibit early Paleoproterozoic Nd model ages (T_{DM} 2.2-2.3 Ga, DePaolo, 1981; T_{CR} 2.35-2.47 Ga, Goldstein et al., 1984), and plot within the field for the early Paleoproterozoic to Archean crust from the study area (Thompson et al., 2011; fig. 5a-b).

All the PUD samples have low radiogenic initial $^{87}Sr/^{86}Sr$ ratios, with those from PUD1a (0.70393-0.70505) exhibiting slightly more radiogenic values compared to those in PUD1b (0.70384-0.70411) and PUD2 (0.70393-0.70428); all these values are slightly higher than the Bulk Silicate Earth (BSE) value at 1 Ga (0.703255;

Workman and Hart, 2005). All the PUD samples exhibit higher initial Sr-isotope ratios compared to the Labrieville dykes and anorthosite massif (table 4.1). The Sr-Nd isotopic signatures in PUD1 and PUD2 are indicative of enriched EM I-type mantle source (fig. 4.5a-b), and comparable to those of the anorogenic lamproites from the Leucite Hills (Mirnejad and Bell, 2006) and Sisimiut (Nelson, 1989), and minettes from the Elkhead Mountains (Thompson et al., 1990). The Sr errorchron age of 996 ± 180 Ma (Valverde Cardenas et al., 2012) is close to the U-Pb zircon crystallization age of 980 ± 3 Ma (Dunning and Indares, 2010), determined from an undeformed PUD2 dyke from the southern part of the domain. However, the scatter of data points in the isochron plot of measured $^{87}Sr/^{86}Sr$ ratios indicates that either the samples were not of the same age, or they were derived from heterogeneous sources, or both (Valverde Cardenas et al., 2012).

The Sr-Nd isotopic signatures in PUD1 and PUD2 (fig. 5c) are comparable to those of the Mesoproterozoic anorogenic lamproites Aillik Bay in eastern Labrador (Tappe et al., 2007) and Sisimiut in west Greenland (Nelson, 1989), and the younger lamproites from the Leucite Hills (Mirnejad and Bell, 2006), Smokey Butte, Prairie Creek (Fraser et al., 1985; Fraser, 1987), and minettes from the Elkhead Mountains (Thompson et al., 1990). The unradiogenic Sr-Nd isotopic signatures of these suites represent the ancient Laurentian SCLM of Tappe et al. (2007) and indicate an enriched EM I-type mantle source.

4.5.3 Pb isotopes

The PUD samples exhibit a wide range of Pb isotopic ratios that are distinct for the PUD1 and PUD2 groups, and are shown on fig. 4.6. The Pb data also permit subdivision of the PUD1 group into subgroups PUD1a and b. For the PUD1 group, five

samples in PUD1a subgroup exhibit significantly higher isotopic ratios ($^{206}Pb/^{204}Pb$: 16.87 to 18.07, $^{207}Pb/^{204}Pb$: 15.37-15.43, $^{208}Pb/^{204}Pb$: 36.12-36.50) than the remaining three samples in PUD1b ($^{206}Pb/^{204}Pb$: 16.25 to 16.53, $^{207}Pb/^{204}Pb$: 15.29-15.33, $^{208}Pb/^{204}Pb$: 36.15-36.77). The PUD1a samples are the most radiogenic and plot farther to the right side of 4.57-0.98 Ga geochron. Four samples from this subgroup yield Stacey and Kramers (1975) model ages between 0.57-0.92 Ga, whereas the sample 11-416 exhibits significantly more radiogenic lead and plots to the right side of the Geochron (fig. 4.6a). This is consistent with this sample being strongly foliated, with the highest Sr isotope ratio. Two unaltered samples with mild or no foliation (RS351 and 408) give model ages (0.91-0.92 Ga) closest to the zircon U-Pb crystallization age of ca. 980 Ma for the PUD interpreted from Dunning and Indares (2010). In the $^{208}Pb/^{204}Pb$ vs. $^{206}Pb/^{204}Pb$ space (fig. 4.6b), the PUD1a samples exhibit a negative trend from the mantle towards lower crustal evolution line of Zartman and Doe (1981), and exhibit the highest thorogenic and uranogenic lead.

The PUD1b samples plot below the average crust evolution curve of Stacey and Kramers (1975), close to the 0.98 Ga geochron (fig. 4.6a), and yield Stacey and Kramers (1975) model ages of 1.06-1.23 Ga (table 4.1). In the $^{208}Pb/^{204}Pb$ vs. $^{206}Pb/^{204}Pb$ space (fig. 4.6b), the PUD1b samples plot above the average crust curve and exhibit a positive trend towards lower crustal evolution line of Zartman and Doe (1981). Overall, the samples in PUD1 are variably deformed, foliated, and show evidence of late-stage alteration in feldspar, features that indicate excess radiogenic Pb could have been acquired by contamination. Alternatively, this could be a consequence of a multi-stage history for Pb in these rocks (e.g., Ayer and Dostal, 2000).

In fig. 4.6a-b, the PUD1 samples overlap with a range of whole-rock and feldspar data from the Grenville anorthosites (Emslie and Hegner, 1993; Owens et al., 1994), Proterozoic orthogneisses from the Grenville Province and eastern Labrador (Ashwal et al., 1986; Schärer, 1991; DeWolf and Mezger, 1994; Loewy et al., 2003; Arcuri and Dickin, 2018; Mumblow et al., 2018), clinopyroxene and paragonite in the Rivard dykes (Corriveau et al., 1996), and with clinopyroxene in xenoliths recovered from the dykes (Corriveau et al., 1996; Amelin et al., 1994). These Mesoproterozoic rocks from the Grenvillian hinterland were derived mainly from Mesoproterozoic mantle sources and involved reworked Proterozoic crust having short crustal residence time (Ashwal et al., 1986; Schärer, 1991; Emslie and Hegner, 1993; Owens et al., 1994). The K-rich plutonic suites from the Central Metasedimentary Belt ("K-S suite" in fig. 4.6) exhibit initial Pb isotope compositions intermediate between the two subgroups of PUD1 (Corriveau and Amelin, 1994). In fig. 4.6c-d, PUD1 samples plot within the field for ancient Laurentian lamproites (Fraser et al., 1985; Thompson et al., 1990; Peterson et al., 1994; Tappe et al., 2007).

The samples in PUD2 yield the most unradiogenic Pb isotopic compositions, exhibiting high $^{206}Pb/^{204}Pb$ at distinctly lower $^{207}Pb/^{204}Pb$ ratios compared to the PUD1 group, and plot to the right side of 0.98 Ga isochron (fig. 4.6a). All the three samples yield two-stage Stacey and Kramers (1975) model ages (0.45-0.84 Ga) significantly younger than their emplacement age. Two of these samples (403 and 462z) are massive and not foliated, whereas sample 338z is weakly foliated, and exhibits no visible sign of late-stage hydrothermal alteration. Several studies on Archean komatiites and sulphides have revealed that although hydrothermal alteration can increase U/Pb ratios, their Th/U and Sm/Nd systematics remain largely unaffected (e.g., Dupré et al., 1984;

Brévart et al., 1986; Dupré and Arndt, 1990). In $^{208}Pb/^{204}Pb$ vs. $^{206}Pb/^{204}Pb$ space (fig. 4.6b), samples 338z and 462z plot above the average crust curve, whereas sample 403 deviates slightly towards higher $^{206}Pb/^{204}Pb$.

In fig. 4.6a-b, the PUD2 samples are compared with the rocks from the Superior and Grenville Province with a known Archean source for Pb. The high $^{206}Pb/^{204}Pb$ may have caused the PUD2 samples to deviate from the fields for the late-Archean to Proterozoic gneisses (Gariépy and Allègre, 1985; Gariépy et al., 1990; Schärer, 1991; DeWolf and Mezger, 1994; Dickin, 1998a) and Aillik Bay galena deposits form the Central Mineral Belt in eastern Labrador (Wilton, 1991). Instead, they plot within the field defined by a range of komatiite, basalt, and magmatic and exhalative sulphide samples from the Abitibi Greenstone Belt in Ontario (Tilton, 1983; Dupré et al., 1984; Brévart et al., 1986; Carignan et al., 1995; Dupré and Arndt, 1990). In fig. 4.6 c-d, PUD2 samples plot below the field for ancient Laurentian lampriotes (Freaser et al., 1985; Peterson et al., 1994; Tappe et al., 2007), and broadly overlap with the Aillik Bay lamproites (Tappe et al., 2007) and the clinopyroxene Pb data (protolith model age of ~2.7 Ga) from the ca. 632 Ma Renard kimberlite in the southeastern Superior Province (Hunt et al., 2012). Whereas large variations in $^{206}Pb/^{204}Pb$ ratios in many of the Abitibi volcanics were attributed to Pb gain due to hydrothermal alteration shortly after their emplacement (mainly samples from thin komatiite layers), or due to later metamorphism (samples from thick basalt layers) (Dupré and Arndt, 1990), others have contested this idea based on the collinearity of the mafic-ultramafic samples with primary magmatic Pb in sulphides and argued for a heterogeneous late-Archean mantle beneath the Superior Province (Carignan et al., 1995). In the present study, the distinct Pb isotopes in PUD2 samples suggest hydrothermal alteration immediately before final

magma crystallization in the late-Rigolet orogenic setting, or they may indicate derivation from a mantle source that has been modified by hydrothermally altered sediments or crust (our preferred interpretation).

4.5.4 O isotopes

Whole-rock oxygen isotopes ($\delta^{18}O_{VSMOW}$) exhibit a wide range of values for the three groups. Samples from PUD1a yield values from 6.2-9.2‰ whereas those from PUD1b exhibit values from 7.7-9.3‰. The samples in PUD2 yield values that range from 3.8‰ to 8.2‰. The range of values in PUD samples exceeds the range for typical mantle-derived mafic rocks ($\delta^{18}O_{WR}$ = 5.5-7.4‰; Taylor, 1968), MORB (5.6-6.0‰; Eiler, 2001), and lower crust (6-7‰; *op. cit.*).

There are no previously published O-isotope data on ultrapotassic rocks from the Grenville Province, but a large number of datasets exist on the Proterozoic AMCG rocks, which have yielded $\delta^{18}O_{WR}$ values of 7-11‰ (Peck and Valley, 2000; Peck et al., 2010). The young (~1 M.y) ultrapotassic rocks from the Roman province in Italy exhibit $\delta^{18}O_{WR}$ values of 5.6-10‰ (Taylor et al., 1979). Primitive basalts with high Mg# were reported from diverse tectonic settings to have $\delta^{18}O_{WR}$ values of 3.6 to 8.7‰ (Harmon and Hoefs, 1995). Archean lamprophyres from the Superior Province yielded high $\delta^{18}O_{WR}$ values of 6.7-11.1‰, and $\delta^{18}O_{clinopyroxene}$ values of 6.1-6.3‰ (Kyser, 1990; Wyman and Kerrich, 1993). Five samples of the Leucite Hills lamproites exhibit whole-rock values of 8.8-12‰ and a phlogopite phenocryst value of 8.8‰ (Kuehner, 1980), which are comparable to the $\delta^{18}O_{WR}$ values of 8.21-8.90‰ reported by Mirnejad and Bell (2006) for these same rocks. In all these examples, higher than mantle values were interpreted to indicate crustal addition either at source and/or during magma ascent through crust (e.g., Eiler, 2001).

4.6 Discussion

4.6.1 Fractional crystallization and crustal contamination

The negative correlation of Rb/Sr vs. Sr (fig. 4.7a) suggests biotite (phlogopite) and amphibole (K-richterite) fractionation, whereas the lack of distinct anomalies in Eu, Sr, and Ba (fig. 4.4) indicate that plagioclase was not a major fractionating phase. The positive covariations between Mg# (MgO) and Cr (fig. 4.7b) and Ni (fig. 4.7c) in our dataset suggest strong effects of fractional crystallization of clinopyroxene and olivine, respectively. It is evident in fig. 4.7b-c that the samples in PUD2 have a different evolutionary path and they also exhibit lower Al, Fe, and Sc and V compared to those in PUD1 (fig. 4.7d-e; table 4.1). Their low Fe and V suggest the role of amphibole or Fe-Ti oxide as also indicated in the Ni vs. V diagram (fig. 4.7e). The high Mg# of the PUD2 samples imply that such fractionation must have occurred at source. PUD1 samples have low Ti/V values (74 - 119) that exhibit a slight decrease with differentiation, whereas PUD2 samples have much higher Ti/V values (198 - 264) that exhibit no correlation with Mg#. P_2O_5 is the highest in PUD2, and exhibits an overall decrease in both groups with decreasing Mg#, suggesting the role of apatite. Their HFSE, REE, Ba, and Sr contents are high and variable but exhibit no particular correlation with Mg#, although Th and U decrease with differentiation.

The overall high abundances in incompatible elements of the PUD samples cannot be produced by fractionation of apatite, Fe-Ti oxides, or amphibole, suggesting they are not related to mineral fractionation. The positive correlation between La and La/Yb indicate that their REE compositions are mainly related by partial melting of an LREE-enriched source (fig. 4.7f). However, the PUD samples form three different

groups, exhibiting distinct radiogenic isotopic compositions that cannot be related to simple fractional crystallization or partial melting, and therefore, require alternative processes such as crustal contamination and/or source heterogeneity.

In general, crustal contamination in potassic and ultrapotassic rocks is difficult to assess due to their extreme enrichment in incompatible LILE and LREE, which can only be diluted by less enriched crust (Conticelli, 1998). Nonetheless, simple mass balance (Conticelli, 1998) and mixing calculations (Mirnejad and Bell, 2006) show that extensive upper crustal contamination can increase SiO_2, Al_2O_3, MnO and Na_2O contents and decrease TiO_2, MgO, K_2O, and P_2O_5 contents in contaminated ultrapotassic to lamproitic magmas. With respect to the high enrichments in incompatible major and trace elements (e.g., K_2O, LREE, Rb, Ba, Sr) and Sr-Nd isotopic values in the late-Grenvillian ultrapotassic and lamprophyric rocks in general (figs. 4.3-4.5), it has been proposed that their parental magmas were derived by partial melting of enriched SCLM, possibly mixed with small volume asthenospheric melts, without significant contribution from continental crust (Owens and Tomascak, 2002; Valverde Cardenas et al., 2012). The PUD samples exhibit extremely coherent trace element patterns in the primitive mantle normalized diagrams (fig. 4.4), which coupled with their overall high concentrations of incompatible elements argue against shallow-level contamination by heterogeneous crust. Therefore, the major and trace elements and isotopic variations of the PUD samples are interpreted to indicate their source heterogeneity, and that crustal contamination in their petrogenesis would have been of secondary importance except only in the most evolved samples with the lowest MgO, Mg#, Ni, and Cr contents.

4.6.2 Source composition and mineralogy

Major elements can provide important clues about primary processes reflecting the composition of mantle sources, whereas incompatible trace element abundances, ratios, and patterns provide information about the nature of metasomatic enrichments or depletions that took place after separation from mantle sources, irrespective of the relative timing of such enrichment or depletion events. The various radiogenic isotope tracers can further provide constraints on the timing of such specific events, which in combination with their major and trace elements can be used to decipher a more complete picture of complex evolutionary history in the ultrapotassic rocks.

Although magmatic differentiation has taken place during petrogenesis of the PUD suite, many of the samples still retain high MgO, Mg#, and relatively high Ni and Cr values, suggesting they represent compositions close to their parental melts. The two groups in PUD exhibit characteristic major and trace element compositions that indicate distinct sources were involved in their respective petrogenesis. Recalculating their major element oxides to a standard MgO value of 6 wt% (following Turner and Hawkesworth, 1995; Williams et al., 2004) still exhibits the compositional differences that we believe to be related to their source characteristics. The PUD1 samples exhibit a wide range in SiO_2 (47 - 57 wt%) and Mg# < 44 - 65 with variable Ni and Cr, high Al_2O_3, TiO_2, Fe_2O_3, Sc and V, and their major element oxide compositions are similar to the experimental melts derived from fertile peridotites (Falloon et al., 1988; Falloon and Green, 1988; Hirose and Kushiro, 1993), suggesting their derivation from such a fertile source. In contrast, the PUD2 samples exhibit higher SiO_2 (53-59 wt%) and Mg# > 69 - 75 with higher Ni and Cr, and lower Al_2O_3, Fe_2O_3, Sc and V indicating their derivation from a relatively depleted source, which coupled with the absence of

clinopyroxene in these samples supports clinopyroxene-poor depleted peridotite source. Depleted peridotite has been suggested as the source for many ultrapotassic rocks on the basis of phase equilibria studies on lamproites and experimental studies at high-pressures on synthetic systems (Edgar and Mitchell, 1997; Foley et al., 1986). It is noteworthy that many group-I and II lamproitic and ultrapotassic rocks exhibit high TiO_2 and low Fe_2O_3 (e.g., Foley et al., 1986; Wyman and Kerrich, 1993; Mirnejad and Bell, 2006) suggesting such features could be inherently related to their source composition.

The REEs can offer significant insights into the source mineralogy and depth of melting, since garnet and spinel have different preferences for HREE versus MREE and LREE. Partial melting in either the spinel or garnet peridotite fields can enrich melt in LREE, but residual garnet can additionally retain HREE and Y, thereby producing strongly fractionated LREE/HREE and MREE/HREE ratios. The PUD1a samples have a broader range of Dy/Yb (1.71 - 3.39), indicating both garnet and spinel in their source regions, and thereby implicating garnet- and spinel-lherzolite mantle sources. In contrast, PUD1b samples exhibit high Dy/Yb (2.90 - 3.44) that suggest their parental melts were in equilibrium with residual garnet, implying a garnet-lherzolite source. For PUD2, the variable Dy/Yb (2.32 - 4.15), coupled with a concave upward HREE pattern in sample #403, indicate both residual garnet and amphibole, implying a depleted amphibole-garnet peridotite (harzburgite or depleted lherzolite) source. However, they also exhibit high K/Yb (5,800-33,000), K_2O and K_2O/Na_2O that are too high to be derived from four-phase mantle peridotite (Foley, 1992; Sun and McDonough, 1989), and suggest the presence of K-bearing phases, e.g., phlogopite or amphibole, most likely located in mica-clinopyroxenitic vein assemblages in the source region (Foley,

1992; Foley et al., 1999). Based on trace element modeling, Duggen et al. (2005) showed that vein assemblages alone with variable proportions of garnet and apatite (0-10%) can produce very high K/Yb (>100,000), but always at low Dy/Yb ratios (< 2.5), whereas dilution of vein melt by garnet-peridotite melt in a vein plus peridotite wall-rock melting model (Foley, 1992; Foley et al., 1999) can produce relatively low K/Yb (~5000-60,000) at high Dy/Yb (2.8-3.8), as observed in the Spanish lamproites. The PUD samples exhibit a range of K/Yb (PUD1a: 6300-19800; PUD1b: 5,800-28,000; PUD2: 14,400-33,000) and Dy/Yb ratios suggesting that a vein plus peridotite wall-rock model (instead of vein assemblage only) would be most applicable for the late-Grenvillian PUD rocks.

Experiments on the high-pressure stability of pargasite and K-richterite suggest that under fluorine-rich conditions these phases (and phlogopite and apatite) can be stable as refractory vein assemblages coexisting with lherzolite (for pargasite) and harzburgite (for K-richterite) over much greater *P-T* ranges (~50 kb, 1300 ºC) than their hydroxy-counterparts (Foley, 1991, 1992). Upon reaching the peridotite solidus, these vein assemblages can melt to impart strong influence on the REE and incompatible element budgets on primitive ultrapotassic melts. Although whole-rock F contents are not available, mineral chemical data for the PUDs (Valverde Cardenas, 2009) exhibit high F contents in apatite (1.54-6.46 wt%), biotite (0.58-3.67 wt%), and amphibole (0.23-3.16 wt%), with the highest F contents in minerals present in PUD2 samples. Experimental studies have shown that high F content under high H_2O/CO_2 conditions in mantle produce silica-rich ultrapotassic melts (Foley et al., 1986).

In comparison to K, Rb has a lower partition coefficient for amphibole (K-richterite) than for fluid ($^{amph\text{-}fluid}K_{D(Rb\text{-}K)}$ = 0.08; Melzer et al., 1998), so amphibole

formed from metasomatic fluids or melts will be Rb-poor and K-rich. On the other hand, Rb prefers to partition into phlogopite rather than coexisting fluid ($^{phl\text{-}fluid}K_{D(Rb\text{-}K)}$ = 1.28; Melzer et al., 1998). Moreover, Ba is highly compatible in phlogopite but moderately compatible in amphibole (Adam et al., 1993; LaTourrette et al., 1995). Consequently, partial melting of a metasomatized lithospheric mantle source in equilibrium with amphibole will produce melts with low Rb/Sr (<0.1), high Ba/Rb (>20) and high K/Rb. In contrast, those in equilibrium with phlogopite have higher Rb/Sr (> 0.1), and lower Ba/Rb (< 20) and K/Rb (Furman and Graham, 1999; Melzer et al., 1998). In the Ba/Rb vs. Rb/Sr diagram (fig. 4.8a), the PUD1a samples exhibit high Rb/Sr, which decreases with increasing Ba/Rb, suggesting a competing role of phlogopite and amphibole in their source regions. The PUD1b samples, on the other hand, show high Ba/Rb at low Rb/Sr (< 0.10), suggesting a predominance of amphibole over phlogopite in their source regions. The PUD2 samples exhibit highest Rb and very high Ba and Sr at low Rb/Sr and Ba/Rb, indicating phlogopite melting at source, possibly in combination with K-richterite. The K/Rb (194-390) ratios in PUDs are low and somewhat overlap between the PUD groups, although they exhibit a negative correlation with Rb/Sr (fig. 4.8b) suggesting phlogopite and amphibole control on both Ba and K (Melzer et al., 1998; Melzer and Wunder, 2001).

The lack of a correlation between TiO_2 and SiO_2, coupled with the negative anomalies in Nb, Ta, and Ti in the primitive mantle-normalized multi-element diagrams, is consistent with the presence of a Ti-bearing mineral phase such as rutile, phlogopite, and amphibole in the source region (Foley and Wheller, 1990; Foley et al., 1999). Accessory phases such as apatite and monazite can exert a strong control on the REE, P, Sr, and Th contents of ultrapotassic melts during mantle melting. Such phases,

if present in trace amounts in the mantle, can change the fluid/rock partitioning behavior of the system, especially with respect to REEs (Rudnick et al., 1993). However, their high LREE, Ti, P, and Sr contents imply that the PUD samples were derived from a mantle source where these elements were incompatible during melting. This is supported by the experiment on Ti solubility that indicates that Ti-rich accessory phases are not residual in mafic melt system (Ryerson and Watson, 1987). Apatite has also been shown to be soluble in mafic alkalic liquids at high pressure mantle conditions (Watson, 1980; Baker and Wyllie, 1992), suggesting such accessory phases most probably melted completely in the source regions of PUD.

In summary, their major and trace element signatures suggest that the two groups of PUD were derived from partial melting of sources that were distinct in terms of their composition and mineralogy. Among the first group of PUD1, the PUD1a samples were derived from fertile garnet- and spinel-peridotite, whereas those in PUD1b were derived from a fertile garnet-peridotite source. The PUD2 samples were derived from a relatively depleted garnet-peridotite source. The peridotite sources for both the PUD1 and PUD2 groups were variably metasomatized at source by melts and fluids derived from vein assemblages containing amphibole, phlogopite, Fe-Ti accessory phases such as rutile and ilmenite, and phosphates such as apatite and monazite. The stability of amphibole at a depth coexisting with garnet peridotite may also suggest F-rich conditions at source. The presence of such minor and accessory phases in EM-I type SCLM source indicate MARID-type metasomatism that has also been suggested for other lamproitic and ultrapotassic rocks derived from the ancient Laurentian SCLM (Tappe et al., 2008). The high solubility of accessory phases during parental ultrapotassic melt genesis indicates that such phases would melt completely

without any significant residue left in the source region, producing the incompatible element depletions and enrichments observed in the PUD samples. Thus, the trace element patterns for the PUD appear to be directly inherited from their source regions.

4.6.3 Orogenic vs. anorogenic characters

It has been shown that potassic and ultrapotassic rocks occur both in orogenic and anorogenic environments, which are related to active subduction zones and stable continental intraplate settings, respectively (Nelson, 1992), although subduction-related processes play an important role in the petrogenesis of such rocks emplaced in both environments (Vollmer, 1989; Lustrino et al., 2016). Based on major elements Al_2O_3 and TiO_2 (fig. 4.9a, b), the PUDs plot in the orogenic field with $Al_2O_3/TiO_2 \geq 4$ (Lustrino et al., 2016), although they exhibit a trend towards anorogenic field. However, in Th/Zr vs. Nb/Zr (fig. 4.9c; Wilson and Bianchini, 1999) and Th-Hf-Nb/2 diagrams (fig. 4.9d; Krmíček et al., 2011), the PUDs straddle between the orogenic and anorogenic fields, with PUD1 samples showing a strong anorogenic signature compared to PUD2 with a strong orogenic signature. The mixed orogenic-anorogenic character in PUDs suggest subduction-metasomatized SCLM sources modified by asthenospheric melts or fluids.

4.6.4 Mantle source metasomatism: trace element constraints

In order to produce primitive potassic to ultrapotassic magmas extremely enriched in incompatible elements (e.g., LREE and LILE), the mantle source must be fertilized by metasomatic fluids or melts of hydrous, alkalic silicate, or carbonatitic composition (Laflèche et al., 1998). Such fluids or melts may be derived from deep

asthenosphere (e.g., Rudnick et al., 1993), or from subduction zones (e.g., Menzies and Hawkesworth, 1987; Hawkesworth et al., 1990), or a combination of both.

4.6.4.1 Subduction–related metasomatism

The role of subduction in the source of the PUD can be readily assessed with reference to their strong depletions in HFSE (e.g., Nb, Ta, P, Ti, Zr, and Hf) relative to enrichments in LREE and LILE (fig. 4.4; Thirlwall et al., 1994), and their low Ti/Zr ratios. The trace element contribution from subduction zones can take place through fluids or melts derived from subducted sediments. Any input from subducted sediment-derived fluids increases Ba/La relative to Th/Yb ratio in the mantle wedge because of the higher solubility of the LILE than the HFSE and REE in fluids compared to melts (Woodhead et al., 2001). In the Th/Yb vs. Ba/La diagram (fig. 4.10a), samples from PUD1 exhibit high Ba/La indicative of metasomatic enrichment from slab-derived fluids, whereas high Th/Yb in those from PUD2 suggests the enrichment was from slab-derived melts.

Partial melting and mantle enrichment processes by hydrous fluids or silicate melts in subduction zones do not significantly deplete HFSE compared to REE (i.e., yielding sub-chondritic Hf/Sm), nor do they result in super-chondritic Nb/Ta ratios as these elements have similar geochemical behavior (McDonough, 1990). Carbonatitic fluids and melts, on the other hand, can deplete HFSE (e.g., Zr, Hf, Nb, Ta, Ti) compared to REE, and can also effectively fractionate HFSE ratios (e.g., Zr/Hf) from chondritic or primitive mantle values due to their higher preference for HFSE over REE, and for Zr over Hf (Laflèche et al., 1992; Rudnick et al., 1993; Ionov et al., 1993). The variable Zr/Sm (4.0-29.1), Zr/Hf (30.8-47.2), and Hf/Sm (0.13-0.70), and low Ti/Eu (769-3930) ratios in PUD samples are variably fractionated from chondritic

values (25.3, 36.3, 0.70, and 7672, respectively; Sun and McDonough, 1989) (fig. 4.10b-d). Moreover, carbonatitic fluids/melts can fractionate Nb from Ta, resulting in super-chondritic Nb/Ta ratios in some of the PUD samples (Ionov et al., 1993; Rudnick et al., 1993; Aulbach et al., 2008; Pfänder et al., 2012). In contrast to Nb enrichment, typical of asthenosphere-derived carbonatite melts or fluids, sub-chondritic Nb/La at variable Zr/Hf and low Hf/Sm ratios (fig. 4.10c and e) in the PUD1b and PUD2 are consistent with subduction-related pelagic and carbonate sediment metasomatism in their mantle source(s) (e.g. Hoernle et al., 2002), rather than terrigenous sediments (terrigenous sources are rich in zircon, yielding high Hf/Sm ratios; Prelević et al., 2012). In contrast, the samples in PUD1a exhibit HF/Sm and Zr/Hf compositions close to chondritic or primitive mantle values at low Nb/La following subduction-related hydrous metasomatism. It is noteworthy that low Hf/Sm ratios are common to many Archean as well as Phanerozoic orogenic alkaline and lamprophyric rocks (e.g., Laflèche et al., 1991; Wyman and Kerrich, 1993). Moreover, the distinct difference in Zr/Hf ratios between the early Ottawan Kensington-Skootamatta suite from the western Grenville Province and the Rigolet PUD suite in the study area is indicative of heterogeneity of their sources, or of different styles of carbonatitic metasomatism. It is noteworthy that a wide range of Zr/Hf ratios were reported from carbonatite metasomatized mantle peridotite from Western Australia (Zr/Hf = 35-102; Yaxley et al., 1991) and Tanzania (25-104; Rudnick et al., 1993).

In summary, the samples from the PUD1a exhibit evidence for hydrous fluid metasomatism, most probably derived from subducted upper crust or terrigenous sediment. In comparison, the source regions for PUD1b and PUD2 were metasomatized by pelagic and carbonatitic fluids and melts, respectively, in subduction-related

environments. Carbonatitic metasomatism is considered to be an essential contributor to the refertilization of lithospheric mantle with LREE and other mobile incompatible elements (Rudnick et al., 1993; Hoernle et al., 2002; and references therein). The source(s) for such complex metasomatism could have been pelagic or chemical marine sediments (such as carbonate and phosphate) that were probably introduced into the lithospheric mantle wedge during long-lived subduction-related processes, as has also been inferred for the lithospheric mantle beneath the northern Tibetan plateau (e.g., Sun et al., 2014). However, the relative timing of metasomatism in the mantle source regions remains unresolved and are addressed through isotopic constraints as discussed below.

4.6.4.2 Asthenosphere-related metasomatism

Evidence for metasomatism by asthenospheric fluids or melts is not directly recorded in the late-Grenvillian PUD rocks. However, two recently investigated ca. 1008-997 Ma suites of mafic tholeiitic rocks from the study area were interpreted to have been derived from asthenospheric upwelling as a result of post-Ottawan lithospheric extension (Maity, *in prep.*). Moreover, one hornblende-lamprophyre from the suite of ca. 1000 Ma. Labrieville dykes (Owens and Tomascak, 2002) exhibit positive anomalies in Nb and Ta (fig. 4h), high Nb/La (fig. 10e), high Th/Yb, and low Zr/Nb. The hornblende-lamprophyre and all three biotite-lamprophyre samples from the Labrieville suite exhibit high Nb/U (41-69), suggesting possible contribution of asthenospheric melts, which is compatible with a post-Ottawan lithospheric extension model. Asthenospheric upwelling may have released a small volume of fluids and melts elevated in incompatible elements that could have migrated upward to metasomatize lithospheric mantle (McKenzie, 1989).

4.6.5 Mantle source metasomatism: isotopic constraints

In deciphering the nature and timing of enrichment of the source(s) of post-collisional shoshonitic volcanism on the Tibetan plateau, Turner et al. (1996) demonstrated that depleted mantle Nd and Pb model ages spanning over the Archean to Mesoproterozoic provide primary constraints on the age of the Tibetan lithospheric mantle source(s) and their multi-stage enrichment history. Similarly, based on major and trace elements and Sr-Nd-Pb-O isotopic data for the Leucite Hills lamproites, Mirnejad and Bell (2006) found evidence indicative of ancient (late-Archean) mantle depletion followed by mid-Proterozoic as well as recent metasomatism of the Wyoming Province lithospheric mantle. The enrichment in incompatible elements, depletion in Nb and Ta, and unradiogenic Nd isotopes in these lamproites were interpreted to indicate ancient subduction-related processes that metasomatized a previously depleted mantle source, and their observed low time-integrated Sr-Nd-Pb isotopic compositions to suggest fractionation of U/Pb, Sm/Nd, and Rb/Sr ratios that were attributed by the authors to high O_2 fugacity and geochemical heterogeneity of subducted sediment containing carbonate and phosphate. Carbonates have inherently high Th and Pb and low U (resulting high Th/U and low U/Pb), and phosphate-rich sediment or phosphate-bearing phases such as monazite have low Sm/Nd and high Th/U (Ben Othman et al., 1989; Plank and Langmuir, 1998; Murphy et al., 2002). Fluids and melts derived from such subducted source materials, with correspondingly wide geochemical and isotopic variations, have been shown to metasomatize the lithospheric mantle wedge above subducting slabs (e.g., Ben Othman et al., 1989; Plank and Langmuir, 1998) to produce EM I-like Sr-Nd-Pb isotopic compositions, as observed in many modern oceanic and

continental carbonatites (e.g., Hoernle et al., 2002), lamproites (e.g., Mirnejad and Bell, 2006), and ultrapotassic rocks (Sun et al., 2014).

The PUD rocks exhibit a wide range of Sr-Nd-Pb-O isotopic compositions that, along with other compositional systematics, clearly indicate source heterogeneity and multi-stage enrichment within their lithospheric mantle sources.

4.6.5.1 Sr-Nd isotopes

The samples from the PUD1 exhibit Paleoproterozoic to Mesoproterozoic Nd model ages (T_{DM} 1.55-1.78 Ga, DePaolo, 1981; T_{CR} 1.70-1.97 Ga, Goldstein et al., 1984), and they plot slightly above, but parallel to, the regression lines for the other Proterozoic crust groupings in the study area (e.g., parallel to the MIZ, Island and Canyon domains, Banded complex, and below the Quebecia crust; fig. 4.5a). The model ages of PUD1 may thus provide a minimum temporal constraint for metasomatic enrichment of their mantle source(s), followed by evolution of metasomatic agents in the SCLM over a period of ~500-800 M.y duration, before their final emplacement at ca. 980 Ma.

Evidence for mantle source depletion for the PUD2 samples has been presented above. Based on their early Paleoproterozoic Nd model ages (T_{DM} 2.2-2.3 Ga, DePaolo, 1981; T_{CR} 2.35-2.47 Ga, Goldstein et al., 1984), it is inferred that this mantle depletion process took place during the extensive late-Archean melt extraction and crust formation events documented in the southeastern margin of the Superior Province. Subsequent subduction-metasomatic re-fertilization of the depleted SCLM, resulting in LREE enrichment, could have taken place during arc-accretionary orogenesis in the late-Archean to Paleoproterozoic (Percival et al., 2012; and references therein).

Following this, metasomatic agents evolved isotopically over a period of >1 B.y, before final emplacement of PUD2 dykes at ca. 980 Ma.

The initial $^{87}Sr/^{86}Sr$ ratios are low for PUD samples, although PUD1a samples exhibit slightly higher values that may indicate source heterogeneity. Overall low time-integrated Rb/Sr ratios suggest that the metasomatic agents for PUD1b and PUD2 were low in Rb, whereas those for PUD1a contained more variable amounts of Rb.

4.6.5.2 Pb isotopes

Pb isotope data may provide more detailed information about depletion and enrichment processes in the source of the late Grenvillian PUD rocks, since the coupled decay of the two U isotopes with greatly different half-lives are more divergent than the Sr-Nd isotope systematics. The ^{235}U has a short half-life (~0.7 Ga), which resulted in formation of ~83% of radiogenic ^{207}Pb by 1.65 Ga and it was largely extinct by the Mesoproterozoic (Tilton, 1983). The $^{207}Pb/^{204}Pb$ ratio is thus least likely to be disturbed by late Grenvillian events, and is strongly indicative of U/Pb differentiation processes that occurred in Archean to early Paleoproterozoic time. Conversely, the half-life of ~4.5 Ga for ^{238}U resulted in the $^{206}Pb/^{204}Pb$ ratio evolving more continuously through time. As a result, the hyperbolic Pb evolution curves for both mantle and crust (Zartman and Doe, 1981) exhibit increasing $^{206}Pb/^{204}Pb$ over $^{207}Pb/^{204}Pb$ ratios in younger mantle and crust.

If Pb in most of the PUD samples was not modified by late-stage alteration, or by shallow-level crustal contamination, then they are likely to reflect multi-stage evolution in a heterogeneously enriched mantle. All the PUD samples plot below the Stacey and Kramers (1975) average crustal evolution line (similar to the orogen

evolution line of Zartman and Doe, 1981) implying a U-depleted mantle source. Based on two-stage Sr-Nd-Pb isotope modelling, Corriveau and Amelin (1994) suggested that the K-rich plutons from the Central Metasedimentary Belt ("K-S suite" in fig. 4.6) were derived from a ca. 1.08 Ga mantle source metasomatized by subducted sediment, and the protoliths of sediment were derived from a depleted Mesoproterozoic mantle with $\mu = 8.0$ at ca. 1.45 Ga. Similar evolution models of Proterozoic depleted mantle-derived materials, with different initial μ ($^{238}U/^{204}Pb$) and κ ($^{232}Th/^{238}U$) values, would fit the heterogeneous Pb isotopic characters of the PUD1a and PUD1b samples. Moreover, the highly uranogenic and thorogenic Pb in PUD1a samples suggests that their source was enriched in U and Th at some stage of their metasomatic evolution.

PUD2 samples exhibit low $^{207}Pb/^{204}Pb$ ratios compared to those fall within the field for ancient Laurentian lamproites (fig. 4.6c-d); the Smokey Butte lamproites were shown to have a two-stage Pb evolution where metasomatic agents were initially separated from Archean depleted mantle at 2.5 Ga with a $\mu 1$ of 8.3, followed by significant reduction in $\mu 2$ to 4.1 (Fraser et al., 1985). A large number of Pb analyses from the late-Archean (~2.72 Ga) mafic-ultramafic rocks (e.g., Abitibi volcanic rocks, fig. 4.6a-b), associated sulphides, and felsic plutonic suites within the Canadian Shield suggest late-Archean mantle sources with lower μ values (7.5-7.8) (Kwon et al., 1989; Gariépy et al., 1990; and references therein). The low $^{207}Pb/^{204}Pb$ ratios in PUD2 samples suggest an ancient mantle source, e.g., late-Archean depleted mantle with low μ and a history of at least two-stage Pb evolution during the Proterozoic with further reduction in μ. This is further supported by the overlap of PUD2 data with those from the Aillik Bay lamproites and clinopyroxene from Renard kimberlites (fig. 4.6c-d), for

which early-Paleoproterozoic to late-Archean sources were inferred (Tappe et al., 2007; Hunt et al., 2012).

However, depletion in U and Th and lowering of μ values probably did not accompany other LILE (e.g., K) and LREE enrichment, as their geochemical behaviours are similar. It is most likely that depletion events lowering U and Th in the mantle sources of PUD2 samples took place prior to enrichment events that increased LILE and LREE contents, and that these subsequent enrichment events did not accompany U and Th addition, as has been suggested for Leucite Hills, Smoky Butte, and Prairie Creek lamproites (Fraser et al., 1985; Mitchell and Bergman, 1991).

4.6.5.3 O isotopes

O isotopes provide constraints on the nature and timing of metasomatism for the sources of PUD samples. The $\delta^{18}O$ values in the PUD (3.8-9.2‰) span +5.4‰, a dispersion that cannot be produced exclusively by fractional crystallization of olivine and clinopyroxene (an effect predicted to be <1‰; Baker et al., 2000). With the exception of the lowest value (sample 403; $\delta^{18}O_{WR}$ = 3.8‰), the remaining data ($\delta^{18}O_{WR}$ = 6.2-9.2‰) range from those corresponding to values for mantle-derived mafic rocks ($\delta^{18}O_{WR}$ = 5.5-7.4‰; Taylor, 1968) to higher values, indicating (weathered?) crustal source(s). In the $\delta^{18}O$ vs. $^{87}Sr/^{86}Sr$ diagram (fig. 4.11a), the PUD samples exhibit an increase in $\delta^{18}O$ compared to only minor or no increase in $^{87}Sr/^{86}Sr$ ratios. Such variations are generally ascribed to crustal contamination rather than source mixing (James, 1981). In the $\delta^{18}O$ vs. Mg# diagram (fig. 4.11b), the most primitive ultrapotassic samples in PUD1b and PUD2 (Mg# ≥ 65) exhibit elevated $\delta^{18}O$ values of 7.6-8.2‰, indicating an ^{18}O-enriched, primitive, ultrapotassic melt source, most likely located within lithospheric mantle. Samples 408 (PUD1a) and 209-2 (PUD1b) exhibit

elevated $\delta^{18}O$ values (9.0-9.2‰) at Mg# < 47 wt%, suggesting these samples could have been contaminated by upper crust or sediment. Conversely, sample RS351 (PUD1a) has low $\delta^{18}O$ (6.2 ‰) at Mg# of only 44, implying a lithospheric mantle source, or contamination at source by lower crust.

Sample 403 from PUD2 exhibits a very low $\delta^{18}O$ value (3.8‰) at very high Mg# (75). Low $\delta^{18}O$, below the upper mantle value, has been reported from many oceanic and continental basalts (Eiler, 2001) and Precambrian anorthosites (Peck et al., 2010), which have been interpreted by these authors to be related to either – (i) assimilation of hydrothermally altered low $\delta^{18}O$ oceanic crust; (ii) post-crystallization, low-temperature alteration by meteoric water; or (iii) original mantle source features. Assimilation of oceanic crust is not considered an alternative here because of the highly unradiogenic $\varepsilon Nd_{(980\ Ma)}$ value of sample 403. Consequently, sample 403 may reflect either low-temperature alteration by meteoric water, or a source feature within the heterogeneous ancient SCLM.

Quantitative modelling shows that crustal contamination can produce large variations in $\delta^{18}O$ values with relatively small changes in Sr-isotope ratios, which define hyperbolic convex upward mixing curves (James, 1981). Conversely, source metasomatism by ^{18}O-enriched fluids and melts derived from subducted sediment and crust produces small changes in $\delta^{18}O$ values at very large variations in Sr-isotope ratios, which define convex downward mixing curves (James, 1981). The $\delta^{18}O$ vs. $^{87}Sr/^{86}Sr$ correlation (fig. 4.11a) suggests at least two stages of enrichment of lithospheric mantle sources for the PUD. The first stage most likely involved source metasomatism in an ancient subduction setting, when lithospheric mantle wedge was enriched in LILE, LREE, and Sr, but with low Rb, most likely by fluids and melts derived from subducted

carbonate and phosphate sediment (e.g., Ben Othman et al., 1989; Plank and Langmuir, 1998). Source metasomatism with low Rb/Sr ratio resulted in low radiogenic $^{87}Sr/^{86}Sr$ and a relatively small increase in $\delta^{18}O$ values in metasomatized lithospheric mantle. In the second stage, ultrapotassic melts derived from these previously metasomatized mantle sources interacted with crustal fluids or melts, resulting in a significant increase in $\delta^{18}O$, with or without increasing their $^{87}Sr/^{86}Sr$ ratios. A similar model was proposed for Neogene K-rich volcanic rocks from SE Spain (Benito et al., 1999).

It is difficult to constrain the timing of this second stage of metasomatic activity based on isotopic correlations alone. High $\delta^{18}O$ values from Leucite Hills lamproites were interpreted by Mirnejad and Bell (2006) to be related to recent metasomatism (<100 M.y) by hydrous fluid or melt at source. They argued for this based on a lack of correlation between εNd and K_2O, suggesting K_2O enrichment was not related to long-term LREE enrichment (e.g., Feeley, 2003) and hence correlates with recent metasomatic activity at the source for the lamproites. The PUD1 samples exhibit no distinguishable correlation between εNd and K_2O (fig. 4.10f), suggesting the second stage of metasomatism could have taken place shortly before their emplacement. PUD2 samples exhibit a weak negative correlation, but more importantly, their lowest εNd values at the highest K_2O (and K_2O/Na_2O) strongly suggest that metasomatic agents added to their mantle source during the second stage were more ancient compared to those for the PUD1, and likely similar in composition in terms of incompatible elements to those of the ultrapotassic melts.

4.6.6 Mantle source components: isotopic constraints

The Sr-Nd-Pb isotopes of the PUD samples suggest three hypothetical source components within the mantle (fig. 4.11c-f) from which PUD rocks were derived: (i)

component C1 contained unradiogenic Nd, moderately radiogenic Sr, and highly radiogenic Pb; (ii) component C2 contained unradiogenic Nd, low radiogenic Sr, and low radiogenic Pb; and (iii) component C3 contained highly unradiogenic Nd, low radiogenic Sr, and highly unradiogenic Pb.

The PUD1a samples exhibit a positive correlation between εNd and $^{87}Sr/^{86}Sr$ (fig. 4.5b) in a sub-horizontal trend, indicating their derivation from mixing between C1 and C2. This is also evident from their highly radiogenic Pb that correlates positively in the $^{87}Sr/^{86}Sr$ vs. $^{207}Pb/^{204}Pb$ (fig. 4.11c, d) and $^{143}Nd/^{144}Nd$ vs. $^{207}Pb/^{204}Pb$ (fig. 4.11e, f) diagrams. Moreover, these same samples exhibit positive correlation of $\delta^{18}O$ vs. $^{87}Sr/^{86}Sr$ (fig. 4.11a), suggesting C1 was a Proterozoic lithospheric mantle source that contained high $\delta^{18}O$ materials such as subducted sediment and/or upper crust. The PUD1b samples, with low radiogenic Sr, unradiogenic Nd, and low radiogenic Pb, plot close to C2 (figs. 4.5b and 4.11c-f), indicating an EM I-type Proterozoic lithospheric mantle source. The ^{18}O-enrichment in PUD1b samples, coupled with both their primitive and evolved compositions suggest they were modified by subducted sediment-derived fluids at source. However, crustal contamination during ascent for the most evolved PUD1 samples is plausible.

Based on the Sr-Nd-Pb-O isotopic constraints presented here, it is inferred that the PUD1 samples were derived from the Proterozoic lithospheric mantle without any involvement of Archean crust or lithospheric mantle. With few exceptions (e.g., the Atikonak River granite; Emslie et al., 1997), the many published geochemical and isotopic data from the Mesoproterozoic mantle-derived rocks emplaced before ca. 1005 Ma in the Grenville hinterland exhibit Paleoproterozoic to Mesoproterozoic Nd model ages, and suggest their derivation from juvenile asthenospheric and depleted

lithospheric mantle sources, modified by Mesoproterozoic subduction along the Laurentian margin, and reworking of Mesoproterozoic to Paleoproterozoic crust with short crustal residence times (Ashwal et al., 1986; Ashwal and Wooden, 1983; Amelin et al., 1994; Corriveau and Amelin, 1994; Owens et al., 1994; Corriveau et al., 1996; Chiarenzelli et al., 2010; Emslie and Hegner, 1993; Thomson et al., 2011; Valverde et al., 2012; Augland et al., 2015, 2017; Maity and Indares, 2018; Maity, *in prep.*).

The PUD2 samples with low radiogenic Sr and the most unradiogenic Nd isotope ratios are similar to C3, indicating an older, late-Archean to early Paleoproterozoic EM I-type mantle source. Their highly unradiogenic $^{207}Pb/^{206}Pb$ ratios also suggest an ancient, strongly U-depleted source similar to ancient lower crust or its attached lithospheric mantle. In the Sr-Nd-Pb isotopes correlation diagrams (fig. 4.11c, e), the PUD2 samples with unradiogenic Nd-Pb and low radiogenic Sr isotopic compositions point towards the field for the Archean Superior crust. The possibility for high-level crustal contamination has been discounted for PUD2 samples, based on their very high incompatible elements along with high Mg#, Ni and Cr. Therefore, component C3 is best explained as a late-Archean to early-Paleoproterozoic lithospheric mantle beneath the Superior margin (S-SCLM), modified at source by late-Archean lower crust and/or Paleoproterozoic cover sequence. The S-SCLM was depleted as a result of extensive melt extraction in the late-Archean (Percival et al., 2012) and subsequently metasomatized during Paleoproterozoic arc-accretionary orogenesis, e.g., Makkovikian and Penokean Orogenies that took place along the southern and southeastern margin of the Superior Province (e.g., Dickin, 1998a, 1998b; Dickin and McNutt, 1989). Paleoproterozoic reworking of the Gagnon terrane has been documented by the ca. 1.70-1.75 Ga granitic magmatism (Dunning and Indares, 2010)

and the ca. 1.74-1.72 Ga metamorphic monazite formed in the KLG paragneiss (Jordan et al., 2006).

Based on trace element and isotopic studies on veined, metasomatic, and MARID xenoliths from South Africa, it has been suggested that Pb partitions into K-richterite more preferentially than into phlogopite (Kramers et al., 1983; Smith, 1983), whereas the opposite is the case for Rb (Schmidt et al., 1999; Tiepolo et al., 2000). Therefore, K-richterite in a metasomatized mantle source (and/or vein assemblages) will produce low U/Pb and Rb/Sr ratios and a negative correlation in Sr-Pb isotopes, whereas phlogopite in this source type will produce high U/Pb and Rb/Sr and a positive correlation between $^{87}Sr/^{86}Sr$ and $^{207}Pb/^{206}Pb$. The C1 component, with high Rb/Sr and U/Pb, implies phlogopite in the source, and therefore the positive correlation between $^{87}Sr/^{86}Sr$ and $^{207}Pb/^{206}Pb$ defined by the PUD1a samples reflects the competing role of phlogopite and K-richterite in their source (e.g., Ionov et al., 1997). These interpretations are consistent with the PUD1a trace element data discussed before (fig. 4.8). The C2 and C3 components have low Rb/Sr and U/Pb, suggesting amphibole in the source, which is also implied by the negative correlations between $^{87}Sr/^{86}Sr$ and $^{207}Pb/^{206}Pb$ exhibited by PUD1b and PUD2 samples (Kramers et al., 1983), although the range of isotope ratios are very restricted.

In summary, the combined Sr-Nd-Pb-O isotope systematics indicate an unambiguous difference between the source regions for PUD1 and PUD2. The trace elements and isotope correlation diagrams support involvement of three distinct sources: (i) a Proterozoic, fertile phlogopite-spinel lherzolite source metasomatized by hydrous fluids from upper crustal materials or subducted sediments (C1); (ii) a Proterozoic, fertile, amphibole-garnet lherzolite source metasomatized by carbonatitic

fluids (C2); and (iii) a late-Archean, depleted phlogopite-amphibole-garnet lherzolite source (S-SCLM) most likely metasomatized by carbonatitic melts (C3). All the three components also exhibit geochemical signatures of heterogeneous MARID-type metasomatism previously reported from other K-rich rocks derived from the Laurnetian SCLM.

Below we discuss the possible tectonic setting of the Rigolet orogenic phase in the hinterland to permit the formation of PUD1 and PUD2 from distinct lithospheric mantle sources.

4.6.7 Tectonic setting

Any tectonic model for the Rigolet PUD samples should explain both their temporally and spatially restricted distinct sources, and their characteristic depletion and multi-stage metasomatic enrichment processes. Previously, the renewed convergence during the Rigolet phase has been proposed to have resulted in one of two kinematically equivalent tectonic movements: thrust propagation of the orogenic hinterland over the Archean foreland (van Gool et al., 2008; Valverde Cardenas et al., 2012); or underthrusting of the rheologically stronger Archean foreland beneath the hinterland (Jordan et al., 2006; Jannin et al., 2018a, 2018b; Turlin et al., 2019). Based on the results obtained in this study, coupled with recent data from the study area, we proposed an intracontinental subduction model for the Rigolet phase as discussed below.

In explaining the source of recent metasomatism in the Leucite Hills lamproites, Mirnejad and Bell (2006) suggested that metasomatic fluids/melts could have been derived from a plume source such as the Yellowstone hotspot, or more likely from

asthenospheric upwelling during back-arc extension and lithospheric thinning related to the Farallon plate subduction. The latter is similar to a model that has been proposed for the Crazy Mountains volcanic rocks by Dudás (1991). In the case of PUDs, fluids/melts that metasomatized SCLM sources prior to their emplacement could have been derived from subducted crust and/or sediment, or from upwelled asthenosphere. Asthenospheric upwelling during the post-Ottawan lithospheric extension has been previously proposed for the central Grenville Province (fig. 4.12a; Maity, *in prep.*). However, we postulate that the ultimate source of high K_2O and other incompatible elements was the SCLM. Moreover, the PUDs do not exhibit evidence for high-grade metamorphism, suggesting their emplacement after the post-Ottawan to early-Rigolet high-grade metamorphism in the study area. Therefore, metasomatic hydrous fluids, responsible for enriching ^{18}O, could have been derived from sediment introduced at the source of the PUD1 samples, i.e., within the Proterozoic SCLM, in a compressional setting via the Rigolet intracontinental subduction (fig. 4.12a). In this model, the foreland lithosphere was subducted beneath the Grenville hinterland along the Grenville Front (Culshaw et al., 1997; Green et al., 1988). This is also compatible with the recent studies from central Grenville Province that suggest underthrusting of the foreland Gagnon terrane beneath the hinterland at the beginning of the Rigolet orogenic phase (Jannin et al., 2018a, 2018b; Turlin et al., 2019).

Although a large portion of sediment (crust) on a downgoing slab may accrete to the base of the over-riding plate, nonetheless, some sediment is still dragged into the mantle wedge by the downgoing slab (Clift and Vannucchi, 2004; Spencer et al., 2015) - where ^{18}O-enriched melts or fluids can be released to metasomatize the SCLM wedge or mix with primitive peridotite melts (e.g., Liu et al., 2014). The isotopic and

geochemical signatures of such metasomatic agents are dependent on the nature of the subducted sediment. The earliest phase of Rigolet subduction could have brought the Paleoproterozoic KLG cover sequences (Rivers, 1983a, 1983b; comparable to the ca. 1.84 Ga Sokoman Formation of western Labrador having $\varepsilon Nd_t = 1.2 \pm 0.8$; Fryer, 1972; Jacobsen and Pimentel-Klose, 1988) beneath the hinterland, leading to metasomatism and melting in the Proterozoic SCLM - from which PUD1 samples were derived and subsequently intruded the Canyon domain (fig. 4.12b-c).

The PUD1a samples have a positive correlation in Dy/Yb vs. La/Yb (not shown) suggesting mixing between low-degree partial melts of amphibole-garnet lherzolite and relatively high-degree partial melts of shallow phlogopite-spinel lherzolite. The PUD1b samples with high Dy/Yb suggest their derivation from amphibole-garnet lherzolite. Based on the foliated texture and lack of high-grade metamorphism in the PUD1 samples, it is inferred that they were syn-tectonically emplaced after ca. 997 Ma (i.e., younger than the maximum age of granulite-facies metamorphism in the study area; Maity, *in prep.*), and before ca. 986 Ma (i.e., the age of the D2 deformation in the foreland Gagnon terrane; Jannin et al., 2018a, 2018b), most likely during the Rigolet channel formation in the study area (Jannin et al., 2018a, 2018b). The geochemical and isotopic contrasts between the PUD1a and PUD1b samples may imply their source heterogeneity and/or slightly different times of emplacement.

Continued subduction brought the currently exposed parts of the Archean Gagnon terrane along the footwall of Allochthon Boundary thereby juxtaposing it with the aM*P* crust on the hanging wall side, whereas the underlying S-SCLM was decoupled from overlying crust, and subducted further down beneath the hinterland towards the orogenic core (fig. 4.12d). Limited crustal extension, lithospheric

relaxation, and far-field stress adjustments towards the end of Rigolet orogeny allowed melting of the most LILE-enriched parts of the S-SCLM at ca. 980 Ma, when the PUD2 samples, with moderate to high Dy/Yb, were derived from previously melt-metasomatized, Archean garnet-peridotite, and were emplaced in a post-tectonic setting. From buoyancy considerations, the subducted S-SCLM would have displaced the asthenosphere beneath it, thereby depressing the asthenospheric thermal boundary layer (T ≈ 1330 °C) to a greater depth, which could have led to conductive heating of the overlying cold S-SCLM as the two bodies equilibrated thermally. One massive sample from PUD1a (408) was most likely emplaced during this period, suggesting its derivation from a sliver of younger Proterozoic SCLM overlying the subducted S-SCLM.

In general, it is well established that the Archean SCLM beneath cratonic interiors is cooler, thicker (up to 250 km or more), more refractory, less hydrous, less dense, and less likely to lose buoyancy relative to the younger Phanerozoic SCLM, which is warmer, thinner (<100 km), more enriched, more hydrous, and denser (Griffin et al., 2009). Subduction-related metasomatism along craton margins has the potential to change the density and buoyancy of the underlying SCLM, as happened along the southern margin of the S-SCLM (Card, 1990; Percival et al., 2012). However, most Proterozoic to Archean SCLM is considered unlikely to have delaminated or melted extensively (Griffin et al., 2009) and so, if subducted, its positive buoyancy compared to the asthenosphere would not have permitted it to sink. Such a situation would, therefore, have led to shallow (low-angle) or flat subduction beneath the base of the orogenic crust in the hinterland, with ongoing convergence eventually displacing the asthenosphere from beneath a large part of the orogenic hinterland.

Several authors have postulated, on the basis of surface mapping and deep seismic imaging studies, that the reworked crust of the Archean Superior Province continues ~300 km to the southeast of the Grenville Front, beneath the hinterland in the central Grenville Province (e.g., Hynes et al., 2000; Rivers, 1997). This architecture is also supported elsewhere in the Grenville Province by geophysical data (e.g., Faure et al., 2011; Aktas and Eaton, 2006; Boyce et al., 2016; Adetunji et al., 2014, 2015). A recent geophysical study based on resistivity data (Adetunji et al., 2014; their figs. 8, 11, and 17) showed that a highly resistive, relict slab of the Archean Superior craton lithosphere above the GF projects at shallow depth (< 150 km; Adetunji et al., 2015), dipping towards southeast and reaching into the middle of the Central Metasedimentary Belt. This distinct resistive layer is restricted on its footwall side by the ca. 1000 Ma GF, which was interpreted by these same authors to indicate the youngest age limit of the event that caused the perturbation of lithospheric resistivity across the GF. Hence, both the geological and geophysical evidence, robust and well established from several datasets, supports the presence of a gently SE-dipping lithospheric slab extending from the margin of the Superior Province into the subsurface beneath the Grenvillian hinterland, towards the orogenic core. Recent studies from the central Grenville Province provide a further time constraint, based on geochronological and isotopic data, that the Archean lithosphere could have entered beneath the orogenic core in the Grenvillian hinterland as a result of Rigolet continental flat subduction.

4.6.8 Implications

The tectonic setting proposed above is compatible with several other observations. First, we propose that flat subduction of the Archean lithosphere resulted in diminishing depleted mantle-derived magmatism in the hinterland between ca. 1000

and 980 Ma. This is analogous to the termination of asthenospheric magmatism ~13 M.y. after underthrusting of the Indian lithosphere beneath southern Tibet (Chen et al., 2017), or to underthrusting of the Eurasian continental lithosphere beneath northern Tibet (DeCelles et al., 2002; Chung et al., 2005; Chen et al., 2012). Continental subduction has also been proposed to have taken place at ca. 980 Ma between the Eastern Segment, composed of the Baltica crust, that was underthrust beneath the western Sveconorwegian terranes (Möller and Andersson, 2018).

Second, the ~30-50 m.y gap in the age of peak high-grade metamorphism, with distinct *P*-*T*-t paths for the allochthonous versus the parautochthonous crust (Indares et al., 1998; Indares et al., 2000; Indares and Dunning, 2004; Jordan et al., 2006), and the distinct gaps in Nd model ages and U-Pb zircon ages between the two adjacent crustal domains on either side of the Allochthon Boundary (Dunning and Indares, 2010; Thomson et al., 2011), suggest that a large part of the early-Paleoproterozoic crust in the foreland was either subducted into the mantle underneath the hinterland during Rigolet continental subduction, or extruded from deep crustal levels through a Rigolet orogenic wedge (e.g., van Gool et al., 2008).

Specifically, it is inferred that the subducted crust on the Superior plate, after detachment from its underlying mantle at depth, was extruded back towards the northwest from crustal depths of ≤ 65 km, forming a metamorphosed orogenic wedge or channel in the footwall of the Allochthon Boundary Thrust (Hynes et al., 2000; Jannin et al., 2018a, 2018b). This subducted crust has been mapped at the surface as the crustal-scale Rigolet thrust-stack in the Gagnon terrane with its classic inverted metamorphic sequence (Rivers, 1983a, 1983b; van Gool et al., 2008). Both structural and geophysical data confirm the presence of a wedge-shaped sliver of Archean crust,

forming the basement of the Superior Province in the Parautochthonous Belt (i.e. the Gagnon terrane; fig. 4.2; Jordan et al., 2006; van Gool et al., 2008), extends in the subsurface beneath the Allochthonous Belt (Rivers et al., 1993; Rivers, 1997; Hynes et al., 2000; Hynes and Rivers, 2010).

Fourth, coeval with and outlasting the Rigolet crustal shortening in the Parautochthonous Belt, there is evidence within the overlying Allochthonous Belt for widespread and dispersed intrusions of small-volume, mantle- and(or) crust(?)-derived, alkaline mafic dykes, Fe-Ti-P-rich jotunitic gabbro bodies, and syenitic to granitic plutons, suggesting derivation from multiple mantle sources, including the subducted cratonic S-SCLM, the overlying remnant of previously thinned Proterozoic SCLM, and possibly a thin asthenospheric wedge sandwiched between them. These unmetamorphosed intrusions occur throughout the central to western Grenville hinterland, e.g., the ca. 1000 Ma LBV lamprophyre dykes, the ca. 1000±6 Ma Lesueur alkaline suite (Davis and Nantel, 2016), the ca. 988 Ma Vénus de Milot syenite (Higgins et al., 2002), the ca. 987 Ma Touladi granite (Hébert et al., 2009), and the ca. 957.5 ± 2.9 Ma Crevier alkaline intrusion (Solgadi et al., 2015). The late- to post-Grenvillian intrusions are especially abundant in the eastern Grenville Province (fig. 4.1; Gower and Krogh, 2002; Greenough and Owen, 1995), where they cluster in two age groups: a weakly foliated to non-foliated 'early post-tectonic' group consisting of anorthosite-alkalic-mafic bodies emplaced between ~985-975 Ma, and an undeformed 'late post-tectonic' group composed of monzonite-syenite-granite bodies emplaced between ~975-955 Ma (Gower and Krogh, 2002).

Fifth, based on paleomagnetic evidence, a crustal shortening of ~4000 ± 1000 km was inferred to have taken place between ca. 1040-1020 and 980 Ma along the

southeastern margin of Laurentia (Halls, 2015). A significant portion of this inferred crustal shortening can be accommodated by the Rigolet flat subduction proposed here.

Sixth, we infer that buoyancy of the late-Archean S-SCLM may have eventually inhibited the progress of subduction, thereby resulting in cessation of the Rigolet phase of continental collision by ca. 980 Ma, although deformation in the parautochthonous belt could have continued as late as ca. 960 Ma (Jannin et al., 2018a). The flat subduction of the cold, refractory S-SCLM also led to an overall decrease in both mantle and crustal melting.

Finally, it is not needed to invoke another episode of extensive delamination or convective thinning of the old S-SCLM (e.g., Ludden and Hynes, 2000). The Parautochthonous Belt does not record either an orogen-wide occurrence of late (i.e., post-Rigolet) granulite-facies metamorphism or a significant volume of asthenospheric magmatism, features that characterized lithospheric thinning in the hinterland during the Ottawan and post-Ottawan orogenic phases. Various modes of geophysical imaging suggest that the subducted S-SCLM remained largely intact beneath the Grenvillian hinterland and eventually contributed to the formation of the lithospheric keel beneath the Grenville Province (e.g., Boyce et al., 2016). However, local thinning or delamination of the S-SCLM as a result of orogenic relaxation following Rigolet convergence is possible and could have played a role in late- to post-Rigolet magmatism.

In concluding this section, it is noted that our model is incompatible with the numerical modelling of the Rigolet phase as a result of gravitationally-driven orogenic collapse (Jamieson et al., 2010, 2011). However, it fits well with many of the generic features of orogenic evolution discussed by Vanderhaeghe (2011), although in detail,

the Rigolet phase is different in that it involves flat subduction of ancient metasomatized cratonic S-SCLM, which was not considered in his study. We also note that the data and interpretations in this current study permit the qualitative refinement of numerical models and may provide constraints useful in future experiments.

4.7 Conclusions

Based on the intensity of deformation, major and trace element geochemistry, and Sr-Nd-Pb-O isotopes, the late-Grenvillian (Rigolet phase) potassic to ultrapotassic dykes (PUD) in the hinterland in central Grenville Province can be subdivided into two groups: (i) an older syn-tectonic group PUD1 (1a and 1b) inferred to have been emplaced before ca. 986 Ma; and (ii) a younger late- to post-tectonic group (PUD2) dated at ca. 980 Ma. Their trace element and isotopic compositions suggest that both groups were derived from EM I-type sources within the Laurentian subcontinental lithospheric mantle that contained MARID-type metasomes derived from ancient subduction-related processes.

The PUD1b samples were derived by partial melting of an unradiogenic fertile garnet lherzolite source with low Sm/Nd, Rb/Sr, and U/Pb. This source was metasomatized by fluids derived from subducted carbonate and phosphate sediments. On the other hand, PUD1a samples were derived by mixing of partial melts from an unradiogenic garnet-lherzolite source similar to that for PUD1b, with that from a more radiogenic spinel-lherzolite source relatively higher in Sm/Nd, Rb/Sr, and U/Pb. This more radiogenic mantle source was metasomatized by hydrous fluids from subducted sediment and/or crust shortly before the emplacement of these syn-tectonic dykes. Overall, the PUD1 group was derived from fertile Proterozoic SCLM that was

previously metasomatized during the late-Paleoproterozoic to Mesoproterozoic subduction-accretionary events along the Laurentian margin, and subsequently by a latest metasomatic event shortly before their emplacement. The latest phase of metasomatism most likely occurred because of Rigolet continental subduction and/or upwelling of small-volume asthenospheric fluids related to post-Ottawan lithospheric extension. Shallow level crustal contamination could have affected only the most evolved PUD1samples.

The highly ultrapotassic PUD2 samples were derived by partial melting of a highly unradiogenic, depleted garnet-lherzolite source, low in Sm/Nd, Rb/Sr, and U/Pb, and this source was metasomatized by melts derived from subducted carbonate, phosphate, and pelagic sediments. This group was derived from melting within the Superior SCLM that was previously depleted as a result of late-Archean crust formation events and was subsequently metasomatized during Paleoproterozoic subduction-accretionary events along the southeastern margin of the Superior Province. The source for PUD2 was also metasomatized by ancient subduction-related sediments and/or lower crust prior to their generation and emplacement.

The tectonic setting for the Rigolet phase at ca. 1005-980 Ma is proposed to be characterized by compressional tectonics driven by flat subduction of the foreland lithosphere under the Grenville hinterland.

4.8 Acknowledgements

This research is part of the Ph.D. project of B.M. and was financially supported for Pb analyses from a NSERC Grant to G.D.L. Sherri Strong (MUN) and Kim Law (Western University) are acknowledged for carrying out Pb and O isotope analyses,

respectively. Aphrodite Indares has kindly provided sample powders for isotope analyses. Toby Rivers is gratefully acknowledged for encouragement and thought-provoking reviews of the manuscript.

4.9 References

Adam, J., Green, T.H., and Sie, S.. 1993. Proton microprobe determined partitioning of Rb, Sr, Ba, Y, Zr, Nb and Ta between experimentally produced amphiboles and silicate melts with variable F content. Chemical Geology, 109: 29–49. doi:10.1016/0009-2541(93)90060-V.

Adetunji, A.Q., Ferguson, I.J., and Jones, A.G. 2014. Crustal and lithospheric scale structures of the Precambrian Superior–Grenville margin. Tectonophysics, 614: 146–169. doi:10.1016/J.TECTO.2013.12.008.

Adetunji, A.Q., Ferguson, I.J., and Jones, A.G. 2015. Reexamination of magnetotelluric responses and electrical anisotropy of the lithospheric mantle in the Grenville Province, Canada. Journal of Geophysical Research: Solid Earth, 120: 1890–1908. doi:10.1002/2014JB011713.

Aktas, K., and Eaton, D.W. 2006. Upper-mantle velocity structure of the lower Great Lakes region. Tectonophysics, 420: 267–281. doi:10.1016/j.tecto.2006.01.020.

Amelin, Y., Corriveau, L., and Morin, D. 1994. Constraints on the evolution of Grenvillian lithosphere from Nd–Sr–Pb cpx and garnet and U–Pb zircon study of pyroxenitic and mafic granulite xenoliths. *In* Abstracts of the Eighth International Conference on Geochronology, Cosmochronology and Isotope Geology. *Edited by* M.A. Lanphere, G.B. Dalrymple, and B.D. Turrin. pp. 5. Available from https://pubs.usgs.gov/circ/1994/1107/report.pdf.

Anderson, A.T. 1966. Mineralogy of the Labrieville anorthosite, Quebec. The American Mineralogist, 51: 1671–1711. Available at: https://pubs.geoscienceworld.org/msa/ammin/article/51/11-12/1671/540380/mineralogy-of-the-labrieville-anorthosite-quebec.

Arcuri, G., and Dickin, A. 2018. Pb Isotope mapping of Paleoproterozoic gneisses in the SW Grenville Province: evidence for a cryptic continental suture. Geosciences, 8: 247. doi:10.3390/geosciences8070247.

Ashwal, L.D., and Wooden, J.L. 1983. Isotopic evidence from the eastern Canadian shield for geochemical discontinuity in the Proterozoic mantle. Nature, 306: 679–680. doi:10.1038/306679a0.

Ashwal, L.D., Wooden, J.L., and Emslie, R.F. 1986. Sr, Nd and Pb isotopes in Proterozoic intrusives astride the Grenville Front in Labrador: implications for crustal contamination and basement mapping. Geochimica et Cosmochimica Acta, 50: 2571–2585. doi:10.1016/0016-7037(86)90211-5.

Augland, L.E., Moukhsil, A., Solgadi, F. 2017. Mantle influence of syn- to late-Grenvillian alkaline magmatism in the Grenville Province: causes and implications. Canadian Journal of Earth Sciences, 15: 1–15. doi:dx.doi.org/10.1139/cjes-2016-0135

Augland, L.E., Moukhsil, A., Solgadi, F., and Indares, A. 2015. Pinwarian to Grenvillian magmatic evolution in the central Grenville Province: new constraints from ID–TIMS U–Pb ages and coupled Lu–Hf S–MC–ICP–MS data. Canadian Journal of Earth Sciences, 52: 701–721. doi:10.1139/cjes-2014-0232.

Aulbach, S., O'Reilly, S.Y., Griffin, W.L., and Pearson, N.J. 2008. Subcontinental lithospheric mantle origin of high niobium/tantalum ratios in eclogites. Nature Geoscience, 1: 468–472. doi:10.1038/ngeo226.

Ayer, J.A., and Dostal, J. 2000. Nd and Pb isotopes from the Lake of the Woods greenstone belt, northwestern Ontario: implications for mantle evolution and the

formation of crust in the southern Superior Province. Canadian Journal of Earth Sciences, 37: 1677–1689. doi:10.1139/e00-067.
Baker, J.A., Macpherson, C.G., Menzies, M.A., Thirlwall, M.F., Al-Kadasi, M., and Mattey, D.P. 2000. Resolving crustal and mantle contributions to continental flood volcanism, Yemen; constraints from mineral oxygen isotope data. Journal of Petrology, 41: 1805–1820. doi:10.1093/petrology/41.12.1805.
Baker, M.B., and Wyllie, P.J. 1992. High-pressure apatite solubility in carbonate-rich liquids: Implications for mantle metasomatism. Geochimica et Cosmochimica Acta, 56: 3409–3422. Pergamon. doi:10.1016/0016-7037(92)90388-Y.
Beaumont, C., Nguyen, M.H., Jamieson, R. A., Ellis, S. 2006. Crustal flow modes in large hot orogens. Geological Society London Special Publication, 268: 91–145. doi:10.1144/GSL.SP.2006.268.01.05
Bell, K., Blenkinsop, J. 1987. Archean depleted mantle: evidence from Nd and Sr initial isotopic ratios of carbonatites. Geochimica et Cosmochimica Acta, 51: 291–298. doi:10.1016/0016-7037(87)90241-9.
Ben Othman, D., White, W.M., Patchett, J. 1989. The geochemistry of marine sediments, island arc magma genesis, and crust-mantle recycling. Earth and Planetary Science Letters, 94: 1–21. doi:10.1016/0012-821X(89)90079-4.
Benito, R., López-Ruiz, J., Cebriá, J.M., Hertogen, J., Doblas, M., Oyarzun, R., and Demaiffe, D. 1999. Sr and O isotope constraints on source and crustal contamination in the high-K calc-alkaline and shoshonitic neogene volcanic rocks of SE Spain. Lithos, 46: 773–802. doi:10.1016/S0024-4937(99)00003-1.
Bouvier, A., Vervoort, J.D., Patchett, P.J. 2008. The Lu–Hf and Sm–Nd isotopic composition of CHUR: constraints from unequilibrated chondrites and implications for the bulk composition of terrestrial planets. Earth and Planetary Science Letters, 273: 48–57. doi:10.1016/j.epsl.2008.06.010.
Boyce, A., Bastow, I.D., Darbyshire, F.A., Ellwood, A.G., Gilligan, A., Levin, V., Menke, W. 2016. Subduction beneath Laurentia modified the eastern North American cratonic edge: evidence from P wave and S wave tomography. Journal of Geophysical Research: Solid Earth, 121: 5013–5030. doi:10.1002/2016JB012838.
Brévart, O., Dupré, B., and Allègre, C.J. 1986. Lead-lead age of komatiitic lavas and limitations on the structure and evolution of the Precambrian mantle. Earth and Planetary Science Letters, 77: 293–302. doi:10.1016/0012-821X(86)90141-X.
Card, K.D. 1990. A review of the Superior Province of the Canadian Shield, a product of Archean accretion. Precambrian Research, 48: 99–156. doi:10.1016/0301-9268(90)90059-Y.
Carignan, J., Machado, N., Gariépy, C. 1995. Initial lead isotopic composition of silicate minerals from the Mulcahy layered intrusion: implications for the nature of the Archean mantle and the evolution of greenstone belts in the Superior Province, Canada. Geochimica et Cosmochimica Acta, 59: 97–105. doi:10.1016/0016-7037(94)00375-V.
Carr, S.D., Easton, R.M., Jamieson, R.A., and Culshaw, N.G. 2000. Geologic transect across the Grenville orogen of Ontario and New York. Canadian Journal of Earth Sciences, 37: 193–216. doi:10.1139/e99-074.
Chen, J.-L., Xu, J.-F., Wang, B.-D., Kang, Z.-Q. 2012. Cenozoic Mg-rich potassic rocks in the Tibetan Plateau: geochemical variations, heterogeneity of subcontinental

lithospheric mantle and tectonic implications. Journal of Asian Earth Sciences, 53: 115–130. doi:10.1016/j.jseaes.2012.03.003.
Chen, M., Niu, F., Tromp, J., Lenardic, A., Lee, C.-T.A., Cao, W., Ribeiro, J. 2017. Lithospheric foundering and underthrusting imaged beneath Tibet. Nature Communications, 8: 15659. doi:10.1038/ncomms15659.
Chiarenzelli, J., Lupulescu, M., Cousens, B., Thern, E., Coffin, L., Regan, S. 2010. Enriched Grenvillian lithospheric mantle as a consequence of long-lived subduction beneath Laurentia. Geology, 38: 151–154. doi:10.1130/G30342.1.
Chung, S.L., Chu, M.F., Zhang, Y., Xie, Y., Lo, C.H., Lee, T.Y., Lan, C.Y., Li, X., Zhang, Q., Wang, Y. 2005. Tibetan tectonic evolution inferred from spatial and temporal variations in post-collisional magmatism. Earth-Science Reviews, 68: 173–196. doi:10.1016/j.earscirev.2004.05.001.
Clarke, P.J. 1977. Région de Gagnon. Québec. Ministère des Richesses Naturelles, RG 178.
Clift, P., and Vannucchi, P. 2004. Controls on tectonic accretion versus erosion in subduction zones: implications for the origin and recycling of the continental crust. Reviews of Geophysics, 42, RG2001: 1–31. doi:10.1029/2003RG000127.
Conticelli, S. 1998. The effect of crustal contamination on ultrapotassic magmas with lamproitic affinity: mineralogical, geochemical and isotope data from the Torre Alfina lavas and xenoliths, central Italy. Chemical Geology, 149: 51–81. doi:10.1016/S0009-2541(98)00038-2.
Corriveau, L. 1990. Proterozoic subduction and terrane amalgamation in the southwestern Grenville province, Canada: Evidence from ultrapotassic to shoshonitic plutonism. Geology, 18: 614–617. doi:10.1130/0091-7613(1990)018<0614:PSATAI>2.3.CO;2.
Corriveau, L., Amelin, Y. 1994. Sources of Proterozoic K-rich alkaline and shoshonitic magmatism in the SW Grenville Province, Quebec: Nd-Sr-Pb isotopic study. *In* Abstracts of the Eighth International Conference on Geochronology, Cosmochronology and Isotope Geology. *Edited by* M.A. Lanphere, G.B. Dalrymple, and B.D. Turrin. pp. 68. Available from: https://pubs.usgs.gov/circ/1994/1107/report.pdf.
Corriveau, L., Gorton, M.P. 1993. Coexisting K-rich alkaline and shoshonitic magmatism of arc affinities in the Proterozoic: a reassessment of syenitic stocks in the southwestern Grenville Province. Contributions to Mineralogy and Petrology, 113: 262–279. doi:10.1007/BF00283233.
Corriveau, L., Heaman, L.M., Marcantonio, F., van Breemen, O. 1990. 1.1 Ga K-rich alkaline plutonism in the SW Grenville Province. Contributions to Mineralogy and Petrology, 105: 473–485. doi:10.1007/BF00286834.
Corriveau, L., Tellier, M.L., Morin, D., Amelin, Y., van Breemen, O. 1996. Le dyke de minette de Rivard et le complexe gneissique cuprifére de Bondy; implications tectoniques et métallogéniques pour la région de Mont-Laurier, province de Grenville, Québec. Commission Géologique du Canada Dossier Public 3078, pp. 73. Available from: https://doi.org/10.4095/207905.
Côté, G., Moukhsil, A., Constantin, M., David, J. 2018. Geochemical characterization, geochronology, and geodynamic implications of Grenville rare earths bearing syenites, Haut-Saint-Maurice, QC, Canada. Minerals, 8: 336. doi:10.3390/min8080336

Cousens, B.L., Aspler, L.B., Chiarenzelli, J.R., Donaldson, J.A., Sandeman, H., Peterson, T.D., and LeCheminant, A.N. 2001. Enriched Archean lithospheric mantle beneath western Churchill Province tapped during Paleoproterozoic orogenesis. Geology, 29: 827. doi:10.1130/0091-7613(2001)029<0827:EALMBW>2.0.CO;2.

Cox, R., Indares, A. 1999a. High-pressure and high-temperature metamorphism of the mafic and ultramafic Lac Espadon suite, Manicouagan Imbricate Zone, eastern Grenville Province, Quebec. Canadian Mineralogist, 37: 335–357.

Cox, R., Indares, A. 1999b. Transformation of Fe-Ti gabbro to coronite, eclogite and amphibolite in the Baie du Nord segment, Manicouagan Imbricate Zone, eastern Grenville Province. Journal of Metamorphic Geology, 17: 537–555. doi:10.1046/j.1525-1314.1999.00216.x.

Cox, R.A. 1999. Eclogite facies metamorphism of mafic and ultramafic rocks in the Tshenukutish Terrane, Manicouagan Imbricate Zone, eastern Grenville Province. Ph.D Thesis. Memorial University of Newfoundland. Available from: https://research.library.mun.ca/6539/.

Cox, R.A., Dunning, G.R., Indares, A.D. 1998. Petrology and U–Pb geochronology of mafic, high-pressure, metamorphic coronites from the Tshenukutish domain, eastern Grenville Province. Precambrian Research, 90: 59–83. doi:10.1016/S0301-9268(98)00033-3.

Culshaw, N.G., Jamieson, R.A., Ketchum, J.W.F., Wodicka, N., Corrigan, D., Reynolds, P.H. 1997. Transect across the northwestern Grenville orogen, Georgian Bay, Ontario: polystage convergence and extension in the lower orogenic crust. Tectonics, 16: 966–982. doi:10.1029/97TC02285.

Darbyshire, F.A., Bastow, I.D., Petrescu, L., Gilligan, A., and Thompson, D.A. 2017. A tale of two orogens: Crustal processes in the Proterozoic Trans-Hudson and Grenville Orogens, eastern Canada. Tectonics, 36: 1633–1659. doi:10.1002/2017TC004479.

Davis, D.W., and Dion, C. 2012a. Datations LA-ICPMS d'échantillons recueillis en 2011-2012 par Géologie Québec. Ministère des Ressources Naturelles et de la Faune, Québec, MB 2012-09. Available from: http://gq.mines.gouv.qc.ca/documents/EXAMINE/MB201209/MB201209.pdf

Davis, D.W., and Dion, C. 2012b. Datations ID-TIMS d'échantillons recueillis en 2011-2012 par Géologie Québec. Ministère des Ressources Naturelles et de la Faune, Québec, MB 2012-07. Available from: http://gq.mines.gouv.qc.ca/documents/EXAMINE/MB201207/MB201207.pdf.

Davis, W.D., and Nantel, S. 2016. Datations U-Pb dans la partie nord de la Ceinture centrale des métasédiments, Province de Grenville, région de Mont-Laurier. Ministère de l'Énergie et des Ressources naturelles, Québec, MB 2016-04: 52. Available from:

DeCelles, P.G., Robinson, D.M., Zandt, G. 2002. Implications of shortening in the Himalayan fold-thrust belt for uplift of the Tibetan Plateau. Tectonics, 21: 12-1-12–25. doi:10.1029/2001TC001322.

DePaolo, D.J. 1981. Neodymium isotopes in the Colorado Front Range and crust-mantle evolution in the Proterozoic. Nature, 291: 193–196. doi:10.1038/291193a0

DeWolf, C.P., Mezger, K. 1994. Lead isotope analyses of leached feldspars: constraints on the early crustal history of the Grenville Orogen. Geochimica et Cosmochimica Acta, 58: 5537–5550. doi:10.1016/0016-7037(94)90248-8.

Dickin, A.P. 1998a. Pb isotope mapping of differentially uplifted Archean basement: a case study from the Grenville Province, Ontario. Precambrian Research, 91: 445–454. doi:10.1016/S0301-9268(98)00069-2.

Dickin, A.P. 1998b. Nd isotope mapping of a cryptic continental suture, Grenville Province of Ontario. Precambrian Research, 91: 433–444. doi:10.1016/S0301-9268(98)00062-X.

Dickin, A.P. 2000. Crustal formation in the Grenville Province: Nd-isotope evidence. Canadian Journal of Earth Sciences, 37: 165–181. doi:10.1139/e99-039.

Dickin, A.P., Higgins, M.D. 1992. Sm/Nd evidence for a major 1.5 Ga crust-forming event in the central Grenville province. Geology, 20: 137–140. doi:10.1130/0091-7613(1992)020<0137:SNEFAM>2.3.CO;2.

Dickin, A.P., McNutt, R.H. 1989. Nd model age mapping of the southeast margin of the Archean foreland in the Grenville province of Ontario. Geology, 17: 299. doi:10.1130/0091-7613(1989)017<0299:NMAMOT>2.3.CO;2.

Dudás, F.Ö. 1991. Geochemistry of igneous rocks from the Crazy Mountains, Montana, and tectonic models for the Montana Alkalic Province. Journal of Geophysical Research: Solid Earth, 96: 13,261-13,277. doi:10.1029/91JB00246.

Duggen, S., Hoernle, K., van den Bogaard, P., and Garbe-Schönberg, D. 2005. Post-Collisional Transition from Subduction- to Intraplate-type Magmatism in the Westernmost Mediterranean: Evidence for Continental-Edge Delamination of Subcontinental Lithosphere. Journal of Petrology, 46: 1155–1201. doi:10.1093/petrology/egi013.

Dunning, G., Indares, A. 2010. New insights on the 1.7–1.0 Ga crustal evolution of the central Grenville Province from the Manicouagan – Baie Comeau transect. Precambrian Research, 180: 204–226. doi:10.1016/j.precamres.2010.04.005.

Dupré, B., Arndt, N.T. 1990. Pb isotopic compositions of Archean komatiites and sulfides. Chemical Geology, 85: 35–56. doi:10.1016/0009-2541(90)90122-N.

Dupré, B., Chauvel, C., Arndt, N.T. 1984. Pb and Nd isotopic study of two Archean komatiitic flows from Alexo, Ontario. Geochimica et Cosmochimica Acta, 48: 1965–1972. doi:10.1016/0016-7037(84)90378-8.

Edgar, A.D., Mitchell, R.H. 1997. Ultra high pressure-temperature melting experiments on an SiO_2-rich lamproite from Smoky Butte, Montana: derivation of siliceous lamproite magmas from enriched sources deep in the continental mantle. Journal of Petrology, 38: 457–477. doi:10.1093/petroj/38.4.457.

Eiler, J.M. 2001. Oxygen Isotope Variations of Basaltic Lavas and Upper Mantle Rocks. Reviews in Mineralogy and Geochemistry, 43: 319–364. doi:10.2138/gsrmg.43.1.319.

Emslie, R.F., Hamilton, M.A., Gower, C.F. 1997. The Michael Gabbro and other Mesoproterozoic lithospheric probes in southern and central Labrador. Canadian Journal of Earth Sciences, 34: 1566–1580. doi:10.1139/e17-127.

Emslie, R.F., Hamilton, M.A., Theriault, R.J. 1994. Petrogenesis of a Mid-Proterozoic anorthosite-mangerite-charnockite-granite (AMCG) complex: isotopic and chemical evidence from the Nain Plutonic Suite. The Journal of Geology, 102: 539–558. doi:10.1086/629697.

Emslie, R.F., Hegner, E. 1993. Reconnaissance isotopic geochemistry of anorthosite-mangerite-charnockite-granite (AMCG) complexes, Grenville Province, Canada. Chemical Geology, 106: 279–298. doi:10.1016/0009-2541(93)90032-E.

Falloon, B.J., Green, D.H., Hatton, C.J., Harris, A.K.L. 1988. Anhydrous partial melting of a fertile and depleted peridotite from 2 to 30 kb and application to basalt petrogenesis. Journal of Petrology, 29: 1257–1282. doi:10.1093/petrology/29.6.1257

Falloon, T.J., Green, D.H. 1988. Anhydrous partial melting of peridotite from 8 to 35 kb and the petrogenesis of MORB. Journal of Petrology, Special Volume, 1: 379–414. doi:10.1093/petrology/Special_Volume.1.379.

Faure, S., Godey, S., Fallara, F., Trepanier, S. 2011. Seismic architecture of the Archean North American mantle and its relationship to diamondiferous kimberlite fields. Economic Geology, 106: 223–240. doi:10.2113/econgeo.106.2.223.

Feeley, T.C. 2003. Origin and tectonic implications of across-strike geochemical variations in the Eocene Absaroka Volcanic Province, United States. The Journal of Geology, 111: 329–346. doi:10.1086/373972

Foley, S. 1991. High-pressure stability of the fluor- and hydroxy-endmembers of pargasite and K-richterite. Geochimica et Cosmochimica Acta, 55: 2689–2694. doi:10.1016/0016-7037(91)90386-J.

Foley, S. 1992. Vein-plus-wall-rock melting mechanisms in the lithosphere and the origin of potassic alkaline magmas. Lithos, 28: 435–453. doi:10.1016/0024-4937(92)90018-T.

Foley, S.F., Musselwhite, D.S., der Laan, S.R. 1999. Melt compositions from ultramafic vein assemblages in the lithospheric mantle: a comparison of cratonic and non-cratonic settings. *In* Proceedings of the VIIth international kimberlite conference, Cape Town. pp. 238–246.

Foley, S.F., Taylor, W.R., Green, D.H. 1986. The role of fluorine and oxygen fugacity in the genesis of the ultrapotassic rocks. Contributions to Mineralogy and Petrology, 94: 183–192. doi:10.1007/BF00592935.

Foley, S.F., Venturelli, G., Green, D.H., Toscani, L. 1987. The ultrapotassic rocks: characteristics, classification, and constraints for petrogenetic models. Earth-Science Reviews, 24: 81–134. doi:10.1016/0012-8252(87)90001-8.

Foley, S.F., Wheller, G.E. 1990. Parallels in the origin of the geochemical signatures of island arc volcanics and continental potassic igneous rocks: the role of residual titanates. Chemical Geology, 85:1-18. doi:10.1016/0009-2541(90)90120-V.

Fraser, K.J. 1987. Petrogenesis of kimberlites from South Africa and lamproites from Western Australia and North America. PhD thesis. The Open University, UK. Available from: http://oro.open.ac.uk/54611/

Fraser, K.J.J., Hawkesworth, C.J.J., Erlank, A.J.J., Mitchell, R.H.H., Scott-Smith, B.H.H. 1985. Sr, Nd and Pb isotope and minor element geochemistry of lamproites and kimberlites. Earth and Planetary Science Letters, 76: 57–70. doi:10.1016/0012-821X(85)90148-7.

Fryer, B.J. 1972. Age determinations in the circum – Ungava geosyncline and the evolution of Precambrian banded iron-formations. Canadian Journal of Earth Sciences, 9: 652–663. doi:10.1139/e72-055.

Furman, T. 1995. Melting of metasomatized subcontinental lithosphere: undersaturated mafic lavas from Rungwe, Tanzania. Contributions to Mineralogy and Petrology, 122: 97–115. doi:10.1007/s004100050115.

Furman, T., Graham, D. 1999. Erosion of lithospheric mantle beneath the East African Rift system: geochemical evidence from the Kivu volcanic province. Lithos, 48:237–262. doi:10.1016/S0024-4937(99)00031-6 .

Gariépy, C., Allègre, C.J. 1985. The lead isotope geochemistry and geochronology of late-kinematic intrusives from the Abitibi greenstone belt, and the implications for late Archaean crustal evolution. Geochimica et Cosmochimica Acta, 49: 2371–2383. doi:10.1016/0016-7037(85)90237-6.

Gariépy, C., Verner, D., Doig, R. 1990. Dating Archean metamorphic minerals southeast of the Grenville front, western Quebec, using Pb isotopes. Geology, 18: 1078. doi:10.1130/0091-7613(1990)018<1078:DAMMSO>2.3.CO;2.

Gobeil, A., Hébert, C., Clark, C., Beaumier, M., Perreault, S. 2002. Géologie de la région du lac De La Blache (22K03/22K04). Ministère des Ressources naturelles du Québec, Québec, RG2002-01.

Gobeil, A., Hébert, C., Clark, T., David, J., Davis, D. 2005. Nouvelles données géochronologiques dans l'est du Grenville: précisions sur l'évolution magmatique. *In* Ministère Des Ressources naturelles du Québec, Résumé Des Conférences et de L'exposition Géoscientifique. Congrès de Québec Exploration. pp. 2003–2005.

Goldstein, S.L., O'Nions, R.K., Hamilton, P.J. 1984. A Sm-Nd isotopic study of atmospheric dusts and particulates from major river systems. Earth and Planetary Science Letters, 70: 221–236. doi:10.1016/0012-821X(84)90007-4

Gower, C.F., Krogh, T.E. 2002. A U-Pb geochronological review of the Proterozoic history of the eastern Grenville Province. Canadian Journal of Earth Sciences, 39: 795. doi:10.1139/e01-090.

Green, A.G., Milkereit, B., Davidson, A., Spencer, C., Hutchinson, D.R., Cannon, W.F., Lee, M.W., Agena, W.F., Behrendt, J.C., and Hinze, W.J. 1988. Crustal structure of the Grenville front and adjacent terranes. Geology, 16: 788. doi:10.1130/0091-7613(1988)016<0788:CSOTGF>2.3.CO;2.

Greenough, J.D., Owen, J. V. 1995. The role of subcontinental lithospheric mantle in massif-type petrogenesis: evidence from the Red Bay pluton, Labrador. Schweizerische Mineralogische und Petrographische Mitteilungen, 75: 1–15. Available from: http://dx.doi.org/10.5169/seals-57141.

Griffin, W.L., O'Reilly, S.Y., Afonso, J.C., Begg, G.C. 2009. The composition and evolution of lithospheric mantle: a re-evaluation and its tectonic implications. Journal of Petrology, 50: 1185–1204. doi:10.1093/petrology/egn033.

Halls, H.C. 2015. Paleomagnetic evidence for ~4000 km of crustal shortening across the 1 Ga Grenville orogen of North America. Geology, G37188.1. doi:10.1130/G37188.1.

Harmon, R.S., and Hoefs, J. 1995. Oxygen isotope heterogeneity of the mantle deduced from global 18O systematics of basalts from different geotectonic settings. Contributions to Mineralogy and Petrology, 120: 95–114. doi:10.1007/BF00311010.

Hauer, K.L. 1995. Protoliths, diagenesis, and depositional history of the upper marble, Adirondack Lowlands, New York. Ph.D Thesis. Miami University (Oxford, Ohio).

Hawkesworth, C.J., Kempton, P.D., Rogers, N.W., Ellam, R.M., van Calsteren, P.W. 1990. Continental mantle lithosphere, and shallow level enrichment processes in

the Earth's mantle. Earth and Planetary Science Letters, 96: 256–268. doi:10.1016/0012-821X(90)90006-J.
Hébert, C., Van Breemen, O., Cadieux, A.-M. 2009. Région du réservoir Pipmuacan, (SNRC 22E) : synthèse géologique. Ministére des Ressources naturelles et de la Faune, Quebec, RG 2009-01: 1–56. Available from: http://collections.banq.qc.ca/ark:/52327/bs1940773.
Higgins, M.D., Ider, M., and Breemen, O. van. 2002. U-Pb ages of plutonism, wollastonite formation, and deformation in the central part of the Lac-Saint-Jean anorthosite suite. Canadian Journal of Earth Sciences, 39: 1093–1105. doi:10.1139/e02-033.
Hirose, K., Kushiro, I. 1993. Partial melting of dry peridotites at high pressures: determination of compositions of melts segregated from peridotite using aggregates of diamond. Earth and Planetary Science Letters, 114(4): 477-489. doi:10.1016/0012-821X(93)90077-M.
Hoernle, K., Tilton, G., Le Bas, M.J., Duggen, S., and Garbe-Schönberg, D. 2002. Geochemistry of oceanic carbonatites compared with continental carbonatites: mantle recycling of oceanic crustal carbonate. Contributions to Mineralogy and Petrology, 142: 520–542. doi:10.1007/s004100100308. http://gq.mines.gouv.qc.ca/documents/EXAMINE/MB201604/MB201604.pdf.
Hunt, L., Stachel, T., Grutter, H., Armstrong, J., McCandless, T.E., Simonetti, A., and Tappe, S. 2012. Small mantle fragments from the Renard Kimberlites, Quebec: powerful recorders of mantle lithosphere formation and modification beneath the Eastern Superior Craton. Journal of Petrology, 53: 1597–1635. doi:10.1093/petrology/egs027.
Hynes, A., Indares, A., Rivers, T., Gobeil, A. 2000. Lithoprobe line 55: integration of out-of-plane seismic results with surface structure, metamorphism, and geochronology, and the tectonic evolution of the eastern Grenville Province. Canadian Journal of Earth Sciences, 37: 341–358. doi:10.1139/e99-076.
Hynes, A., Rivers, T. 2010. Protracted continental collision – evidence from the Grenville Orogen. Canadian Journal of Earth Sciences, 47: 591–620. doi:10.1139/E10-003.
Indares, A. 1997. Garnet-kyanite clinopyroxenites and garnet-kyanite restites from the Manicouagan Imbricate Zone: a case of high-P - High-T metamorphism in the Grenville Province. Canadian Mineralogist, 35: 1161–1171.
Indares, A., Dunning, G. 2004. Crustal architecture above the high-pressure belt of the Grenville Province in the Manicouagan area: new structural, petrologic and U-Pb age constraints. Precambrian Research, 130: 199–228. doi:10.1016/j.precamres.2003.11.005
Indares, A., Dunning, G., and Cox, R. 2000. Tectono-thermal evolution of deep crust in a Mesoproterozoic continental collision setting: the Manicouagan example. Canadian Journal of Earth Sciences, 37: 325–340. doi:10.1139/cjes-37-2-3-325.
Indares, A., Dunning, G., Cox, R., Gale, D., Connelly, J. 1998. High-pressure, high-temperature rocks from the base of thick continental crust: geology and age constraints from the Manicouagan Imbricate Zone, eastern Grenville Province. Tectonics, 17: 426–440. doi:10.1029/98TC00373; doi:10.1029/9.
Indares, A., Moukhsil, A. 2013. Geon 12 crustal extension in the central Grenville Province, implications for the orogenic architecture, and potential influence on

the emplacement of anorthosites. Canadian Journal of Earth Sciences, 50: 955–966. NRC Research Press. doi:10.1139/cjes-2012-0161.
Indares, A., White, R.W., Powell, R. 2008. Phase equilibria modelling of kyanite-bearing anatectic paragneisses from the central Grenville Province. Journal of Metamorphic Geology, 26: 815–836. doi:10.1111/j.1525-1314.2008.00788.x.
Ionov, D.A., Dupuy, C., O'reilly, S.Y., Kopylova, M.G., Genshaft, Y.S. 1993. Carbonated peridotite xenoliths from Spitsbergen: implications for trace element signature of mantle carbonate metasomatism. Earth and Planetary Science Letters, 119: 283–297. doi:10.1016/0012-821X(93)90139-Z
Ionov, D.A., Griffin, W.L., O'Reilly, S.Y. 1997. Volatile-bearing minerals and lithophile trace elements in the upper mantle. Chemical Geology, 141:153-184. doi:10.1016/S0009-2541(97)00061-2.
Jacobsen, S.B., Pimentel-Klose, M.R. 1988. Nd isotopic variations in Precambrian banded iron formations. Geophysical Research Letters, 15: 393–396. Wiley-Blackwell. doi:10.1029/GL015i004p00393.
James, D.E. 1981. The combined use of oxygen and radiogenic isotopes as indicators of crustal contamination. Annual Review of Earth and Planetary Sciences, 9: 311–344. doi:10.1146/annurev.ea.09.050181.001523.
Jamieson, R.A., and Beaumont, C. 2011. Coeval thrusting and extension during lower crustal ductile flow - implications for exhumation of high-grade metamorphic rocks. Journal of Metamorphic Geology, 29: 33–51. doi:10.1111/j.1525-1314.2010.00908.x.
Jamieson, R.A., Beaumont, C., Nguyen, M.H., Culshaw, N.G. 2007. Synconvergent ductile flow in variable-strength continental crust: numerical models with application to the western Grenville orogen. Tectonics, 26: 1–23. doi:10.1029/2006TC002036
Jamieson, R.A., Beaumont, C., Warren, C.J., and Nguyen, M.H. 2010. The Grenville Orogen explained? Applications and limitations of integrating numerical models with geological and geophysical data. Canadian Journal of Earth Sciences, 47: 517–539. doi:10.1139/E09-070.
Jannin, S., Gervais, F., Moukhsil, A., Augland, L.E. 2018a. Late-Grenvillian channel flow in the central Grenville Province (Manicouagan Reservoir area): new constraints from a structural and geochronological study of the Allochthon Boundary Thrust. Journal of Structural Geology, 115: 132–151. doi:10.1016/j.jsg.2018.07.019.
Jannin, S., Gervais, F., Moukhsil, A., Augland, L.E., Crowley, J.L. 2018b. Déformations tardi-grenvilliennes dans la ceinture parautochtone (Province de Grenville centrale) : contraintes géochronologiques par couplage de méthodes U–Pb de haute résolution spatiale et de haute précision. Canadian Journal of Earth Sciences, 55: 406–435. doi:10.1139/cjes-2017-0129.
Jordan, S.L., Indares, A., Dunning, G. 2006. Partial melting of metapelites in the Gagnon terrane below the high-pressure belt in the Manicouagan area (Grenville Province): pressure–temperature (P–T) and U–Pb age constraints and implications. Canadian Journal of Earth Sciences, 43: 1309–1329. doi:10.1139/e06-038.
Kerr, A.C., Kempton, P.D., and Thompson, R.N. 1995. Crustal assimilation during turbulent magma ascent (ATA); new isotopic evidence from the Mull Tertiary

lava succession, N. W. Scotland. Contributions to Mineralogy and Petrology, 119: 142–154. doi:10.1007/BF00307277.

Kramers, J.D., Roddick, J.C.M., Dawson, J.B. 1983. Trace element and isotope studies on veined, metasomatic and "MARID" xenoliths from Bultfontein, South Africa. Earth and Planetary Science Letters, 65: 90–106. Elsevier. doi:10.1016/0012-821X(83)90192-9.

Krmíček, L., Cempírek, J., Havlín, A., Přichystal, A., Houzar, S., Krmíčková, M., Gadas, P. 2011. Mineralogy and petrogenesis of a Ba–Ti–Zr-rich peralkaline dyke from Šebkovice (Czech Republic): recognition of the most lamproitic Variscan intrusion. Lithos, 121: 74–86. doi:10.1016/J.LITHOS.2010.10.005.

Kuehner, S.M. 1980. Petrogenesis of ultrapotassic rocks, Leucite Hills, Wyoming. MSc. Thesis. University of Western Ontario, London, Ontario.

Kwon, S.T., Tilton, G.R., Griinenfelder, M.H. 1989. Pb isotope relationships in carbonatites and alkalic complexes: an overview. *In* Carbonatites - Genesis and Evolution. *Edited by* K. Bell. Unwin-Hyman, London. pp. 360–387.

Kyser, T.K. 1990. Stable isotopes in the continental lithospheric mantle. *In* Continental Mantle. *Edited by* M.A. Menzies. Oxford monographs on geology and geophysics. pp. 127–156.

Laflèche, M.R., Camiré, G., Jenner, G.A. 1998. Geochemistry of post-Acadian, Carboniferous continental intraplate basalts from the Maritimes Basin, Magdalen Islands, Quebec, Canadá. Chemical Geology, 148: 115–136. doi:10.1016/S0009-2541(98)00002-3.

Laflèche, M.R., Dupuy, C., and Bougault, H. 1992. Geochemistry and petrogenesis of Archean mafic volcanic rocks of the southern Abitibi Belt, Québec. Precambrian Research, 57: 207–241. doi:10.1016/0301-9268(92)90003-7.

Laflèche, M.R.R., Dupuy, C., and Dostal, J. 1991. Archaean orogenic ultrapotassic magmatism: an example from the southern Abitibi greenstone belt. Precambrian Research, 52: 71–96. Elsevier. doi:10.1016/0301-9268(91)90014-2.

Lasalle, S., Dunning, G., Indares, A., McFarlane, C. 2014. In situ LA–ICP–MS dating of monazite from aluminous gneisses: insights on the tectono-metamorphic history of a granulite-facies domain in the central Grenville Province. Canadian Journal of Earth Sciences, 51: 558–572. doi:10.1139/cjes-2013-0170

Lasalle, S., Fisher, C.M., Indares, A., Dunning, G. 2013. Contrasting types of Grenvillian granulite facies aluminous gneisses: insights on protoliths and metamorphic events from zircon morphologies and ages. Precambrian Research, 228: 117–130. doi:10.1016/j.precamres.2013.01.014

Lasalle, S., Indares, A. 2014. Anatectic record and contrasting P–T paths of aluminous gneisses from the central Grenville Province. Journal of Metamorphic Geology, 32: 627–646. doi:10.1111/jmg.12083

LaTourrette, T., Hervig, R.L., Holloway, J.R. 1995. Trace element partitioning between amphibole, phlogopite, and basanite melt. Earth and Planetary Science Letters, 135:13-30. doi:10.1016/0012-821X(95)00146-4.

Le Bas, M.J., Maitre, R.W.L., Streckeisen, A., Zanettin, B. 1986. A chemical classification of volcanic rocks based on the total alkali-silica diagram. Journal of Petrology, 27: 745–750. doi:10.1093/petrology/27.3.745.

Liu, D., Zhao, Z., Zhu, D.-C., Niu, Y., DePaolo, D.J., Harrison, T.M., Mo, X., Dong, G., Zhou, S., Sun, C., Zhang, Z., and Liu, J. 2014. Postcollisional potassic and ultrapotassic rocks in southern Tibet: mantle and crustal origins in response to

India–Asia collision and convergence. Geochimica et Cosmochimica Acta, 143: 207–231. doi:10.1016/j.gca.2014.03.031.
Loewy, S.L., Connelly, J.N., Dalziel, I.W., and Gower, C.F. 2003. Eastern Laurentia in Rodinia: constraints from whole-rock Pb and U/Pb geochronology. Tectonophysics, 375: 169–197. doi:10.1016/S0040-1951(03)00338-X.
Ludden, J., and Hynes, A. 2000. The Lithoprobe Abitibi-Grenville transect: two billion years of crust formation and recycling in the Precambrian Shield of Canada. Canadian Journal of Earth Sciences, 37: 2-3. doi:10.1139/e99-120.
Lustrino, M., Agostini, S., Chalal, Y., Fedele, L., Stagno, V., Colombi, F., and Bouguerra, A. 2016. Exotic lamproites or normal ultrapotassic rocks? The Late Miocene volcanic rocks from Kef Hahouner, NE Algeria, in the frame of the circum-Mediterranean lamproites. Journal of Volcanology and Geothermal Research, 327: 539–553. doi:10.1016/J.JVOLGEORES.2016.09.021.
Maity, B., and Indares, A. 2018. The Geon 14 arc-related mafic rocks from the central Grenville Province. Canadian Journal of Earth Sciences, 55: 545–570. doi:10.1139/cjes-2017-0197.
Mattey, D., Lowry, D., and Macpherson, C. 1994. Oxygen isotope composition of mantle peridotite. Earth and Planetary Science Letters, 128: 231–241. doi:10.1016/0012-821X(94)90147-3.
McCulloch, M.T., and Wasserburg, G.J. 1978. Sm-Nd and Rb-Sr Chronology of Continental Crust Formation. Science, 200: 1003–1011. doi:10.1126/science.200.4345.1003.
McDonough, W.F. 1990. Constraints on the composition of the continental lithospheric mantle. Earth and Planetary Science Letters, 101: 1–18. doi:10.1016/0012-821X(90)90119-I.
McKenzie, D. 1989. Some remarks on the movement of small melt fractions in the mantle. Earth and Planetary Science Letters, 95: 53–72. doi:10.1016/0012-821X(89)90167-2.
McLennan, S., Taylor, S., McCulloch, M., and Maynard, J. 1990. Geochemical and Nd-Sr isotopic composition of deep-sea turbidites: crustal evolution and plate tectonic associations. Geochimica et Cosmochimica Acta, 54: 2015–2050. doi:10.1016/0016-7037(90)90269-Q.
Melzer, S., Gottschalk, M., Heinrich, W. 1998. Experimentally determined partitioning of Rb between richterites and aqueous (Na, K)-chloride solutions. Contributions to Mineralogy and Petrology, 133: 315–328. doi:10.1007/s004100050455.
Melzer, S., Wunder, B. 2001. K–Rb–Cs partitioning between phlogopite and fluid: experiments and consequences for the LILE signatures of island arc basalts. Lithos, 59: 69–90. doi:10.1016/S0024-4937(01)00061-5
Menzies, M.A., Hawkesworth, C.J. 1987. Upper mantle processes and composition. *In* Mantle Xenolith. *Edited by* P.H. Nixon. John Wiley and Sons, Chichester, pp. 725-738.
Miller, C., Schuster, R., Klötzli, U., Frank, W., Purtscheller, F. 1999. Post-collisional potassic and ultrapotassic magmatism in SW Tibet: geochemical and Sr-Nd-Pb-O isotopic constraints for mantle source characteristics and petrogenesis. Journal of Petrology, 40: 1399–1424. doi:10.1093/petroj/40.9.1399.
Mirnejad, H., Bell, K. 2006. Origin and source evolution of the Leucite Hills lamproites: evidence from Sr-Nd-Pb-O isotopic compositions. Journal of Petrology, 47: 2463–2489. doi:10.1093/petrology/egl051.

Möller, C., and Andersson, J. 2018. Metamorphic zoning and behaviour of an underthrusting continental plate. Journal of Metamorphic Geology, 36: 567–589. doi:10.1111/jmg.12304.

Morin, D., Hébert, R., Corriveau, L. 2005. Mesoproterozoic deep K-magmatism recorded in a megacryst- and xenolith-bearing minette dyke, western Grenville Province. Canadian Journal of Earth Sciences, 42: 1881–1906. doi:10.1139/e05-083.

Moukhsil, A., Solgadi, F., Lacoste, P., Gagnon, M., David, J. 2012. Géologie de la région du lac du Milieu (SNRC 22O03, 22O04, 22O06, 22J13 et 22J14), RG 2012-01. Available from: http://collections.banq.qc.ca/ark:/52327/bs2108637.

Moukhsil, A., Solgadi, F., Thomas, C., Séverine, B., Indares, A., Davis, D.W. 2013. Géologie du nord-ouest de la région du barrage Daniel-Johnson (Manic 5), Côte-Nord. Available from: http://collections.banq.qc.ca/ark:/52327/bs2272082.

Moumblow, R.M., Arcuri, G.A., Dickin, A.P., and Gower, C.F. 2019. Nd and Pb isotope mapping of crustal domains within the Makkovik Province, Labrador. Geological Magazine, 156: 833–848. doi:10.1017/S0016756818000195.

Murphy, D.T., Collerson, K.D., Kamber, B.S. 2002. Lamproites from Gaussberg, Antarctica: possible transition zone melts of Archaean subducted sediments. Journal of Petrology, 43: 981–1001. doi:10.1093/petrology/43.6.981.

Nelson, D.R. 1989. Isotopic characteristics and petrogenesis of the lamproites and kimberlites of central west Greenland. Lithos, 22: 265–274. doi:10.1016/0024-4937(89)90029-7.

Nelson, D.R. 1992. Isotopic characteristics of potassic rocks: evidence for the involvement of subducted sediments in magma genesis. Lithos, 28: 403–420. doi:10.1016/0024-4937(92)90016-R.

Owens, B.E., Dymek, R.F., Tucker, R.D., Brannon, J.C., Podosek, F.A. 1994. Age and radiogenic isotopic composition of a late- to post-tectonic anorthosite in the Grenville Province: the Labrieville massif, Quebec. Lithos, 31: 189–206. doi:10.1016/0024-4937(94)90009-4.

Owens, B.E., Tomascak, P.B. 2002. Mesoproterozoic lamprophyres in the Labrieville Massif, Quebec: clues to the origin of alkalic anorthosites? Canadian Journal of Earth Sciences, 39: 983–997. doi:10.1139/e02-010.

Patrick, M.E., Indares, A. 2017. Petrography and phase equilibria modeling of mid-P aluminous gneisses derived from hydrothermally altered protoliths, Grenville Province, Canada. Canadian Journal of Earth Sciences, 54: 1103–1118. doi:10.1139/cjes-2016-0162.

Pearce, J.A., and Parkinson, I.J. 1993. Trace element models for mantle melting: application to volcanic arc petrogenesis. Geological Society, London, Special Publications, 76: 373–403. doi:10.1144/GSL.SP.1993.076.01.19.

Peck, W.H., Clechenko, C.C., Hamilton, M.A., and Valley, J.W. 2010. Oxygen isotopes in the Grenville and Nain AMCG suites: regional aspects of the crustal component in massif anorthosites. The Canadian Mineralogist, 48: 763–786. doi:10.3749/canmin.48.4.763.

Peck, W.H., Valley, J.W. 2000. Large crustal input to high δ18O anorthosite massifs of the southern Grenville Province: new evidence from the Morin Complex, Quebec. Contributions to Mineralogy and Petrology, 139: 402–417. doi:10.1007/s004100000149.

Percival, J.A., Skulski, T., Sanborn-Barrie, M., Stott, G.M., Leclair, A.D., Corkery, M.T., Boily, M. 2012. Geology and tectonic evolution of the Superior Province, Canada. Chapter 6 *In* Tectonic Styles in Canada: The Lithoprobe Perspective. *Edited by* J.A. Percival, F.A. Cook, and R.M. Clowes. Geological Association of Canada, Special Paper 49, pp. 321–378.

Peterson, T.D., Esperança, S., and LeCheminant, A.N. 1994. Geochemistry and origin of the Proterozoic ultrapotassic rocks of the Churchill Province, Canada. Mineralogy and Petrology, 51: 251–276. doi:10.1007/BF01159732.

Petrescu, L., Bastow, I.D., Darbyshire, F.A., Gilligan, A., Bodin, T., Menke, W., and Levin, V. 2016. Three billion years of crustal evolution in eastern Canada: Constraints from receiver functions. Journal of Geophysical Research: Solid Earth, 121: 788–811. doi:10.1002/2015JB012348.

Pfänder, J.A., Jung, S., Münker, C., Stracke, A., Mezger, K. 2012. A possible high Nb/Ta reservoir in the continental lithospheric mantle and consequences on the global Nb budget – evidence from continental basalts from Central Germany. Geochimica et Cosmochimica Acta, 77: 232–251. doi:10.1016/J.GCA.2011.11.017.

Plank, T., Langmuir, C.H. 1998. The chemical composition of subducting sediment and its consequences for the crust and mantle. Chemical Geology, 145: 325–394. doi:10.1016/S0009-2541(97)00150-2

Prelević, D., Akal, C., Foley, S.F., Romer, R.L., Stracke, A., Van den Bogaard, P. 2012. Ultrapotassic mafic rocks as geochemical proxies for post-collisional dynamics of orogenic lithospheric mantle: the case of Southwestern Anatolia, Turkey. Journal of Petrology, 53: 1019–1055. doi:10.1093/petrology/egs008.

Rivers, T. 1980. Revised stratigraphic nomenclature for Aphebian and other rock units, southern Labrador Trough, Grenville Province. Canadian Journal of Earth Sciences, 17: 668–670. NRC Research Press Ottawa, Canada. doi:10.1139/e80-062.

Rivers, T. 1983a. The northern margin of the Grenville Province in western Labrador – anatomy of an ancient orogenic front. Precambrian Research, 22: 41–73. doi:10.1016/0301-9268(83)90058-X

Rivers, T. 1983b. Progressive metamorphism of pelitic and quartzofeldspathic rocks in the Grenville Province of western Labrador – tectonic implications of bathozone 6 assemblages. Canadian Journal of Earth Sciences, 20: 1791–1804. doi:10.1139/e83-171

Rivers, T. 1997. Lithotectonic elements of the Grenville Province: review and tectonic implications. Precambrian Research, 86: 117–154. doi:10.1016/S0301-9268(97)00038-7

Rivers, T. 2008. Assembly and preservation of lower, mid, and upper orogenic crust in the Grenville Province—implications for the evolution of large hot long-duration orogens. Precambrian Research, 167: 237–259. doi:10.1016/j.precamres.2008.08.005.

Rivers, T. 2009. The Grenville Province as a large hot long-duration collisional orogen - insights from the spatial and thermal evolution of its orogenic fronts. Geological Society, London, Special Publications, 327: 405–444. doi:10.1144/SP327.17.

Rivers, T. 2015. Tectonic Setting and Evolution of the Grenville Orogen: An Assessment of Progress Over the Last 40 Years. Geoscience Canada, 42: 77–124. doi:10.12789/geocanj.2014.41.057.

Rivers, T., Culshaw, N., Hynes, A., Indares, A., Jamieson, R., Martignole, J. 2012. The Grenville Orogen–a post-Lithoprobe perspective. *In* Tectonic Styles in Canada: the Lithoprobe perspective. *Edited by* J.A. Percival, F.A. Cook, and R.M. Clowes. Geological Association of Canada, Special Paper. pp. 97–236.

Rivers, T., Gool, J.A.M. van, Connelly, J.N. 1993. Contrasting tectonic styles in the northern Grenville province: implications for the dynamics of orogenic fronts. Geology, 21: 1127. doi:10.1130/0091-7613(1993)021<1127:CTSITN>2.3.CO;2

Rivers, T., Martignole, J., Gower, C.F., and Davidson, A. 1989. New tectonic divisions of the Grenville Province, Southeast Canadian Shield. Tectonics, 8: 63–84. doi:10.1029/TC008i001p00063.

Rudnick, R.L., Gao, S. 2014. 4.1 – Composition of the Continental Crust. *In* Treatise on Geochemistry (2nd ed.), 4:1–51. doi:10.1016/B978-0-08-095975-7.00301-6.

Rudnick, R.L., McDonough, W.F., Chappell, B.W. 1993. Carbonatite metasomatism in the northern Tanzanian mantle: petrographic and geochemical characteristics. Earth and Planetary Science Letters, 114: 463–475. doi:10.1016/0012-821X(93)90076-L.

Ryerson, F.J., and Watson, E.B. 1987. Rutile saturation in magmas: implications for Ti-Nb-Ta depletion in island-arc basalts. Earth and Planetary Science Letters, 86: 225–239. doi:10.1016/0012-821X(87)90223-8.

Schärer, U. 1991. Rapid continental crust formation at 1.7 Ga from a reservoir with chondritic isotope signatures, eastern Labrador. Earth and Planetary Science Letters, 102: 110–133. doi:10.1016/0012-821X(91)90002-Y.

Schmidt, K.H., Bottazzi, P., Vannucci, R., and Mengel, K. 1999. Trace element partitioning between phlogopite, clinopyroxene and leucite lamproite melt. Earth and Planetary Science Letters, 168: 287–299. doi:10.1016/S0012-821X(99)00056-4.

Scott, D.J., Hynes, A. 1994. U-Pb geochronology along the Manicouagan corridor, preliminary results: evidence for ca. 1.47 Ga metamorphism. Lithoprobe Abitibi-Grenville Transect. Lithoprobe Report, 41: 109–110.

Shieh, Y.-N., Schwarcz, H.P. 1978. The oxygen isotope composition of the surface crystalline rocks of the Canadian Shield. Canadian Journal of Earth Sciences, 15: 1773–1782. doi:10.1139/e78-185.

Smith, C.B. 1983. Pb, Sr and Nd isotopic evidence for sources of southern African Cretaceous kimberlites. Nature, 304: 51–54. doi:10.1038/304051a0.

Solgadi, F., Groulier, P.-A., Moukhsil, A., Ohnenstetter, D., André-Mayer, A.-S., and Zeh, A., 2015. Nb-Ta-REE mineralization associated with the Crevier alkaline intrusion. *In* Symposium on Strategic and Critical Materials Proceedings, *Edited by* Simandl, G.J. and Neetz, M. November 13-14, 2015, Victoria, British Columbia. British Columbia Ministry of Energy and Mines, British Columbia Geological Survey Paper 2015-3, pp. 69-74.

Spencer, C.J., Cawood, P. a., Hawkesworth, C.J., Prave, A.R., Roberts, N.M.W., Horstwood, M.S. a., and Whitehouse, M.J. 2015. Generation and preservation of continental crust in the Grenville Orogeny. Geoscience Frontiers, 6: 357–372. doi:10.1016/j.gsf.2014.12.001.

Stacey, J.S., Kramers, J.D. 1975. Approximation of terrestrial lead isotope evolution by a two-stage model. Earth and Planetary Science Letters, 26: 207–221. doi:10.1016/0012-821X(75)90088-6.

Stevenson, R., Henry, P., Gariépy, C. 1999. Assimilation–fractional crystallization origin of Archean sanukitoid suites: western Superior Province, Canada. Precambrian Research, 96: 83–99. doi:10.1016/S0301-9268(99)00009-1.

Sun, S. -s., McDonough, W.F. 1989. Chemical and isotopic systematics of oceanic basalts: implications for mantle composition and processes. Geological Society, London, Special Publications, 42: 313–345. doi:10.1144/GSL.SP.1989.042.01.19.

Sun, Y., Ying, J., Zhou, X., An Shao, J., Chu, Z., Su, B. 2014. Geochemistry of ultrapotassic volcanic rocks in Xiaogulihe NE China: implications for the role of ancient subducted sediments. Lithos, 208–209: 53-66. doi:10.1016/j.lithos.2014.08.026.

Tappe, S., Foley, S.F., Stracke, A., Romer, R.L., Kjarsgaard, B.A., Heaman, L.M., and Joyce, N. 2007. Craton reactivation on the Labrador Sea margins: 40Ar/39Ar age and Sr–Nd–Hf–Pb isotope constraints from alkaline and carbonatite intrusives. Earth and Planetary Science Letters, 256: 433–454. doi:10.1016/J.EPSL.2007.01.036.

Tatsumoto, M., Knight, R.J., Allegre, C.J. 1973. Time differences in the formation of meteorites as determined from the ratio of Lead-207 to Lead-206. Science, 180: 1279–1283. doi:10.1126/science.180.4092.1279.

Taylor, H.P. 1968. The oxygen isotope geochemistry of igneous rocks. Contributions to Mineralogy and Petrology, 19: 1–71. doi:10.1007/BF00371729.

Taylor, H.P., Giannetti, B., and Turi, B. 1979. Oxygen isotope geochemistry of the potassic igneous rocks from the Roccamonfina volcano, Roman comagmatic region, Italy. Earth and Planetary Science Letters, 46: 81–106. doi:10.1016/0012-821X(79)90067-0.

Thirlwall, M.F., Upton, B.G.J., Jenkins, C. 1994. Interaction between continental lithosphere and the Iceland plume – Sr-Nd-Pb isotope geochemistry of Tertiary basalts, NE Greenland. Journal of Petrology, 35: 839–879. doi:10.1093/petrology/35.3.839.

Thompson, R., Leat, P., Dickin, A.P., Morrison, M., Hendry, G., Gibson, S. 1990. Strongly potassic mafic magmas from lithospheric mantle sources during continental extension and heating: evidence from Miocene minettes of northwest Colorado, U.S.A. Earth and Planetary Science Letters, 98: 139–153. doi:10.1016/0012-821X(90)90055-3.

Thomson, S.D., Dickin, A.P., Spray, J.G. 2011. Nd isotope mapping of Grenvillian crustal terranes in the vicinity of the Manicouagan Impact Structure. Precambrian Research, 191: 184–193. doi:10.1016/j.precamres.2011.08.006.

Tiepolo, M., Vannucci, R., Bottazzi, P., Oberti, R., Zanetti, A., and Foley, S. 2000. Partitioning of rare earth elements, Y, Th, U, and Pb between pargasite, kaersutite, and basanite to trachyte melts: implications for percolated and veined mantle. Geochemistry, Geophysics, Geosystems, 1. doi:10.1029/2000GC000064.

Tilton, G.R. 1983. Evolution of depleted mantle: the lead perspective. Geochimica et Cosmochimica Acta, 47: 1191–1197. doi:10.1016/0016-7037(83)90061-3.

Tilton, G.R., Bell, K. 1994. Sr-Nd-Pb isotope relationships in Late Archean carbonatites and alkaline complexes: applications to the geochemical evolution of Archean mantle. Geochimica et Cosmochimica Acta, 58: 3145–3154. doi:10.1016/0016-7037(94)90042-6.

Tollo, R., Corriveau, L., McLelland, J., Bartholomew, M. 2004. Proterozoic tectonic evolution of the Grenville orogen in North America: an introduction. *In* Proterozoic tectonic evolution of the Grenville Orogen in North America. *Edited by* R.P. Tollo, L. Corriveau, J. McLelland, and M.J. Bartholomew. GSA Memoirs, 197(03): 1-18.

Turlin, F., André-Mayer, A.-S., Moukhsil, A., Vanderhaeghe, O., Gervais, F., Solgadi, F., Groulier, P.-A., Poujol, M. 2017. Unusual LREE-rich, peraluminous, monazite- or allanite-bearing pegmatitic granite in the central Grenville Province, Québec. Ore Geology Reviews, 89: 627–667. doi:10.1016/j.oregeorev.2017.04.019

Turlin, F., Vanderhaeghe, O., Gervais, F., André-Mayer, A.-S., Moukhsil, A., Zeh, A., Solgadi, F., I.P.T.N. 2019. Petrogenesis of LREE-rich pegmatitic granite dykes in the central Grenville Province by partial melting of Paleoproterozoic-Archean metasedimentary rocks: evidence from zircon U-Pb-Hf-O isotope and trace element analyses. Precambrian Research, 327: 327-360. doi:10.1016/j.precamres.2019.02.009.

Turner, S., and Hawkesworth, C. 1995. The nature of the sub-continental mantle: constraints from the major-element composition of continental flood basalts. Chemical Geology, 120: 295–314. doi:10.1016/0009-2541(94)00143-V.

Turner, S., Arnaud, N., Liu, J., Rogers, N., Hawkesworth, C., Harris, N., Kelley, S., Van Calsteren, P., Deng, W. 1996. Post-collision, shoshonitic volcanism on the Tibetan Plateau: implications for convective thinning of the lithosphere and the source of Ocean Island Basalts. Journal of Petrology, 37: 45–71. doi:10.1093/petrology/37.1.45.

Valley, J.W., Lackey, J.S., Cavosie, A.J., Clechenko, C.C., Spicuzza, M.J., Basei, M.A.S., Bindeman, I.N., Ferreira, V.P., Sial, A.N., King, E.M., Peck, W.H., Sinha, A.K., Wei, C.S. 2005. 4.4 billion years of crustal maturation: oxygen isotope ratios of magmatic zircon. Contributions to Mineralogy and Petrology, 150: 561–580. doi:10.1007/s00410-005-0025-8.

Valverde Cardenas, C. 2009. Geochemical constraints on the origin of mafic and ultrapotassic dykes from the southern Manicouagan area, Grenville Province. Memorial University of Newfoundland. Available from: http://collections.mun.ca/PDFs/theses/Cardenas_CarolinaValverde.pdf.

Valverde Cardenas, C., Indares, A., Jenner, G. 2012. Mafic and ultrapotassic rocks from the Canyon domain (central Grenville Province): geochemistry and tectonic implications. Canadian Journal of Earth Sciences, 49: 412–433. doi:10.1139/e11-065.

van Gool, J.A.M., Rivers, T., Calon, T. 2008. Grenville Front zone, Gagnon terrane, southwestern Labrador: configuration of a midcrustal foreland fold-thrust belt. Tectonics, 27: 1–35. doi:10.1029/2006TC002095.

Vanderhaeghe, O. 2011. The thermal–mechanical evolution of crustal orogenic belts at convergent plate boundaries: a reappraisal of the orogenic cycle. Journal of Geodynamics, 56–57: 124–145. doi:10.1016/j.jog.2011.10.004.

Veizer, J., Compston, W. 1976. $^{87}Sr/^{86}Sr$ in Precambrian carbonates as an index of crustal evolution. Geochimica et Cosmochimica Acta, 40: 905–914. doi:10.1016/0016-7037(76)90139-3.

Veizer, J., Hoefs, J. 1976. The nature of O^{18}/O^{16} and C^{13}/C^{12} secular trends in sedimentary carbonate rocks. Geochimica et Cosmochimica Acta, 40: 1387–1395. doi:10.1016/0016-7037(76)90129-0.

Veizer, J., Hoefs, J., Lowe, D.R., Thurston, P.C. 1989. Geochemistry of Precambrian carbonates: II. Archean greenstone belts and Archean sea water. Geochimica et Cosmochimica Acta, 53: 859–871. doi:10.1016/0016-7037(89)90031-8.

Vervoort, J.D., and Blichert-Toft, J. 1999. Evolution of the depleted mantle: Hf isotope evidence from juvenile rocks through time. Geochimica et Cosmochimica Acta, 63: 533–556. doi:10.1016/S0016-7037(98)00274-9.

Vollmer, R. 1989. On the origin of the Italian potassic magmas: 1. A discussion contribution. Chemical Geology, 74: 229–239. doi:10.1016/0009-2541(89)90034-X.

Watson, E.B. 1980. Apatite and phosphorus in mantle source regions: an experimental study of apatite/melt equilibria at pressures to 25 kbar. Earth and Planetary Science Letters, 51: 322–335. doi:10.1016/0012-821X(80)90214-9.

Whalen, J.B., Percival, J.A., McNicoll, V.J., Longstaffe, F.J. 2002. A mainly crustal origin for tonalitic granitoid rocks, Superior Province, Canada: implications for late Archean tectonomagmatic processes. Journal of Petrology, 43: 1551–1570. doi:10.1093/petrology/43.8.1551.

Williams, H.M. 2004. Nature of the source regions for post-collisional, potassic magmatism in southern and northern Tibet from geochemical variations and inverse trace element modelling. Journal of Petrology, 45: 555–607. doi:10.1093/petrology/egg094.

Wilson, M., Bianchini, G. 1999. Tertiary-Quaternary magmatism within the Mediterranean and surrounding regions. *In* The Mediterranean Basins: Tertiary extension within the Alpine Orogen. *Edited by* B. Durand, L. Jolivet, F. Horváth, and M. Séranne. The Geological Society London, Geological Society Special Publication No. 156. pp. 141–168. Available from: https://sp.lyellcollection.org/content/specpubgsl/156/1/141.full.pdf.

Wilton, D.H.C. 1991. Metallogenic and tectonic implications of Pb isotope data for galena separates from the Labrador Central mineral belt. Economic Geology, 86: 1721–1736. doi:10.2113/gsecongeo.86.8.1721.

Woodhead, J.D., Hergt, J.M., Davidson, J.P., Eggins, S.M. 2001. Hafnium isotope evidence for 'conservative' element mobility during subduction zone processes. Earth and Planetary Science Letters, 192: 331–346. doi:10.1016/S0012-821X(01)00453-8.

Workman, R.K., and Hart, S.R. 2005. Major and trace element composition of the depleted MORB mantle (DMM). Earth and Planetary Science Letters, 231: 53–72. doi:10.1016/J.EPSL.2004.12.005.

Wyman, D.A., and Kerrich, R. 1993. Archean shoshonitic lamprophyres of the Abitibi Subprovince, Canada: petrogenesis, age, and tectonic setting. Journal of Petrology, 34: 1067–1109. doi:10.1093/petrology/34.6.1067.

Yang, P., and Indares, A.D. 2005. Mineral zoning, phase relations, and P-T evolution of high-pressure granulites from the Lelukuau terrane, northeastern Grenville Province, Quebec. The Canadian Mineralogist, 43: 443–462. doi:10.2113/gscanmin.43.1.443.

Yaxley, G.M., Crawford, A.J., and Green, D.H. 1991. Evidence for carbonatite metasomatism in spinel peridotite xenoliths from western Victoria, Australia.

Earth and Planetary Science Letters, 107: 305–317. doi:10.1016/0012-821X(91)90078-V.
Zartman, R.E., and Doe, B.R. 1981. Plumbotectonics—the model. Tectonophysics, 75: 135–162. doi:10.1016/0040-1951(81)90213-4.

Table 4.1. Major and trace element and Sr-Nd-Pb-O isotope data for potassic to ultrapotassic dykes, Canyon domain.

Sample no	RS351*	408	404	361-z	11-416*	209-2	398A	361	403(3)	462-z	338-z
Geol. Domain	Canyon	Canyon	Canyon	Canyon	Canyon	Canyon	Canyon	Canyon	Canyon	Canyon	Canyon
Groups	PUD1a	PUD1a	PUD1a	PUD1a	PUD1a	PUD1b	PUD1b	PUD1b	PUD2	PUD2	PUD2
SiO2	54.10	49.41	47.36	50.19	47.32	54.07	50.24	57.28	53.50	59.39	53.95
TiO2	2.14	2.36	3.25	1.98	2.05	2.59	2.05	2.42	2.49	2.05	1.50
Al2O3	15.23	16.85	12.78	14.36	15.86	15.38	12.92	15.15	10.79	12.73	11.96
Fe2O3	9.02	11.54	11.46	10.58	10.33	12.51	11.52	10.48	4.42	4.01	5.66
FeO*	8.12	10.38	10.31	9.52	9.29	11.26	10.37	9.43	3.98	3.61	5.09
MnO	0.11	0.14	0.13	0.10	0.15	0.22	0.15	0.15	0.08	0.06	0.09
MgO	3.55	5.02	7.45	6.05	5.64	5.37	10.99	3.18	6.80	4.84	6.42
CaO	6.62	7.20	9.07	5.92	6.52	7.76	7.37	5.52	6.42	3.86	6.49
Na2O	2.83	2.69	0.29	1.30	2.99	0.63	0.99	1.41	0.19	0.90	0.56
K2O	3.28	2.21	3.54	5.73	4.01	2.73	4.93	4.84	8.32	9.11	5.74
P2O5	0.84	0.89	2.30	1.15	1.17	1.99	1.45	1.48	4.80	2.34	4.07
LOI	1.34	1.22	1.57	1.25	1.09	1.92	1.46	1.81	1.13	0.92	2.21
Total	99.06	98.38	98.05	97.55	98.86	103.91	102.91	103.29	98.49	99.81	98.08
Na2O+K2O	6.11	4.90	3.83	7.03	7.00	3.36	5.92	6.25	8.51	10.01	6.30
K2O/Na2O	1.16	0.82	12.21	4.41	1.34	4.33	4.98	3.43	43.79	10.12	10.25
#Mg	44	46	56	53	52	46	65	38	75	71	69
Sc	14.0	21.0	22.0	17.0	20.0	20.0	20.0	14.0	7.0	11.0	4.0
V	121	142	164	169	193	143	166	136	65	62	34
Cr	30		98	145	80	64	638	52	270	169	151
Co	171	127	160	110	53	121	107	146	166	145	194
Ni	10	25	45	102	30	21	230	0	139	115	82
Cu	100				50	43					
Zn	130				110	213					
Ga	21				20	23					
Rb	104	65	97	216	152	77	153	103	193	263	245
Cs	0.25				0.9						
Sr	1727	1091	2456	1415	936	4301	1918	2618	6521	2889	2701
Ba	2999	2098	4771	5208	2650	7621	9017	6156	7117	3642	4960
Ti	12829	14148	19484	11870	12296	15527	12290	14508	14928	12290	8993
K	27227	18345	29386	47565	33287	22662	40924	40177	69064	75622	47648
Al	80597	89170	67632	75993	83931	81391	68373	80174	57101	67367	63292
Zr	245.0	355.0	709.0	408.0	369.0	391.0	348.0	330.0	911.0	382.0	191.0
Hf	6.8	8.8		10.2	8.5	9.0	8.8	7.9	19.3	12.1	6.2
Nb	11.0	18.0	29.0	23.0	23.0	20.2	16.7	20.9	28.0	38.0	13.0
Ta	0.70	0.80	1.20	1.30	2.00	1.06	0.84	1.15	1.00	2.10	0.90
Nb/Ta	15.7	22.5	24.2	17.7	11.5	19.0	19.9	18.2	28.0	18.1	14.4
Th	2.10	3.40	6.10	5.10	3.90	6.06	2.62	3.04	16.20	10.80	11.60
U	0.8	0.9	1.7	1.5	3.4	1.28	0.73	0.94	5.2	2.8	2.5
Pb	9				13						
Y	23	32.7	40.2	26.7	37	56	24	31	39	31.6	54
La	51.60	95.60	220.00	92.50	55.20	256.00	79.50	115.00	245.00	137.00	252.00
Ce	115	187	441	196	121	500	177	253	526	285	511
Pr	14.7	21.3	52.4	22.6	15.7	66.5	22.6	31.6	62.4	33.3	61.7
Nd	58.6	80.7	199	89	66.6	244	88.5	120	240	124	249
Sm	10.7	13.5	30.6	14.6	12.7	36.8	15	18.7	36.6	19.3	47.3
Eu	3.56	3.6	7.67	3.97	3.27	9.93	4.53	5.96	9.04	4.4	11.7
Gd	8.3	10.2	19.6	9.8	9.1	26.1	10.67	12.9	22.0	12.6	32.1
Tb	1.00	1.50	2.20	1.30	1.20	2.76	1.15	1.36	2.20	1.50	3.60
Dy	4.6	7.1	9.5	5.6	6.5	11.48	5.02	6.07	8.6	6.8	13.7
Ho	0.8	1.2	1.4	0.9	1.3	1.91	0.84	1.05	1.3	1.1	1.9
Er	2	3.5	3.5	2.7	3.8	4.78	1.99	2.62	3.7	3	4.6
Tm	0.27	0.47	0.45	0.37	0.57	0.63	0.25	0.35	0.52	0.39	0.54
Yb	1.6	2.9	2.8	2.4	3.8	3.93	1.46	2.09	3.7	2.3	3.3
Lu	0.23	0.4	0.37	0.35	0.57	0.57	0.2	0.29	0.65	0.3	0.46
ΣREE	273	429	990	442	301	1165	409	571	1162	631	1193
U-Pb (Ma)									980		
$^{147}Sm/^{144}Sm$	0.1051	0.0973			0.1120	0.0857	0.0965	0.0912	0.0876	0.0887	0.1087
$^{143}Nd/^{144}Nd$	0.511785	0.511853			0.511844	0.511560	0.511763	0.511672	0.511183	0.511224	0.511450
$^{143}Nd/^{144}Nd$ (t)	0.511109	0.511227			0.511124	0.511009	0.511143	0.511086	0.510620	0.510654	0.510751
εNd(t)	-5.1	-2.8			-4.8	-7.1	-4.5	-5.6	-14.7	-14	-12.1
T_{DM}	1753	1546			1783	1755	1652	1694	2243	2212	2309
T_{CR}	1924	1708			1966	1900	1812	1846	2379	2350	2472
$^{87}Sr/^{86}Sr$(t)	0.70394	0.704742	0.704844	0.704471	0.705053	0.703897	0.703839	0.704113	0.704283	0.704272	0.703925
εSr(t)	8	20	21	16	24	8	7	11	13	13	8
$^{206}Pb/^{204}Pb$	16.8704	17.006	17.1722	17.401	18.067	16.526	16.406	16.2840	16.768	16.5306	16.419
2σ	0.0005	0.001	0.0005	0.001	0.001	0.001	0.001	0.0005	0.001	0.0003	0.001
$^{207}Pb/^{204}Pb$	15.3759	15.438	15.4281	15.418	15.4211	15.3097	15.331	15.2976	15.125	15.1421	15.160
2σ	0.0005	0.002	0.0005	0.001	0.0004	0.0004	0.001	0.0005	0.001	0.0003	0.001
$^{208}Pb/^{204}Pb$	37.368	37.267	37.175	37.127	37.503	36.774	36.487	36.155	36.250	36.705	36.389
2σ	0.001	0.005	0.001	0.003	0.001	0.001	0.002	0.001	0.001	0.001	0.004
SK75 Age (207/206)	0.903	0.915	0.766	0.565	0.032	1.056	1.194	1.232	0.452	0.705	0.844
$\delta^{18}O$ (VSMOW ‰)	6.219	9.001				9.210	7.691		3.790	8.184	7.578

Note:

* indicates new samples, remaining data from Valverde Cardenas et al. (2012).

T_{DM} is calculated following DePaolo, 1981; T_{CR} is calculated following Goldstein et al. (1984).

SK 75, Stacey and Kramers (1975).

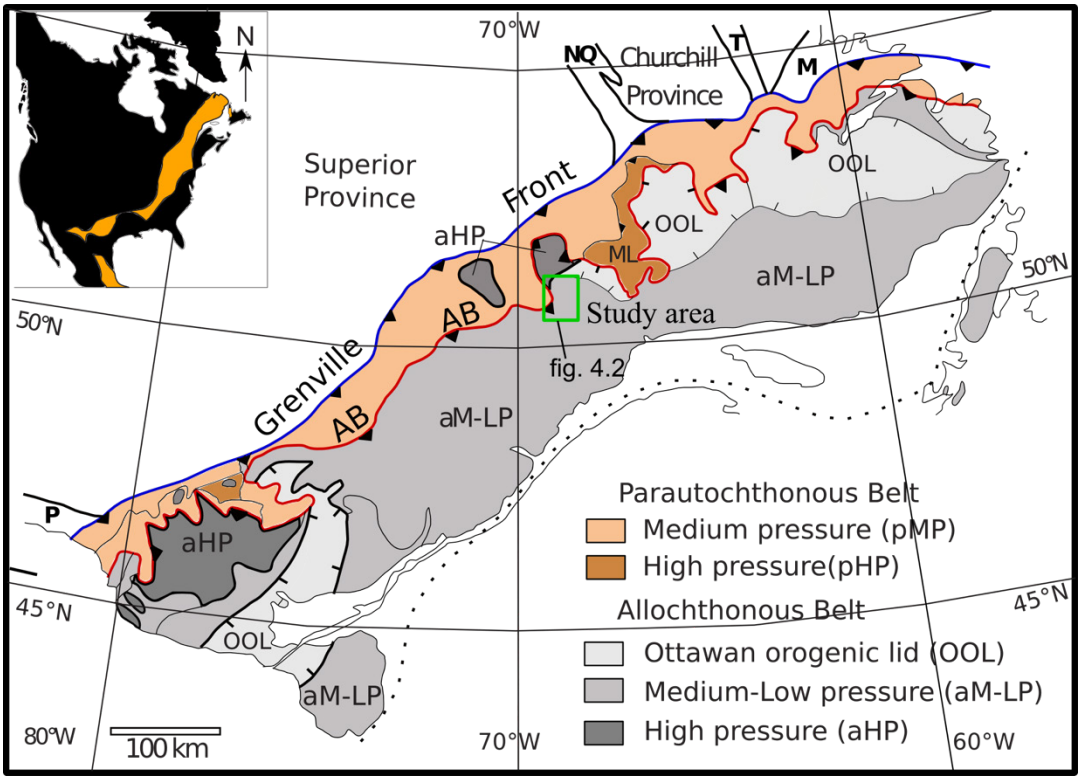

Figure 4.1. Major tectonic divisions of the Grenville Province (modified after Rivers et al., 2012). The orogen is composed of belts defined on the basis of tectonic characteristics, and belts are subdivided into terranes and domains. AB, allochthonous boundary, which worked both as thrust and normal fault; NQ, New Quebec Orogen; P, Penokean Orogen; M, Makkovik Orogen; and T, Torngat Orogen. Inset, Grenville Province in North America (Tollo et al., 2004).

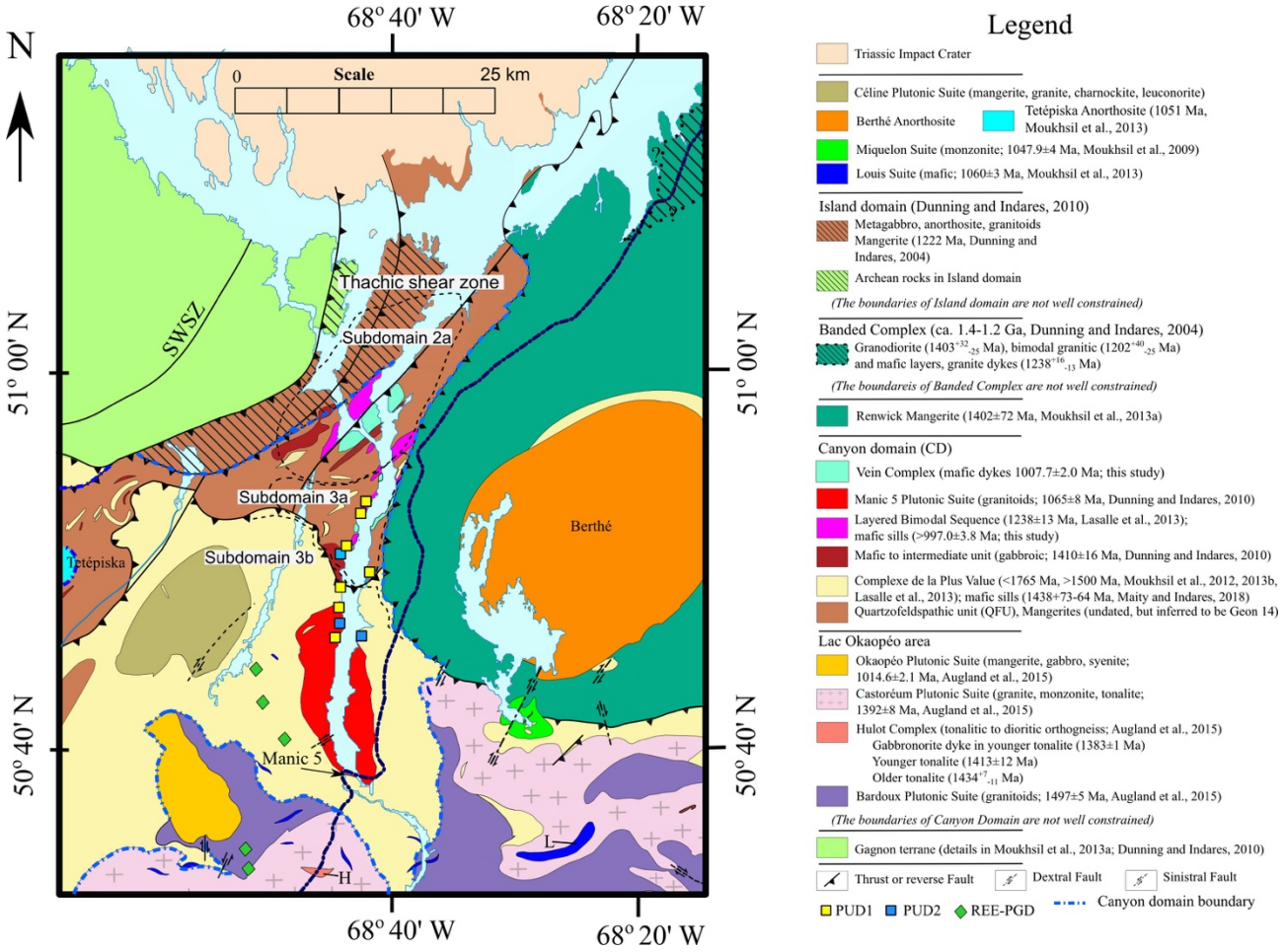

Figure 4.2. Geological map of the study area in the Canyon domain located to the south of the Manicouagan Impact Crater (modified from Maity and Indares, 2018); structural subdomains and the Thachic Shear Zone are shown (Jannin et al., 2018a, b); REE-PGD, REE-rich pegmatite granite dykes (Turlin et al., 2017, 2019).

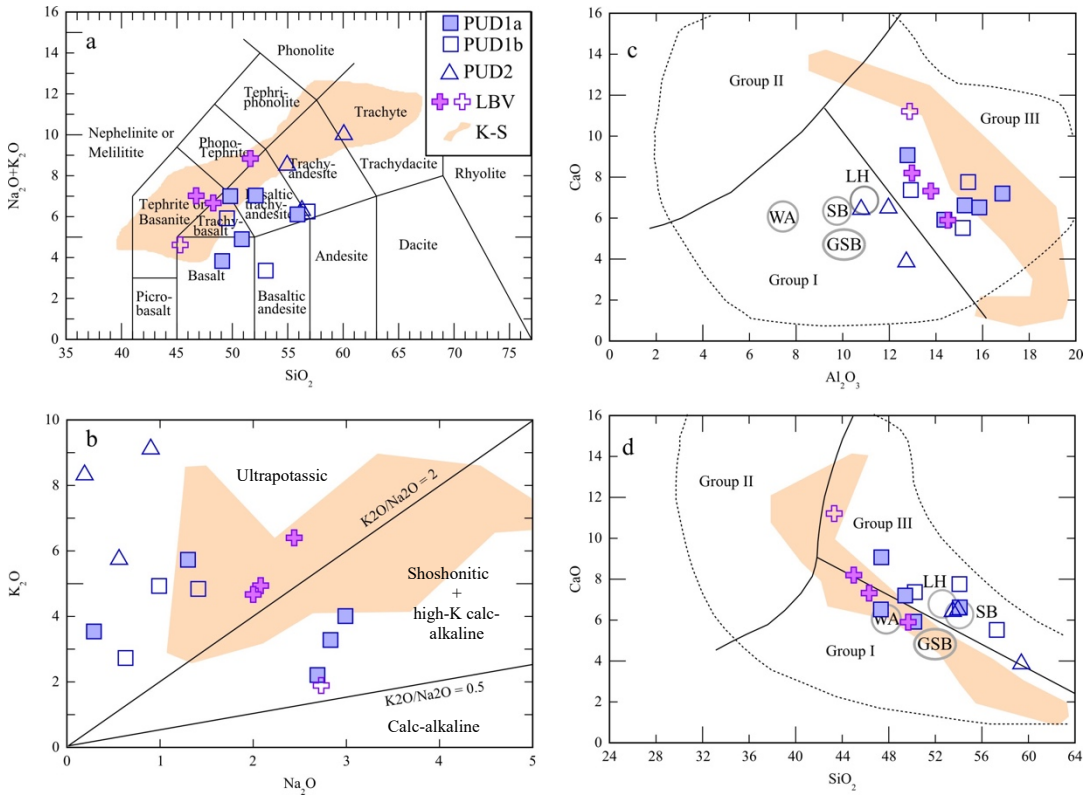

Figure 4.3. Rock types classification diagrams for the potassic to ultrapotassic dykes (PUD) from Canyon domain. (a) SiO_2 vs. $Na_2O + K_2O$ (Le Bas et al., 1986); (b) K_2O vs. Na_2O; (c) CaO vs. Al_2O_3; (d) CaO vs. SiO_2 (Foley et al., 1987). Data source: WA, Western Australia; LH, Leucite Hills; GSB, Gaussberg; SB, Smoky Butte (Fraser et al., 1985; Fraser, 1987); K-S, Kensington-Scoottamatta suite and Rivard minette dykes (Corriveau, 1990; Corriveau et al., 1990, 1996; Corriveau and Gorton, 1993; Morin et al., 2005); LBV, Labrieville dykes (Owens and Tomascak, 2002).

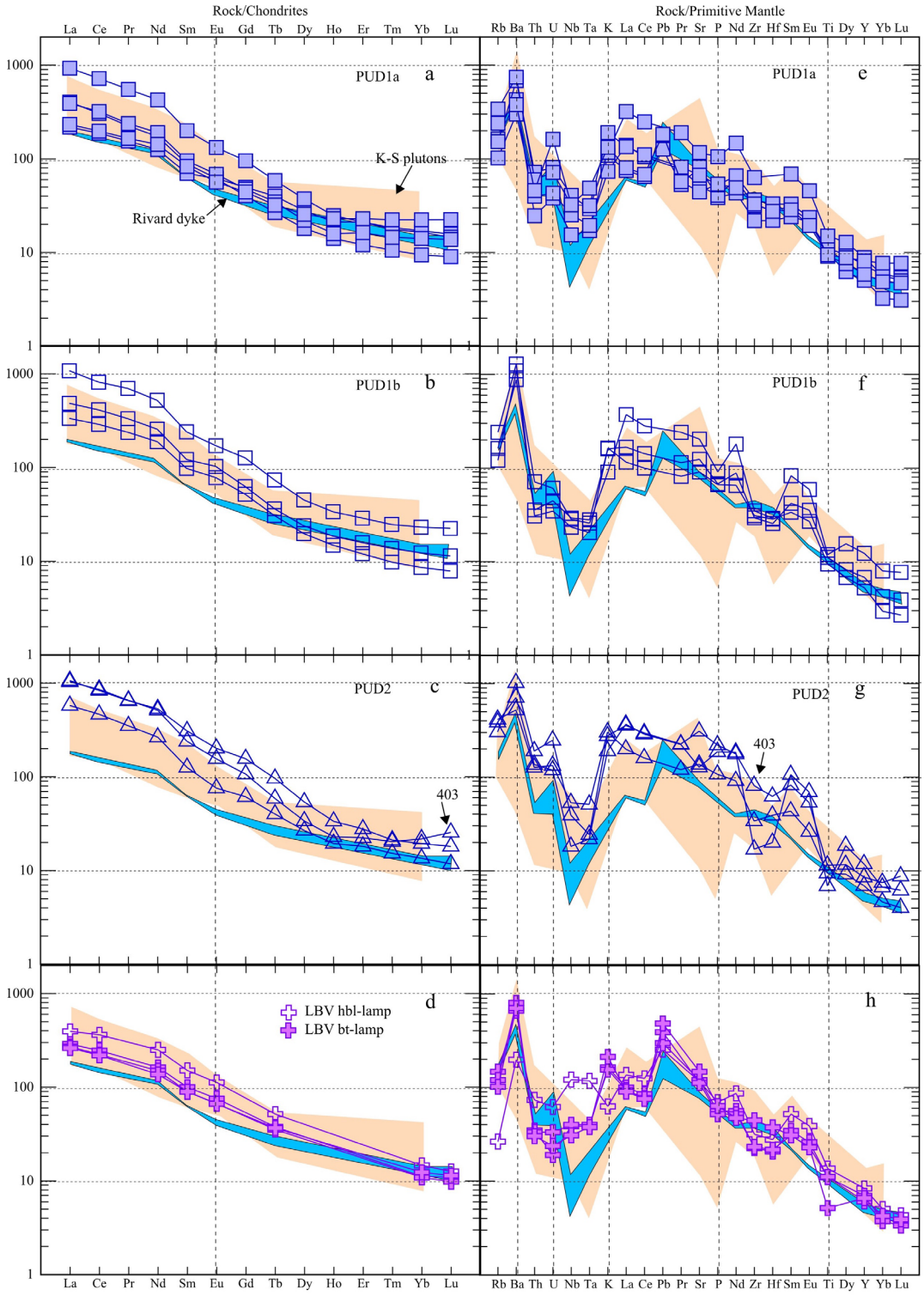

Figure 4.4. (a-d) Chondrite-normalized; and (e-h) Primitive mantle-normalized multi-element diagrams for the PUD. Normalization values are from Sun and McDonough (1989). The Labrieville dykes (LBV) (Owens and Tomascak, 2002), Rivard lamprophyre dyke (Corriveau et al., 1996; Morin et al., 2005), and Kensington-Schoottamatta suite (K-S) (Corriveau et al., 1990; Corriveau and Gorton, 1993) are shown for comparison.

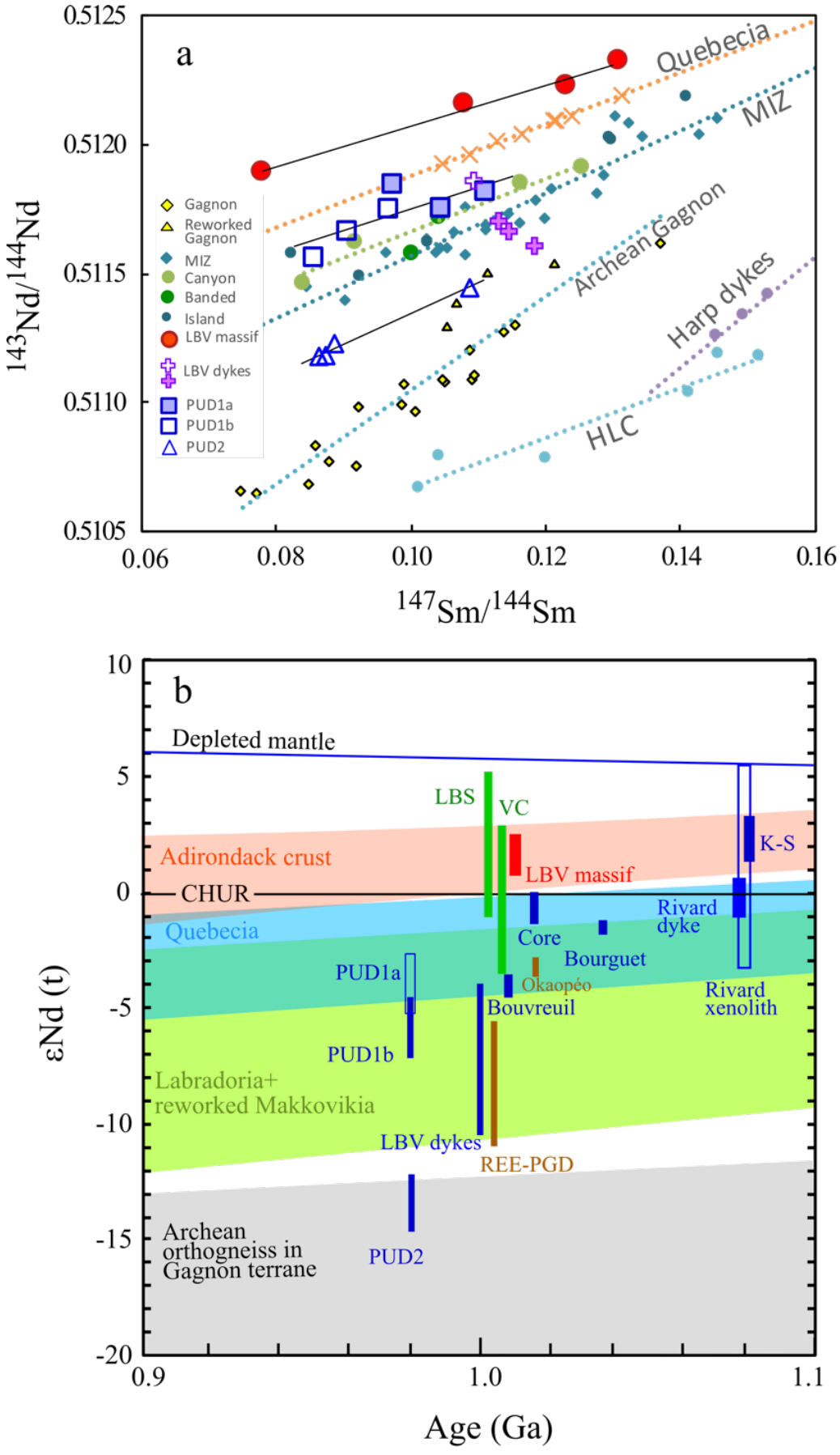
a
Quebecia
MIZ
Archean Gagnon
Harp dykes
HLC
Gagnon
Reworked Gagnon
MIZ
Canyon
Banded
Island
LBV massif
LBV dykes
PUD1a
PUD1b
PUD2
0.5125
0.5120
0.5115
0.5110
0.5105
0.06
0.08
0.10
0.12
0.14
0.16
143Nd/144Nd
147Sm/144Sm
b
Depleted mantle
LBS
VC
K-S
Adirondack crust
LBV massif
CHUR
Rivard dyke
Quebecia
Core
Bourguet
PUD1a
Okaopéo
Bouvreuil
Rivard xenolith
PUD1b
Labradoria+
reworked Makkovikia
LBV dykes
REE-PGD
Archean
orthogneiss in
Gagnon terrane
PUD2
10
5
0
-5
-10
-15
-20
0.9
1.0
1.1
εNd (t)
Age (Ga)

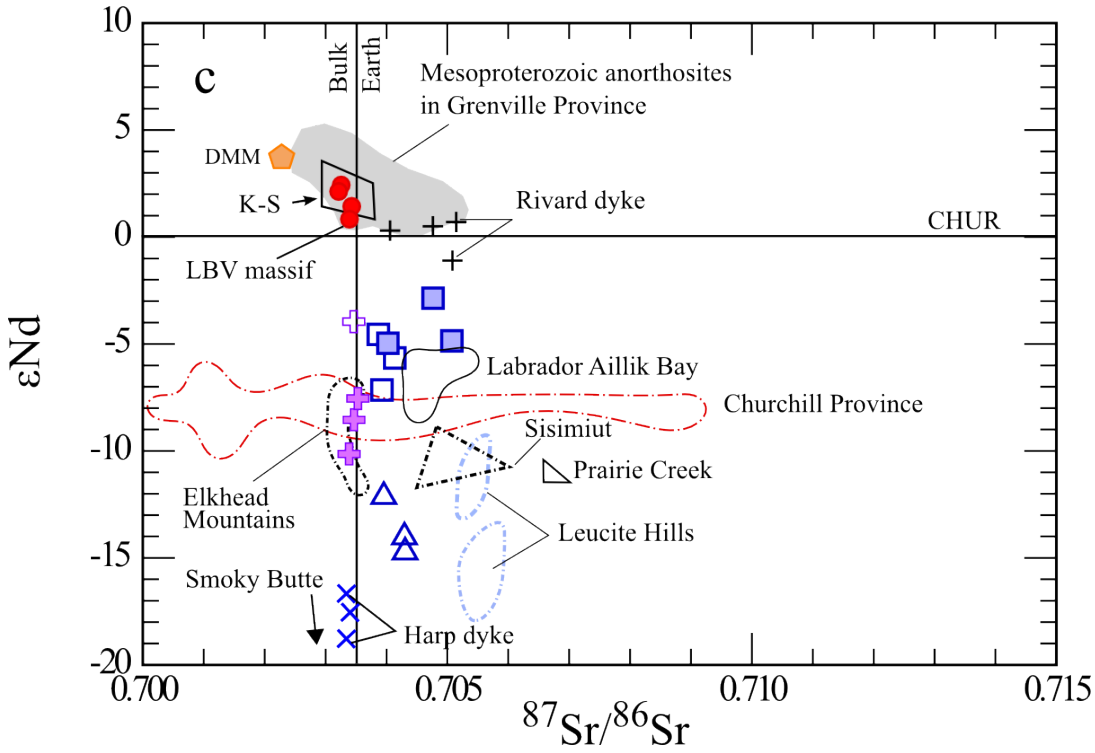

Figure 4.5. Sr-Nd-Pb isotopes for the PUD. (a) $^{143}Nd/^{144}Nd$ vs. $^{147}Sm/^{144}Nd$; (b) εNd (t) vs. Time (Ga); (c) εNd vs. $^{87}Sr/^{86}Sr$ diagrams. Data source: Gagnon terrane, Manicouagan Imbricate Zone (MIZ), Island domain, Canyon domain, Banded Complex, Canyon domain orthogneiss, and Archean orthogneiss in Gagnon terrane (Thomson et al., 2011); Labradoria and reworked Makkovikia (Schärer, 1991; Thomson et al., 2011); Adirondack crust (Chiarenzelli et al., 2010; and references therein); Quebecia (Dickin, 2000; Dickin and Higgins, 1992), Labrieville (LBV) massif anorthosite (Owens et al., 1994); Labrieville lamprophyre dykes (Owens and Tomascak, 2002); Okaopéo mangerite, syenite plutons from Bourguet, Bouvreuil, and Core (Augland et al., 2015, 2017; εNd values estimated from zircon εHf value following Vervoort and Blichert-Toft; 1999); Vein Complex (VC) and Layered bimodal suite (LBS) (Maity, *in prep.*); Rivard minette dyke (Corriveau et al., 1996); Kensington-Schoottamatta suite (K-S) (Corriveau and Amelin, 1994); Elkhead Mountains (Thompson et al., 1990); Sisimiut (Nelson, 1989); Smokey Butte, Prairie Creek, Leucite Hills (Mirnejad and Bell, 2006); Churchill Province (Peterson et al., 1994); depleted mantle (DePaolo, 1981); CHUR, chondrite uniform reservoir (Bouvier et al., 2008).

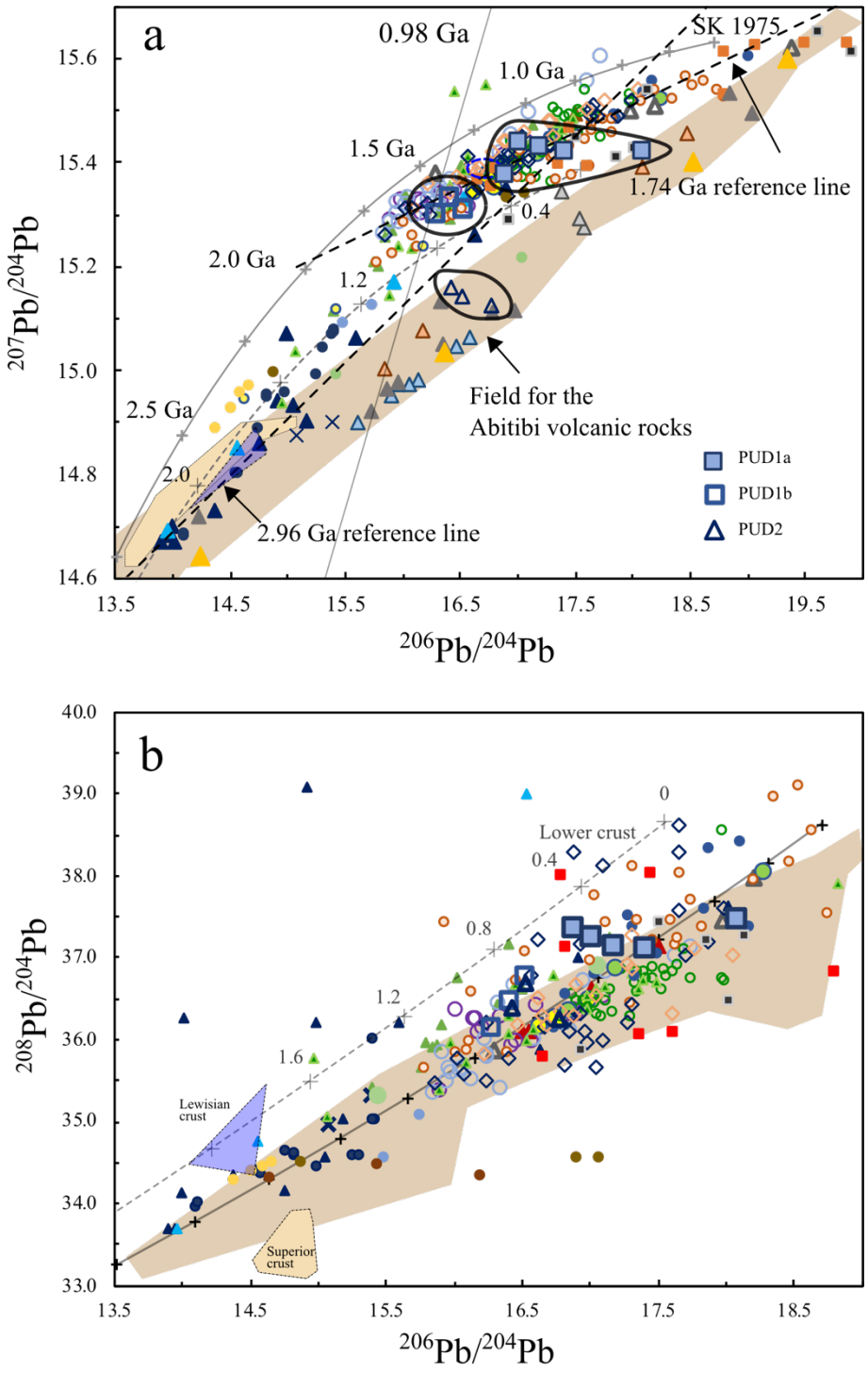

Archean

- Big Bight-Ford, Ferguson Lake, Moran Lake; Makkovik Zone, Mink Trap, Michein Zone } (Wilton, 1991)
- Levack gneiss, Grenville gneiss } (Dickin, 1998)
- NGA (DeWorlf and Mezger, 94)
- Harp Lake Complex, Harp Dykes } (Ashwal et al., 1984)

Abitibi volcanics Rock

- Pyke Hills, Fred's Flow, Theo's Flow } (Brévart et al., 1986)
- Munro Township (Tilton, 1983)
- Alexo komatiite (Dupre et al., 1984)

Proterozoic

- Grenville anorthosite feldspar (Emslie and Hegner, 1993)
- Mealy Mountain Complex, Mealy dykes } (Ashwal et al., 1986)
- Labrieville anorthosite (Owens et al., 1994)
- Rivard xenolith cpx, Rivard dyke minerals } (Corriveau et al., 1996)
- SGA (DeWolf and Mezger, 1994)
- Eastern Labrador K-feldspar (Schärer, 1991)
- K-S suite (Corriveau and Amelin, 1994)
- Suture Suite, Ontario (Arcuri and Dickin, 2018)
- Labradorian gneiss (Loewy et al., 2003)
- Pinwarian gneiss (Loewy et al., 2003)
- Cape Harisson North and South (Mumblow et at., 2018)

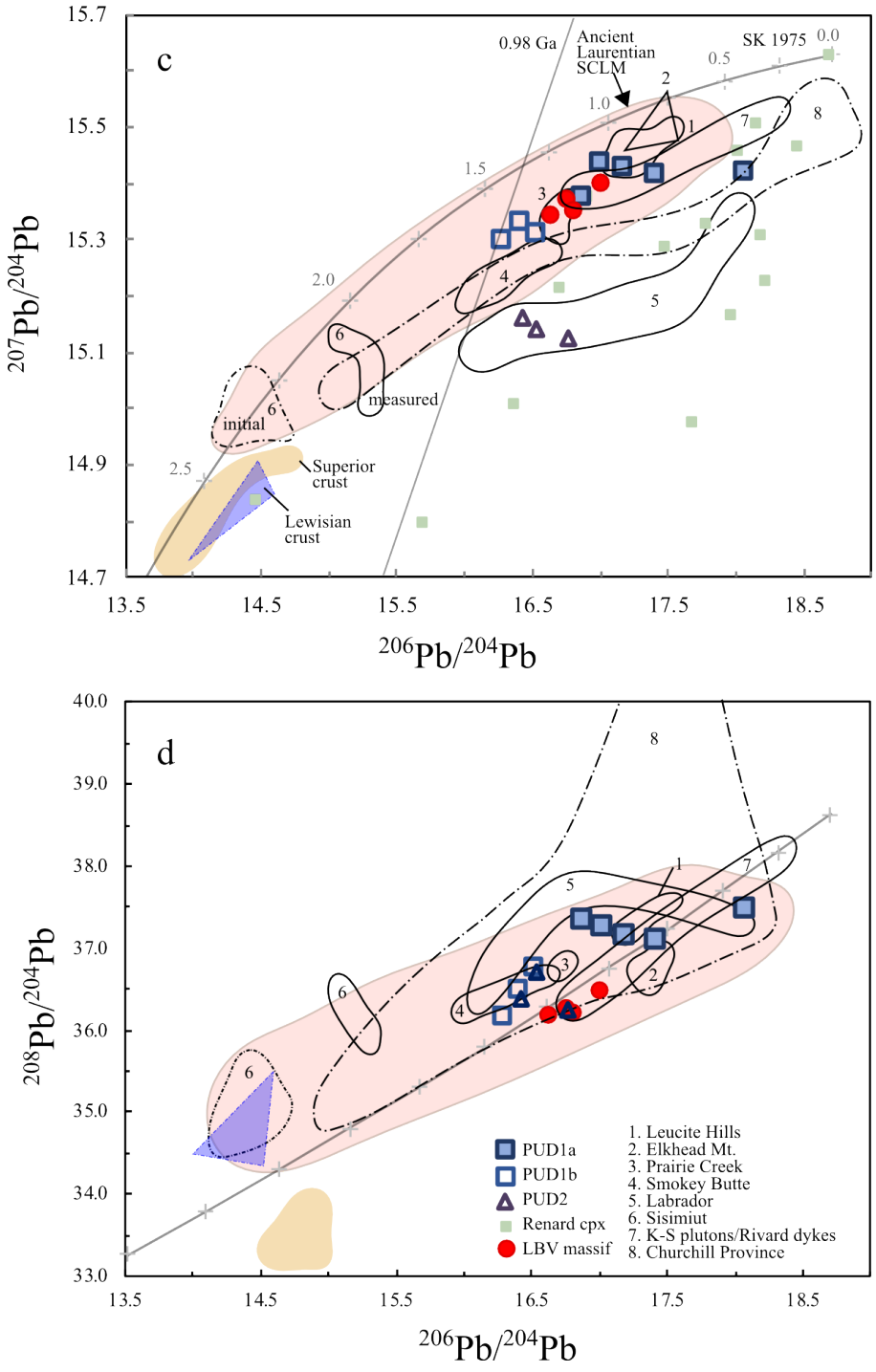

Figure 4.6. Pb-Pb isotope ratios for the PUD compared with (a-b) Archean orthogneisses (n = 46), galena deposits (n = 34), Abitibi volcanic rocks (n = 54), and Proterozoic orthogneisses (n = 232); data source mentioned on the diagram; (c-d) Laurentian lamproites and ultrapotassic rocks (n = 46), and kimberlite clinopyroxene (n = 15) data from the Superior Province. Data source: Renard kimberlite clinopyroxene (Hunt et al., 2012); ancient Laurentian SCLM (Tappe et al., 2007); Superior lower crust (Gariépy et al., 1990; Stevenson et al., 1999); Lewisian crust (Kerr et al., 1995); SK 1975, average crust (Stacey and Kramers, 1975); remaining data source as in fig. 4.5. Pb evolution line for lower crust (Zartman and Doe, 1981) and average crust (Stacey

and Kramers, 1979), 0.98 Ga geochron is drawn for T = 4.55 Ga (age of the Earth) and primeval lead data for Canyon Diablo Troilite (Tatsumoto et al., 1973); the 1.74 Ga and 2.96 Ga reference lines are for a mantle source with μ = 8.0 (Arcuri and Dickin, 2018).

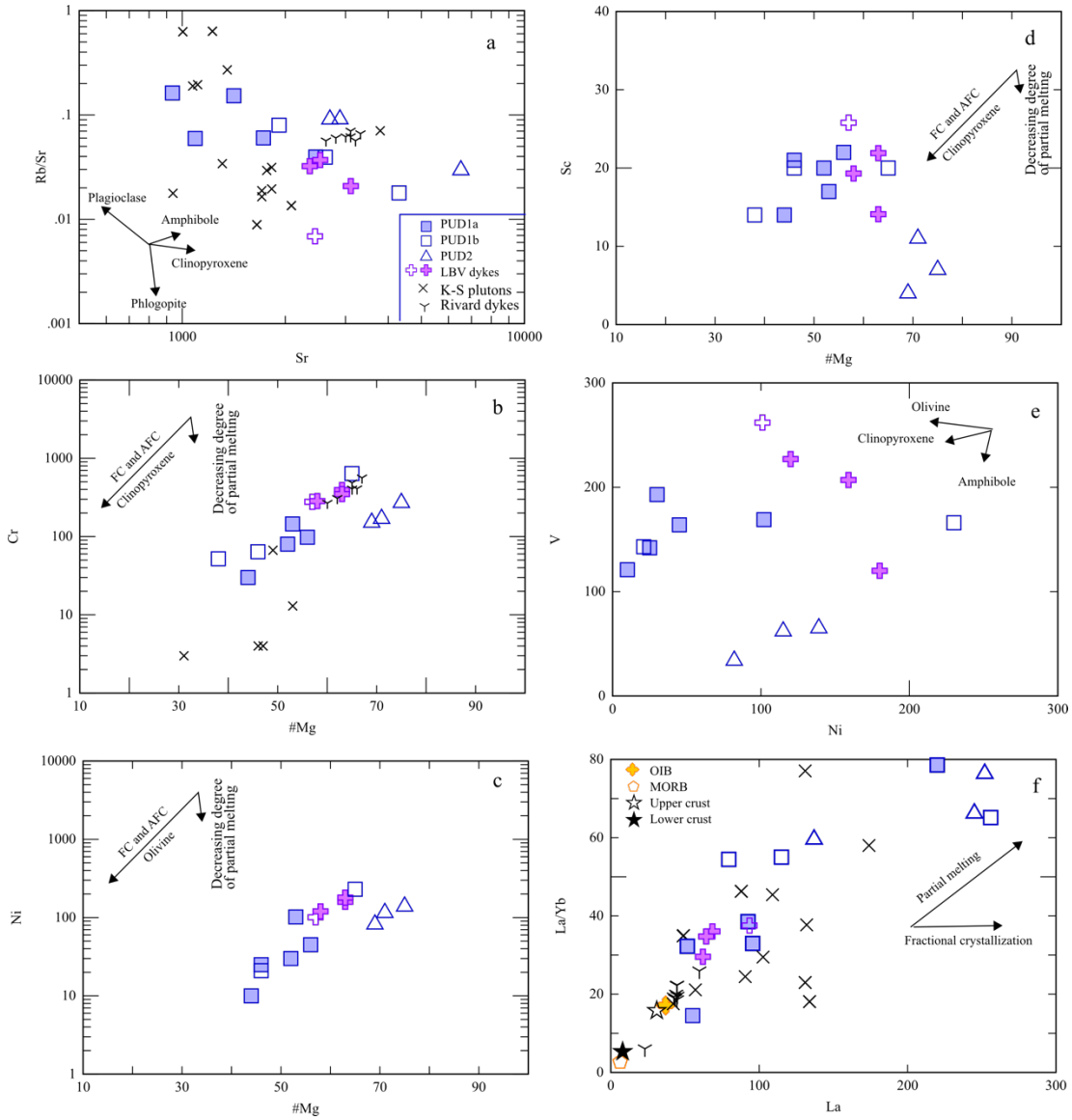

Figure 4.7. (a) Rb/Sr vs. Sr (ppm); (b) Cr (ppm); (c) Ni (ppm); and (d) Sc (ppm) vs. Mg#; (e) V vs. Ni (ppm); and (f) La/Yb vs. La diagrams for the PUD. Data from Labrieville (LBV) lamprophyre dykes (Owens and Tomascak, 2002), K-S suite and Rivard dykes (Corriveau et al., 1996) are shown for comparison. Crystal fractionation vectors are shown using partition coefficients from Pearce and Parkinson (1993). Data for OIB and MORB (Sun and McDonough, 1989), and for upper and lower crust (Rudnick and Gao, 2014).

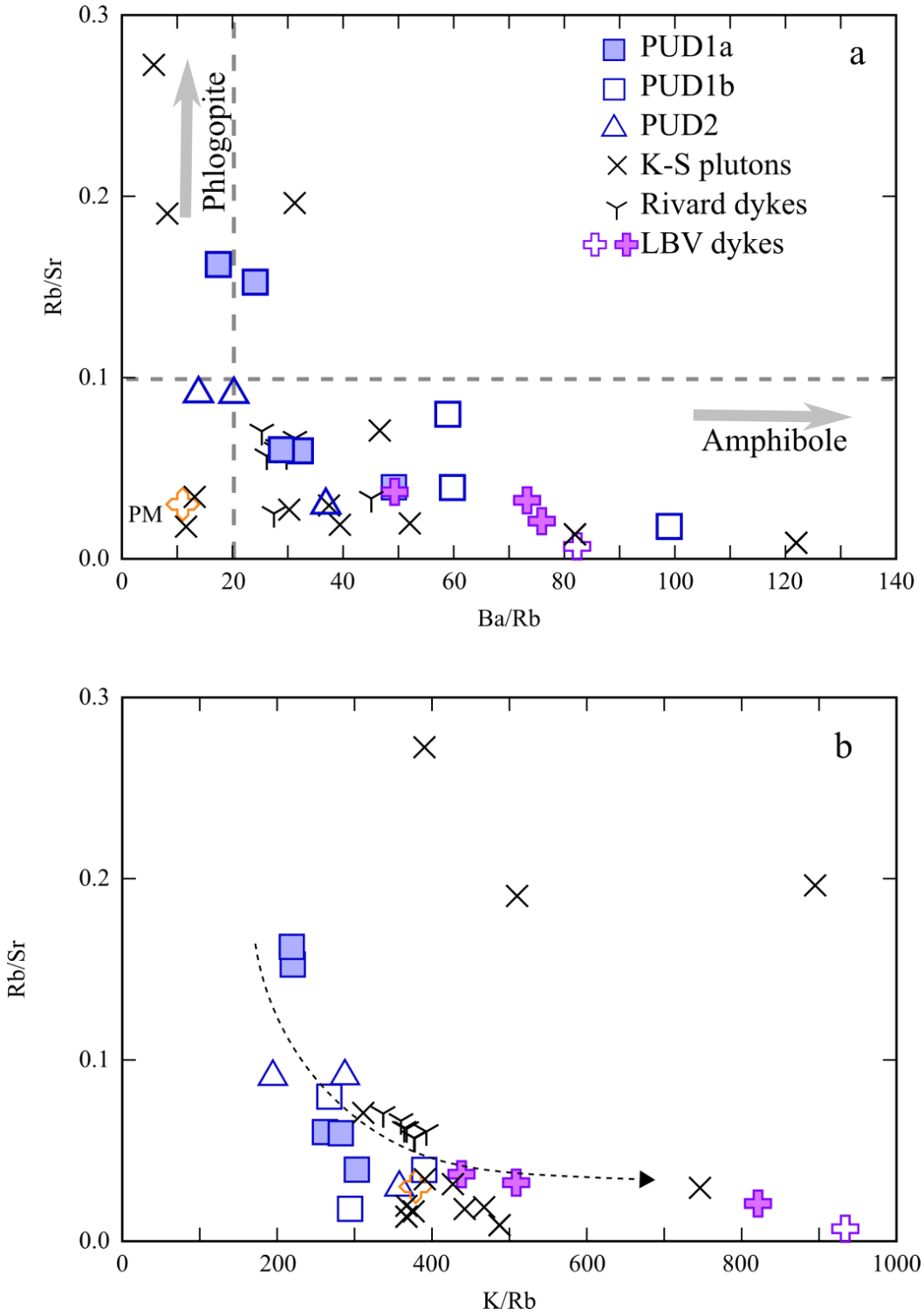

Figure 4.8. (a) Rb/Sr vs. Ba/Rb (Furman, 1995; Furman and Graham, 1999); and (b) Rb/Sr vs. K/Rb diagram for the PUD. The downward pointing arrow in (b) indicates phlogopite fractionation at source. PM, primitive mantle (Sun and McDonough, 1989).

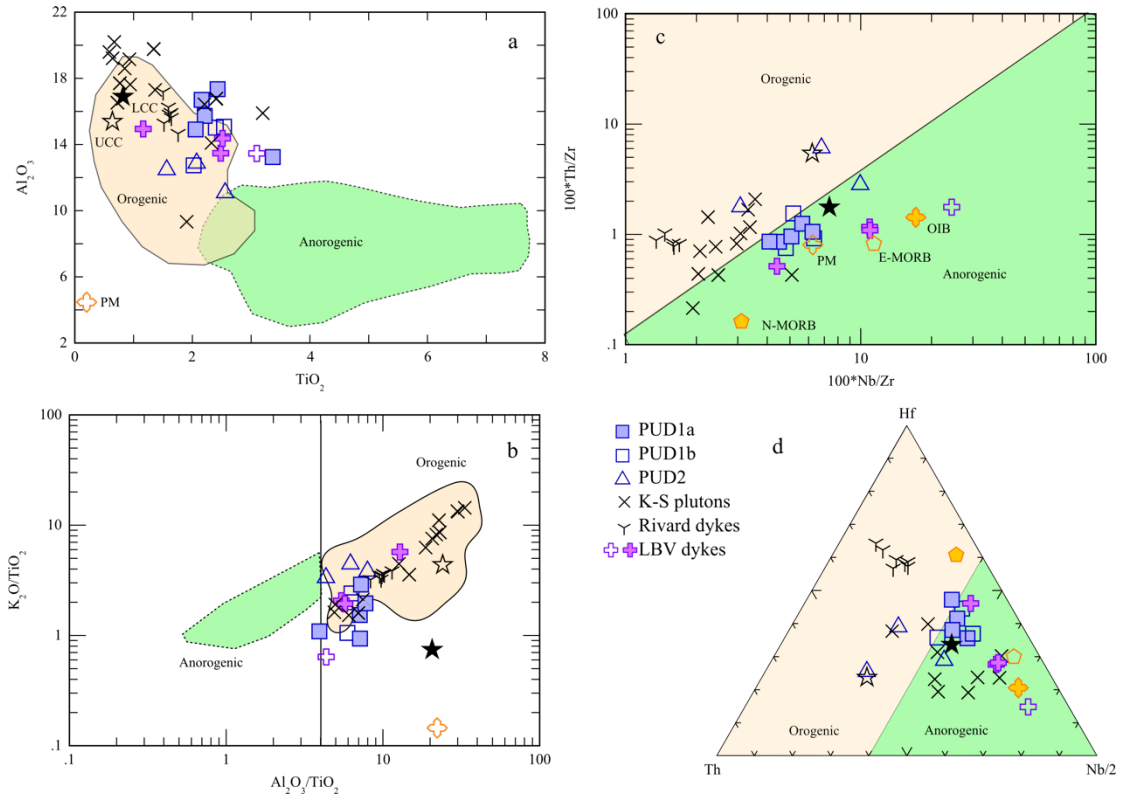

Figure 4.9. (a) Al_2O_3 vs. TiO_2; (b) K_2O/TiO_2 vs. Al_2O_3/TiO_2 (Lustrino et al., 2016); (c) 100*Th/Zr vs. 100*Nb/Zr (modified after Wilson and Bianchini, 1999); and (d) Th-Hf-Nb/2 (Krmíček et al., 2011) diagrams showing mixed orogenic-anorogenic character of PUDs, with the fields for worldwide orogenic and anorogenic lamproites (Lustrino et al., 2016) shown for comparison. Remaining data source as in figs. 4.5 and 4.7.

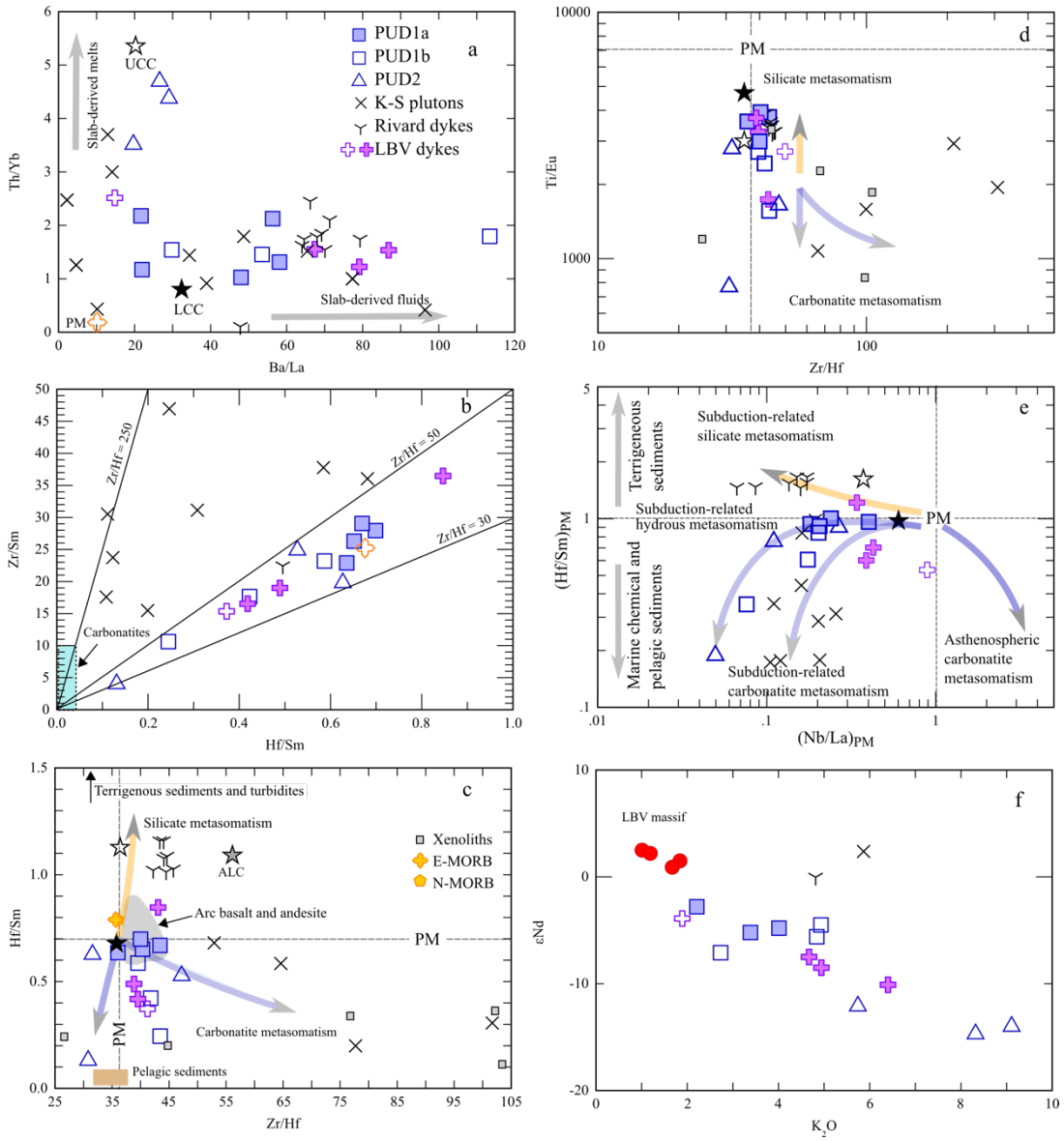

Figure 4.10. (a) Th/Yb vs. Ba/La; (b) Zr/Sm vs. Hf/Sm; (c) Hf/Sm vs. Zr/Hf; (d) Ti/Eu vs. Zr/Hf; (e) $(Hf/Sm)_{PM}$ vs. $(Nb/La)_{PM}$ (modified after Laflèche et al., 1998; Prelević et al., 2012); and (f) εNd vs. K_2O (wt%) for the PUD. Data source: carbonatite metasomatized xenoliths (Rudnick et al., 1993), turbidites (McLennan et al., 1990), pelagic sediments (Ben Othman et al., 1989), remaining data source as in fig. 4.5.

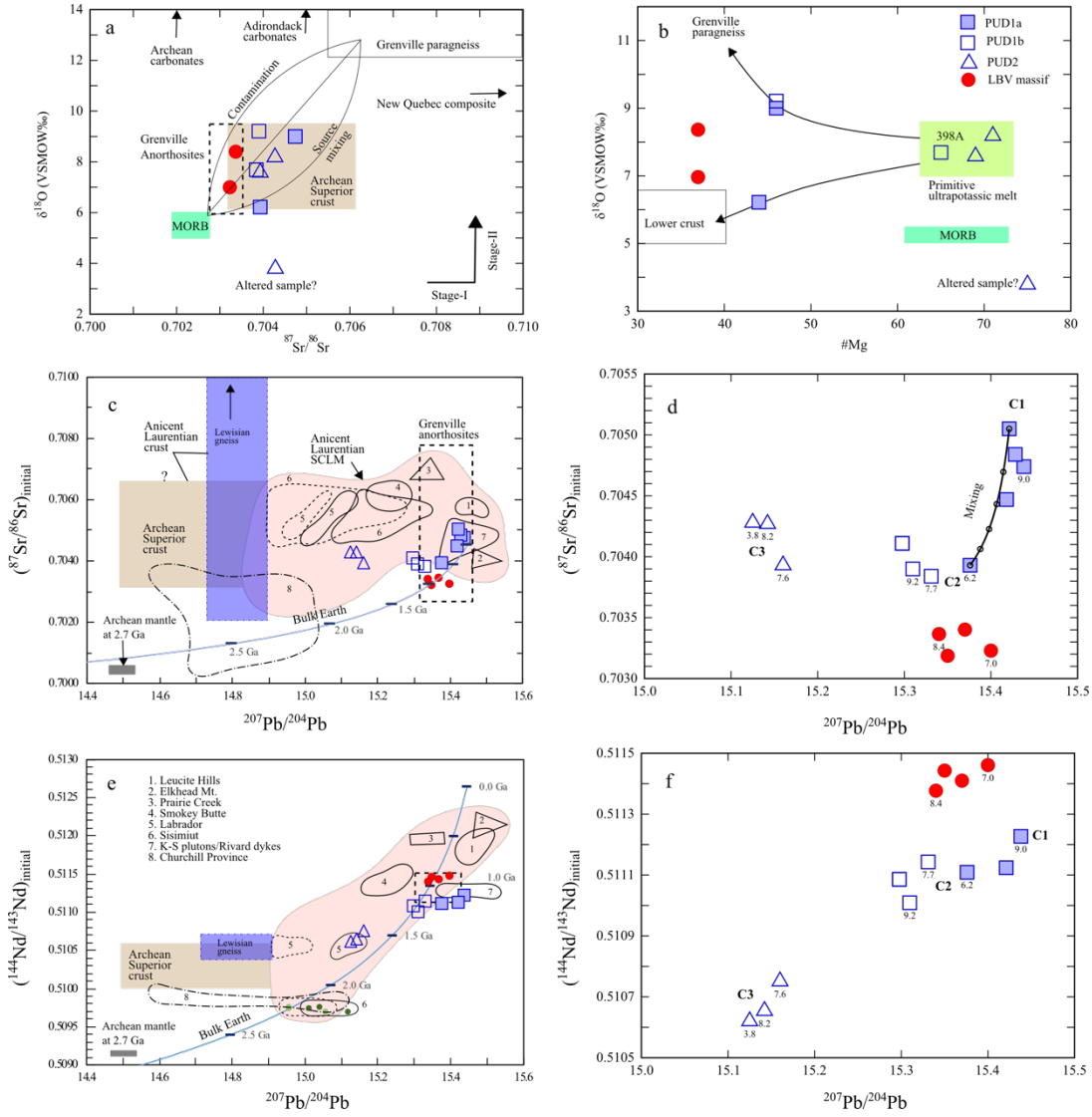

Figure 4.11. Whole-rock Sr-Nd-Pb-O isotopes and Mg# for PUD. (a) $\delta^{18}O_{VSMOW}$ vs. $^{87}Sr/^{86}Sr$ (1Ga); (b) $\delta^{18}O_{VSMOW}$ vs. #Mg; (c) $^{87}Sr/^{86}Sr$ (1Ga) vs. $^{207}Pb/^{204}Pb$; (d) close up of (c); (e) $^{143}Nd/^{144}Nd$ vs. $^{207}Pb/^{204}Pb$; and (f) close up of (e). Small numbers below data symbols in (d) and (f) indicate $\delta^{18}O$ values from table 4.1. Data source: New Quebec composite (McCulloch and Wasserburg, 1978; Shieh and Schwarcz, 1978), Archean carbonate (Shieh and Schwarcz, 1978; Veizer et al., 1989; Veizer and Compston, 1976; Veizer and Hoefs, 1976), Archean Superior crust (Ashwal et al., 1986; Gariépy et al., 1990; Emslie et al., 1994; Stevenson et al., 1999; Valley et al., 2005; Whalen et al., 2002; Thomson et al., 2011), Lewisian crust (Kerr et al., 1995); Archean mantle at 2.7 Ga (Bell and Blenkinsop, 1987; Tilton and Bell, 1994), Grenville anorthosite and Labrieville (LBV) massif (Anderson, 1966; Owens et al., 1994; Peck et al., 2010; Peck and Valley, 2000), Grenville paragneiss (Schärer, 1991; Peck and Valley, 2000; Thomson et al., 2011), Adirondack carbonate (Hauer, 1995; Shieh and Schwarcz, 1978), MORB and mantle (Eiler, 2001; Mattey et al., 1994; Workman and Hart, 2005), CHUR (Bouvier et al., 2008); Bulk earth evolution curve (Kwon et al., 1989); Laurentian lamproites and ultrapotassic rocks as in fig. 4.5.

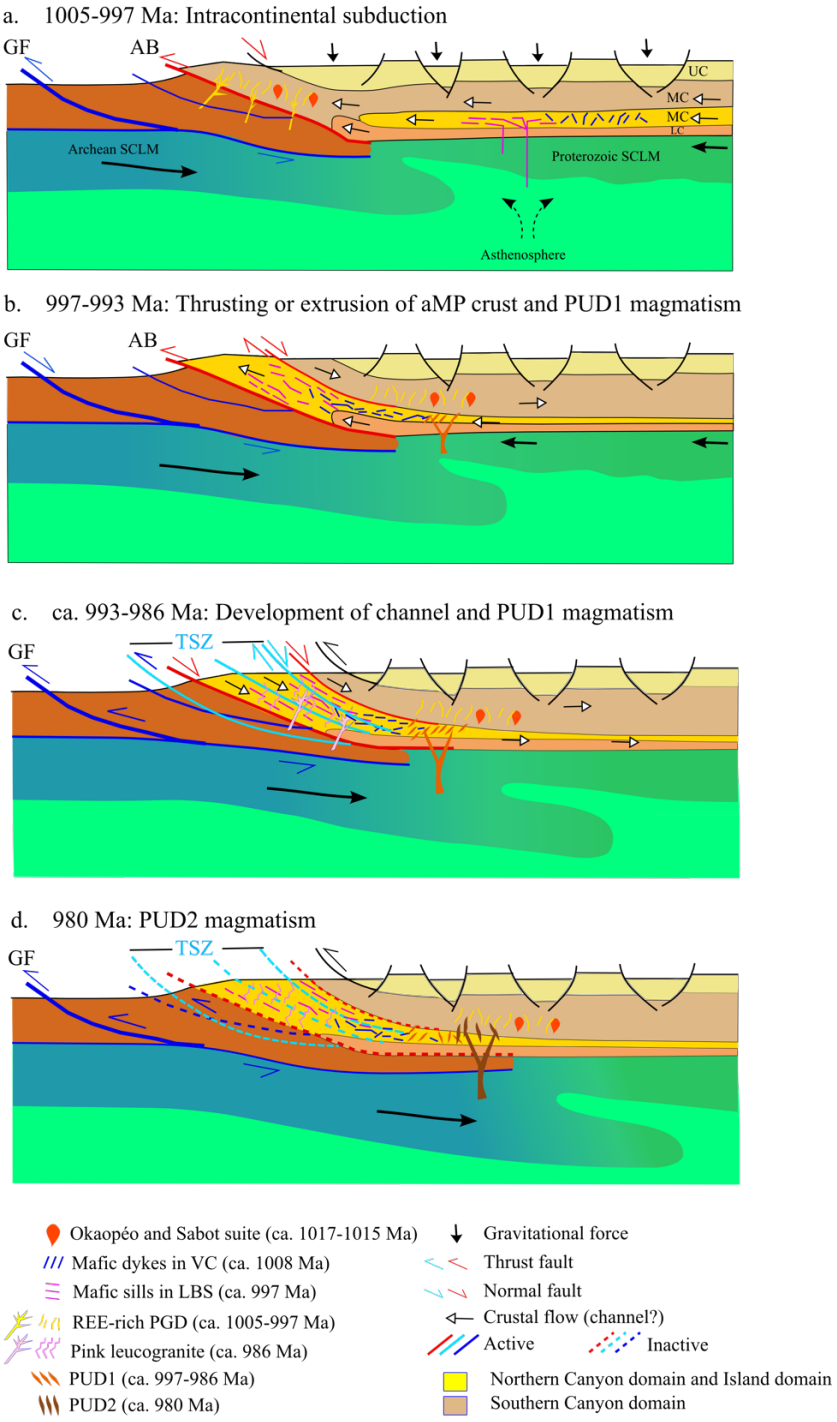

Figure 4.12. Cartoon illustrating proposed tectonic model (inspired by Rivers et al., 2012; Jannin et al., 2018a, 2018b) for the evolution of Rigolet phase in the Grenville hinterland. (a) Initiation of intracontinental subduction and crustal thickening at ca. 1005 Ma, intrusion of PGDs; (b) thrusting or extrusion of northern Canyon domain between ca. 997-993 Ma, and possible derivation of syn-tectonic PUD1 from Proterozoic SCLM; (c) development of Rigolet channel and the normal-sense Thachic Shear Zone (TSZ) at ca. 990 Ma and intrusion of syn-tectonic PUD1 from Proterozoic SCLM ≤ 986 Ma; (d) intrusion of late- to post-tectonic PUD2 from late-Archean S-SCLM at ca. 980 Ma. UC, upper crust; MC middle crust; LC, lower crust.

5 Summary and Conclusions

The main objectives of this thesis were: (i) to constrain the age, petrogenesis and tectonic setting of the mafic rocks from the MIU and PLV to provide information on the Mesoproterozoic evolution of the Laurentian continental margin; (ii) to constrain the age, petrogenesis, and tectonic setting of the mafic rocks in the VC and LBS to characterize the late-orogenic evolution of the Grenvillian hinterland; and (iii) to characterize the nature and multi-stage metasomatism of lithospheric mantle sources for the PUDs, and to better constrain the tectonic evolution of the Rigolet phase in the Grenvillian LHO. As summarized below, the combined results of petrography, U-Pb geochronology, major and trace element geochemistry, and radiogenic and stable isotope geochemistry of mafic and potassic to ultrapotassic rocks, integrated with published data, provide fundamental constraints about the Mesoproterozoic arc-accretionary evolution of the active Laurentian margin, as well as its late-orogenic intracontinental subduction evolution as part of the large hot long-duration Grenville Orogen. The results presented here also provide evidence that the Grenville Province preserves all the three types of orogens of Cawood et al., (2009): accretionary, collisional, and intracratonic orogens.

5.1 Summary of the thesis

5.1.1 Mesoproterozoic evolution of the Laurentian margin

The magmatic and metamorphic events during Geon 14 in the central Grenville Province constitute a significant part of the pre-Grenvillian tectonic evolution of the southeastern margin of Laurentia. The two suites of mid-pressure mafic granulites from the MIU and PLV have provided more detailed information about the pre-orogenic

magmatism and hence the inferred architecture of this part of the Laurentian margin during Geon 14 and its implications for the pre-Grenvillian evolution of SE Laurentia. The $1439\,^{+76}_{-68}$ Ma high Fe-Ti-P, tholeiitic, mafic sills were derived from variably depleted to enriched MORB-type mantle modified by minor subduction components and crustal contamination. They intruded the >1500 Ma PLV supracrustal sequence during limited extension of arc/back-arc crust that resulted in thinning of the Laurentian continental margin. The 1410 ± 16 Ma mafic intrusive rocks in the MIU and the mafic samples from QFU (inferred to be ca. 1.4 Ga) have depleted to enriched MORB- and arc-type geochemical signatures. They were formed in a compressional back-arc setting in which shortening of the Laurentian crust decreased the distance between the back-arc to the more outboard arc source, as suggested by increased crustal input from subduction components and/or crustal contamination. The various magmatic components in the MIU were mingled in a shallow closed-system magma chamber before their final emplacement. When considered collectively with published literature from the area, the repetitive intrusion of the high Fe-Ti-P mafic rocks during Geon 14 in the central Grenville Province suggests that arc/back-arc extension was an intermittent process in an overall compressional arc regime on southeast Laurentia during the Mesoproterozoic.

5.1.2 Late-orogenic evolution of the Grenvillian LHO

Combining the results from the ca. 1008-997 Ma mafic dykes and sills in the Vein Complex (VC) and Layered Bimodal Suite (LBS) with other recently published data, the late-orogenic tectonic setting in the central Grenville Province is proposed to have involved the late- to post-Ottawan lithospheric extension, which resulted in melting of the subduction-metasomatized SCLM, decompression melting of upwelling

asthenosphere, and high-grade metamorphism and crustal melting. During this extension, previously thinned lithospheric mantle underwent partial melting resulting in emplacement of alkaline plutonic suites and AMCG complexes. Continued extension caused shallow spinel-facies melting of upwelled asthenosphere, and melts thus derived were variably contaminated by overlying lithosphere before being emplaced within the orogenic mid-crust.

Subsequent Rigolet crustal shortening resulted in underthrusting of foreland beneath the Grenville hinterland. Partial melting of parautochthonous crust at depth produced the ca. 1004-1002 Ma REE-rich pegmatitic granite dykes (PGDs) that intruded the PLV in the southern Canyon domain and Lac Okaopéo area (Turlin et al., 2017, 2019), and the ca. 984 Ma pink leucogranite dyke swarm in the northern Canyon domain (Jannin et al., 2018b). However, the apparent absence of REE-rich PGDs in the northern Canyon domain, which was intruded by coeval mafic rocks of the VC and LBS (this study), and later by the pink leucogranite dykes, suggests a more complex tectonic setting for the Canyon domain during the post-Ottawan period. It is proposed that during this period, the structurally lower northern Canyon domain was situated in a more distal location with respect to the AB than the structurally higher southern Canyon domain and the Lac Okaopéo area; and that during the early-Rigolet compression the northern Canyon domain was extruded from beneath the southern Canyon domain and Lac Okaopéo area such that their relative positions were reversed. Subsequent normal faulting along the Thachic shear zone and the development of a mid-Rigolet crustal channel (Jannin et al., 2018a, 2018b) affected the structurally lower parts of the aM*P* belt, including the northern Canyon domain.

5.1.3 Rigolet orogenic evolution of the Grenvillian LHO

A suite of previously reported ca. 980 Ma potassic to ultrapotassic dykes in the Canyon domain was studied to further characterize the geochemical evolution of the subcontinental lithospheric mantle beneath the Grenville Orogen in the central Grenville Province, and to constrain the tectonic evolution during the Rigolet phase. Based on Sr-Nd-Pb-O isotopic constraints, it is inferred that the group of syn-tectonic PUD1 dykes were derived from fertile Proterozoic subcontinental lithospheric mantle, contaminated at source by crustal fluids. In contrast, the late- to post-tectonic PUD2 samples were derived from the depleted, late-Archean to early-Paleoproterozoic, subcontinental lithospheric mantle that was metasomatized by carbonatitic and pelagic sediment-derived melt in an ancient subduction setting beneath the southeastern margin of the Superior Province. The evidence for $\delta^{18}O$-enrichment above mantle value also indicates contamination at source by ^{18}O-rich fluids and melts derived from subducted crust or sediment, although contamination during magma ascent through crust cannot be excluded for a small number of highly fractionated samples.

Consequent to the above findings, an intracontinental subduction model is invoked for the Rigolet tectonic evolution of the central Grenville Province. In this scenario, the syn-tectonic PUD1 samples were derived from thickened Proterozoic SCLM and were emplaced in the Canyon domain before ca. 986 Ma. Continued underthrusting resulted in flat subduction of the refractory, metasomatically enriched, and buoyant late-Archean SCLM beneath the hinterland in PLV in southern Canyon domain by late-Rigolet time. We propose that subsequent orogenic relaxation, possibly coupled with local delamination of the thickened Rigolet lithosphere, induced melting

in the most incompatible element-enriched parts of the late-Archean SCLM to produce the PUD2 dykes that intruded the Canyon domain at ca. 980 Ma.

Finally, the Rigolet flat subduction of Laurentian SCLM beneath the Grenvillian hinterland during the Rigolet phase could also have resulted in the intrusion of several late- to post-tectonic alkalic mafic and syenitic rocks, and crust-derived felsic suites reported by others. Moreover, underthrusting of the SCLM largely diminished asthenospheric magmatism and high-grade metamorphism in the hinterland.

5.2 Outlook and suggestion for future research

The research described in the second chapter of this thesis highlights the underlying challenges in studying Precambrian high-grade gneisses and in unravelling the petrotectonic evolution of ancient crustal terranes. By employing multiple robust, immobile-incompatible-element-based geochemical tools, we have been able to screen out altered samples and constrain the tectonic settings of formation of the protoliths of the two suites of mafic, Geon 14 granulite-facies gneisses emplaced in the PLV and MIU. This research shows that the central Grenville Province in Geon 14 evolved as an active margin arc and intermittent back-arc setting. The early Geon 13 intrusions in the Hulot Complex farther south exhibited similar arc and back-arc geochemical signatures to those of the Geon 14 rocks in the study area (Augland et al., 2015). The Geon 12 mafic and felsic rocks in the study area exhibit predominantly arc to minor within-plate geochemical signatures (Indares and Dunning, 2004; Valverde Cardenas et al., 2012; Hindemith et al., 2017; Moukhsil and Solgadi, 2017), that are probably indicative of arc magmatism related to back-arc closure, comparable to the Elzevirian Orogeny in the southwestern Grenville Province (Rivers and Corrigan, 2000). These results

collectively suggest that the ca. 1.24 Ga supracrustal sequence comprising the Layered Bimodal Suite was deposited in an arc setting, possibly related to back-arc closure, rather than an intracontinental extensional setting. It would be beneficial to investigate further the age and depositional setting of the Quartzofeldspathic Unit, for which a ca. 1.4 Ga depositional age was inferred, and to constrain whether it is a part of the PLV, or was deposited as a separate lithologic unit. Moreover, if the northern Canyon domain represents Geon 12 crust accreted to, and/or developed on a Geon 14 continental margin, it was feasible that this crustal section was emplaced beneath the PLV in the hanging wall of the AB as a result of the Grenvillian thrust tectonics.

A robust conclusion of this study, coupled with the results of other recent publications (Augland et al., 2015, 2017; Turlin et al., 2017, 2018, 2019; Jannin et al., 2017, 2018a, b), is that the post-Ottawan to pre-Rigolet "hiatus" in tectonic activity in the Grenville Province can now be defined as a period of lithospheric extension, tholeiitic and alkaline magmatism, high-grade metamorphism and crustal melting. In this research, we have designated this "hiatus" as a distinct 'post-Ottawan' phase separating the longer duration Ottawan orogenic phase from the shorter duration Rigolet phase. However, several studies (e.g., Jamieson et al., 2010; Jannin, 2017; Jannin et al., 2018b) have considered the tectonometamorphic evolution of the Grenvillian hinterland to have been continuous from the Ottawan through to the post-Ottawan period (~1090-1005 Ma). Moreover, contrary to the conventional wisdom of metamorphism and deformation during the Ottawan phase being largely restricted to the hinterland, and those of the Rigolet to the foreland (Rivers, 2008, 2015; Rivers et al., 2012), recent studies in the central Grenville Province have shown that the northern parts of the hinterland and the adjacent Allochthonous Boundary were overprinted by

the Rigolet compressional phase (Jannin et al., 2018b; this study), as the orogen advanced from the hinterland to the foreland.

The emplacement of the mafic dykes and sills in the northern Canyon domain (this study), and coeval emplacement of the REE-rich PGDs in the southern Canyon domain and the Lac Okaopéo area, coupled with the detailed structural, geophysical, geochronological, and metamorphic studies by others in the Canyon domain, have established the complex evolution of the northern Canyon domain during the post-Ottawan to Rigolet period. Most importantly, underthrusting of the footwall Gagnon terrane beneath the Canyon domain in the early Rigolet phase was closely followed by extrusion of the northern Canyon domain along the hanging wall of the Allochthonous Boundary from relatively deeper parts of orogenic mid-crust in the hinterland. This early-Rigolet extrusion event, which was not adequately described or constrained in previous studies, most likely took place by the mechanism of orogenic wedge propagation due to Rigolet intracontinental flat subduction, as the Rigolet channel was established only by ca. 990 Ma (Jannin et al., 2018b). If this was the case, then the channel developed within a larger orogenic wedge similar to that in the eastern Labrador (van Gool et al., 2008). More research is required to constrain the timing and mechanism of extrusion of this mid-crustal section at the beginning of the Rigolet phase, and its relationship to the overlying crustal section. Moreover, unlike the aH*P* MIZ to the north of the Manicouagan Reservoir, the absence of a lower crustal ramp-flat structure beneath the aM*P* area to the south, as evident from geophysical and structural studies (Hynes et al., 2000; Jannin, 2017; Jannin et al., 2018b), could have been crucial in controlling the extrusion of crustal slices during the Grenvillian orogeny.

The potassic to ultrapotassic dykes provide important constraints on the nature of the SCLM beneath the late-Grenvillian orogenic hinterland. However, U-Pb dating of zircon from PUD1 samples would undoubtedly provide more robust constraints on the timing of their emplacement. Future studies might also focus on radiogenic and stable isotopes in minerals, to further characterize the sources of the potassic to ultrapotassic dykes, and to compare them with apparently similar K-rich intrusions elsewhere in the Grenville Province. Delineating the extent and timing of flat subduction of the late-Archean SCLM beneath the orogenic core, and performing similar studies throughout the orogen would provide significant improvement in characterizing the Rigolet orogenic evolution, as well as establishing the Grenvillian LHO as a doubly-vergent orogen comparable in magnitude to the modern Himalaya-Tibet Orogen (Toby Rivers, personal communication).

Several recent tectonic models proposed for the evolution of the Grenvillian Orogeny have involved mid-Ottawan arc-accretionary orogenesis followed by post-Ottawan to early-Rigolet slab break-off or retreat (Augland et al., 2015, 2017; Côté et al., 2018; Turlin et al., 2019). However, to be robust such models require more detailed geochemical studies to demonstrate the presence of tholeiitic to calc-alkaline basalt and arc andesites, calcic to calc-alkaline to alkaline arc granitoids, and the characteristic isotopic "pull-ups" and "pull-downs" that are typical of modern arc-accretionary orogens (DeCelles et al., 2009; Moyen et al., 2017). In the absence of such evidence, and respecting decades of work by numerous researchers, we have maintained in this thesis that the Grenville Orogen is an eroded, ancient analogue of a classic continental collisional large hot long-duration orogen, similar in scale and magnitude to the Himalaya-Tibet Orogen.

5.3 References

Augland, L.E., Moukhsil, A., Solgadi, F., and Indares, A. 2015. Pinwarian to Grenvillian magmatic evolution in the central Grenville Province: new constraints from ID–TIMS U–Pb ages and coupled Lu–Hf S–MC–ICP–MS data. Canadian Journal of Earth Sciences, 52: 701–721. doi:10.1139/cjes-2014-0232.

Augland, L.E., Moukhsil, A., Solgadi, F. 2017. Mantle influence of syn- to late-Grenvillian alkaline magmatism in the Grenville Province: causes and implications. Canadian Journal of Earth Sciences, 15: 1–15. doi:dx.doi.org/10.1139/cjes-2016-0135

Cawood, P. a., Kroner, a., Collins, W.J., Kusky, T.M., Mooney, W.D., Windley, B.F. 2009. Accretionary orogens through Earth history. Geological Society, London, Special Publications, 318: 1–36. doi:10.1144/SP318.1.

Côté, G., Moukhsil, A., Constantin, M., David, J. 2018. Geochemical characterization, geochronology, and geodynamic implications of Grenville rare earths bearing syenites, Haut-Saint-Maurice, QC, Canada. Minerals, 8: 336. doi:10.3390/min8080336

DeCelles, P.G., Ducea, M.N., Kapp, P., Zandt, G. 2009. Cyclicity in Cordilleran orogenic systems. Nature Geoscience, 2: 251–257. doi:10.1038/ngeo469

Hindemith, M., Indares, A., Piercey, S. 2017. Hydrothermally altered volcanic rocks metamorphosed at granulite-facies conditions: an example from the Grenville Province. Canadian Journal of Earth Sciences, 54: 622–638. doi:10.1139/cjes-2016-0146

Hynes, A., Indares, A., Rivers, T., Gobeil, A. 2000. Lithoprobe line 55: integration of out-of-plane seismic results with surface structure, metamorphism, and geochronology, and the tectonic evolution of the eastern Grenville Province. Canadian Journal of Earth Sciences, 37: 341–358. doi:10.1139/e99-076

Indares, A., Dunning, G. 2004. Crustal architecture above the high-pressure belt of the Grenville Province in the Manicouagan area: new structural, petrologic and U-Pb age constraints. Precambrian Research, 130: 199–228. doi:10.1016/j.precamres.2003.11.005

Jamieson, R.A., Beaumont, C., Warren, C.J., Nguyen, M.H. 2010. The Grenville Orogen explained? Applications and limitations of integrating numerical models with geological and geophysical data. Canadian Journal of Earth Sciences, 47: 517–539. doi:10.1139/E09-070.

Jannin, S., Gervais, F., Moukhsil, A., Augland, L.E. 2018a. Late-Grenvillian channel flow in the central Grenville Province (Manicouagan Reservoir area): New constraints from a structural and geochronological study of the Allochthon Boundary Thrust. Journal of Structural Geology, 115: 132–151. doi:10.1016/j.jsg.2018.07.019.

Jannin, S., Gervais, F., Moukhsil, A., Augland, L.E., Crowley, J.L. 2018b. Déformations tardi-grenvilliennes dans la ceinture parautochtone (Province de Grenville centrale) : contraintes géochronologiques par couplage de méthodes U–Pb de haute résolution spatiale et de haute précision. Canadian Journal of Earth Sciences, 55: 406–435. doi:10.1139/cjes-2017-0129.

Jannin, S., Gervais, F., Moukhsil, A., Crowley, J.L., Augland, L.E. 2017. Datation U/Pb des déformations inverses et normales dans la Province de Grenville central (Manicouagan, Québec): évidence d'un chenal orogénique dans le Parautochtone.

In Géologie et ressources minérales de la partie centrale de la Province de Grenville. Moukhsil, A. coordonnateur. Ministère de l'Énergie et des Ressources naturelles, Québec, MM 2017-1: 99-148. Available from: http://gq.mines.gouv.qc.ca/documents/EXAMINE/MM201701/MM201701.pdf.

Moukhsil, A., Fabien, S. 2017. Géologie, potentiel minéral et cadre géodynamique des roches de la région du réservoir Daniel-Johnson (Manicouagan), partie centrale de la Province de Grenville. In Géologie, potentiel minéral et cadre géodynamique des roches de la région du réservoir Daniel-Johnson (Manicouagan), partie centrale de la Province de Grenville. Moukhsil, A. coordonnateur. Ministère de l'Énergie et des Ressources naturelles, Québec, MM 2017-1: 7-92. Available from: http://gq.mines.gouv.qc.ca/documents/EXAMINE/MM201701/MM201701.pdf.

Moyen, J.-F., Laurent, O., Chelle-Michou, C., Couzinié, S., Vanderhaeghe, O., Zeh, A., Villaros, A., Gardien, V. 2017. Collision vs. subduction-related magmatism: Two contrasting ways of granite formation and implications for crustal growth. Lithos, 277: 154–177. doi:10.1016/j.lithos.2016.09.018

Rivers, T. 2015. Tectonic setting and evolution of the Grenville Orogen: an assessment of progress over the last 40 years. Geoscience Canada, 42: 77–124. doi:10.12789/geocanj.2014.41.057.

Rivers, T., Corrigan, D. 2000. Convergent margin on southeastern Laurentia during the Mesoproterozoic: tectonic implications. Canadian Journal of Earth Sciences, 37: 359–383. doi:10.1139/e99-067

Turlin, F., André-Mayer, A.-S., Moukhsil, A., Vanderhaeghe, O., Gervais, F., Solgadi, F., Groulier, P.-A., Poujol, M. 2017. Unusual LREE-rich, peraluminous, monazite- or allanite-bearing pegmatitic granite in the central Grenville Province, Québec. Ore Geology Reviews, 89: 627–667. doi:10.1016/j.oregeorev.2017.04.019

Turlin, F., Deruy, C., Eglinger, A., Vanderhaeghe, O., André-Mayer, A.-S., Poujol, M., Moukhsil, A., Solgadi, F. 2018. A 70 Ma record of suprasolidus conditions in the large, hot, long-duration Grenville Orogen. Terra Nova, 30: 233–243. doi:10.1111/ter.12330

Turlin, F., Vanderhaeghe, O., Gervais, F., André-Mayer, A.-S., Moukhsil, A., Zeh, A., Solgadi, F., I.P.T.N. 2019. Petrogenesis of LREE-rich pegmatitic granite dykes in the central Grenville Province by partial melting of Paleoproterozoic-Archean metasedimentary rocks: evidence from zircon U-Pb-Hf-O isotope and trace element analyses. Precambrian Research, in press. doi:10.1016/j.precamres.2019.02.009.

Valverde Cardenas, C., Indares, A., Jenner, G. 2012. Mafic and ultrapotassic rocks from the Canyon domain (central Grenville Province): geochemistry and tectonic implications. Canadian Journal of Earth Sciences, 49: 412–433. doi:10.1139/e11-065.

van Gool, J.A.M., Rivers, T., Calon, T. 2008. Grenville Front zone, Gagnon terrane, southwestern Labrador: configuration of a midcrustal foreland fold-thrust belt. Tectonics, 27: 1–35. doi:10.1029/2006TC002095.

6 Appendices

6.1 Appendix A

6.1.1 Analytical techniques

6.1.1.1 CA-TIMS U-Pb in zircon (after Sparkes and Dunning, 2014)

The zircon grains analyzed in sample 11-383c, 11-331b, and 11-208 were hand-picked using tweezers from mineral concentrates under a binocular microscope according to the criteria of clarity, similarity of crystal form and lack of inclusions. All grains were chemically abraded using the Mattinson (2005) chemical abrasion thermal ionization mass spectrometry (CA-TIMS) technique. The selected crystals of zircon were annealed at 900° C for 36 hours prior to etching in concentrated HF acid in a pressure bomb at 200° C for a few hours. This procedure is designed to remove any altered domains from the crystal that may have undergone lead loss. It is a remarkably effective and simple procedure and has now largely replaced physical abrasion (Krogh, 1982) for zircon analysis.

Single grains or a small number of zircon grains were grouped into fractions of like morphology to allow precise measurement of all Pb masses on the mass spectrometer. At an age of ca. 1000 Ma, for clear high quality zircon, this amounts to 2-5 grains of zircon per fraction. These etched zircon fractions were washed in distilled HNO_3, then doubly distilled H_2O, prior to loading in Krogh-type TEFLON dissolution bombs. A mixed $^{205}Pb/^{235}U$ tracer was added in proportion to the sample weight, along with ca. 15 drops of distilled HF, then the bomb was sealed and placed in an oven at 210° C for 5 days. Ion exchange chemistry was carried out according to the procedure

of Krogh (1973), with modified columns and reagent volumes scaled down to one tenth of those reported in 1973. The purified Pb and U were collected in a clean beaker in a single drop of ultrapure H_3PO_4.

Lead and uranium were loaded together on outgassed single Re filaments with silica gel and dilute H_3PO_4. Mass spectrometry was carried out using a multi-collector MAT 262. The Faraday cups were calibrated with NBS 981 lead standard and the ion-counting secondary electron multiplier (SEM) detector was calibrated against the Faraday cups by measurement of known lead isotopic ratios. The small amounts of Pb were measured by peak jumping on the SEM, with measurement times weighted according to the amounts of each mass present. U was measured by peak jumping on the SEM. A series of sets of data were measured in the temperature range 1400 to 1550^{o} C for Pb and 1550 to 1640^{o} C for U, and the best sets combined to produce a mean value for each ratio. The measured ratios were corrected for Pb and U fractionation of 0.1% /amu and 0.03%/amu respectively as determined from repeat measurements of NBS standards. The ratios were also corrected for laboratory procedure blanks (1-2 picograms - Pb, 0.3 picogram - U) and for common lead above the laboratory blank with lead of the composition predicted by the two-stage model of Stacey and Kramers (1975) for the age of the sample. Ages are calculated using the decay constants recommended by Jaffey et al. (1971).

The uncertainties on the isotopic ratios and ages were calculated using an unpublished program and are reported at the two sigma (σ) level. Ages are reported as the weighted average of the $^{206}Pb/^{238}U$ ages calculated using ISOPLOT (Ludwig, 2003), and are reported at the 95% confidence interval.

As a check on the accuracy of the entire laboratory procedure, nine U-Pb analyses of the TEMORA zircon standard (Black et al., 2003) were carried out overlapping in time with the measurement of these samples, using the same detector and measurement conditions. These were reported by Sparkes and Dunning (2014). Eight of nine analyses overlap and yielded a weighted average $^{206}Pb/^{238}U$ age of 416.84 Ma (MSWD = 0.18), in close agreement with the published value (416.75 Ma, Black et al., 2003).

6.1.1.2 Whole rock major and trace elements

Selected samples were crushed and powdered using standard clean laboratory protocols at MUN. These samples were then sent to the Activation Laboratories where they were mixed with a flux of lithium metaborate and lithium tetraborate and fused in an induction furnace. The melt was immediately poured into a solution of 5% nitric acid containing an internal standard, and mixed continuously until completely dissolved (~30 minutes). The samples were then run for major oxides and selected trace elements (Ba, Be, Sc, Sr, V, Y, Zr; Code 4B) on a combination of simultaneous/sequential Thermo Jarrell-Ash ENVIRO II ICP or a Varian Vista 735 ICP. Calibration was performed using 7 prepared USGS and CANMET certified reference materials. One of the 7 standards was used during the analysis for every group of ten samples. Totals are expected to be between 98.5% and 101%. For lower results, samples were scanned for base metals as low results may indicate sulphate or other elements like Li, which are normally not scanned for. Samples with low totals were re-fused and reanalyzed. For the remaining trace elements (code 4B2-STD), samples were diluted and analyzed by Perkin Elmer Sciex ELAN (6000, 6100, or 9000 series) inductively coupled plasma mass spectrometer (FUS-MS). Three blanks and five controls (three before the samples

group and two after) were analyzed per group of samples; duplicates were fused and analyzed for every 15 samples; and the instrument was recalibrated after every 40 samples analyses. Typical precision and accuracy for these analyses (excluding those close to their detection limit) is 3%–5% for the major elements and 5%–20% for the trace elements. All the elements and detection limits for both analyses are listed below.

Analyte Symbol	Unit Symbol	Detection Limit	Analysis Method	Analyte Symbol	Unit Symbol	Detection Limit	Analysis Method
SiO2	%	0.01	FUS-ICP	Nb	ppm	1	FUS-MS
Al2O3	%	0.01	FUS-ICP	Mo	ppm	2	FUS-MS
Fe2O3(T)	%	0.01	FUS-ICP	Ag	ppm	0.5	FUS-MS
MnO	%	0.001	FUS-ICP	In	ppm	0.2	FUS-MS
MgO	%	0.01	FUS-ICP	Sn	ppm	1	FUS-MS
CaO	%	0.01	FUS-ICP	Sb	ppm	0.5	FUS-MS
Na2O	%	0.01	FUS-ICP	Cs	ppm	0.5	FUS-MS
K2O	%	0.01	FUS-ICP	La	ppm	0.1	FUS-MS
TiO2	%	0.001	FUS-ICP	Ce	ppm	0.1	FUS-MS
P2O5	%	0.01	FUS-ICP	Pr	ppm	0.05	FUS-MS
LOI	%		FUS-ICP	Nd	ppm	0.1	FUS-MS
Total	%	0.01	FUS-ICP	Sm	ppm	0.1	FUS-MS
Sc	ppm	1	FUS-ICP	Eu	ppm	0.05	FUS-MS
Be	ppm	1	FUS-ICP	Gd	ppm	0.1	FUS-MS
V	ppm	5	FUS-ICP	Tb	ppm	0.1	FUS-MS
Ba	ppm	3	FUS-ICP	Dy	ppm	0.1	FUS-MS
Sr	ppm	2	FUS-ICP	Ho	ppm	0.1	FUS-MS
Y	ppm	2	FUS-ICP	Er	ppm	0.1	FUS-MS
Zr	ppm	4	FUS-ICP	Tm	ppm	0.05	FUS-MS
Cr	ppm	20	FUS-MS	Yb	ppm	0.1	FUS-MS
Co	ppm	1	FUS-MS	Lu	ppm	0.04	FUS-MS
Ni	ppm	20	FUS-MS	Hf	ppm	0.2	FUS-MS
Cu	ppm	10	FUS-MS	Ta	ppm	0.1	FUS-MS
Zn	ppm	30	FUS-MS	W	ppm	1	FUS-MS
Ga	ppm	1	FUS-MS	Tl	ppm	0.1	FUS-MS
Ge	ppm	1	FUS-MS	Pb	ppm	5	FUS-MS
As	ppm	5	FUS-MS	Bi	ppm	0.4	FUS-MS
Rb	ppm	2	FUS-MS	Th	ppm	0.1	FUS-MS
Nb	ppm	1	FUS-MS	U	ppm	0.1	FUS-MS

6.1.1.3 Whole-rock Rb-Sr and Sm-Nd isotope analysis

In order to carry out whole rock Sm-Nd isotope ratio analyses of selected samples by thermal ionization mass spectrometer (TIMS), whole rock powders were dissolved in Savillex© Teflon beakers using an 8 ml (4:1) mixture of 29 M HF – 15 M HNO_3. Prior to acid digestion, a mixed $^{150}Nd/^{149}Sm$ spike was added to each sample with both sample and spike being weighed on a high-precision balance. After five days of digestion, the solution was evaporated to dryness and then redissolved in 6 M HCl for 2-3 days. The sample was dried down and then re-dissolved in 1.0 ml of 2.5 M HCL. Samples were then loaded into a column containing cation exchange resin AG-50W-X8, H^+ form, 200-400 mesh where a Sr fraction could be isolated followed by collection of bulk rare earth elements (REE). This solution was then dried and taken up in 0.18 M HCl and loaded on a second column containing Eichrom© Ln resin (50-100 mesh) to isolate Sm and Nd separately from the other REEs. Sm and Nd concentrations and the Nd isotopic compositions were determined using a multi-collector Finnigan Mat 262 mass spectrometer in static mode for concentration determination, and dynamic mode for isotopic composition determination. Sm and Nd were loaded onto a double rhenium filament assembly and instrumental mass fractionation of Sm and Nd isotopes was corrected using a Raleigh law relationship relative to $^{146}Nd/^{144}Nd = 0.7219$ and $^{152}Sm/^{147}Sm = 1.783$. The measured values were adjusted to the JNdi-1 standard ($^{143}Nd/^{144}Nd = 0.512115$, Tanaka et al., 2000). Our current measurement of JNdi-1 at the time of this study yielded a mean $^{143}Nd/^{144}Nd = 0.512098 \pm 6$ (2σ, n = 15). We also analyzed USGS whole rock reference material BCR-2 with each analysis comprising a separate dissolution, providing the best estimate of the reproducibility of an individual whole-rock analysis. The mean values of BCR-2 are as follows, where the relative two

standard deviations of the mean (n = 11) are given in parentheses in percent; $^{143}Nd/^{144}Nd$ = 0.512636 (0.0021%); $^{147}Sm/^{144}Nd$ = 0.1383 (0.389%); Nd ppm = 27.7 (0.7%); Sm = 6.33 (0.6%). These results are in agreement with the results reported by Raczek et al. (2003). For Sr, the measured chemical blank is below 0.7 ng and is considered negligible. The Sr isotopic ratios were normalized to $^{88}Sr/^{86}Sr$ = 8.375209. The reported values were adjusted to the National Bureau of Standards-987 Sr standard ($^{87}Sr/^{86}Sr$ = 0.710240), for which the mean value measured at MUN was 0.710245 ± 19 (2σ, n = 20).

6.1.1.4 Whole-rock Pb isotope analyses

For the Pb isotope analysis, approximately 0.2 g of whole-rock powder was dissolved in Savilex© Teflon beakers using a mixture of HF – HNO3 acids. After five days of digestion, the solution was evaporated to dryness and then taken up in 6 N HCl acid for two days. The solution was then evaporated again and taken up in HBr. Pb elution was achieved using the standard anionic HBr – HCl chromatography. All reagents were purified by sub-boiling in order to minimize contamination. Isotopic ratios were obtained using a multicollector Finnigan Mat 262 mass spectrometer in static mode. The reported Pb isotopic ratios are corrected for mass fractionation by a factor of 0.126% per amu, which was obtained by measuring the deviation from repeated (n = 11) analyses of the NBS 981 standard. In-run precisions on all isotopic ratios are given at 95% confidence level.

6.1.1.5 Whole-rock oxygen isotope analyses

For the oxygen isotope analysis, performed at the Western University, Ontario, Canada, whole-rock powders of about 8 mg of each sample are placed in spring-loaded

sample holders, and heated while pumping in vacuo overnight at 150 °C to remove sorbed water. The samples were then loaded into Ni-reaction vessels under dry nitrogen and heated while pumping under vacuum at 300°C for an additional three hours to eliminate any remaining water from the system. Structural oxygen was then liberated using chlorine trifluoride, and the oxygen was then reacted with incandescent carbon to produce carbon dioxide gas, following Clayton & Mayeda (1963), as modified by Borthwick & Harmon (1982). The oxygen isotope measurements were conducted using a dual-inlet, triple-collecting Thermo Scientific Delta Plus XL IRMS. All results are reported in the standard δ-notation in parts per thousand (‰) relative to Vienna Standard Mean Ocean Water (VSMOW) on the VSMOW-SLAP scale, to which internal laboratory standards have been calibrated following the protocol of Coplen (1996). The target reproducibility of duplicate analyses of samples is ± 0.2‰.

6.1.2 References

Black, L.P., Kamo, S.L., Allen, C.M., Aleinikoff, J.N., Davis, D.W., Korsch, R.J., Foudoulis, C. 2003. TEMORA 1: a new zircon standard for Phanerozoic U–Pb geochronology. Chemical Geology, 200: 155–170. doi: 10.1016/S0009-2541(03)00165-7

Borthwick, J., Harmon, R.S. 1982. A note regarding CIF3 as an alternative to BrF5 for oxygen isotope analysis. Geochimica et Cosmochimica Acta, 46: 1665–1668. doi:10.1016/0016-7037(82)90321-0

Clayton, R.N., Mayeda, T.K. 1963. The use of bromine pentafluoride in the extraction of oxygen from oxides and silicates for isotopic analysis. Geochimica et Cosmochimica Acta, 27: 43–52. doi:10.1016/0016-7037(63)90071-1.

Coplen, T.B. 1996. New guidelines for reporting stable hydrogen, carbon, and oxygen isotope-ratio data. Geochimica et Cosmochimica Acta, 60: 3359–3360. doi:10.1016/0016-7037(96)00263-3

Jaffey, A.H., Flynn, K.F., Glendenin, L.E., Bentley, W.C., Essling, A.M. 1971. Precision measurement of half-lives and specific activities of U235 and U238. Physical Review, C 4: 1889–1906. doi: 10.1103/PhysRevC.4.1889

Krogh, T.E. 1973. A low-contamination method for hydrothermal decomposition of zircon and extraction of U and Pb for isotopic age determinations. Geochimica et Cosmochimica Acta, 37(3): 485–494. doi:10.1016/0016-7037(73)90213-5

Krogh, T.E. 1982. Improved accuracy of U-Pb zircon ages by the creation of more concordant systems using an air abrasion technique. Geochimica et Cosmochimica Acta, 46(4): 637–649. doi:10.1016/0016-7037(82)90165-X

Ludwig, K.R. 2003. ISOPLOT 3.0: a geochronological toolkit for Microsoft Excel. Berkeley Geochronology Center. Special publication, 4: 1–71.

Mattinson, J.M. 2005. Zircon U–Pb chemical abrasion ("CA-TIMS") method: combined annealing and multi-step partial dissolution analysis for improved precision and accuracy of zircon ages. Chemical Geology, 220(1-2): 47–66. doi:10.1016/j.chemgeo.2005.03.011

Raczek, I., Jochum, K.P., and Hofmann, A.W. 2003. Neodymium and Strontium isotope data for USGS reference materials BCR-1, BCR-2, BHVO-1, BHVO-2, AGV-1, AGV-2, GSP-1, GSP-2 and eight MPI-DING reference glasses. Geostandards and Geoanalytical Research, 27: 173–179. doi:10.1111/j.1751-908X.2003.tb00644.x.

Sparkes, G.W., Dunning, G.R. 2014. Late Neoproterozoic epithermal alteration and mineralization in the western Avalon zone: a summary of mineralogical investigations and new U/Pb geochronological results. Current Research, Newfoundland and Labrador Department of Natural Resources, Geological Survey, Report 14-1: 99–128. Available from: https://www.nr.gov.nl.ca/nr/mines/geoscience/publications/currentresearch/2014/Sparkes-2014.pdf.

Stacey, J.S., Kramers, J.D. 1975. Approximation of terrestrial lead isotope evolution by a two-stage model. Earth and Planetary Science Letters, 26: 207–221. doi:10.1016/0012-821X(75)90088-6

Tanaka, T., Togashi, S., Kamioka, H., Amakawa, H., Kagami, H., Hamamoto, T., Yuhara, M., Orihashi, Y., Yoneda, S., Shimizu, H., Kunimaru, T., Takahashi, K., Yanagi, T., Nakano, T., Fujimaki, H., Shinjo, R., Asahara, Y., Tanimizu, M., Dragusanu, C. 2000. JNdi-1: a neodymium isotopic reference in consistency with LaJolla neodymium. Chemical Geology, 168: 279–281. doi:10.1016/S0009-2541(00)00198-4.

6.2 Appendix B

6.2.1 Effects of high-grade metamorphism and hydrothermal alteration

Chemical mobility in hydrothermally altered rocks can be assessed by using geochemical indices that have the potential to indicate changes in major element compositions resulting from the formation of sericite, chlorite, pyrite, and carbonates during hydrothermal alteration. The mafic rocks from both the VC and LBS suites exhibit negligible carbonate, but contain variable proportions of sericite and minor chlorite, with the LBS sample 11-331b exhibiting the highest proportions (0.10%, 18%, and 0.24%, respectively). LBS sample 11-317a has a thin K-feldspar vein that cuts across the entire thin section. For whole-rock analysis, these alteration zones were removed as much as possible and only fresh-looking parts were analyzed. The mafic rocks in our study exhibit an alteration index (A.I = [(MgO + K_2O)/ (MgO + K_2O + Na_2O + CaO)] × 100; Ishikawa et al., 1976) between 36-49, and a peraluminous index (PI = Al_2O_3/ (CaO + Na_2O + $K_2O)_{mol.}$) (Hashiguchi et al., 1983) between 0.56-0.86 (except samples 11-317a and 11-331b having P.Is of 0.97 and 1.15, respectively). These ranges are similar to fresh MORB and arc-related mafic volcanic rocks (A.I = 36 ± 8 and 34 ± 10, respectively, and P.I = 0.8 ± 0.2; Laflèche et al., 1992), suggesting no significant mobility in major elements, except for alkalis compared to aluminium in the two samples. All the samples exhibit low loss on ignition (table 3.2).

The values of chlorite-carbonate-pyrite index (CCPI = 100 × (MgO + FeO_t)/ (MgO + FeO_t + Na_2O + K_2O) (Large et al., 2001) plotted against AI show a trend from the field for least altered basalt and andesite towards dolomite/ankerite extending outside the least altered box (fig. 6.1a). This trend is interpreted to be a result of Na loss

compared to Fe-Mg, as the samples contain minor chlorite, sericite and K-feldspar veins. This is further supported in the $K_2O + Na_2O$ vs. $100 \times K_2O/(K_2O+Na_2O)$ diagram (fig. 6.1b; Hughes, 1972), where most of the samples plot within the igneous spectrum, but three exhibit a trend towards increasing K_2O suggestive of K-metasomatism or relative Na-loss. The alteration index Al_2O_3/Na_2O plotted against Na_2O (fig. 6.1c; Spitz and Darling, 1978) shows that most of the mafic samples fall within the field for fresh to weakly altered rocks with two exhibiting relative Na-loss. The effect of sericite alteration is probably reflected in the low CaO value in the sample (11-331b) exhibiting the highest sericite content. Fe_2O_3 is fluid-mobile under reducing conditions and hence can be lost, whereas TiO_2 and P_2O_5 are immobile and remain unchanged during hydrothermal alteration (Rollinson, 1993). The positive correlation between Fe_2O_3, TiO_2, and P_2O_5 with Zr (fig. 3.8) in the mafic rocks suggests magmatic differentiation rather than alteration was the main process determining their major element characteristics. Extreme Fe-Ti enrichment in mafic tholeiites can also increase the CCPI values, but the major element compositions of most of the mafic samples in our study are interpreted to have been largely unaffected by hydrothermal alteration and granulite-facies metamorphism, except for mobility of alkalis in three samples and CaO in one sample.

Thorium is generally considered to be immobile below amphibolite-facies conditions, although it can be mobilized during high-grade metamorphism in a water-dominated system (Jenner, 1996). Th mobility can be assessed in the La/Th vs. Th/U diagram (fig. 6.1d) where four mafic samples exhibit La/Th ratios higher than common igneous rocks ($La/Th \leq 21$; Rudnick et al., 1985; Sun and McDonough, 1989) suggesting minor Th and/or U mobility. However, low Th and La/Th ratios in many

granulites are considered as original features (Rudnick et al., 1985; Rudnick, 1992), and Th and U have been shown to be isochemically redistributed in mafic and calc-alkaline rocks following the breakdown of accessory phases and dehydration reactions during granulite-facies metamorphism (Bingen et al., 1996; Bea and Montero, 1999; Bea et al., 1999). Our data exhibit comparable ratios for these elements to other least altered mafic granulites from the Grenville Province (e.g., Blein et al., 2003; Bonnet et al., 2005; Montreuil and Constantin, 2010), suggesting their La/Th ratios are original features.

The K/Rb ratios (<500) in the mafic rocks from the LBS mostly fall within the range of the igneous fractionation trend (fig. 6.1e; Shaw, 1968; Rudnick et al., 1985), whereas the samples from the VC exhibit highly variable K/Rb ratios that do not correlate with their K_2O contents. Overall, the samples from the LBS have higher Rb and K_2O at relatively low K/Rb, possibly related to their higher modal proportions of biotite. The samples from the VC, with lower modal biotite, exhibit increase in K/Rb at K_2O < 1 wt%, possibly suggesting these samples lost Rb because of biotite breakdown (Shaw, 1968; Rudnick et al., 1985).

Partial melting and melt loss during metamorphism in mafic rocks would result in restitic compositions exhibiting LREE depletion along with either positive Eu anomalies or a decrease in original negative anomalies inherited from their protoliths (Rudnick, 1992). Samples from both the mafic suites exhibit a narrow range in Eu/Eu* (fig. 6.1f), suggesting that they have not been modified by partial melting. In N-MORB-normalized REE and HFSE diagrams (fig. 6.1g-h), the HFSE and REE patterns of the most altered mafic samples from both suites are similar to the least altered samples

except 11-331b, which exhibits slight but noticeable depletion in LREE compared to the OIB pattern.

Dehydration melting in mafic migmatites has been shown to produce leucosomes that are not significantly different than their original protolith compositions (Sawyer, 1991), and many subsequent studies have shown that such process may have only minor effect on immobile element remobilization in mafic gneisses (e.g., Blein et al., 2003). For example, poikiloblastic garnet-bearing mafic migmatites in the marginal gabbro from the Baie du Nord segment in the MIZ (north of the study area) were shown to have broadly retained their protolith compositions inasmuch as they are identical to samples from the main unaltered Fe-Ti gabbro body (Cox et al., 1998). Several studies of high-grade gneisses in the Grenville Province and elsewhere have demonstrated that high-grade metamorphism can be effectively isochemical for immobile-incompatible major and trace elements e.g., HFSE and REE (Ludden et al., 1982; Blein et al., 2003; Bonnet et al., 2005; Dickin and McNutt, 2007; Sappin et al., 2009; Yardley, 2012; Corriveau and Spry, 2014).

The screening process indicates minor hydrothermal alteration in a few samples, but most exhibit major and trace element features indicating they are not restites and that hydrothermal alteration has not significantly changed their whole-rock immobile incompatible element concentrations and ratios. This conclusion is supported by other studies that suggest the incompatible element concentrations remain largely unchanged in tholeiitic rocks during high-grade metamorphism and hydrothermal alteration (e.g., Laflèche et al., 1992, 1998; Blein et al., 2003; Bonnet et al., 2005; Corriveau and Bonnet, 2005; Sappin et al., 2009; Yardley et al., 2012; Corriveau and Spry, 2014).

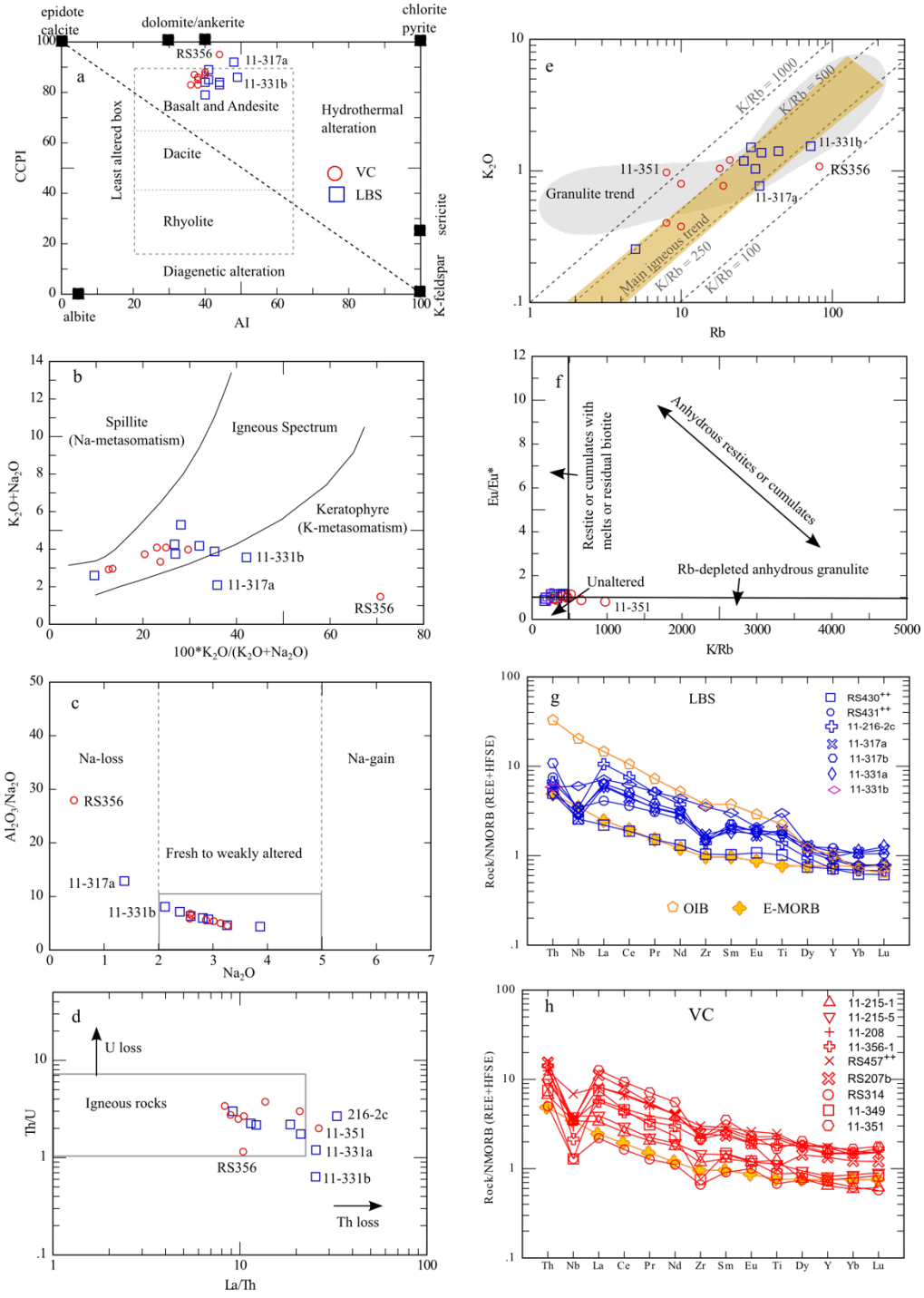

Figure 6.1. Plots the data for the mafic rocks from VC and LBS to assess the effects post-magmatic alteration. (a) CCPI vs. AI (alteration box plot; Large et al., 2001); (b) $K_2O + Na_2O$ vs $(100 \times K_2O)/ (K_2O + Na_2O)$ (Hughes et al., 1972); (c) Al_2O_3/Na_2O vs. Na_2O (modified after Spitz and Darling, 1978); (d) Th/U vs. La/Th plot (modified after Rudnick et al., 1985); (e) K_2O vs. Rb plot (modified after Rudnick et al., 1985); (f) Eu/Eu* vs. K/Rb plot (modified after Rudnick, 1992); N-MORB normalized REE, Th, Nb, Zr, and Ti plots for the mafic rocks from the (g) LBS and (h) VC. N-MORB normalization values from Sun and McDonough (1989).

6.2.2 References

Bea, F., Montero, P. 1999. Behavior of accessory phases and redistribution of Zr, REE, Y, Th, and U during metamorphism and partial melting of metapelites in the lower crust: an example from the Kinzigite Formation of Ivrea-Verbano, NW Italy. Geochimica et Cosmochimica Acta, 63: 1133–1153. doi:10.1016/S0016-7037(98)00292-0.

Bea, F., Montero, P., Molina, J.F. 1999. Mafic precursors, peraluminous granitoids, and late lamprophyres in the Avila batholith: a model for the generation of Variscan Batholiths in Iberia. The Journal of Geology, 107: 399–419. doi:10.1086/314356.

Bingen, B., Demaiffe, D., Hertogen, J. 1996. Redistribution of rare earth elements, thorium, and uranium over accessory minerals in the course of amphibolite to granulite facies metamorphism: the role of apatite and monazite in orthogneisses from southwestern Norway. Geochimica et Cosmochimica Acta, 60: 1341–1354. Pergamon. doi:10.1016/0016-7037(96)00006-3.

Blein, O., Marc R., L., Corriveau, L. 2003. Geochemistry of the granulitic Bondy gneiss complex: a 1.4 Ga arc in the Central Metasedimentary Belt, Grenville Province, Canada. Precambrian Research, 120: 193–217. doi:10.1016/S0301-9268(02)00112-2.

Bonnet, A.-L., Corriveau, L., La Flèche, M.R. 2005. Chemical imprint of highly metamorphosed volcanic-hosted hydrothermal alterations in the La Romaine Supracrustal Belt, eastern Grenville Province, Quebec. Canadian Journal of Earth Sciences, 42: 1783–1814. doi:10.1139/e05-098.

Corriveau, L., Bonnet, A.-L. 2005. Pinwarian (1.50 Ga) volcanism and hydrothermal activity at the eastern margin of the Wakeham Group, Grenville Province, Quebec. Canadian Journal of Earth Sciences, 42: 1749–1782. doi:10.1139/e05-086.

Corriveau, L., Spry, P. 2014. Metamorphosed hydrothermal ore deposits. *In* Treatise on Geochemistry (Second Edition). *Edited by* H.D. Holland and K.K. Turekian. Oxford, Elsevier. pp. 175–194.

Cox, R.A., Dunning, G.R., Indares, A.D. 1998. Petrology and U–Pb geochronology of mafic, high-pressure, metamorphic coronites from the Tshenukutish domain, eastern Grenville Province. Precambrian Research, 90: 59–83. doi:10.1016/S0301-9268(98)00033-3.

Dickin, A.P., McNutt, R.H. 2007. The Central Metasedimentary Belt (Grenville Province) as a failed back-arc rift zone: Nd isotope evidence. Earth and Planetary Science Letters, 259: 97–106. doi:10.1016/j.epsl.2007.04.031.

Hashiguchi, H., Inoue, T. 1983. Practical application of low Na_2O anomalies in footwall acid lavas for delimiting promising areas around the Kosaka and Fukazawa Kuroko deposits, Akita Prefecture, Japan. Economic Geology Monograph, 5: 387–394.

Hughes, C.J. 1972. Spilites, keratophyres and the igneous spectrum. Geological Magazine, 109: 513–527. doi:10.1017/S0016756800042795.

Ishikawa, Y., Sawaguchi, T., Iwaya, S., Horiuchi, M. 1976. Delineation of prospecting targets for Kuroko deposits based on modes of volcanism of underlying dacite and alteration halos. Mining Geology, 26: 105–117.

Jenner, G.A. 1996. Trace element geochemistry of igneous rocks: geochemical nomenclature and analytical geochemistry. *In* Trace element geochemistry of

volcanic rocks: applications for massive sulphide exploration. *Edited by* D.A. Wyman. Geological Association of Canada. Short Course Notes. pp. 51–77.

Laflèche, M.R., Camiré, G., Jenner, G.A. 1998. Geochemistry of post-Acadian, Carboniferous continental intraplate basalts from the Maritimes Basin, Magdalen Islands, Quebec, Canadá. Chemical Geology, 148: 115–136. doi:10.1016/S0009-2541(98)00002-3.

Laflèche, M.R., Dupuy, C., Bougault, H. 1992. Geochemistry and petrogenesis of Archean mafic volcanic rocks of the southern Abitibi Belt, Québec. Precambrian Research, 57: 207–241. doi:10.1016/0301-9268(92)90003-7.

Large, R.R., Gemmell, J.B., Paulick, H., Huston, D.L. 2001. The alteration box plot: a simple approach to understanding the relationship between alteration mineralogy and lithogeochemistry associated with volcanic-hosted massive sulfide deposits. Economic Geology, 96: 957–971. doi:10.2113/gsecongeo.96.5.957.

Ludden, J., Gélinas, L., Trudel, P. 1982. Archean metavolcanics from the Rouyn–Noranda district, Abitibi Greenstone Belt, Quebec. 2. Mobility of trace elements and petrogenetic constraints. Canadian Journal of Earth Sciences, 19: 2276–2287. doi:10.1139/e82-200.

Montreuil, J.F., Constantin, M. 2010. The geochemistry of mafic gneisses from the Renzy terrane, western Grenville Province, Quebec: implications for the geodynamic setting of the early Mesoproterozoic Laurentian margin. Precambrian Research, 181: 150–166. doi:10.1016/j.precamres.2010.06.001.

Rollinson, H. 1993. Using geochemical data. 352 pp., Longman, London.

Rudnick, R.L. 1992. Restites, Eu anomalies and the lower continental crust. Geochimica et Cosmochimica Acta, 56: 963–970. doi:10.1016/0016-7037(92)90040-P.

Rudnick, R.L., McLennan, S.M., Taylor, S.R. 1985. Large ion lithophile elements in rocks from high-pressure granulite facies terrains. Geochimica et Cosmochimica Acta, 49: 1645–1655. doi:10.1016/0016-7037(85)90268-6.

Sappin, A.-A., Constantin, M., Clark, T., van Breemen, O. 2009. Geochemistry, geochronology, and geodynamic setting of Ni–Cu ± PGE mineral prospects hosted by mafic and ultramafic intrusions in the Portneuf–Mauricie Domain, Grenville Province, Quebec. Géologie Québec Contribution 8439-2008-2009-5. Geological Survey of. Canadian Journal of Earth Sciences, 46: 331–353. doi:10.1139/E09-022.

Sawyer, E.W. 1991. Disequilibrium melting and the rate of melt-residuum separation during migmatization of mafic rocks from the Grenville Front, Quebec. Journal of Petrology, 32: 701–738. doi:10.1093/petrology/32.4.701.

Shaw, D.M. 1968. A review of K-Rb fractionation trends by covariance analysis. Geochimica et Cosmochimica Acta, 32: 573–601. doi:10.1016/0016-7037(68)90050-1.

Spitz, G., Darling, R. 1978. Major and minor element lithogeochemical anomalies surrounding the Louvem copper deposit, Val d'Or, Quebec. Canadian Journal of Earth Sciences, 15: 1161–1169. doi:10.1139/e78-122.

Sun, S. -s., McDonough, W.F. 1989. Chemical and isotopic systematics of oceanic basalts: implications for mantle composition and processes. Geological Society, London, Special Publications, 42: 313–345. doi:10.1144/GSL.SP.1989.042.01.19.

Yardley, B.W.D. 2012. The chemical composition of metasomatic fluids in the crust. *In* Lecture Notes in Earth System Sciences. *Edited by* D.E. Harlov and H. Austrheim. pp. 17–52.

6.3 Appendix C

6.3.1 Isotope and trace element modelling

6.3.1.1 The assimilation fractional crystallization model (AFC)

The assimilation fractional crystallization (AFC) model is based on a strict relationship between the amount of material assimilated and the amount of material crystallized during cooling of the magma. The AFC is expressed by the following equations (DePaolo, 1981):

For an element:

$$C_l^{AFC} = C_0[F^{-Z} + \left(\frac{r}{r-1}\right)\frac{C_a}{ZC_0}(1 - F^Z)]$$

For an isotopic ratio:

$$IC_l^{AFC} = \frac{\left(\frac{r}{r-1}\right)\left(\frac{C_a}{Z}\right)(1 - F^{-Z})IC_a + C_0F^{-Z}IC_0}{\left(\frac{r}{r-1}\right)\left(\frac{C_a}{Z}\right)(1 - F^{-Z}) + C_0F^{-Z}}$$

where C_l^{AFC}, C_0, and C_a are the concentrations of an element in the resulting magma, parental magma and assimilating material (wall-rock), respectively. IC_l^{AFC}, IC_0 *and* IC_a are isotopic ratios in the magma undergoing AFC process, in the parental magma, and isotopic ratios in the assimilating material (wall-rock), respectively. F is the fraction of melt during cooling of the magma. The r value describes the relative ratio of assimilated material to crystallized material, and it is expressed by $r = \frac{m_a}{m_c}$, where m_a is the amount of assimilated material and m_c is the amount of crystallized material. The z value in AFC equations are expressed by $z = \frac{r+D-1}{r-1}$

where D is the bulk partition coefficient calculated by:

$$D = \Sigma_i^n x_i kd_i = x_a k_d^{mineral\ a} + x_b k_d^{mineral\ b} + \cdots + x_n k_d^{mineral\ n}$$

where x is the weight fraction of the mineral phase i in the fractionation assemblage, and k_d is the partition coefficient of an element (i.e., Sr and Nd) for each mineral phase in the fractionation assemblages.

6.3.1.2 Bulk mixing

Concentration of an element in a magma resulted from simple mixing of two different magmas is expressed by the following equations (Powell 1984):

For an element: $C_m = X(C_a - C_b) + C_b$

For isotopic ratio: $IC_m = IC_a \left(\frac{C_a X}{C_m}\right) + IC_b \left(\frac{C_b(1-x)}{C_m}\right)$

where C_a, C_b, and C_m are the concentrations of an element in the assimilating material a (e.g., wall-rock), in the parental magma b, and in mixed magma m resulted from mixing of a and b, respectively. IC_a, IC_b, IC_m are the isotopic ratios in the assimilating material, in the parental magma, and in the mixed magma resulting from bulk mixing of a and b, respectively. X is the degree of mixing.

6.3.1.3 Non-modal batch melting

For a mass of solid M_o with concentration of some element as C_s^o, if partial melting produces melt of volume L with concentration of the element as C_l and in the residual solid C_s with mass as M, then batch melting assumes that total melt fraction attains equilibrium with the solid, and only then the melt is extracted fully. From mass balance consideration we get the following relationship:

$M_0 = M + L$, and $C_s^o M_o = C_l L + C_S M$, which gives us $C_s^o = FC_l + (1 - F)C_s$

where melt fraction $F = \frac{L}{M_o}$, and partition coefficient $D = \frac{C_s}{C_l}$.

For non-modal batch melting, proportions of mineral phases entering melt p_i differ from those in the residual solid so that at any point during melting $D = \frac{D_o - FP}{1-F}$, where the original value of bulk partition $D_o = \sum_i X_i^o D_i$ and the bulk partition coefficient of phases melting to form liquid is $P = \sum_i p_i D_i$. The equation for non-modal batch melting given by Shaw (1970) is $\frac{C_l}{C_s^o} = \frac{1}{D_o + F(1-P)}$.

6.3.2 References

DePaolo, D.J. 1981. Trace element and isotopic effects of combined wallrock assimilation and fractional crystallization. Earth and Planetary Science Letters, 53: 189–202. doi:10.1016/0012-821X(81)90153-9.

Powell, R. 1984. Inversion of the assimilation and fractional crystallization (AFC) equations; characterization of contaminants from isotope and trace element relationships in volcanic suites. Journal of the Geological Society, 141: 447–452. doi:10.1144/gsjgs.141.3.0447.

Shaw, D.M. 1970. Trace element fractionation during anatexis. Geochimica et Cosmochimica Acta, 34: 237–243. doi:10.1016/0016-7037(70)90009-8.